

2007

Interactions of the Triaquatricarbonylrhenium(I) Cation with Nucleotides and Other N-Donor Ligands

Kristie Marie Adams

Louisiana State University and Agricultural and Mechanical College, kadams9@lsu.edu

Follow this and additional works at: https://digitalcommons.lsu.edu/gradschool_dissertations



Part of the [Chemistry Commons](#)

Recommended Citation

Adams, Kristie Marie, "Interactions of the Triaquatricarbonylrhenium(I) Cation with Nucleotides and Other N-Donor Ligands" (2007). *LSU Doctoral Dissertations*. 2149.

https://digitalcommons.lsu.edu/gradschool_dissertations/2149

This Dissertation is brought to you for free and open access by the Graduate School at LSU Digital Commons. It has been accepted for inclusion in LSU Doctoral Dissertations by an authorized graduate school editor of LSU Digital Commons. For more information, please contact gradetd@lsu.edu.

**INTERACTIONS OF THE TRIQUATRICARBONYLRHENIUM(I) CATION WITH
NUCLEOTIDES AND OTHER N-DONOR LIGANDS**

A Dissertation

Submitted to the Graduate Faculty of the
Louisiana State University and
Agricultural and Mechanical College
in partial fulfillment of the
requirements for the degree of
Doctor of Philosophy

in

The Department of Chemistry

by
Kristie Marie Adams
B.S., Louisiana State University, 2002
December 2007

©Copyright 2007
Kristie Marie Adams
All rights reserved

This one is for you, Mom.
I am forever grateful for your patience, love, and guidance.
Thank you, and I love you.

*“...Always remember that what
does not kill you
only makes you stronger.
This is just a snapshot in time...
... it too shall pass.”*

ACKNOWLEDGMENTS

I owe the completion of this dissertation to an extremely capable team of highly trained individuals, each of whom has played an integral role in this extremely lengthy process. I must first thank my advisor, **Dr. Luigi G. Marzilli**, for his unique brand of guidance and support throughout my graduate career. I'm sure that I would never have earned my Ph.D. without his constantly pushing me to do my best (but mostly pushing me to do better!) I must thank **Dr. Patricia A. Marzilli**, for her sharp eye, endless reading of my manuscripts, and gardening hints. I would like to thank the members of my committee, **Dr. George Stanley**, **Dr. Andy Maverick**, **Dr. Robert Hammer** and **Dr. Carol Taylor**, for offering advice, or lending an ear on a rough day (of which there were more than a few), and putting up with me in general. Finally, I want to thank **Dr. Dale Treleaven** and **Dr. Thomas Weldeghiorghis**, for being endlessly patient with me, and making sure that I had (mostly) functioning NMR spectrometers on which to conduct my research; and **Dr. Frank Fronczek**, for determining all of the X-ray crystal structures reported herein (and doing it with a smile!).

My thanks also go to my colleagues, "The Fabulous Women of the Marzilli Lab", **Dr. Anna Maria Christoforou**, **Janet Manono**, **Vidhi Maheshwari**, and **Theshini Perera**, (and those in the Italian chapter, **Dr. Rosita Ranaldo** and **Dr. Patrizia Siega**) for making me laugh (and sometimes cry!), for being united against a common enemy, and for being there to share the "experience" of graduate school. I enjoyed all of the interesting conversations that took my mind off of my troubles, if even for just a moment. I must also thank the former members of the Marzilli Lab, for laying a solid foundation of work from which to draw from. Additional thanks go to **Dr. Debadeep Bhattacharyya**, for putting up with my endless questions as a first-year graduate student, and **Dr. Mike Reily**, who left behind some very large shoes to fill.

My sincere thanks go to those brave individuals who befriended me during my tenure at LSU. Thanks go to the “boys”, **Derek Dorman**, **Chris Haftek**, **Dr. Garrett Doucet**, **Arther Gates**, and **Adam Sonnier**, for always being game for tailgating or grabbing a drink at the Chimes. I thank **M. Scott Moreau** for being my first “real” friend, a friend I can trust with anything. I thank **Kelly Pitre-Small** for letting me “borrow” her children for awhile as a welcome break from thinking all the time; **Karla Lemoine**, for being like a second mom; and **Kim Mollere**, for always keeping the candy dish full!

Last but certainly not least, I reserve my most sincere thanks for the two most important people in my life, **Elaine Adams** and **John Grubb**, who somehow found the strength to not only support me while I was pursuing my Ph.D., but also to tolerate me! I am immeasurably grateful that Mom raised me right, teaching me never to give up, and that anything worth having is worth working hard for. She also taught me the meaning of strength and love, spirit and dedication. She always told me that I could do or have absolutely anything I wanted, if I was willing to work for it. You never think that your parents know what they are talking about. Now I understand that she’s been right all along. I am also very lucky to have come across John during this fabulous higher-learning experience, and I am forever grateful for his understanding, love and support. I thank him for taking care of all of the things that fell by the wayside as I got closer to (finally) finishing this journey. I don’t know what I would have done if he hadn’t made sure I was eating enough, sleeping enough, and maintaining a reasonable standard of hygiene. You’d be surprised what you can forget to do when you are intently focused on research!

If I forgot anyone, and I’m sure I did, I apologize. And I almost forgot. I must thank **Dr. Lashman Soriya** for being the best neurosurgeon on the planet. I quite literally owe him my life.

TABLE OF CONTENTS

ACKNOWLEDGMENTS	iv
LIST OF TABLES	ix
LIST OF FIGURES	xi
LIST OF ABBREVIATIONS	xiv
ABSTRACT	xix
CHAPTER 1. INTRODUCTION	1
1.1 Metals in Medicine	1
1.2 Cisplatin, <i>cis</i> -[Pt(NH ₃) ₂ Cl ₂]	1
1.3 Triaquatricarbonylrhenium(I), <i>fac</i> -[Re(CO) ₃ (H ₂ O) ₃] ⁺	3
1.4 References	6
CHAPTER 2. <i>fac</i> -[Re(CO) ₃ (H ₂ O) ₃] ⁺ NUCLEOSIDE MONOPHOSPHATE ADDUCTS INVESTIGATED IN AQUEOUS SOLUTION BY MULTINUCLEAR NMR SPECTROSCOPY	8
2.1 Introduction	8
2.2 Experimental Section	10
2.2.1 Materials and Sample Preparation	10
2.2.2 NMR Spectroscopy	11
2.2.3 Circular Dichroism (CD) Spectroscopy	12
2.3 Results and Discussion	12
2.3.1 Characteristic Features of Metal–NMP Adducts	12
2.3.2 Overview of Products Formed by <i>fac</i> -[Re(CO) ₃ (H ₂ O) ₃] ⁺ and NMPs	15
2.3.3 5'-GMP Reaction Products	15
2.3.4 3'-GMP Reaction Products	21
2.3.5 Further Aspects of the GMP Reactions	22
2.3.6 Mixed Nucleotide Approach	26
2.3.7 Effects of Modifying the Nucleotides	29
2.3.8 Competition and Challenge Reactions Using Methionine and 5'-GMP	31
2.4 Conclusions	33
2.5 References	34
CHAPTER 3. REACTIONS OF <i>fac</i> -[Re(CO) ₃ (H ₂ O) ₃] ⁺ WITH NUCLEOSIDE DIPHOSPHATES AND THIAMINE DIPHOSPHATE IN AQUEOUS SOLUTION INVESTIGATED BY MULTINUCLEAR NMR SPECTROSCOPY	39
3.1 Introduction	39
3.1.1 Stereochemistry and Nomenclature	40
3.2 Experimental Section	44
3.2.1 Materials and Sample Preparation	44
3.2.2 NMR Spectroscopy	44
3.2.3 Computational Methods	45

3.3	Results and Discussion.....	46
3.3.1	Overview of Products Formed by <i>fac</i> -[Re(CO) ₃ (H ₂ O) ₃] ⁺ and MDPs	48
3.3.2	TDP Reaction Products.....	48
3.3.3	5'-UDP Reaction Products.....	50
3.3.3.1	Mixed-Nucleotide Experiment.....	52
3.3.4	5'-GDP Reaction Products.....	52
3.3.5	Further Considerations.....	56
3.3.5.1	pH Study of <i>fac</i> -[Re(CO) ₃ (H ₂ O)({N ₇ ,P _β }GDP)] ⁻ Isomers	58
3.3.5.2	Mn ²⁺ Relaxation NMR Titrations of <i>fac</i> -[Re(CO) ₃ (H ₂ O)({N ₇ ,P _β }GDP)] ⁻ Isomers	58
3.3.6	Rate Constants of Interchange for TDP, 5'-UDP, and 5'-GDP Products.....	60
3.4	Conclusions	63
3.5	References	64
CHAPTER 4. <i>fac</i> -[Re(CO) ₃ (H ₂ O) ₃] ⁺ NUCLEOSIDE TRIPHOSPHATE ADDUCTS INVESTIGATED IN AQUEOUS SOLUTION BY MULTINUCLEAR NMR SPECTROSCOPY		
4.1 Introduction		
4.2 Experimental Section		
4.2.1 Materials and Sample Preparation		
4.2.2 NMR Spectroscopy.....		
4.2.3 Computational Methods.....		
4.3 Results and Discussion.....		
4.3.1 General Considerations, Including Nomenclature.....		
4.3.2 Overview of Products Formed by <i>fac</i> -[Re(CO) ₃ (H ₂ O) ₃] ⁺ and NTPs.....		
4.3.3 5'-UTP Reaction Products.....		
4.3.4 5'-GTP Reaction Products.....		
4.3.5 Effect of Re(I) Binding on P _γ pK _a of the <i>fac</i> -[Re(CO) ₃ ({N ₇ ,P _β ,P _γ }GTP)] ²⁻ and <i>fac</i> -[Re(CO) ₃ ({P _α ,P _β ,P _γ }UTP)] ²⁻ Adducts.....		
4.3.6 Nature of the GTP Products.....		
4.3.7 5'-ATP Reaction Products.....		
4.3.8 Considerations Regarding the Solution Structure of [Mg(ATP)].....		
4.4 Conclusions		
4.5 References		
CHAPTER 5. PROGRESS TOWARDS X-RAY CRYSTALLOGRAPHIC CHARACTERIZATION OF COMPLEXES CONTAINING 5-6 BICYCLIC BIOLIGANDS BOUND TO THE <i>fac</i> -[Re(CO) ₃] ⁺ CORE		
5.1 Introduction		
5.2 Experimental Section		
5.2.1 Starting Materials.....		
5.2.2 Synthetic Procedures.....		
5.2.3 NMR Spectroscopy.....		
5.2.4 X-Ray Crystallographic Data Collection and Structure Determination		
5.3 Results and Discussion.....		
5.3.1 X-ray Characterization.....		

5.3.1.1	Crystal Packing	106
5.3.1.2	Hydrogen Bonding.....	108
5.3.1.3	Base Orientation.....	109
5.3.1.4	Dihedral Angles	111
5.4	Conclusions	113
5.5	References	113
CHAPTER 6. PROGRESS TOWARDS SYNTHESIS, CHARACTERIZATION AND X-RAY CRYSTALLOGRAPHIC STUDIES OF <i>fac</i> -[Re(CO) ₃] ⁺ COMPLEXES CONTAINING N,N'-BIDENTATE AROMATIC N-DONOR LIGANDS		116
6.1	Introduction	116
6.2	Experimental Section	117
6.2.1	Starting Materials.....	117
6.2.2	Synthetic Procedures.....	118
6.2.3	NMR Spectroscopy.....	120
6.2.4	X-Ray Crystallographic Data Collection and Structure Determination	120
6.3	Results and Discussion.....	121
6.3.1	X-Ray Characterization	121
6.3.2	Distortion of Re(I) Complexes Containing Bipyridine Ligands.....	127
6.3.2.1	Out-of-Plane Distortions.....	130
6.3.2.2	In-plane Bending Distortions.....	132
6.4	Conclusions	133
6.5	References	133
CHAPTER 7. CONCLUSION.....		136
APPENDIX A SUPPORTING INFORMATION FOR CHAPTER 2		137
A.1	Sugar Pucker of Nucleotides Coordinated to <i>fac</i> -[Re(CO) ₃ (H ₂ O) ₃] ⁺	137
A.2	Exclusion of the Presence of 2:2 Cyclic Dimer	137
A.3	References.....	140
APPENDIX B SUPPORTING INFORMATION FOR CHAPTER 3		141
APPENDIX C SUPPORTING INFORMATION FOR CHAPTER 4		144
APPENDIX D REGARDING THE SYNTHESIS, PURIFICATION, AND CHARACTERIZATION OF THIAMINE TRIPHOSPHATE.....		146
D.1	Synthesis, Purification and Characterization of Thiamine Triphosphate	146
D.2	References.....	148
VITA.....		149

LIST OF TABLES

Table 1.1. Selected Nuclear Properties of some Tc and Re Radionuclides	3
Table 2.1. ^1H and ^{31}P NMR Shifts (ppm) and $^3J_{\text{H1}'\text{-H2}'}$ Coupling Constants (Hz, in parentheses) of Nucleotides and Complexes Formed with $\text{fac-}[\text{Re}(\text{CO})_3(\text{H}_2\text{O})_3]^+{}^a$	18
Table 2.2. Concentrations (mM) of 1:1, 1:2 and Dinuclear Adducts of 5'-GMP, 3'-GMP, 5'-IMP, and 3'-IMP at Different Nucleotide Concentrations and Times after Mixing with $\text{fac-}[\text{Re}(\text{CO})_3(\text{H}_2\text{O})_3]^+{}^a$	24
Table 2.3. Concentrations (mM) of 1:1, 1:2 and Mixed Bis Adducts of 5'- and 3'-GMP at Different Nucleotide Concentrations and Times after Mixing with $\text{fac-}[\text{Re}(\text{CO})_3(\text{H}_2\text{O})_3]^+{}^a$	28
Table 2.4. ^1H and ^{31}P NMR Shifts (ppm) and $^3J_{\text{H1}'\text{-H2}'}$ Coupling Constants (Hz, in parentheses) of 5'-GMP, 3'-GMP and 5'-dGMP and Complexes Formed with $\text{fac-}[\text{Re}(\text{CO})_3(\text{H}_2\text{O})_3]^+{}^a$ at Different Times after Mixing with $\text{fac-}[\text{Re}(\text{CO})_3(\text{H}_2\text{O})_3]^+{}^a$	31
Table 2.5. Concentrations (mM) of 1:1 and 1:2 Adducts of 5'-GMP and Methionine at Different Times after Mixing with $\text{fac-}[\text{Re}(\text{CO})_3(\text{H}_2\text{O})_3]^+{}^a$ in a Competition Reaction.....	32
Table 3.1. Possible Isomers Formed by the Reaction of $\text{fac-}[\text{Re}(\text{CO})_3(\text{H}_2\text{O})_3]^+{}^a$ with MDPs	43
Table 3.2. ^1H and ^{31}P NMR Chemical Shifts (ppm), Coupling Constants (Hz) of TDP, 5'-UDP, PP, and Complexes Formed with $\text{fac-}[\text{Re}(\text{CO})_3(\text{H}_2\text{O})_3]^+{}^a$	47
Table 3.3. ^1H and ^{31}P NMR Chemical Shifts (ppm), Coupling Constants (Hz) of 5'-GDP and Complexes Formed with $\text{fac-}[\text{Re}(\text{CO})_3(\text{H}_2\text{O})_3]^+{}^a$	54
Table 3.4. Ribose ^1H NMR Chemical Shifts (ppm) of 5'-GDP and Complexes Formed with $\text{fac-}[\text{Re}(\text{CO})_3(\text{H}_2\text{O})_3]^+{}^a$	57
Table 3.5. Characteristics of Selected Pt(II) and Re(I) Nucleotide Complexes.....	60
Table 3.6. Distances (Å) between H8 Proton and Phosphate Oxygens of $\text{fac-}[\text{Re}(\text{CO})_3(\text{H}_2\text{O})_3](\{\text{N7},\text{P}_\beta\}\text{GDP})^-$ Macrochelate Models.....	60
Table 3.7. Rate Constants of Interchange Obtained from ^1H - ^1H ROESY and ^{31}P - ^{31}P NOESY Experiments ^a	61
Table 4.1. Possible Isomers Formed by the Reaction of $\text{fac-}[\text{Re}(\text{CO})_3(\text{H}_2\text{O})_3]^+{}^a$ with NTPs	74
Table 4.2. ^1H and ^{31}P NMR Chemical Shifts (ppm), Coupling Constants (Hz) of $\text{H}_2\text{PPP}^{3-}$, 5'-UTP, and Complexes Formed with $\text{fac-}[\text{Re}(\text{CO})_3(\text{H}_2\text{O})_3]^+{}^a$	75
Table 4.3. ^{31}P NMR Chemical Shift Data (ppm) of Selected Reference Co(III) and Rh(III) Complexes Compared to Similar Re(I) Complexes.....	76
Table 4.4. ^1H and ^{31}P NMR Chemical Shifts (ppm), Coupling Constants (Hz) of 5'-GTP and Complexes Formed with $\text{fac-}[\text{Re}(\text{CO})_3(\text{H}_2\text{O})_3]^+{}^a$	85

Table 4.5. Characteristics of <i>fac</i> -[Re(CO) ₃ ({N ₇ ,P _β ,P _γ }GTP)] ²⁻ Model Complexes ^a	88
Table 4.6. ¹ H and ³¹ P NMR Chemical Shifts (ppm), Coupling Constants (Hz) of 5'-ATP and Complexes Formed with <i>fac</i> -[Re(CO) ₃ (H ₂ O) ₃] ⁺ ^a	90
Table 5.1. Crystal Data and Structure Refinement for [(Bzm) ₂ Re(CO) ₃ Br] (5.1), [(MeBzm) ₂ Re(CO) ₃ Br] (5.2), [(Me ₂ Bzm) ₂ Re(CO) ₃ Br] (5.3), [(MeBzm) ₂ Re(CO) ₃ (H ₂ O)]OTf (5.6), [(Me ₂ Bzm) ₂ Re(CO) ₃ (H ₂ O)]OTf (5.7), and [(Me ₂ Bzm) ₂ Re(CO) ₃ (OTf)] (5.7a).....	105
Table 5.2. Selected Bond Distances (Å) and Angles (°) for [(Bzm) ₂ Re(CO) ₃ Br] (5.1), [(MeBzm) ₂ Re(CO) ₃ Br] (5.2), [(Me ₂ Bzm) ₂ Re(CO) ₃ Br] (HH, 5.3a ; HT, 5.3b), [(MeBzm) ₂ Re(CO) ₃ (H ₂ O)]OTf (5.6), [(Me ₂ Bzm) ₂ Re(CO) ₃ (H ₂ O)]OTf (5.7) and [(Me ₂ Bzm) ₂ Re(CO) ₃ OTf] (5.7a)	107
Table 5.3. Hydrogen bond geometry.....	109
Table 5.4. Relevant Conformational Parameters for [(Bzm) ₂ Re(CO) ₃ Br] (5.1), [(MeBzm) ₂ Re(CO) ₃ Br] (5.2), [(Me ₂ Bzm) ₂ Re(CO) ₃ Br] (HH, 5.3a ; HT, 5.3b), [(MeBzm) ₂ Re(CO) ₃ (H ₂ O)]OTf (5.6), [(Me ₂ Bzm) ₂ Re(CO) ₃ (H ₂ O)]OTf (5.7) and [(Me ₂ Bzm) ₂ Re(CO) ₃ OTf] (5.7a)	112
Table 6.1. Crystal Data and Experimental Details for [(5,5'-Me ₂ bpy)Re(CO) ₃ Br] (6.1), [(6,6'-Me ₂ bpy)Re(CO) ₃ Br] (6.2), [(2,9-Me ₂ phen)Re(CO) ₃ Br] (6.5), [(4,4'-Me ₂ bpy)Re(CO) ₃ (H ₂ O)]OTf (6.6), [(5,5'-Me ₂ bpy)Re(CO) ₃ (H ₂ O)]OTf (6.7), and [(6,6'-Me ₂ bpy)Re(CO) ₃ (H ₂ O)]OTf (6.8) .	123
Table 6.2. Selected Bond Distances (Å) and Angles (°) for [(5,5'-Me ₂ bpy)Re(CO) ₃ Br] (6.1), [(6,6'-Me ₂ bpy)Re(CO) ₃ Br] (6.2), [(2,9-Me ₂ phen)Re(CO) ₃ Br] (6.5), [(4,4'-Me ₂ bpy)Re(CO) ₃ (H ₂ O)]OTf (6.6), [(5,5'-Me ₂ bpy)Re(CO) ₃ (H ₂ O)]OTf (6.7), and [(6,6'-Me ₂ bpy)Re(CO) ₃ (H ₂ O)]OTf (6.8)	125
Table 6.3. Crystal Data and Experimental Details for [(6,6'-Me ₂ bpy)Re(CO) ₃ (OTf)] (6.9a and 6.9b)	126
Table 6.4. Selected Bond Distances (Å) and Angles (°) for [(6,6'-Me ₂ bpy)Re(CO) ₃ (OTf)] (6.9a and 6.9b)	128
Table 6.5. Ligand Deformation in Octahedral Re(I) and Square-Planar Pt(II)/Pd(II) Complexes.....	129

LIST OF FIGURES

Figure 1.1. Molecular structures of (A) cisplatin, (B) auranofin, (C) Gd-DOTA, and (D) ^{99m}Tc -sestamibi (Cardiolite).....	1
Figure 1.2. Models of (left) a 9-mer with native B-DNA structure and (right) a 9-mer containing a 1,2-intrastrand cross-link effected by cisplatin. Model structures were determined using distances obtained by NMR methods. ²	2
Figure 1.3. Protolytic behavior of $[\text{Re}_2(\text{CO})_6(\mu\text{-OH})_3]^-$	4
Figure 1.4. <i>fac</i> - $[\text{Re}(\text{CO})_3(\text{H}_2\text{O})_3]^+$ binds two guanosine (R = ribosyl) or 9-methylguanine (R = methyl) ligands in a stepwise fashion.	5
Figure 2.1. Guanine (left) and hypoxanthine (right) derivatives. The arrow and its head represent the base and the H8 atom respectively.....	10
Figure 2.2. (top) Diagram showing coordination positions relative to each other; (bottom) HHa, ΔHT , HHb and ΔHT orientations for an octahedral metal center. NMPs in coordination positions 1 and 2 are distinct and all four conformers can interchange only if the type of NMP is identical in both coordination positions.....	14
Figure 2.3. H8 (left), H1' (center) and P_α (right) NMR signals of equilibrated mixtures of <i>fac</i> - $[\text{Re}(\text{CO})_3(\text{H}_2\text{O})_3]^+$ (25 mM) and 5'-GMP at pH 3.6. (A) Re/GMP $r = 4:1$, (B) $r = 1:1$, (C) $r = 1:2$. The red arrow points to the small amount of 2:1 adduct in spectrum (B). See text for conditions and spectral assignments for signals not identified in Figure.	17
Figure 2.4. Possible Re/GMP adducts.	19
Figure 2.5. H8 (left), H1' (center) and P_α (right) NMR signals of equilibrated mixtures of <i>fac</i> - $[\text{Re}(\text{CO})_3(\text{H}_2\text{O})_3]^+$ (25 mM) and 3'-GMP at pH 3.6. (A) Re/GMP $r = 4:1$, (B) $r = 1:1$, (C) $r = 1:2$. See text for conditions and spectral assignments for signals not identified in Figure.....	22
Figure 2.6. CD spectra recorded soon after dilution of equilibrated NMR solutions ($[\text{Re}] = 25$ mM, pH 3.6) of 5'-GMP ($r = 1:2$, red line), 3'-GMP ($r = 1:2$, blue line) and mixed 5'-GMP/3'-GMP ($r = 1:1:1$, black line).	26
Figure 2.7. H8 NMR signals of equilibrated mixtures ($r = 1:1:1$, pH 3.6) of <i>fac</i> - $[\text{Re}(\text{CO})_3(\text{H}_2\text{O})_3]^+$ with the NMPs indicated. See text for signal assignments.....	27
Figure 2.8. (top) Diagram showing coordination position numbering; (bottom) The pairs of HT conformers of each of the two possible <i>fac</i> - $[\text{Re}(\text{CO})_3(\text{H}_2\text{O})(5'\text{-GMP})(3'\text{-GMP})]^-$ adducts. In the pair on the left, the ΔHT conformer can form a favorable phosphate-to-coordinated water H-bond.....	27
Figure 2.9. H8 and H1' NMR signals of a mixture containing <i>fac</i> - $[\text{Re}(\text{CO})_3(\text{H}_2\text{O})_3]^+$ (5 mM), 5'-GMP (5 mM), and 5'-dGMP (5 mM) at pH 3.6 and 1 h after mixing. Symbol alone denotes	

signals due to free nucleotide. In this $r = 1:1:1$ experiment, only trace amounts of 1:2 adducts are formed at 1 h; these adducts account for the weak signals observed just above the baseline. 30

Figure 3.1. TDP (top). Base portion of 5'-UDP (middle left) and 5'-GDP (middle right) and the R group bearing the diphosphate moiety (bottom). 40

Figure 3.2. Four possible isomers of $fac-[Re(CO)_3(\{P_\alpha, P_\beta\}MDP)]^-$; $R_{Re}\Delta/S_{Re}\Lambda$ and $R_{Re}\Lambda/S_{Re}\Delta$ are mirror image pairs if the attached ester moiety has no chiral groups. Arrows indicate sense of rotation defining chirality at Re(I). The blue O and the red O are the pro- Δ and pro- Λ oxygens in the free nucleotide, respectively. 41

Figure 3.3. R_{Re} and S_{Re} isomers of $fac-[Re(CO)_3(H_2O)(\{N7, P_\beta\}GDP)]^-$. Only these two isomers are possible when P_α is not bound to Re(I). The R_{Re} and S_{Re} isomers are tentatively assigned as M and m , respectively. 42

Figure 3.4. ^{31}P NMR (A), ^{31}P - ^{31}P COSY (B), and ^{31}P - ^{31}P NOESY (C) spectra of an equilibrium mixture of $fac-[Re(CO)_3(H_2O)_3]^+$ (25 mM, $r = 1:1$) and TDP at pH 3.6. Asterisk labels indicate peaks arising from free TDP. 49

Figure 3.5. 1H NMR (A), ^{31}P NMR (B), ^{31}P - ^{31}P COSY (C), and ^{31}P - ^{31}P NOESY (D) spectra of an equilibrium mixture of $fac-[Re(CO)_3(H_2O)_3]^+$ (25 mM, $r = 1:1$) and 5'-UDP at pH 3.6. Asterisk labels indicate peaks arising from free 5'-UDP. 51

Figure 3.6. 1H NMR (A), ^{31}P NMR (B) and ^{31}P - ^{31}P COSY (C) spectra of an equilibrium mixture of $fac-[Re(CO)_3(H_2O)_3]^+$ (25 mM, $r = 1:1$) and 5'-GDP at pH 3.6. Asterisk labels indicate peaks arising from free 5'-GDP. 53

Figure 3.7. 1H - 1H ROESY (A) and ^{31}P - ^{31}P NOESY (B) spectra of an equilibrium mixture of $fac-[Re(CO)_3(H_2O)_3]^+$ (25 mM, $r = 1:1$) and 5'-GDP at pH 3.6. 55

Figure 3.8. Possible mode of conversion between the R_{Re} and S_{Re} isomers of $fac-[Re(CO)_3(H_2O)(\{N7, P_\beta\}GDP)]^-$ 62

Figure 4.1. 5'-UTP (top), 5'-GTP (middle), and 5'-ATP (bottom). At pH ~ 3.6 , the P_γ group of the free NTP is protonated and the phosphate chain carries three negative charges. See text for protocol used to designate phosphate oxygen atoms. 71

Figure 4.2. The four possible isomers of $fac-[Re(CO)_3(\{P_\alpha, P_\beta, P_\gamma\}NTP)]^{2-}$. The asymmetry of the Re(I) center (R_{Re} or S_{Re}) is based on the direction of rotation of the NTP around a reference axis defined by a line passing through the Re(I) atom perpendicular to the P_α -Re(I)- P_γ chelate ring (assumed to be planar as shown above) and passing through the CO (away from the viewer). *Endo* and *exo* isomers result from $P_\alpha O''$ and $P_\alpha O'$ coordination to Re(I), respectively. 72

Figure 4.3. The four possible isomers of $fac-[Re(CO)_3(\{N7, P_\beta, P_\gamma\}NTP)]^{2-}$. The asymmetry of the Re(I) center (R_{Re} or S_{Re}) is based on the direction of rotation of the NTP around a reference axis defined by a line passing through the Re(I) atom perpendicular to the P_β -Re(I)- P_γ chelate ring (assumed to be planar as shown above) and passing through the CO (away from the viewer). *Endo* and *exo* isomers result from $P_\beta O''$ and $P_\beta O'$ coordination to Re(I), respectively. 73

- Figure 4.4.** ^1H NMR (A), ^{31}P NMR (B) and expanded region of ^{31}P NMR (C) spectra of an equilibrium mixture of *fac*- $[\text{Re}(\text{CO})_3(\text{H}_2\text{O})_3]^+$ (25 mM, $r = 1:1$) and 5'-UTP at pH 3.6. Asterisk labels indicate peaks arising from free 5'-UTP..... 79
- Figure 4.5.** ^{31}P - ^{31}P COSY spectrum of an equilibrium mixture of *fac*- $[\text{Re}(\text{CO})_3(\text{H}_2\text{O})_3]^+$ (25 mM, $r = 1:1$) and 5'-UTP at pH 3.6. Expansion of cross-peaks encircled by dotted line appears in Appendix C..... 80
- Figure 4.6.** Comparison of P_α and P_γ NMR signals of (A) $[\text{Rh}(\text{H}_2\text{O})_3(\{\text{P}_\alpha, \text{P}_\beta, \text{P}_\gamma\}\text{ATP})]$, (B) *fac*- $[\text{Re}(\text{CO})_3(\{\text{P}_\alpha, \text{P}_\beta, \text{P}_\gamma\}\text{UTP})]^{2-}$, and (C) $[\text{Co}(\text{NH}_3)_3(\{\text{P}_\alpha, \text{P}_\beta, \text{P}_\gamma\}\text{ATP})]$. Plots (A) and (C) are derived from refs 10 and 15, respectively..... 82
- Figure 4.7.** ^1H NMR (A), ^{31}P NMR (B) and ^{31}P - ^{31}P COSY (C) spectra of an equilibrium mixture of *fac*- $[\text{Re}(\text{CO})_3(\text{H}_2\text{O})_3]^+$ (25 mM, $r = 1:1$) and 5'-GTP at pH 3.6. Asterisk labels indicate peaks arising from free 5'-GTP..... 84
- Figure 4.8.** Models of four possible diastereomers of *fac*- $[\text{Re}(\text{CO})_3(\{\text{N}7, \text{P}_\beta, \text{P}_\gamma\}\text{GTP})]^{2-}$ 89
- Figure 5.1.** Perspective drawings of $[(\text{Bzm})_2\text{Re}(\text{CO})_3\text{Br}]$ (5.1), $[(\text{MeBzm})_2\text{Re}(\text{CO})_3\text{Br}]$ (5.2), $[(\text{Me}_2\text{Bzm})_2\text{Re}(\text{CO})_3\text{Br}]$ (HH, 5.3a), $[(\text{MeBzm})_2\text{Re}(\text{CO})_3(\text{H}_2\text{O})]\text{OTf}$ (5.6), $[(\text{Me}_2\text{Bzm})_2\text{Re}(\text{CO})_3(\text{H}_2\text{O})]\text{OTf}$ (5.7) and $[(\text{Me}_2\text{Bzm})_2\text{Re}(\text{CO})_3\text{OTf}]$ (5.7a). Counter ions have been omitted for clarity. Thermal ellipsoids are drawn with 50% probability..... 104
- Figure 5.2.** Perspective drawing of $[(\text{Me}_2\text{Bzm})_2\text{Re}(\text{CO})_3\text{Br}]$ (HT, 5.3b). Thermal ellipsoids are drawn with 50% probability..... 104
- Figure 5.3.** The arrow and its head represent the 6-membered ring and B2H, respectively. The red and blue arrows represent ligands B and B'; these designations are used in the text to refer to coordination positions occupied by benzimidazole ligands..... 110
- Figure 6.1.** Graphical representation and atom numbering schemes for coordinated (A) dimethyl-2,2'-bipyridine derivatives, and (B) 2,9-dimethyl-1,10-phenanthroline (2,9-Me₂phen)..... 117
- Figure 6.2.** Perspective drawings of $[(5,5'\text{-Me}_2\text{bpy})\text{Re}(\text{CO})_3\text{Br}]$ (6.1), $[(6,6'\text{-Me}_2\text{bpy})\text{Re}(\text{CO})_3\text{Br}]$ (6.2), $[(2,9\text{-Me}_2\text{phen})\text{Re}(\text{CO})_3\text{Br}]$ (6.5), $[(4,4'\text{-Me}_2\text{bpy})\text{Re}(\text{CO})_3(\text{H}_2\text{O})]\text{OTf}$ (6.6), $[(5,5'\text{-Me}_2\text{bpy})\text{Re}(\text{CO})_3(\text{H}_2\text{O})]\text{OTf}$ (6.7), and $[(6,6'\text{-Me}_2\text{bpy})\text{Re}(\text{CO})_3(\text{H}_2\text{O})]\text{OTf}$ (6.8). Counter ions have been omitted for clarity. Thermal ellipsoids are drawn with 50% probability..... 122
- Figure 6.3.** Perspective drawings of $[(6,6'\text{-Me}_2\text{bpy})\text{Re}(\text{CO})_3(\text{OTf})]$ (6.9a and 6.9b). Thermal ellipsoids are drawn with 50% probability..... 125
- Figure 6.4.** Distortions in N-N ligands as defined by Hazell: (A) in-plane bending (θ_p , in deg); (B) twisting (θ_T , in deg); (C) bowing (θ_B , in deg); (D) S-shaped distortion (d_S , in Å). θ_T , θ_B and θ_p are the angles between the best straight lines ($ax + c = z$) through each pyridyl ring of the bipyridine ligand in the XY, YZ, and XZ projections, respectively..... 128

LIST OF ABBREVIATIONS

<u>Abbreviation</u>	<u>Definition</u>
MRI	magnetic resonance imaging
DOTA	1,4,7,10-tetraazacyclododecane-1,4,7,10-tetraacetic acid
FDA	Food and Drug Administration
DNA	deoxyribonucleic acid
HMG	high-mobility group
NMR	nuclear magnetic resonance
1D	one-dimensional
2D	two-dimensional
RNA	ribonucleic acid
A ₂	two amines or a diamine carrier ligand
X	anionic leaving group
M or M	metal
G	guanine base derivative
9-MeG	9-methylguanine
Guo	guanosine
dGuo	2-deoxyguanosine
HH	head-to-head
HT	head-to-tail
5'-GMP	guanosine 5'-monophosphate
5'-GDP	guanosine 5'-diphosphate
5'-GTP	guanosine 5'-triphosphate

5'-dGMP	2'-deoxyguanosine-5'-monophosphate
3'-GMP	guanosine 3'-monophosphate
5'-IMP	inosine 5'-monophosphate
3'-IMP	inosine 3'-monophosphate
NMP	6-oxopurine nucleotide monophosphate
OTf	trifluoromethanesulfonate
h	hour
FID	free induction decay
TMP	trimethyl phosphate
Hz	hertz
MHz	megahertz
ROESY	Rotating frame nuclear Overhauser Effect Spectroscopy
ms	millisecond
CD	circular dichroism spectroscopy
mM	millimolar
nm	nanometer
min	minute
μL	microliter
<i>r</i>	ratio of <i>fac</i> -[Re(CO) ₃ (H ₂ O) ₃] ⁺ to nucleotide in a given sample
mL	milliliter
P _α	α-phosphate group
P _β	β-phosphate group
P _γ	γ-phosphate group

d(GpG)	2'-deoxyguanylyl(3'→5')-2'-deoxyguanosine
NOE	Nuclear Overhauser Effect
SSC	“second-sphere” interactions
ppm	parts per million
p <i>K</i> _a	negative logarithm of the ionization constant <i>K</i> _a
NOESY	Nuclear Overhauser Effect Spectroscopy
Δε	molar circular dichroism (M ⁻¹ cm ⁻¹)
conc	concentration
equiv	equivalent
μM	micromolar
MDP	monoester diphosphate
TDP	thiamine diphosphate
5'-UDP	uridine 5'-diphosphate
H ₂ PP ²⁻	diprotonated pyrophosphate
COSY	COrelated Spectroscopy
rms	root-mean-square
<i>t</i> _{1/2}	half-life
HMQC	Heteronuclear Multiple Quantum Coherence
EXSY	EXchange Spectroscopy
P	pseudorotation phase angle
χ	N-glycosidic bond torsion angle, defined by O4'–C1'–N9–C4
<i>t</i> _{<i>m</i>}	mixing time
<i>k</i>	rate constant of interchange

fwhh	full width at half height
NTP	nucleoside triphosphate
5'-ATP	adenosine 5'-triphosphate
5'-UTP	uridine 5'-triphosphate
H ₂ PPP ³⁻	diprotonated tripolyphosphate, H ₂ P ₃ O ₁₀ ³⁻
ccs	coordination chemical shift
T ₁	spin-lattice relaxation time
γ	torsion angle describing orientation of the sugar-phosphate linkage, given by O5'–C5'–C4'–C3'
gg	<i>gauche, gauche</i>
HSAB	hard and soft acids and bases
MeG	9-methylguanine, 7-methylguanine
Bzm	benzimidazole
MeBzm	1-methylbenzimidazole
Me ₂ Bzm	5,6-dimethylbenzimidazole
Me ₃ Bzm	1,5,6-trimethylbenzimidazole
L	planar aromatic N-donor ligand
O-donor	oxygen donor ligand, such as H ₂ O or OTf
HH _u	head-to-head “up”, refers to H2 atom pointing towards axial CO
HH _d	head-to-head “down”, refers to H2 atom pointing towards axial X
CP	coordination plane
1,3,9-TMX	1,3,9-trimethylhypoxanthine
N–N	<i>N,N'</i> -bidentate aromatic N-donor ligand

4,4'-Me ₂ bpy	4,4'-dimethyl-2,2'-bipyridine
5,5'-Me ₂ bpy	5,5'-dimethyl-2,2'-bipyridine
6,6'-Me ₂ bpy	6,6'-dimethyl-2,2'-bipyridine
bpy	2,2'-bipyridine
2,9-Me ₂ phen	2,9-dimethyl-1,10-phenanthroline; neocuproine
TMS	tetramethylsilane
θ_P	in-plane bending
θ_B	out-of-plane bending deformation
θ_T	out-of-plane twisting deformation
d_S	S-shaped deformation
θ_{di}	dihedral angle between the best planes through bipyridine rings
TDP	thiamine diphosphate
TTP	thiamine triphosphate
DMSO	dimethyl sulfoxide
DCC	1,3-dicyclohexylcarbodiimide
HPLC	high performance liquid chromatography

ABSTRACT

Transition metal centers possessing an octahedral geometry are useful for understanding the natural role of metal ions in biology. Complexes based on such metals might improve upon the widely used square planar Pt(II) anticancer drug cisplatin, *cis*-[Pt(NH₃)₂Cl₂]. The octahedral triaquatricarbonylrhenium(I) cation, *fac*-[Re(CO)₃(H₂O)₃]⁺, has been shown to possess anticancer activity. Furthermore, Re(I) complexes containing unstable rhenium isotopes have found utility as radiodiagnostic and radiotherapeutic agents. Thus, this work focuses on elucidating the fundamental coordination chemistry of *fac*-[Re(CO)₃(H₂O)₃]⁺.

Adducts formed in reactions of nucleoside mono-, di-, and triphosphates with *fac*-[Re(CO)₃(H₂O)₃]OTf are examined by using a combination of 1D and 2D multinuclear nuclear magnetic resonance (NMR) spectroscopy, circular dichroism (CD) spectroscopy, and molecular modeling techniques. Mixtures containing *fac*-[Re(CO)₃(H₂O)₃]⁺ and nucleotides attain equilibrium, in contrast to cisplatin, and the nature of the adduct formed depends on the number of phosphate groups and the base present.

Nucleoside di- and triphosphate adducts consist of diastereomers having distinct, sharp NMR signals, thus allowing accurate measurement of ¹H and ³¹P NMR chemical shifts and coupling constants. Re(I) coordination at N7 is observed for all adducts with guanine bases, and the reactions proceed to near completion. {N7,P_β} and {N7,P_β,P_γ} macrochelates are formed for 5'-GDP and 5'-GTP, respectively, but only N7 binding is observed for 5'-GMP. The lack of P_α binding for 5'-GTP indicates that formation of an N7–Re–P_α chelate ring is sterically unfavorable. When methionine and 5'-GMP are allowed to compete for *fac*-[Re(CO)₃(H₂O)₃]⁺, the N7-bound Re/5'-GMP 1:1 adduct is the kinetic product, while the S-bound Re/methionine adduct is thermodynamically favored, a result opposite to that typically found for cisplatin.

No base interaction was noted for adducts with uridine bases, and these reactions were incomplete at equilibrium. *fac*-[Re(CO)₃(H₂O)₃]⁺ forms {P_α,P_β} and {P_α,P_β,P_γ} phosphato chelates with 5'-UDP and 5'-UTP, respectively, but no significant reaction occurred with 5'-UMP. Notably, *fac*-[Re(CO)₃(H₂O)₃]⁺ forms both an {N7,P_β,P_γ} macrochelate and a {P_α,P_β,P_γ} phosphato chelate with 5'-ATP, suggesting that the *fac*-[Re(CO)₃]⁺ core could provide a model for the kinetically labile biorelevant [Mg(ATP)] complex. These results offer hope that (radio)pharmaceuticals based on Re(I) could be developed with lower toxicity than drugs based on Pt(II).

CHAPTER 1.

INTRODUCTION

1.1 Metals in Medicine

Inorganic compounds have found use in a variety of medicinal applications.¹ Examples include the anticancer agent cisplatin (cis -[Pt(NH₃)₂Cl₂])², the antirheumatic agent auranofin (an organogold compound), magnetic resonance imaging (MRI) contrast agents (usually based on Gd(III)), and radiotherapeutic and radiodiagnostic agents containing radionuclides such as ^{99m}Tc and ^{186/188}Re (Figure 1.1).³

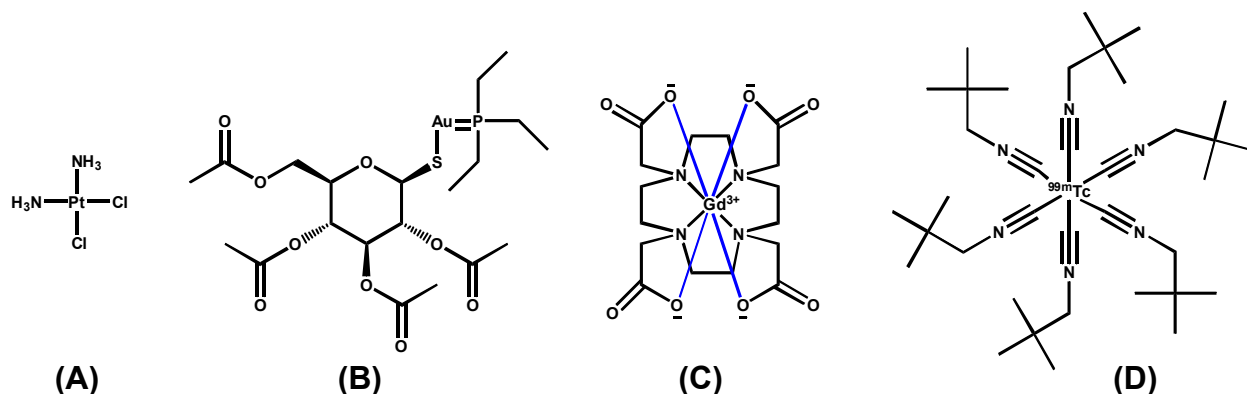


Figure 1.1. Molecular structures of (A) cisplatin, (B) auranofin, (C) Gd-DOTA, and (D) ^{99m}Tc-sestamibi (Cardiolite)

1.2 Cisplatin, cis -[Pt(NH₃)₂Cl₂]

First approved by the FDA for use in humans in 1978, cisplatin has been the mainstay for chemotherapeutic treatment of ovarian, testicular, and head and neck tumors for nearly thirty years.⁴ Upon cellular uptake, the two chloro ligands of cisplatin are displaced by water ligands, as the intracellular chloride concentration is much lower than the extracellular chloride

concentration. For this reason, the cytotoxic species *in vivo* is believed to be the diaqua cation $cis-[Pt(NH_3)_2(H_2O)_2]^{2+}$. Within the cell, $cis-[Pt(NH_3)_2(H_2O)_2]^{2+}$ reacts with a variety of biomolecules, such as proteins, nucleic acids, and peptides. However, DNA is now generally accepted to be the ultimate target of $cis-[Pt(NH_3)_2(H_2O)_2]^{2+}$; $cis-[Pt(NH_3)_2(H_2O)_2]^{2+}$ binds to the N7 atoms of two adjacent purine residues, forming a 1,2-intrastrand crosslink.⁵ The 1,2-intrastrand crosslink causes local unwinding and destacking of DNA base pairs, thus causing the DNA strand to bend at an angle between 30° and 60° (Figure 1.2). The platinated DNA lesion is then recognized by HMG-domain proteins, which then bind to the lesion and effectively shield the lesion from DNA repair mechanisms.⁶ However, upon attempting to replicate the DNA in preparation for cellular division, the DNA replication machinery simply stops upon encountering the lesion, and the lack of replicated genetic material eventually leads to cell death.

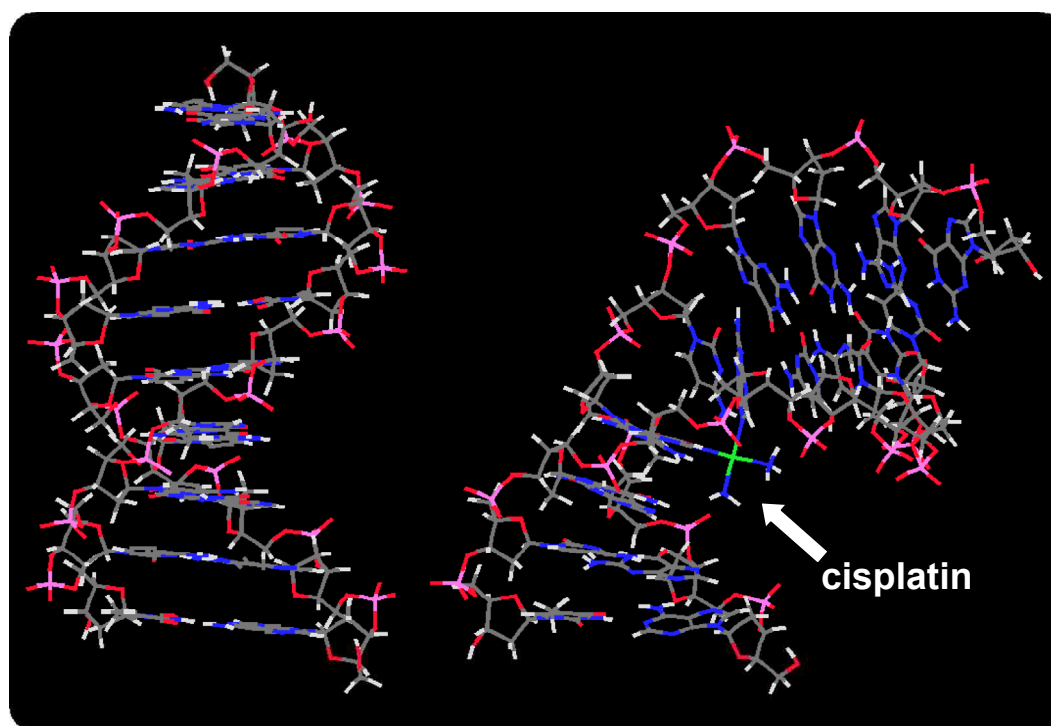


Figure 1.2. Models of (left) a 9-mer with native B-DNA structure and (right) a 9-mer containing a 1,2-intrastrand cross-link effected by cisplatin. Model structures were determined using distances obtained by NMR methods.²

The incredible success of cisplatin in cancer therapy has led to the development of similar chemotherapeutic agents based on Pt(II). However, the overall success of agents based on Pt(II) is limited by toxic side effects, believed to be the result of reaction of Pt(II) with the soft sulfur atoms in cysteine, methionine, and other intracellular thiols and thioethers.⁷ Thus, the search for other potential chemotherapeutic agents has expanded to include inert, redox-stable metal centers with octahedral geometry, such as Ru(III) and Rh(II), and most recently, Re(I).⁸⁻²⁰

1.3 Triaquatricarbonylrhenium(I), *fac*-[Re(CO)₃(H₂O)₃]⁺

Another application of metals in medicine involves the use of radioactive metal complexes for molecular and functional imaging, diagnosis, and radiotherapy. The nuclear properties of ^{99m}Tc and ^{186/188}Re are amenable for use as radiodiagnostic and radiotherapeutic agents, respectively (Table 1.1).²¹ In addition, ^{99m}Tc and ¹⁸⁸Re are readily available from generator systems that can be kept and maintained at medical facilities.

Table 1.1. Selected Nuclear Properties of some Tc and Re Radionuclides

Isotope	Half-life	Emissions	Comments
^{99m} Tc	6.0 h	γ, 143 KeV no β-	Generator produced, “no carrier added”
⁹⁹ Tc	2.1 x 10 ⁵ y	no γ β-, 0.292 MeV	Available in gram quantities
¹⁸⁶ Re	90 h	γ, 137 MeV β-, 1.07, 0.93 MeV	Reactor produced; contains carrier ¹⁸⁵ Re and ¹⁸⁷ Re; contaminated with ¹⁸⁸ Re
¹⁸⁸ Re	17 h	γ, 155 KeV β-, 2.12 MeV	Generator produced, “no carrier added”

Routine investigations into the coordination chemistry of unstable Re and Tc isotopes (“hot” radionuclides) often first take place with model complexes containing stable, “cold” metal centers. $^{185/187}\text{Re}$, the stable isotopes of rhenium, are used as a model for “hot” $^{186/188}\text{Re}$ and the (man-made) second-row congeners, ^{99}Tc and $^{99\text{m}}\text{Tc}$. One such model complex, *fac*- $[\text{Re}(\text{CO})_3(\text{H}_2\text{O})_3]^+$, possesses particularly attractive properties, as the metal center is in the low +1 oxidation state, resulting in a kinetically inert d^6 electronic configuration.²² Re (and Tc) are not often found in the +1 oxidation state; however, the low oxidation state is stabilized by the presence of three π -backbonding CO ligands. The CO ligands withdraw electron density from the metal center, effectively creating an electronic environment emulating that of a higher oxidation state. The *fac*- $[\text{Re}(\text{CO})_3]^+$ core is small in size, compact and nearly spherical; these characteristics lessen the steric impact of the metal center.²² In addition, the three facial water ligands are readily substituted by a variety of donor atoms, thus providing available sites for cross-linking interactions with DNA bases.^{23,24}

Interest in the coordination chemistry of *fac*- $[\text{Re}(\text{CO})_3(\text{H}_2\text{O})_3]^+$ has increased significantly since 2000, when Hall et al. demonstrated that the hydroxo-bridged dirhenium complex $[\text{Re}_2(\text{CO})_6(\mu\text{-OH})_3]^-$ was effective at suppressing the growth of murine and human leukemias and lymphomas in vitro.¹⁷ It was then discovered that $[\text{Re}_2(\text{CO})_6(\mu\text{-OH})_3]^-$ is readily cleaved under protic conditions to yield the mononuclear *fac*- $[\text{Re}(\text{CO})_3(\text{H}_2\text{O})_3]^+$, thus leading to the suggestion that the cation may be the active species in vitro (Figure 1.3).²⁵

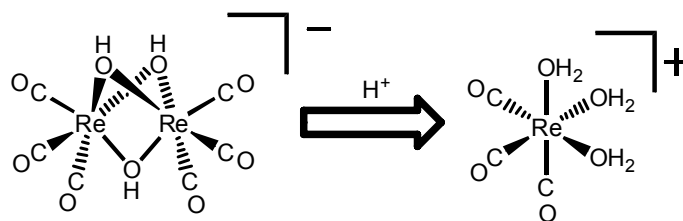


Figure 1.3. Protolytic behavior of $[\text{Re}_2(\text{CO})_6(\mu\text{-OH})_3]^-$

Zobi et al. found that the fac -[Re(CO)₃]⁺ core preferred to bind to the N7 atoms of two guanine base derivatives, such as guanosine, 2-deoxyguanosine, and 9-methylguanine, in a stepwise fashion.^{18,19} This finding led these researchers to propose that a cisplatin-like binding mechanism (Figure 1.4) could be responsible for the cytotoxic activity displayed by compounds containing the fac -[Re(CO)₃]⁺ core^{18,19}

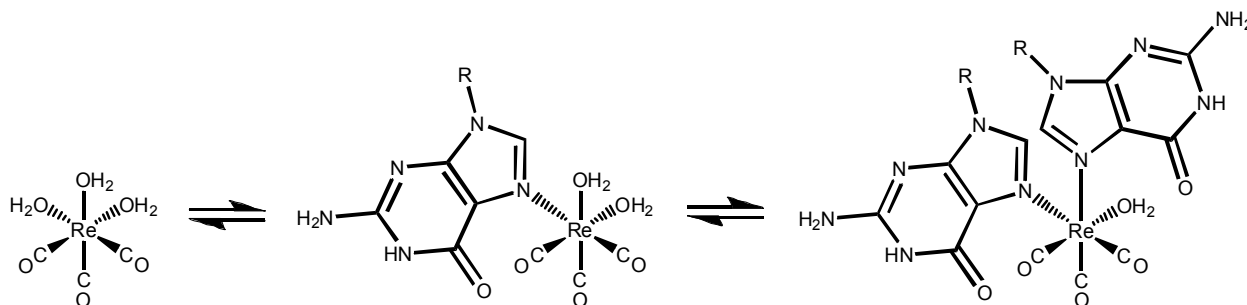


Figure 1.4. fac -[Re(CO)₃(H₂O)₃]⁺ binds two guanosine (R = ribosyl) or 9-methylguanine (R = methyl) ligands in a stepwise fashion.

However, compared to Pt(II) compounds, the fac -[Re(CO)₃]⁺ core may have a higher affinity for oxygen donors²³ and its binding equilibria are likely to be more dynamic and less complete. Thus, interactions between the fac -[Re(CO)₃]⁺ core and the phosphate groups in the sugar-phosphate backbone of DNA, and the phosphate groups in nucleoside mono-, di- and triphosphates, are likely to be important factors in the coordination behavior of the fac -[Re(CO)₃]⁺ core.

To our knowledge, interactions between the fac -[Re(CO)₃]⁺ core and nucleotides have not been investigated. Thus, the current study features fundamental investigations into the coordination chemistry of fac -[Re(CO)₃(H₂O)₃]⁺ with purine and pyrimidine nucleotides in aqueous solution using multinuclear NMR spectroscopic methods. In addition, the synthesis and characterization of complexes containing the fac -[Re(CO)₃]⁺ core and various biologically

relevant N-donor ligands (such as benzimidazole and bipyridine) are reported, with the intention of increasing insight into the coordination chemistry of the *fac*-[Re(CO)₃]⁺ core.

1.4 References

1. Orvig, C.; Abrams, M. J. *Chem. Rev.* **1999**, *99*, 2201-2203.
2. Marzilli, L. G.; Saad, J. S.; Kuklenyik, Z.; Keating, K. A.; Xu, Y. *J. Am. Chem. Soc.* **2001**, *123*, 2764-2770.
3. Lippard, S. J.; Berg, J. M. *Principles of Bioinorganic Chemistry*; University Science Books: Mill Valley, CA, 1994.
4. Jamieson, E. R.; Lippard, S. J. *Chem. Rev.* **1999**, *99*, 2467-2498.
5. *Cisplatin: Chemistry and Biochemistry of a Leading Anticancer Drug*; Wiley-VCH: Weinheim, Germany, 1999.
6. Ohndorf, U.-M.; Rould, M. A.; He, Q.; Pabo, C. O.; Lippard, S. J. *Nature* **1999**, 708-712.
7. Djuran, M. I.; Lempers, E. L. M.; Reedijk, J. *Inorg. Chem.* **1991**, *30*, 2648-2652.
8. Alessio, E.; Mestroni, G.; Bergamo, A.; Sava, G. *Curr. Top. Med. Chem.* **2004**, *4*, 1525-1535.
9. Chifotides, H. T.; Dunbar, K. R. *Acc. Chem. Res.* **2005**, *38*, 146-156.
10. Chifotides, H. T.; Koshlap, K. M.; Pérez, L. M.; Dunbar, K. R. *J. Am. Chem. Soc.* **2003**, *125*, 10714-10724.
11. Frausin, F.; Scarcia, V.; Cocchietto, M.; Furlani, A.; Serli, B.; Alessio, E.; Sava, G. *J. Pharmacol. Exp. Ther.* **2005**, *313*, 227-233.
12. Galanski, M.; Arion, V. B.; Jakupec, M. A.; Keppler, B. *Curr. Pharm. Des.* **2003**, *9*, 2078-2089.
13. Guichard, S. M.; Else, R.; Reid, E.; Zeitlin, B.; Aird, R.; Muir, M.; Dodds, M.; Fiebig, H.; Sadler, P. J.; Jodrell, D. I. *Biochem. Pharmacol.* **2006**, *71*, 408-415.
14. Hayward, R. L.; Schornagel, Q. C.; Tente, R.; Macpherson, J. S.; Aird, R. E.; Guichard, S.; Habtemariam, A.; Sadler, P.; Jodrell, D. I. *Cancer Chemother. Pharmacol.* **2005**, *55*, 577-583.
15. Velders, A. H.; Bergamo, A.; Alessio, E.; Zangrando, E.; Haasnoot, J. G.; Casarsa, C.; Cocchietto, M.; Zorzet, S.; Sava, G. *J. Med. Chem.* **2004**, *47*, 1110-1121.
16. Yan, Y. K.; Melchart, M.; Habtemariam, A.; Sadler, P. J. *Chem. Commun.* **2005**, 4764-4776.
17. Yan, Y.-K.; Cho, S. E.; Shaffer, K. A.; Rowell, J. E.; Barnes, B. J.; Hall, I. H. *Pharmazie* **2000**, *55*, 307-313.

18. Zobi, F.; Alberto, R.; Spingler, B.; Fox, T. In *Technetium, Rhenium and Other Metals in Chemistry and Nuclear Medicine*; Nicolini, M., Mazzi, U., Eds.; SGEEditoriali: Padova, Italy, 2002; Vol. 6, pp 97-105.
19. Zobi, F.; Blacque, O.; Schmalte, H. W.; Spingler, B.; Alberto, R. *Inorg. Chem.* **2004**, *43*, 2087-2096.
20. Zobi, F.; Spingler, B.; Fox, T.; Alberto, R. *Inorg. Chem.* **2003**, *42*, 2818-2820.
21. Deutsch, E.; Libson, K.; Vanderhayden, J.-L.; Ketring, A. R.; Maxon, H. R. *Int. J. Radiat. Appl. Instrum. Part B* **1986**, *13*, 465-477.
22. Schibli, R.; Schubiger, P. A. *Eur. J. Nucl. Med.* **2002**, *29*, 1529-1542.
23. Egli, A.; Hegetschweiler, K.; Alberto, R.; Abram, U.; Schibli, R.; Hedinger, R.; Gramlich, V.; Kissner, R.; Schubiger, P. A. *Organometallics* **1997**, *16*, 1833-1840.
24. Salignac, B.; Grundler, P. V.; Cayemittes, S.; Frey, U.; Scopelliti, R.; Merbach, A. E.; Hedinger, R.; Hegetschweiler, K.; Alberto, R.; Prinz, U.; Raabe, G.; Kölle, U.; Hall, S. *Inorg. Chem.* **2003**, *42*, 3516-3526.
25. Jiang, C.; Hor, T. S. A.; Yan, Y.-K.; Henderson, W.; McCaffrey, L. J. *J. Chem. Soc., Dalton Trans.* **2000**, *18*, 3197-3203.

CHAPTER 2.

fac-[Re(CO)₃(H₂O)₃]⁺ NUCLEOSIDE MONOPHOSPHATE ADDUCTS INVESTIGATED IN AQUEOUS SOLUTION BY MULTINUCLEAR NMR SPECTROSCOPY*

2.1 Introduction

The success of cisplatin (*cis*-[Pt(NH₃)₂Cl₂]) in the treatment of various cancers has led to intensive efforts to determine its mode of action in order to guide development of other metal-based chemotherapeutic drugs.^{1,2} The primary intracellular target of cisplatin is DNA, with the major DNA lesion being an intrastrand N7–Pt–N7 cross-link between two adjacent guanine residues.³⁻⁶ The anticancer activity of *cis*-[PtA₂X₂] compounds (A₂ = two amines or a diamine carrier ligand; X = anionic leaving group) correlates with the number of NH groups. Models have suggested to us that this correlation could be related to the small size of the hydrogen atom rather than its hydrogen-bonding ability.⁶ Indeed, as the bulk of the diamine carrier ligand increases, anticancer activity decreases.^{5,7} Carrier-ligand bulk also influences the relative stability of single-strand vs duplex forms of oligonucleotides with the intrastrand cross-link.⁸

The great long-term clinical success of cisplatin makes it imperative to continue the search for other potential inorganic chemotherapeutic agents. This search has focused primarily on Pt(II), a square-planar, inert, and redox-stable metal center and one of a limited number of metal centers having all of these properties. Metal centers forming inert, redox-stable complexes typically have an octahedral geometry. Octahedral complexes are generally more bulky and more sterically crowded than square-planar complexes.⁹ As mentioned, bulk decreases the anticancer

* Reproduced with permission from American Chemical Society: Adams, K. M., Marzilli, L. G., “*fac*-[Re(CO)₃(H₂O)₃]⁺ Nucleoside Monophosphate Adducts Investigated in Aqueous Solution by Multinuclear NMR Spectroscopy,” *Inorganic Chemistry*, **2007**, *46*, 4926-4936. Copyright 2007 American Chemical Society.

activity of *cis*-[PtA₂X₂] compounds.⁵ Octahedral complexes do not bind so well as Pt(II) compounds to DNA and have a high propensity to bind to biomolecular targets other than cellular DNA; protein binding over nucleic acid binding can cause considerable toxicity, preventing the use of octahedral metal complexes as anticancer agents.⁵ Several octahedral metal complexes do, however, have modest anticancer properties, with some of the most promising complexes containing Re(I), Ru(II), Ru(III), or dinuclear Rh(II)/Rh(II) metal centers.⁹⁻²¹

With the goal of gaining a better understanding of the coordination chemistry of octahedral metal complexes relevant to nucleic acid binding, we chose to investigate the *fac*-[Re(CO)₃(H₂O)₃]⁺ cation. Dinuclear complexes, such as [Re₂(CO)₆(μ-OH)₃]⁻ and [Re₂(μ-OH)(μ-OPh)₂(CO)₆]⁻, suppressed the growth of murine and human leukemias and lymphomas in cell culture studies.¹⁹ Subsequent mass spectrometry studies demonstrated that [Re₂(CO)₆(μ-OH)₃]⁻ is readily cleaved under protic conditions to yield the *fac*-[Re(CO)₃(H₂O)₃]⁺ cation, leading to a suggestion that this cation may be the species possessing anticancer properties.²² The three water ligands in *fac*-[Re(CO)₃(H₂O)₃]⁺ are readily substituted by a variety of donor atoms, thus providing available sites for cross-linking interactions with DNA bases.^{23,24} Notable similarities in the reactions/adducts of cisplatin and *fac*-[Re(CO)₃(H₂O)₃]⁺ include the following: First, both form M/G 1:1 and 1:2 adducts with 9-methylguanine (9-MeG), guanosine (Guo) and 2-deoxyguanosine (dGuo).^{9,21} Second, both bind these guanine derivatives at N7, and the bases in 1:2 adducts adopt both head-to-head (HH) and head-to-tail (HT) orientations.^{9,21} Third, the rate constant for the binding of Guo to *fac*-[Re(CO)₃(H₂O)₃]⁺ is very similar to that for Guo binding to *cis*-[Pt(NH₃)₂(H₂O)₂]²⁺.²¹ Fourth, both readily bind N- and/or S-containing ligands such as Guo and thiourea.^{9,21,24}

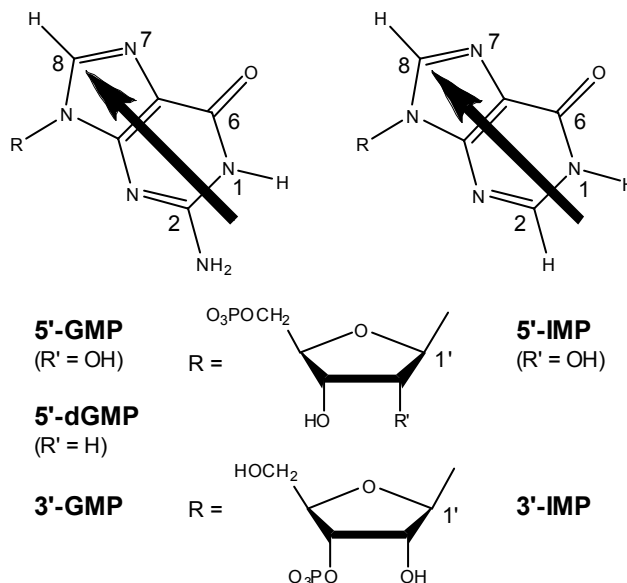


Figure 2.1. Guanine (left) and hypoxanthine (right) derivatives. The arrow and its head represent the base and the H8 atom respectively.

However, compared to Pt(II) compounds, the *fac*-[Re(CO)₃(H₂O)₃]⁺ cation may have a higher affinity for oxygen donors,²³ and its binding equilibria are likely to be more dynamic and less complete.²⁵⁻³⁰ Therefore, the likelihood that an investigation of the interaction of *fac*-[Re(CO)₃(H₂O)₃]⁺ with 6-oxopurine nucleotide monophosphates (NMPs) would prove to be informative led us to study the binding of guanosine 5'-monophosphate (5'-GMP) and guanosine 3'-monophosphate (3'-GMP). We also performed studies with inosine monophosphates (5'-IMP and 3'-IMP) and 2'-deoxyguanosine 5'-monophosphate (5'-dGMP) to assess the effect of the C2–NH₂ substituent and/or N7 basicity (Figure 2.1).

2.2 Experimental Section

2.2.1 Materials and Sample Preparation

Stock solutions (50 mM and 200 mM) of *fac*-[Re(CO)₃(H₂O)₃]OTf in water were prepared by published procedures and maintained at pH ~1.8.³¹ 5'-GMP, 3'-GMP, 5'-IMP, 3'-IMP and 5'-dGMP (disodium salts) and D₂O (99.9%) (Sigma-Aldrich) were used as received.

The H8 of 5'- or 3'-GMP was exchanged to D8 by incubating a solution of the nucleotide in D₂O at 100 °C for 5 h.³² The solution was then filtered and taken to dryness by rotary evaporation, yielding solid D8–5'-GMP (*d*-5'-GMP) or D8–3'-GMP (*d*-3'-GMP) as the disodium salt.

Except as noted, a typical preparation involved treatment of an appropriate amount of NMP in 0.3 mL of H₂O with 0.4 mL of *fac*-[Re(CO)₃(H₂O)₃]OTf (~50 mM or ~10 mM, depending on required final concentration); a small amount (0.1 mL) of D₂O was added to establish a lock signal. Dilute HCl or NaOH stock solutions (in H₂O) were used to adjust the pH (uncorrected) of the samples to ~3.6 in the NMR tubes as required.

2.2.2 NMR Spectroscopy

All NMR spectra were obtained on either a Bruker DPX400 spectrometer (400.1 MHz) or a Varian INOVA500 spectrometer (500.1 MHz); both were equipped with a variable-temperature probe that was equilibrated at 25 °C unless otherwise indicated. 1D ¹H NMR spectra were referenced to the residual HOD peak, and presaturation was used to reduce the residual HOD peak. Each FID was accumulated for 64 transients, each containing 16K data points. Before Fourier transformation, an exponential apodization window function with a 0.2 Hz line broadening was applied. 1D proton-decoupled ³¹P NMR spectra (¹H}-³¹P) were referenced to external trimethyl phosphate (TMP); each FID was accumulated for 64 transients, each containing 32K data points. Before Fourier transformation, an exponential apodization window function with a 2 Hz line broadening was applied. One hundred twenty-eight scans per block (256 blocks) were collected in a 2D rotating frame nuclear Overhauser effect spectroscopy (ROESY) experiment conducted at 32 °C by using a spectral width of ~4000 Hz and a 500 ms mixing time. All NMR data were processed with either XWINNMR (Bruker) or VnmrJ (Varian) software.

2.2.3 Circular Dichroism (CD) Spectroscopy

CD samples were prepared from the respective NMR samples and diluted to ~1 mM GMP with deionized water (pH ~3.6). Three acquisitions, collected from 400 to 200 nm on a JASCO J-710 CD spectropolarimeter at a scan speed of 50 nm/min, were averaged to improve the signal-to-noise ratio.

Although NMR data indicate that the exchange rate is slow, we employed a set of additional experiments to determine if the re-equilibration after dilution would affect the CD results. For this, an aliquot (5 μ L) of a Re/NMP NMR sample ($[fac-[Re(CO)_3(H_2O)_3]^+]$ = 25 mM, $r = 1:2$) was added to 0.3 mL of H₂O (pH ~3.6) and the sample immediately transferred to the CD instrument. Ten acquisitions, collected from 280 to 230 nm, were averaged to improve the signal-to-noise ratio. CD spectra were recorded from 2 min to 2 days after dilution. The CD spectrum of the diluted sample did not change significantly from 2 min to 3 h after dilution. At 6 h after dilution, the CD spectrum had changed considerably. These results indicate that CD spectra measured promptly after dilution are representative of the NMR solution and can be used to assess the chirality of the dominant HT conformer.

2.3 Results and Discussion

2.3.1 Characteristic Features of Metal–NMP Adducts

Shift changes of the ¹H and ³¹P NMR signals of the NMP upon coordination are informative. Extensive studies with *cis*-[PtA₂G₂] complexes indicate that, upon coordination via N7 to Pt, the G H8 singlet shifts downfield more for a Pt/NMP 1:1 adduct than for a 1:2 adduct with *cis* nucleotides.³ This pattern can be explained by an inductive effect of the metal, causing H8 deshielding that is offset somewhat by H8 shielding from the anisotropic *cis* purine bases in

1:2 adducts.³ Upon formation of a 1:1 adduct, the H1' doublet shifts downfield slightly (inductive effect); conversely, the H1' doublet shifts upfield upon formation of a 1:2 adduct (base anisotropic effect). An {N7,P_α} macrochelate, in which the 5'-nucleotide is coordinated via both N7 and P_α, has an H1' singlet because the sugar pucker is forced to be virtually 100% N.³³⁻³⁵ However, this {N7,P_α} macrochelate is rare, occurring for 5'- but not for 3'-monophosphates.³⁵⁻³⁷ Direct inner-sphere coordination of phosphate oxygen to Pt causes the P_α ³¹P NMR signal to shift ~4 to 12 ppm downfield.^{24,34,35,38,39}

At pH ~3.6 (used here) the P_α group (Figure 2.1) of the free NMP is protonated and carries a single negative charge, the same as that of the phosphodiester group in DNA. Also, because deprotonation of *fac*-[Re(CO)₃(H₂O)₃]⁺ begins around pH 4, the choice of pH ~3.6 avoids formation of *fac*-[Re(CO)₃(H₂O)₂(OH)] and *fac*-[Re(CO)₃(H₂O)(OH)₂]⁻ species.²³

The fact that the guanine base bound to a metal is not C₂ symmetrical with respect to rotation about the M–N7 bond allows for rotamers. For square-planar metal geometries, there are two distinct rotamers at most for a given M/G 1:1 adduct. When the metal moiety lacks high symmetry, these rotamers are not equivalent, and thus there are two conformers. Introduction of a chiral sugar at the G N9 also influences the number of conformers. For octahedral or square-planar M/G 1:2 adducts with two *cis* N7-coordinated identical G's, head-to-head (HH) and head-to-tail (HT) conformers are possible. HH conformers and HT conformers have the two H8 atoms on the same and opposite sides, respectively, of the N7–M–N7 plane. When the starting complex has high symmetry, one HH and two HT conformers are possible. An additional HH conformer can exist if the complex has lower symmetry (as in the adducts studied here, see Figure 2.2) or if the two G's are not identical, such as in d(GpG) adducts.^{40,41} If the starting complex has lower symmetry and the two G's are not identical, two 1:2 adducts with two *cis* N7-coordinated

nonidentical **G**'s can form, each having 2 HH and 2 HT conformers; hence, a solution having a total of 4 HH and 4 HT conformers could be created.

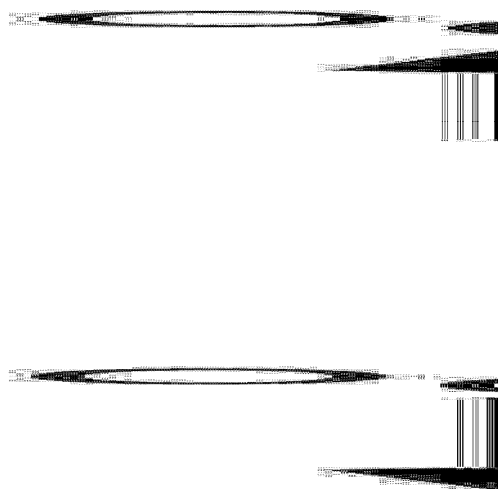


Figure 2.2. (top) Diagram showing coordination positions relative to each other; (bottom) HHa, Δ HT, HHb and Δ HT orientations for an octahedral metal center. NMPs in coordination positions **1** and **2** are distinct and all four conformers can interchange only if the type of NMP is identical in both coordination positions.

In typical *cis*-[PtA₂G₂] models with non-bulky amines, the rate of rotation about the Pt–N7 bonds is too rapid to detect distinct NMR signals for the conformers.⁴² By using chiral carrier ligands with sufficient bulk to slow rotation, **G** H8 signals for the HH and HT rotamers could be observed, and the Δ HT and Λ HT absolute conformations could be established by NOE cross-peaks between the **G** H8 signals and the carrier ligand signals.^{41,43,44} In turn, the CD signatures for these conformations were characterized.⁴⁴ For these adducts, the dominant HT conformer appears to be stabilized by hydrogen bonding of the phosphate group of one **G** with the N1H of

the *cis* **G** and these “second-sphere” interactions, or SSC, have been identified as important factors that stabilize the Δ HT and Δ HT conformers in 5'-GMP and 3'-GMP complexes, respectively.^{43,45-49} In addition, such studies with *cis*-[PtA₂G₂] complexes with unlinked **G** nucleotides has shown that, while the HH conformer does form, the two HT conformers, Δ HT and Δ HT, are typically favored.^{42,43,50-56} In addition, Pt/5'-GMP 1:2 adducts adopt the HH conformation more readily than do Pt/3'-GMP 1:2 adducts.^{47,48,57}

2.3.2 Overview of Products Formed by *fac*-[Re(CO)₃(H₂O)₃]⁺ and NMPs

In describing the ¹H and ³¹P NMR spectral results for NMP binding to *fac*-[Re(CO)₃(H₂O)₃]⁺, we state the nature of the adducts formed before presenting all the evidence and the reasoning for such designations. In general for a given NMP, two principal adducts were formed: a 1:1 adduct, *fac*-[Re(CO)₃(H₂O)₂(NMP)], and a 1:2 adduct, *fac*-[Re(CO)₃(H₂O)(NMP)₂]⁻ having inequivalent NMPs (Figure 2.2). We also found evidence for the formation of both a dinuclear 2:1 complex, *fac*-[Re₂(CO)₆(H₂O)₄(NMP)] (in which a phosphate oxygen and N7 are each bound to a *fac*-[Re(CO)₃(H₂O)₂]⁺ moiety), and a trinuclear 3:1 complex, *fac*-[Re₃(CO)₉(H₂O)₆(NMP)]⁺ (in which two phosphate oxygens and N7 are each bound to a *fac*-[Re(CO)₃(H₂O)₂]⁺ moiety). When two different NMPs (NMP and N'MP) were present in the reaction mixture, two 1:2 adducts, *fac*-[Re(CO)₃(H₂O)(NMP)(N'MP)]⁻, formed, as expected because the coordination positions are not equivalent (Figure 2.2).

2.3.3 5'-GMP Reaction Products

Upon treatment of *fac*-[Re(CO)₃(H₂O)₃]⁺ with 5'-GMP ([Re] = 25 mM, *r* = 1:1), four new H8 singlets appeared (although one H8 singlet is very small, Figure 2.3). These signals are relatively downfield and are insensitive to pH from 3.6 to 1.4, properties indicating that the

signals are from adducts with Re bound to 5'-GMP via N7. The predominant H8 signal appears immediately after mixing and dominates the spectrum, even at long reaction times. Because this major adduct signal has no partner H8 signal, it could arise from either a 1:1 or 1:3 Re/nucleotide adduct (Figure 2.4). The following observations demonstrate that this major product is the 1:1 adduct, *fac*-[Re(CO)₃(H₂O)₂(5'-GMP)]: First, the intensity of the predominant H8 signal decreases upon addition of more 5'-GMP (*vide infra*), whereas the intensity of this signal could increase only if it were due to the 1:3 adduct. Second, the downfield shifts of the H8 singlet (~0.4 ppm) and the H1' doublet (~0.1 ppm) of this major adduct relative to free 5'-GMP are consistent with a 1:1 adduct (Table 2.1). Third, the ³J_{H1'-H2'} coupling constant decreases from ~6 Hz (free GMP) to ~3.6 Hz, a feature consistent with metal coordination at N7 (Table 2.1 and Appendix A). Fourth, the chemical shift of the P_α signal of this adduct is similar (Table 2.1) to that for 5'-GMP, ruling out the only other 1:1 adduct with 5'-GMP bound via N7, a macrochelate (Figure 2.4) expected to have a P_α signal shifted downfield by 4–12 ppm.^{24,34,35,38,39} These results, as well as those obtained at *r* values higher than 1:1 and with a mixture of nucleotides (*vide infra*), establish beyond question that when *r* = 1:1, the predominant adduct formed is *fac*-[Re(CO)₃(H₂O)₂(5'-GMP)], with 5'-GMP bound only through N7.

The next most abundant adduct in the *r* = 1:1 solution is *fac*-[Re(CO)₃(H₂O)(5'-GMP)₂]⁻. This 1:2 adduct has two closely spaced H8 singlets of approximately equal intensity (Figure 2.3). Relative to free 5'-GMP, the H8 signals are shifted ca. 0.2 ppm downfield, the two H1' doublets are shifted slightly *upfield*, and neither of the two corresponding P_α signals is shifted significantly (Table 2.1, Figure 2.3). Two H8 singlets of equal intensity are expected for a 1:2 adduct. A 1:2 adduct lacks both a plane of symmetry (because of a chiral sugar) and a C₂ axis (because the *fac*-[Re(CO)₃(H₂O)]⁺ moiety lacks C₂ symmetry). Addition of another equivalent of

5'-GMP ($r = 1:2$) resulted in a higher intensity for these H8 signals relative to that of *fac*-[Re(CO)₃(H₂O)₂(5'-GMP)]; therefore, these signals undoubtedly arise from the 1:2 adduct, *fac*-[Re(CO)₃(H₂O)(5'-GMP)₂]⁻.

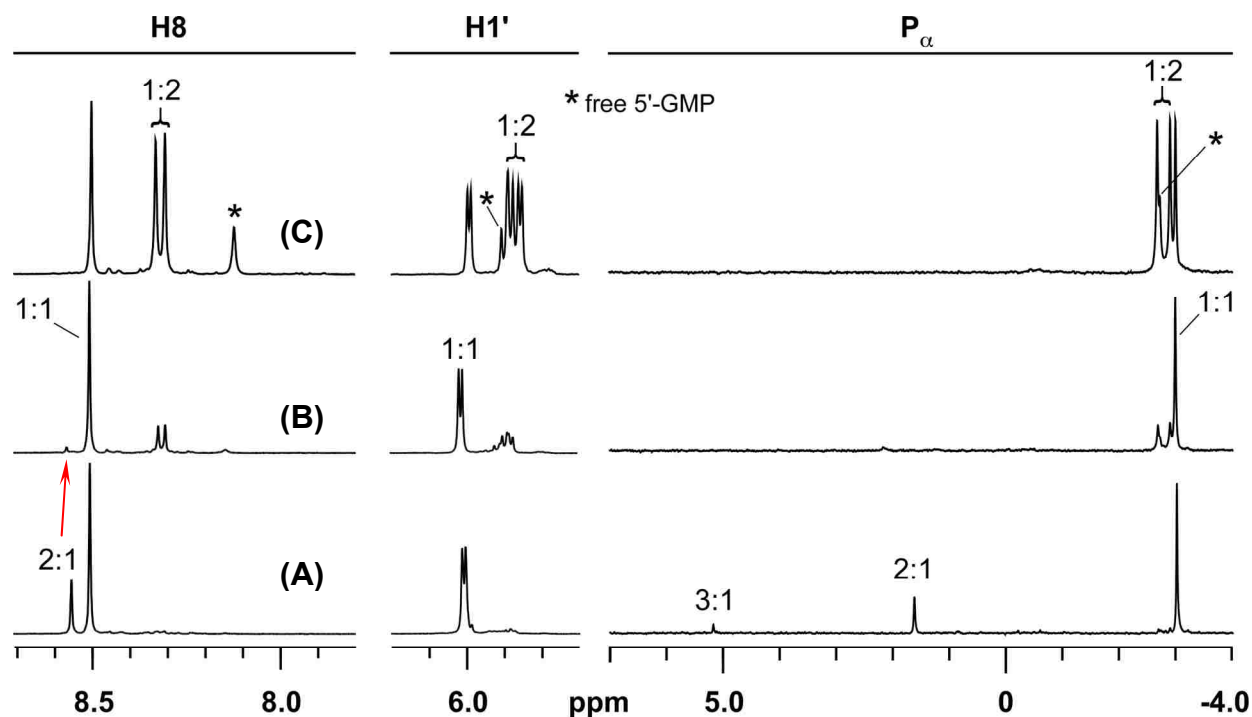


Figure 2.3. H8 (left), H1' (center) and P_α (right) NMR signals of equilibrated mixtures of *fac*-[Re(CO)₃(H₂O)₃]⁺ (25 mM) and 5'-GMP at pH 3.6. **(A)** Re/GMP $r = 4:1$, **(B)** $r = 1:1$, **(C)** $r = 1:2$. The red arrow points to the small amount of 2:1 adduct in spectrum **(B)**. See text for conditions and spectral assignments for signals not identified in Figure.

The third most abundant adduct in the $r = 1:1$ solution is *fac*-[Re₂(CO)₆(H₂O)₄(5'-GMP)]. This dinuclear adduct gives a small H8 singlet (Figure 2.3) downfield from the H8 singlet of *fac*-[Re(CO)₃(H₂O)₂(5'-GMP)]; the H1' signal of this adduct is obscured by the H1' signals of other adducts. The corresponding P_α signal is ca. 5 ppm downfield from the P_α resonance of 5'-GMP. Taken together, these results indicate that both N7 and P_α are coordinated to Re in this minor product in the $r = 1:1$ solution (Table 2.1). Three conceivable and reasonable adducts with 5'-GMP coordinated via both N7 and P_α can explain the observation of one H8 and one P_α signal

for this third product. The first possibility is a C_2 -symmetric cyclic dimeric 2:2 adduct with two 5'-GMP's linking two fac -[Re(CO)₃(H₂O)]⁺ moieties (Figure 2.4). The abundance of this dimer relative to the 1:1 adduct should remain constant above $r = 1:1$ at a given GMP concentration because each contains one 5'-GMP per Re. The other two conceivable adducts have less than one 5'-GMP per Re. These are a dinuclear 2:1 adduct with N7 bound to one Re and P_α bound to a second Re, and a trinuclear 3:1 adduct with N7 bound to one Re and P_α bound to two different Re's (Figure 2.4). At a given GMP concentration, increasing the Re concentration above $r = 1:1$ would increase the abundance of both the di- and trinuclear adducts relative to the 1:1 adduct.

Table 2.1. ¹H and ³¹P NMR Shifts (ppm) and ³J_{H1'-H2'} Coupling Constants (Hz, in parentheses) of Nucleotides and Complexes Formed with fac -[Re(CO)₃(H₂O)₃]⁺^a

complex	δ ¹ H		δ ³¹ P
	H8	H1'	P _α
5'-GMP	8.12	5.90 (6.1)	-2.74
fac -[Re(CO) ₃ (H ₂ O) ₂ (5'-GMP)]	8.50	5.99 (3.7)	-3.02
fac -[Re(CO) ₃ (H ₂ O)(5'-GMP) ₂] ⁻	8.32, 8.30	5.88 (5.1), 5.86 (3.9)	-2.69, -2.91 ^b
fac -[Re ₂ (CO) ₆ (H ₂ O) ₄ (5'-GMP)]	8.55	^c	1.62 ^d
fac -[Re ₃ (CO) ₉ (H ₂ O) ₆ (5'-GMP)] ⁺	^c	^c	5.17
3'-GMP	8.00	5.93 (6.0)	-3.00
fac -[Re(CO) ₃ (H ₂ O) ₂ (3'-GMP)]	8.52	6.00 (3.6)	-3.06
fac -[Re(CO) ₃ (H ₂ O)(3'-GMP) ₂] ⁻	8.40, 8.34	5.90 (3.8), 5.90 (3.8)	-3.04
fac -[Re ₂ (CO) ₆ (H ₂ O) ₄ (3'-GMP)]	8.53	6.02 (4.0)	1.63 ^d
fac -[Re ₃ (CO) ₉ (H ₂ O) ₆ (3'-GMP)] ⁺	8.54	6.04 (3.9)	5.09
<i>M</i>-5'-GMP^e	8.48	5.90 ^c	-3.11 ^b
<i>M</i>-3'-GMP	8.38	5.90 ^c	-3.04 ^b
<i>m</i>-5'-GMP	8.40	5.90 ^c	-3.11 ^b
<i>m</i>-3'-GMP	8.14	5.90 ^c	-3.04 ^b

^a[Re] = 25 mM, pH 3.6, 32 °C. ^bSignal assigned to adduct only. ^cSignal obscured by other signals. ^dShift highly dependent on pH (see text). ^e***M*** and ***m*** = major and minor adducts, respectively.

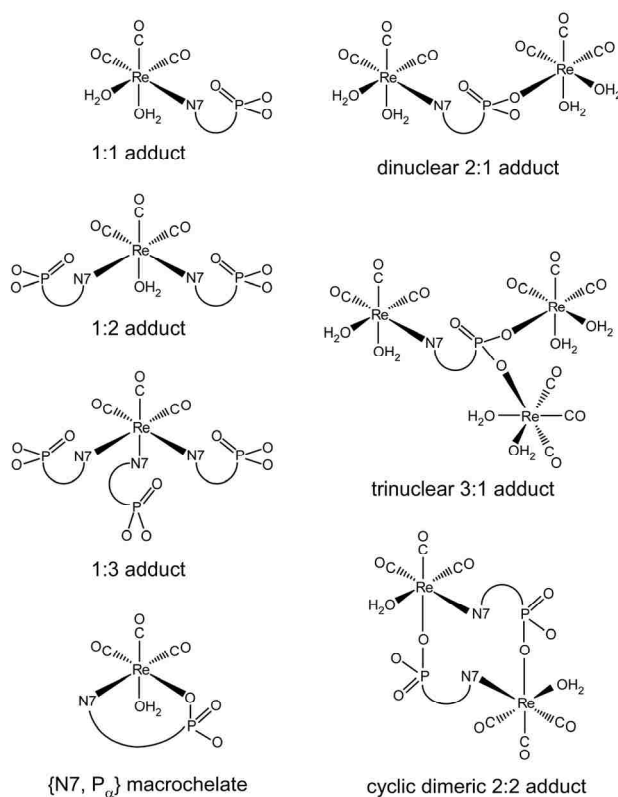


Figure 2.4. Possible Re/GMP adducts.

To distinguish among these possibilities for the third product, we performed the formation reaction twice more but by using different total concentrations and different r values. At high concentrations (100 mM) of both Re and 5'-GMP, the intensities of ^1H and ^{31}P NMR signals of the third product relative to those of the 1:1 adduct were the same as those found in the 25 mM $r = 1:1$ reaction. At the higher $r = 4:1$ ($[\text{Re}] = 25$ mM) the H8 and P_α signals of the third product had a higher intensity relative to the 1:1 adduct signals. Thus, there is more than one Re bound per 5'-GMP. The third product with the ca. 5 ppm downfield P_α signal cannot be a cyclic dimeric 2:2 adduct.

The nature of the third product was established in this $r = 4:1$ experiment. A small additional P_α signal (Figure 2.3) was found ~8 ppm downfield from the P_α resonance of free 5'-

GMP. Because the P_{α} signal of the fourth product appears only at higher r values and is one-fourth the size of the P_{α} signal of the third product, the fourth product contains more Re per 5'-GMP than the third product. Most reasonably, the third and fourth products are the 2:1 and 3:1 adducts. Although no H8 signal could be located for the 3:1 adduct, we should note that in 3'-GMP reactions at $r = 4:1$, both the H8 and P_{α} signals of this fourth product are evident (*vide infra*, Figure 2.5).

To assess our conclusions, we examined the effect of low pH on the ^{31}P NMR shifts (Appendix A). When the pH of a solution containing the 1:1, 1:2, 2:1, and 3:1 adducts was decreased from 4 to 2, the P_{α} signal of the 1:1 adduct (with a shift similar to that of free 5'-GMP) did not shift significantly, consistent with the P_{α} group being uncoordinated and monoprotonated throughout the pH range. However, the P_{α} signal of the 2:1 adduct (shifted 5 ppm downfield from that of free 5'-GMP) shifted significantly upfield (ca. 3.5 ppm) over this pH range, consistent with a coordinated deprotonated P_{α} group becoming protonated. The pK_a of this P_{α} group is thus about 3.2, a value much lower than the pK_a for 5'-GMP (~ 6.3).⁵⁷⁻⁶⁰ The much lower pK_a of the phosphate group in *fac*-[Re₂(CO)₆(H₂O)₄(5'-GMP)], compared to N7-bound Pt adducts,⁶¹⁻⁶⁴ is undoubtedly due to the direct binding of Re to this P_{α} group.^{35,38,39} The very downfield P_{α} signal of the fourth adduct was insensitive to changes in pH between 4 and ~ 3 (this P_{α} signal disappeared below pH ~ 3); this lack of pH dependence, indicating a phosphate group pK_a below 2, is consistent with such a 3:1 adduct with two Re moieties bound to the P_{α} group. The binding of the second Re is expected to be weak, and thus it does not compete well with the proton as the pH drops below the pK_a of the 2:1 adduct. However, because two Re's are bound to it, the P_{α} group is always deprotonated in the 3:1 adduct.

The coordination of N7 of a nucleotide to inert metal centers can be demonstrated by addition of Cu^{2+} ions. The paramagnetic Cu^{2+} ion binds to N7 of the free nucleotide, causing the broadening and eventual disappearance of the H8 resonance.⁶⁵ Alternatively, if N7 of the nucleotide is bound to another metal, such as Pt or Re, Cu^{2+} coordination at N7 is blocked and the H8 resonance remains sharp.³⁵ Addition of a Cu^{2+} solution to 5 μM to an $r = 1:1$ solution ($[\text{Re}] = 5 \text{ mM}$) caused the H8 and P_α signals of free 5'-GMP to disappear. The H8 signals of the 1:1 and 1:2 adducts remained sharp and the P_α signals of these adducts were still present but broadened considerably. Addition of Cu^{2+} solution to 50 μM did not cause broadening of the H8 signals of the 1:1 and 1:2 adducts; however, no ^{31}P signals were detected. These results thus confirm that N7 is bound to Re in both the *fac*- $[\text{Re}(\text{CO})_3(\text{H}_2\text{O})_2(5'\text{-GMP})]$ 1:1 and *fac*- $[\text{Re}(\text{CO})_3(\text{H}_2\text{O})(5'\text{-GMP})_2]^-$ 1:2 adducts.

2.3.4 3'-GMP Reaction Products

To evaluate the effect of phosphate group position on the adducts formed, we examined 3'-GMP reactions. Treatment of *fac*- $[\text{Re}(\text{CO})_3(\text{H}_2\text{O})_3]^+$ with 3'-GMP ($[\text{Re}] = 25 \text{ mM}$, $r = 1:1$) led to the appearance of three new H8 singlets (Figure 2.5, Table 2.1); these signals can be attributed to the 1:1 adduct, *fac*- $[\text{Re}(\text{CO})_3(\text{H}_2\text{O})_2(3'\text{-GMP})]$, and the 1:2 adduct, *fac*- $[\text{Re}(\text{CO})_3(\text{H}_2\text{O})(3'\text{-GMP})_2]^-$, for reasons given above for adducts of 5'-GMP. Signals arising from the 1:2 adduct were confirmed with an $r = 1:2$ experiment. In solutions initially 25 mM in *fac*- $[\text{Re}(\text{CO})_3(\text{H}_2\text{O})_3]^+$, the downfield shoulder on the H8 signal of *fac*- $[\text{Re}(\text{CO})_3(\text{H}_2\text{O})_2(3'\text{-GMP})]$ and the downfield P_α signal at $\sim 5 \text{ ppm}$ were relatively larger in an $r = 4:1$ reaction mixture than in an $r = 1:1$ reaction mixture (Figure 2.5). The third product is clearly the dinuclear 2:1 adduct, *fac*- $[\text{Re}_2(\text{CO})_6(\text{H}_2\text{O})_4(3'\text{-GMP})]$. A fourth product with an H8 signal just downfield from the H8 signal of *fac*- $[\text{Re}(\text{CO})_3(\text{H}_2\text{O})_2(3'\text{-GMP})]$ and with an P_α signal $\sim 8 \text{ ppm}$ downfield from the P_α

signal of free 3'-GMP is the 3:1 trinuclear adduct, $fac-[Re_3(CO)_9(H_2O)_6(3'-GMP)]^+$. As was found for 5'-GMP, a 100 mM, $r = 1:1$ experiment supported this interpretation by ruling out the cyclic dimeric 2:2 adduct. To summarize, for both 3'-GMP and 5'-GMP, four products were found: two abundant products, $fac-[Re(CO)_3(H_2O)_2(GMP)]$ and $fac-[Re(CO)_3(H_2O)(GMP)_2]^-$, and two minor products, $fac-[Re_2(CO)_6(H_2O)_4(GMP)]$ and $fac-[Re_3(CO)_9(H_2O)_6(GMP)]^+$.

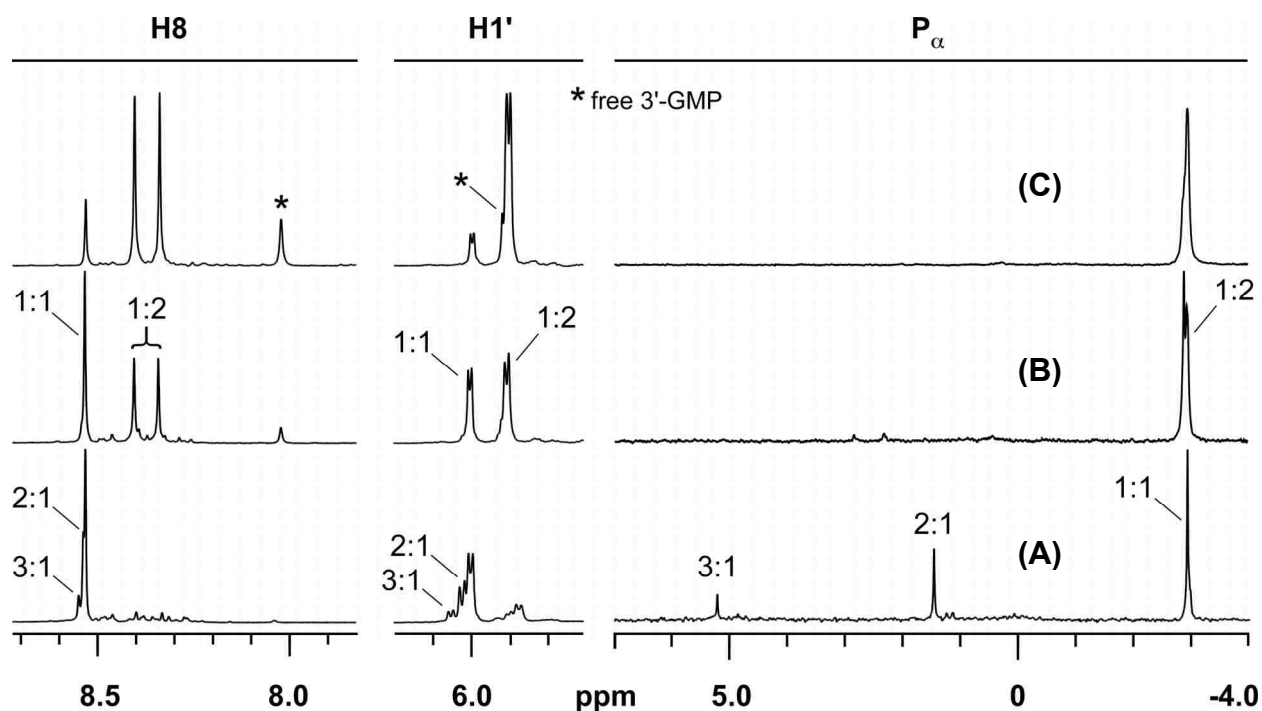


Figure 2.5. H8 (left), H1' (center) and P_α (right) NMR signals of equilibrated mixtures of $fac-[Re(CO)_3(H_2O)_3]^+$ (25 mM) and 3'-GMP at pH 3.6. (A) Re/GMP $r = 4:1$, (B) $r = 1:1$, (C) $r = 1:2$. See text for conditions and spectral assignments for signals not identified in Figure.

2.3.5 Further Aspects of the GMP Reactions

Reactions at $r = 1:1$ and $r = 1:2$ of both 5'- and 3'-GMP with $fac-[Re(CO)_3(H_2O)_3]^+$ (at 5 mM, a concentration at which H8 signals did not overlap) at 1 h and at 6 days were compared (Table 2.2). The solutions were at equilibrium after 6 days, as no spectral changes occurred between 4 and 6 days. At 1 h, the 1:1 adduct was the predominant product at $r = 1:1$; however,

more 1:1 adduct was present at 1 h for 5'-GMP than for 3'-GMP. In the normal nucleotide anti conformation, the 5'-phosphate group is closer to N7 than the 3'-phosphate group. In an initial ion pair interaction of the nucleotide with the metal cation, the stabilizing electrostatic and H-bonding interactions of the phosphate group with the cation place the N7 in a position closer to the metal center for a 5'-nucleotide than for a 3'-nucleotide. We attribute the faster reaction of 5'-GMP to this proximity.

At equilibrium (6 days), the 1:1 adduct remained the predominant product for 5'-GMP at both $r = 1:1$ and at $r = 1:2$, but for 3'-GMP this was the case only at $r = 1:1$. At $r = 1:1$, more 1:1 adduct was present in the 5'-GMP reaction than in the 3'-GMP reaction (Table 2.2). The factors (H-bonding and electrostatic interactions) facilitating the formation of $fac-[Re(CO)_3(H_2O)_2(5'-GMP)]$ also stabilize the 1:1 adduct. These factors are either absent (H-bonding) or weaker (electrostatic) in $fac-[Re(CO)_3(H_2O)_2(3'-GMP)]$, accounting for its lower abundance at $r = 1:1$. However, at equilibrium, the amount of $fac-[Re(CO)_3(H_2O)(3'-GMP)_2]^-$ formed was greater than the amount of $fac-[Re(CO)_3(H_2O)(5'-GMP)_2]^-$ formed under both $r = 1:1$ and $r = 1:2$ conditions (Table 2.2).

Factors favoring the Re/5'-GMP 1:1 adduct are less likely to be important in contributing to the stability of the Re/5'-GMP 1:2 adduct. First, $fac-[Re(CO)_3(H_2O)(5'-GMP)_2]^-$ has only one coordinated H₂O for H-bonding to phosphate. Second, the greater conformational freedom for the 5'-phosphate group will lead to some electrostatic repulsion between the bound nucleotides. In contrast, because the 3'-phosphate groups of $fac-[Re(CO)_3(H_2O)(3'-GMP)_2]^-$ are directed away from the center of the complex, electrostatic repulsion is less in this 1:2 adduct. Although the 3'-phosphate group cannot participate in H-bonding interactions with the coordinated H₂O,

this group can form stabilizing H-bonds with N1H of the cis 3'-GMP.⁶⁶ Thus, differences in the relative abundance of the 1:1 adduct and 1:2 adduct between 5'-GMP and 3'-GMP are explained.

Table 2.2. Concentrations (mM) of 1:1, 1:2 and Dinuclear Adducts of 5'-GMP, 3'-GMP, 5'-IMP, and 3'-IMP at Different Nucleotide Concentrations and Times after Mixing with *fac*-[Re(CO)₃(H₂O)₃]⁺^a

complex	<i>r</i> = 1:1		<i>r</i> = 1:2	
	1 h	6 d	1 h	6 d
5'-GMP	2.6	0.9	6.2	3.6
<i>fac</i> -[Re(CO) ₃ (H ₂ O) ₂ (5'-GMP)]	2.3	3.2	3.0	2.9
<i>fac</i> -[Re(CO) ₃ (H ₂ O)(5'-GMP) ₂] ⁻	0.1	0.5	0.4	1.8
3'-GMP	4.3	1.1	8.6	2.9
<i>fac</i> -[Re(CO) ₃ (H ₂ O) ₂ (3'-GMP)]	0.7	2.2	1.2	2.3
<i>fac</i> -[Re(CO) ₃ (H ₂ O)(3'-GMP) ₂] ⁻	^b	0.8	0.1	2.3
<i>fac</i> -[Re ₂ (CO) ₆ (H ₂ O) ₄ (3'-GMP)]	^b	0.2	^b	0.2
5'-dGMP	2.8	0.6	5.7	3.1
<i>fac</i> -[Re(CO) ₃ (H ₂ O) ₂ (5'-dGMP)]	2.1	3.5	3.1	3.5
<i>fac</i> -[Re(CO) ₃ (H ₂ O)(5'-dGMP) ₂] ⁻	^b	0.5	0.6	1.7
5'-IMP	3.7	1.7	5.8	4.7
<i>fac</i> -[Re(CO) ₃ (H ₂ O) ₂ (5'-IMP)]	1.3	3.0	4.0	4.0
<i>fac</i> -[Re(CO) ₃ (H ₂ O)(5'-IMP) ₂] ⁻	^b	0.2	^b	0.7
<i>fac</i> -[Re ₂ (CO) ₆ (H ₂ O) ₄ (5'-IMP)]	^b	^b	0.2	^b
3'-IMP	4.2	2.2	8.6	4.6
<i>fac</i> -[Re(CO) ₃ (H ₂ O) ₂ (3'-IMP)]	0.9	2.0	1.4	3.2
<i>fac</i> -[Re(CO) ₃ (H ₂ O)(3'-IMP) ₂] ⁻	^b	0.4	^b	1.0
<i>fac</i> -[Re ₂ (CO) ₆ (H ₂ O) ₄ (3'-IMP)]	^b	0.2	^b	0.3

^a[Re] = 5 mM. ^bNot observed.

To understand better the role of phosphate group H-bonding to N1H of the cis GMP, we must consider which conformers are likely to be present. As mentioned above, the number of conformers depends on the symmetry of the complex. For a *fac*-[Re(CO)₃(H₂O)(NMP)₂]⁻ adduct, two HH (HHa and HHb) and two HT conformers (ΔHT and ΛHT, Figure 2.2) are possible.

Distinguishing between HH and HT conformers in solution is best accomplished by using NOESY techniques, as the two H8 protons are normally close enough to give an NOE cross-peak for an HH conformer but too far to give a cross-peak for an HT conformer.^{41,51,67-69} No H8–H8 NOE cross-peaks were observed for *fac*-[Re(CO)₃(H₂O)(5'-GMP)₂]⁻ or *fac*-[Re(CO)₃(H₂O)(3'-GMP)₂]⁻, thus providing evidence that these adducts exist mainly as HT conformers.

Because of rapid rotation about the Re–N7 bond, the NMR signal detected for each coordinated NMP is a weighted average of the respective signals for all conformers but the signals reflect mainly the HT conformers. For a dynamic adduct, differentiating between the Δ HT and Λ HT conformers is best accomplished by using CD methods.⁴⁸ It has been established that the CD signals of both 1:1 adducts and of HH conformers of 1:2 adducts are weak, while the CD signal of the HT conformers is much stronger.⁶⁹ Therefore, the sign of the CD spectrum reflects the conformation of the major HT conformer present. The CD signal of a Δ HT conformer has negative features at ~227 and ~285 nm and a positive feature at ~252 nm, while the CD signal of a Λ HT conformer has positive features at ~227 and ~285 nm and a negative feature at ~252 nm.⁶⁹ At pH ~3.6, CD spectra of equilibrated solutions ([Re] = 25 mM, *r* = 1:2, pH ~3.6) containing both the 1:1 and 1:2 adducts of 5'-GMP or 3'-GMP were recorded. The 5'-GMP solution exhibited a negative feature at ~267 nm and a positive feature at ~238 nm (Figure 2.6). A similar pattern was observed for the 3'-GMP solution (Figure 2.6). This pattern in both cases is indicative of the Δ HT conformer; therefore, we can conclude that *both fac*-[Re(CO)₃(H₂O)(5'-GMP)₂]⁻ and *fac*-[Re(CO)₃(H₂O)(3'-GMP)₂]⁻ exist primarily as Δ HT conformers. Past studies have found that the Δ HT conformation allows favorable phosphate interligand H–bonding to the carrier ligands for 5'-GMP adducts and to the N1H of the *cis* 3'-GMP for 3'-GMP adducts.^{43,45-48} In the Δ HT conformation, only one phosphate group is well

positioned to form H-bonds (to the coordinated H₂O) for 5'-GMP but both phosphate groups are positioned to form H-bonds (to the cis GMP) for 3'-GMP; thus, the preference for the Δ HT conformation for 3'-GMP is explained, as is the higher amount of 1:2 adduct for 3'-GMP than for 5'-GMP. However, the preference for the Δ HT conformation for the 5'-GMP 1:2 adduct was unexpected because two favorable N1H-5'-phosphate H-bonds are possible for the Δ HT conformer of 5'-GMP 1:2 adducts.

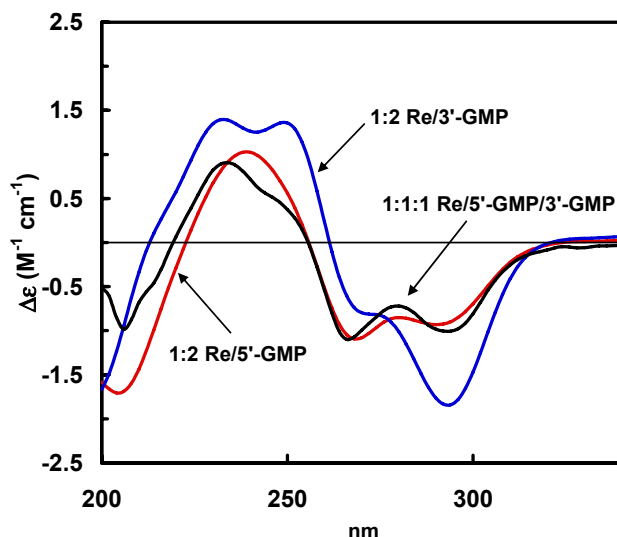


Figure 2.6. CD spectra recorded soon after dilution of equilibrated NMR solutions ($[Re] = 25$ mM, pH 3.6) of 5'-GMP ($r = 1:2$, red line), 3'-GMP ($r = 1:2$, blue line) and mixed 5'-GMP/3'-GMP ($r = 1:1:1$, black line).

2.3.6 Mixed Nucleotide Approach

Mixed 5'-GMP/3'-GMP experiments were performed to elucidate the properties of 1:2 adducts, particularly the preference for the Δ HT conformation by the 5'-GMP 1:2 adduct. In such mixtures, two Re/5'-GMP/3'-GMP 1:1:1 adducts are expected (Figure 2.8), in addition to the previously identified adducts containing 5'-GMP or 3'-GMP. Three $r = 1:1:1$ solutions at pH 3.6, all starting with $[Re] = 5$ mM, were studied. In one, 3'-GMP and 5'-GMP were added initially. In the other solutions, one GMP was added initially, the solution was allowed to equilibrate, and

then the other GMP was added. All three solutions gave identical NMR spectra. The H8 signals of previously discussed adducts were observed, as expected. In addition, three new H8 singlets (8.48, 8.38, and 8.14 ppm, Figure 2.7) were observed. Because the conformers of each adduct will interchange rapidly on the NMR time scale, four new H8 singlets are expected. We deduced that one new H8 singlet was overlapped with a previously discussed signal; consequently, we exchanged H8 with deuterium, preparing *d*-3'-GMP and *d*-5'-GMP.³² The mixed nucleotide experiment utilizing one of these deuterated nucleotides allows assignment of all H8 signals arising from the undeuterated nucleotide.

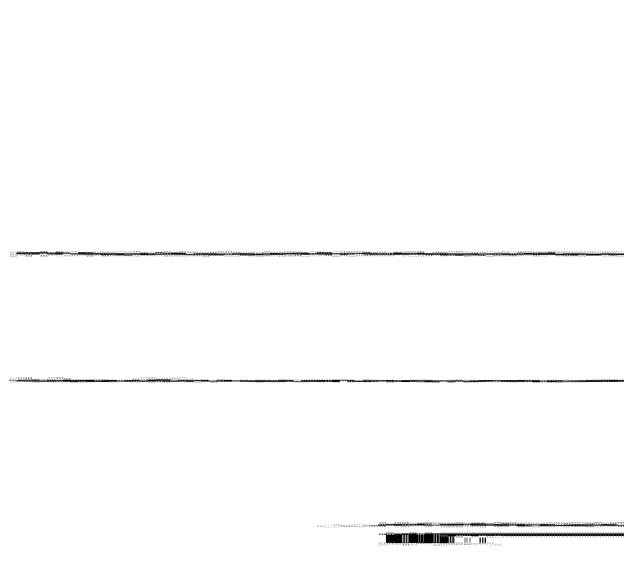


Figure 2.7. H8 NMR signals of equilibrated mixtures ($r = 1:1:1$, pH 3.6) of *fac*-[Re(CO)₃(H₂O)₃]⁺ with the NMPs indicated. See text for signal assignments.

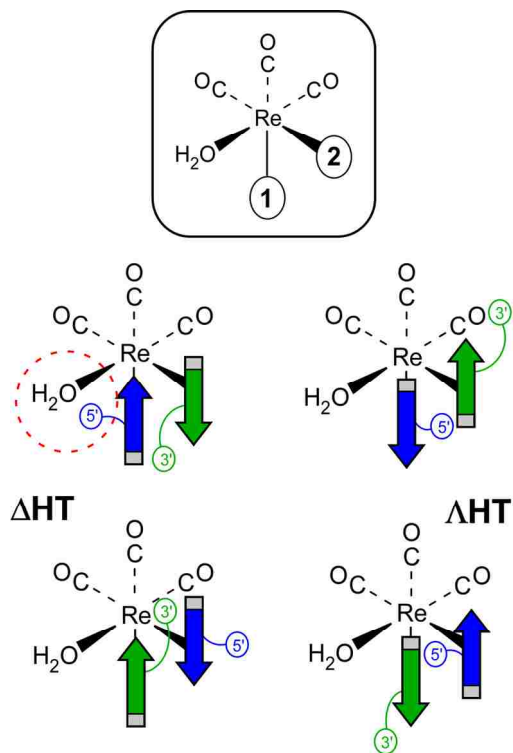


Figure 2.8. (top) Diagram showing coordination position numbering; (bottom) The pairs of HT conformers of each of the two possible *fac*-[Re(CO)₃(H₂O)(5'-GMP)(3'-GMP)]⁻ adducts. In the pair on the left, the Δ HT conformer can form a favorable phosphate-to-coordinated water H-bond.

In a typical experiment, 1 equiv of 5'-GMP was added to an equilibrated sample containing equimolar concentrations of *d*-3'-GMP and *fac*-[Re(CO)₃(H₂O)₃]⁺ (5 mM, *r* = 1:1:1) at pH 3.6. New H8 singlets (at 8.48 and 8.40 ppm, Figure 2.7) can be assigned to the 5'-GMP's in the two Re/5'-GMP/3'-GMP 1:1:1 adducts. In the competition experiment with *d*-5'-GMP, the H8 singlets (at 8.38 and 8.14 ppm, Figure 2.7) can be assigned to the 3'-GMP's in these two Re/5'-GMP/3'-GMP adducts. The relative intensity of the H8 signals from the Re/5'-GMP/3'-GMP adducts permits pairing of signals arising from the same complex. In this way, it was determined that the more abundant 1:1:1 adduct (***M***, 60%) has a 5'-GMP H8 signal at 8.48 ppm and a 3'-GMP H8 signal at 8.38 ppm, while the minor adduct (***m***) has a 5'-GMP H8 signal at 8.40 ppm and a 3'-GMP H8 signal at 8.14 ppm. At equilibrium (6 days, *r* = 1:2), the stability order was ***M***, *fac*-[Re(CO)₃(H₂O)(3'-GMP)₂]⁻, ***m***, and *fac*-[Re(CO)₃(H₂O)(5'-GMP)₂]⁻ (Table 2.3).

Table 2.3. Concentrations (mM) of 1:1, 1:2 and Mixed Bis Adducts of 5'- and 3'-GMP at Different Nucleotide Concentrations and Times after Mixing with *fac*-[Re(CO)₃(H₂O)]⁺^a

complex	<i>r</i> = 1:1		<i>r</i> = 1:2	
	1 h	6 d	1 h	6 d
5'-GMP	2.0	0.4	3.9	1.4
<i>fac</i> -[Re(CO) ₃ (H ₂ O) ₂ (5'-GMP)]	0.5	1.6	1.2	1.8
<i>fac</i> -[Re(CO) ₃ (H ₂ O)(5'-GMP) ₂] ⁻	^b	0.1	^b	0.4
3'-GMP	2.3	0.6	4.2	1.6
<i>fac</i> -[Re(CO) ₃ (H ₂ O) ₂ (3'-GMP)]	0.3	1.1	0.7	1.0
<i>fac</i> -[Re(CO) ₃ (H ₂ O)(3'-GMP) ₂] ⁻	^b	0.2	^b	0.6
<i>M</i> ^c	^b	0.3	^b	0.8
<i>m</i> ^c	^b	0.2	^b	0.5

^a[Re] = 5 mM. ^bNot observed. ^c***M*** and ***m*** refer to the major and minor forms, respectively, of *fac*-[Re(CO)₃(H₂O)(5'-GMP)(3'-GMP)]⁻.

The two Re/5'-GMP/3'-GMP 1:1:1 adducts can have a total of four HT conformers. Each adduct has a pair of ΔHT and ΛHT conformers (Figure 2.8). The conformers in each pair rapidly

interchange. The CD pattern of an equilibrated solution containing the 1:1:1 adducts retains the Δ HT-type signal, indicating that **M** most likely favors the Δ HT conformation (Figure 2.6).

While for both *fac*-[Re(CO)₃(H₂O)(5'-GMP)(3'-GMP)]⁻ adducts, the Δ HT conformer can be stabilized by an N1H–3'-phosphate H-bond between the cis nucleotides, only the Δ HT conformer of the 1:1:1 adduct with 5'-GMP in coordination position 1 can form a favorable H-bond to the coordinated water (Figure 2.8, left). An idealized model of the Δ HT conformer of this preferred adduct (Appendix A) reveals that, in addition to these two H bonds, an O6 to coordinated water H-bond is also possible. Therefore, we suggest that adduct **M** is the adduct in which 5'-GMP occupies coordination position 1 and 3'-GMP occupies coordination position 2. Because **M** is more stable than the 3'-GMP 1:2 adduct (which has two N1H–3'-phosphate H-bonds), the results suggest that phosphate–water H-bonding is more favorable than N1H–3'-phosphate H-bonding. The strength of this bond appears to be sufficient to overcome the normal preference of 5'-GMP 1:2 adducts to favor the Δ HT conformation.

2.3.7 Effects of Modifying the Nucleotides

To assess the effect of the exocyclic amino group at the C2 position of the guanine ring, we conducted some studies with 5'-IMP and 3'-IMP (Table 2.4, Figure 2.1). In general, we found products similar to those found above for 5'- and 3'-GMP. At equilibrium, the relative amounts of 1:1 vs 1:2 products formed with IMP's were similar to those with GMP. Therefore, we suggest that the exocyclic amino group of GMP does not contribute to the relative stability of the 1:1 vs 1:2 adducts. This conclusion agrees with a previous report with Pt adducts which indicate that the exocyclic amino group of GMP does not form H-bonds to the cis nucleotide.⁴⁸ The overall amount of 1:1 and 1:2 adducts formed with 5'-IMP and 3'-IMP was slightly less than the amount formed with 5'-GMP and 3'-GMP (data not shown). We believe that the less favorable

formation of adducts by 5'- and 3'-IMP is related to the low N7 basicity of the hypoxanthine base of the IMP's versus that of 5'-GMP.^{70,71}

The rate of reaction of 5'-dGMP and *cis*-[Pt(NH₃)₂(H₂O)₂]²⁺ was reported to be ~10 times faster than that of 5'-GMP and *cis*-[Pt(NH₃)₂(H₂O)₂]²⁺.⁷² This "anomalous" behavior was explained by the lack of flexibility in the ribose ring as compared to the 2'-deoxyribose ring due to the presence of a bulky -OH group on the former.⁷² If this explanation were correct, the difference between 5'-GMP and 5'-dGMP should be even larger for the reactions with the *fac*-[Re(CO)₃(H₂O)₃]⁺ cation, which is somewhat bulkier than the *cis*-[Pt(NH₃)₂(H₂O)₂]²⁺ cation. Therefore, we decided to study the reaction of *fac*-[Re(CO)₃(H₂O)₃]⁺ with 5'-dGMP at *r* = 1:1 and *r* = 1:2 (Table 2.4). We found types of products similar to those found for 5'-GMP. In addition, we performed a mixed experiment with both 5'-GMP and 5'-dGMP at *r* = 1:1:1 ([Re] = 5 mM, pH 3.6). The 5'-dGMP 1:1 adduct formed to about the same extent as the 5'-GMP 1:1 adduct at 1 h (Figure 2.9). Also, the 5'-GMP 1:2 adduct, the 5'-dGMP 1:2 adduct, and the two mixed 5'-GMP/5'-dGMP 1:1:1 adducts are present to about the same extent at equilibrium. These results are an indication that the 2'-substituent of the ribose ring does not exert a great effect on the binding affinity of N7, and the results call into question the proposed effect of the 2'-OH in the reactions of *cis*-[Pt(NH₃)₂(H₂O)₂]²⁺ with 5'-dGMP and 5'-GMP.

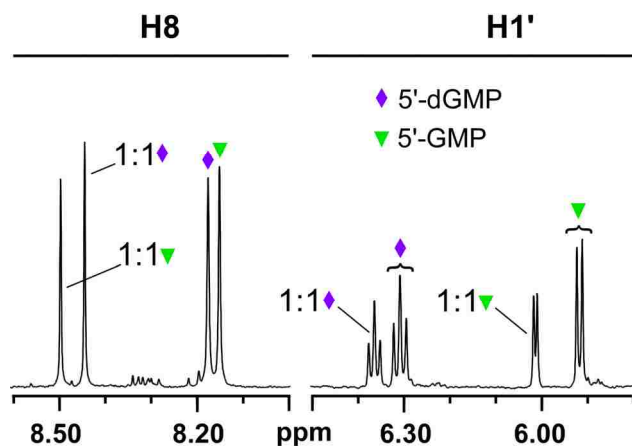


Figure 2.9. H8 and H1' NMR signals of a mixture containing *fac*-[Re(CO)₃(H₂O)₃]⁺ (5 mM), 5'-GMP (5 mM), and 5'-dGMP (5 mM) at pH 3.6 and 1 h after mixing. Symbol alone denotes signals due to free nucleotide. In this *r* = 1:1:1 experiment, only trace amounts of 1:2 adducts are formed at 1 h; these adducts account for the weak signals observed just above the baseline.

Table 2.4. ^1H and ^{31}P NMR Shifts (ppm) and $^3J_{\text{H1}'\text{-H2}'}$ Coupling Constants (Hz, in parentheses) of 5'-GMP, 3'-GMP and 5'-dGMP and Complexes Formed with $\text{fac-}[\text{Re}(\text{CO})_3(\text{H}_2\text{O})_3]^+$ at Different Times after Mixing with $\text{fac-}[\text{Re}(\text{CO})_3(\text{H}_2\text{O})]^+$ ^a

	δ ^1H		
	H8	H1'	H2
5'-IMP	8.41	6.10 (6.0)	8.17
$\text{fac-}[\text{Re}(\text{CO})_3(\text{H}_2\text{O})_2(5'\text{-IMP})]$	8.78	6.21 (3.0)	8.26
$\text{fac-}[\text{Re}(\text{CO})_3(\text{H}_2\text{O})(5'\text{-IMP})_2]^-$	8.62, 8.49	6.09 (3.5), 6.08 (3.0)	8.17, 8.15
3'-IMP	8.30	6.07 (6.0)	8.16
$\text{fac-}[\text{Re}(\text{CO})_3(\text{H}_2\text{O})_2(3'\text{-IMP})]$	8.83	6.17 (3.5)	8.25
$\text{fac-}[\text{Re}(\text{CO})_3(\text{H}_2\text{O})(3'\text{-IMP})_2]^-$	8.68, 8.63	<i>b</i>	8.16, 8.14
5'-dGMP	8.16	6.31 (7.0)	—
$\text{fac-}[\text{Re}(\text{CO})_3(\text{H}_2\text{O})_2(5'\text{-dGMP})]$	8.45	6.37 (6.5)	—
$\text{fac-}[\text{Re}(\text{CO})_3(\text{H}_2\text{O})(5'\text{-dGMP})_2]^-$	8.34, 8.20	6.22 (6.0), 6.30 (6.5)	—

^a $[\text{Re}] = 5 \text{ mM}$, $r = 1:2$, pH 3.6, 25 °C. ^bSignal obscured by other signals.

2.3.8 Competition and Challenge Reactions Using Methionine and 5'-GMP

The well-known toxicity of Pt drugs has been attributed partially to reactions with sulfur-containing biomolecules.⁷³ In methionine vs GMP competition reactions with Pt complexes, Pt binds first to S of methionine, and over time this S-bound product converts to an N7-bound GMP adduct.^{73,74} To assess the binding affinity of 5'-GMP for $\text{fac-}[\text{Re}(\text{CO})_3(\text{H}_2\text{O})_3]^+$, we used a competition reaction in which equimolar amounts of 5'-GMP, methionine, and $\text{fac-}[\text{Re}(\text{CO})_3(\text{H}_2\text{O})_3]^+$ ($[\text{Re}] = 5 \text{ mM}$, $r = 1:1:1$) were present in the reaction mixture. Shortly after mixing (~30 min), approximately half of the 5'-GMP had reacted with $\text{fac-}[\text{Re}(\text{CO})_3(\text{H}_2\text{O})_3]^+$ to form $\text{fac-}[\text{Re}(\text{CO})_3(\text{H}_2\text{O})_2(5'\text{-GMP})]$, while very little methionine had reacted to form products (Table 2.5). After 2 days the reaction mixture contained primarily $\text{fac-}[\text{Re}(\text{CO})_3(\text{H}_2\text{O})_2(5'\text{-GMP})]$

(2.8 mM) and *fac*-[Re(CO)₃(H₂O)_x(methionine)] (1.4 mM, *x* = 1 or 2, Table 2.5). At 1 month after mixing, the reaction mixture contained mostly free 5'-GMP (3.5 mM) and *fac*-[Re(CO)₃(H₂O)_x(methionine)] (3.4 mM). No signals providing evidence for the formation of mixed 5'-GMP/methionine adducts were detected. Therefore, the kinetic product of such a competition reaction is *fac*-[Re(CO)₃(H₂O)₂(5'-GMP)]; however, the thermodynamic product is *fac*-[Re(CO)₃(H₂O)_x(methionine)].

Table 2.5. Concentrations (mM) of 1:1 and 1:2 Adducts of 5'-GMP and Methionine at Different Times after Mixing with *fac*-[Re(CO)₃(H₂O)₃]⁺ ^a in a Competition Reaction

	conc at 30 min	conc at 2 d	conc at 1 month
5'-GMP	2.6	1.6	3.5
<i>fac</i> -[Re(CO) ₃ (H ₂ O) ₂ (5'-GMP)]	2.0	2.8	1.0
<i>fac</i> -[Re(CO) ₃ (H ₂ O)(5'-GMP) ₂] ⁻	<i>b</i>	0.6	0.5
Methionine	4.7	3.6	1.6
<i>fac</i> -[Re(CO) ₃ (H ₂ O) _x (methionine)]	0.3	1.4	3.4

^a[Re] = 5 mM, *r* = 1:1:1. ^bNot observed; amount of 5'-GMP present at 30 min not equal to 5 mM due to formation of ca. 0.4 mM *fac*-[Re₂(CO)₆(H₂O)₄(5'-GMP)]; no *fac*-[Re₂(CO)₆(H₂O)₄(5'-GMP)] was detectable ca. 3 h after mixing.

These results are the opposite of what occurs in similar competition reactions of typical Pt(II) complexes with methionine and 5'-GMP.⁷⁴ To compare the results found here to those of a typical Pt complex, we carried out a Pt/methionine/5'-GMP competition reaction⁷⁴ under the conditions used here ([Pt] = 5 mM, *r* = 1:1:1, pH = 3.6). Again, the methionine adduct was the kinetic product, and this product converted over time to the N7-bound 5'-GMP thermodynamic product (unpublished data). Therefore, even under our low pH conditions, a typical Pt(II) complex has kinetic and thermodynamic preferences opposite to those found here for *fac*-[Re(CO)₃(H₂O)₃]⁺.

2.4 Conclusions

For NMP = GMP or IMP, *fac*-[Re(CO)₃(H₂O)₃]⁺ forms the Re/5'-NMP 1:1 adduct more rapidly than the Re/3'-NMP 1:1 adduct. This result most likely arises from the stabilization of the 5'-NMP 1:1 adduct precursor, which we envision as being an encounter ion pair having inter-ion H-bonding between the 5'-phosphate and a coordinated water molecule. This finding agrees with results for reactions of aquated *cis*-[PtA₂X₂] complexes with 5'- and 3'-NMPs.

In contrast to the normal situation for reactions of *cis*-[PtA₂X₂] complexes with 5'- and 3'-NMPs, the reactions of *fac*-[Re(CO)₃(H₂O)₃]⁺ with 5'- and 3'-NMPs do not go to completion under normal conditions in the presence of 2 equiv of NMP. At equilibrium both 1:1 and 1:2 adducts are present, indicating that the 1:2 adduct may be disfavored because of steric crowding. Adducts with IMP are less stable than those with GMP, a result undoubtedly related to the decreased electron-donating capability of the hypoxanthine base of the IMP's.

The NMR data confirm that all of these adducts have purine bases that rotate rapidly about the Re–N7 bond. This dynamic interchange of rotamers is attributed to the small size of the *cis* CO and H₂O ligands. NOESY data show that HH conformers are not present in significant amounts, and these data plus CD measurements suggest that the Re/NMP 1:2 adducts favor the ΔHT conformation.

Normally, 5'-GMP 1:2 adducts favor the ΔHT conformation.⁴⁵ However, it is proposed that favorable H-bonding interactions of the 5'-GMP phosphate with the coordinated water increases the stability of the ΔHT conformer over the ΛHT conformer. This interaction with coordinated water also explains why for 1:1 adducts, the 5'-NMP 1:1 adduct is favored over the 3'-NMP 1:1 adduct. In the latter, the 3'-phosphate group cannot interact with coordinated water.

In contrast, Re/3'-NMP 1:2 adducts are favored over Re/5'-NMP 1:2 adducts. This preference most likely stems from the presence in the Re/3'-NMP 1:2 adducts of stabilizing H-bonds between the N1H of each 3'-NMP with the phosphate group of the cis-bound 3'-NMP. This type of stabilizing interaction is most favorable in the Δ HT conformation.

Mixed nucleotide experiments, in which two different NMPs are present to react with $fac\text{-}[\text{Re}(\text{CO})_3(\text{H}_2\text{O})_3]^+$, reveal the formation of mixed 1:1:1 adducts; for example, two new mixed Re/5'-GMP/3'-GMP adducts were formed in a 60(*M*):40(*m*) ratio. The most favored mixed species, *M*, was more favored than even the Re/3'-GMP 1:2 adduct. This behavior is attributed to a favorable Δ HT conformer of the 1:1:1 adduct with 5'-GMP in coordination position 1. Only in this 1:1:1 adduct does one expect to have a Δ HT conformer with both phosphate groups participating in stabilizing H-bonds.

A 5'-GMP/methionine competition experiment indicated that $fac\text{-}[\text{Re}(\text{CO})_3(\text{H}_2\text{O})_3]^+$ binds faster to the harder 5'-GMP nitrogen atom, forming $fac\text{-}[\text{Re}(\text{CO})_3(\text{H}_2\text{O})_2(5'\text{-GMP})]$ as a kinetic product, but with time, the softer sulfur atom of methionine is preferred; thus, $fac\text{-}[\text{Re}(\text{CO})_3(\text{H}_2\text{O})_x(\text{methionine})]$ is the thermodynamic product. This relationship of kinetic and thermodynamic preferences is opposite to that for typical Pt complexes. The results offer hope that an anticancer drug based on Re(I) compounds could be developed with lower toxicity than drugs based on Pt.

2.5 References

1. Wang, D.; Lippard, S. J. *Nat. Rev. Drug Discovery* **2005**, *4*, 307-320.
2. *Cisplatin: Chemistry and Biochemistry of a Leading Anticancer Drug*; Wiley-VCH: Weinheim, Germany, 1999.
3. Ano, S. O.; Kuklenyik, Z.; Marzilli, L. G. In *Cisplatin: Chemistry and Biochemistry of a Leading Anticancer Drug*; Lippert, B., Ed.; Wiley-VCH: Weinheim, 1999, pp 247-291.

4. Fichtinger-Schepman, A. M. J.; van der Veer, J. L.; den Hartog, J. H. J.; Lohman, P. H. M.; Reedijk, J. *Biochemistry* **1985**, *24*, 707-713.
5. Hambley, T. W. *Coord. Chem. Rev.* **1997**, *166*, 181-223.
6. Marzilli, L. G.; Saad, J. S.; Kuklenyik, Z.; Keating, K. A.; Xu, Y. *J. Am. Chem. Soc.* **2001**, *123*, 2764-2770.
7. Jamieson, E. R.; Lippard, S. J. *Chem. Rev.* **1999**, *99*, 2467-2498.
8. Beljanski, V.; Villanueva, J. M.; Doetsch, P. W.; Natile, G.; Marzilli, L. G. *J. Am. Chem. Soc.* **2005**, *127*, 15833-15842.
9. Zobi, F.; Blacque, O.; Schmalle, H. W.; Spingler, B.; Alberto, R. *Inorg. Chem.* **2004**, *43*, 2087-2096.
10. Alessio, E.; Mestroni, G.; Bergamo, A.; Sava, G. *Curr. Top. Med. Chem.* **2004**, *4*, 1525-1535.
11. Chifotides, H. T.; Dunbar, K. R. *Acc. Chem. Res.* **2005**, *38*, 146-156.
12. Chifotides, H. T.; Koshlap, K. M.; Pérez, L. M.; Dunbar, K. R. *J. Am. Chem. Soc.* **2003**, *125*, 10714-10724.
13. Frausin, F.; Scarcia, V.; Cocchietto, M.; Furlani, A.; Serli, B.; Alessio, E.; Sava, G. *J. Pharmacol. Exp. Ther.* **2005**, *313*, 227-233.
14. Galanski, M.; Arion, V. B.; Jakupec, M. A.; Keppler, B. *Curr. Pharm. Des.* **2003**, *9*, 2078-2089.
15. Guichard, S. M.; Else, R.; Reid, E.; Zeitlin, B.; Aird, R.; Muir, M.; Dodds, M.; Fiebig, H.; Sadler, P. J.; Jodrell, D. I. *Biochem. Pharmacol.* **2006**, *71*, 408-415.
16. Hayward, R. L.; Schornagel, Q. C.; Tente, R.; Macpherson, J. S.; Aird, R. E.; Guichard, S.; Habtemariam, A.; Sadler, P.; Jodrell, D. I. *Cancer Chemother. Pharmacol.* **2005**, *55*, 577-583.
17. Velders, A. H.; Bergamo, A.; Alessio, E.; Zangrando, E.; Haasnoot, J. G.; Casarsa, C.; Cocchietto, M.; Zorzet, S.; Sava, G. *J. Med. Chem.* **2004**, *47*, 1110-1121.
18. Yan, Y. K.; Melchart, M.; Habtemariam, A.; Sadler, P. J. *Chem. Commun.* **2005**, 4764-4776.
19. Yan, Y.-K.; Cho, S. E.; Shaffer, K. A.; Rowell, J. E.; Barnes, B. J.; Hall, I. H. *Pharmazie* **2000**, *55*, 307-313.

20. Zobi, F.; Alberto, R.; Spingler, B.; Fox, T. In *Technetium, Rhenium and Other Metals in Chemistry and Nuclear Medicine*; Nicolini, M., Mazzi, U., Eds.; SGEEditoriali: Padova, Italy, 2002; Vol. 6, pp 97-105.
21. Zobi, F.; Spingler, B.; Fox, T.; Alberto, R. *Inorg. Chem.* **2003**, *42*, 2818-2820.
22. Jiang, C.; Hor, T. S. A.; Yan, Y.-K.; enderson, W.; McCaffrey, L. J. *J. Chem. Soc., Dalton Trans.* **2000**, *18*, 3197-3203.
23. Egli, A.; Hegetschweiler, K.; Alberto, R.; Abram, U.; Schibli, R.; Hedinger, R.; Gramlich, V.; Kissner, R.; Schubiger, P. A. *Organometallics* **1997**, *16*, 1833-1840.
24. Salignac, B.; Grundler, P. V.; Cayemittes, S.; Frey, U.; Scopelliti, R.; Merbach, A. E.; Hedinger, R.; Hegetschweiler, K.; Alberto, R.; Prinz, U.; Raabe, G.; Kölle, U.; Hall, S. *Inorg. Chem.* **2003**, *42*, 3516-3526.
25. den Hartog, J. H. J.; Altona, C.; van der Marel, G. A.; Reedijk, J. *Eur. J. Biochem.* **1985**, *147*, 371-379.
26. Dijt, F.; Canters, G. W.; den Hartog, J. H. J.; Marcelis, A. T. M.; Reedijk, J. *J. Am. Chem. Soc.* **1984**, *106*, 3644-3647.
27. Marcelis, A. T. M.; Erkelens, C.; Reedijk, J. *Inorg. Chim. Acta* **1984**, *91*, 129-135.
28. Marcelis, A. T. M.; van Kralingen, C. G.; Reedijk, J. *J. Inorg. Biochem.* **1980**, *13*, 213-222.
29. Miller, S. K.; Marzilli, L. G. *Inorg. Chem.* **1985**, *24*, 2421-2425.
30. Wirth, W.; Blotevogel-Baltronat, J.; Kleinkes, U.; Sheldrick, W. S. *Inorg. Chim. Acta* **2002**, *339*, 14-26.
31. He, H.; Lipowska, M.; Xu, X.; Taylor, A. T.; Carlone, M.; Marzilli, L. G. *Inorg. Chem.* **2005**, *44*, 5437-5446.
32. Schweizer, M. P.; Chan, S. I.; Helmkamp, G. K.; Ts'o, P. O. P. *J. Am. Chem. Soc.* **1964**, *86*, 696-700.
33. Girault, J.-P.; Chottard, G.; Lallemand, J.-Y.; Chottard, J.-C. *Biochemistry* **1982**, *21*, 1352-1356.
34. Reily, M. D.; Hambley, T. W.; Marzilli, L. G. *J. Am. Chem. Soc.* **1988**, *110*, 2999-3007.
35. Reily, M. D.; Marzilli, L. G. *J. Am. Chem. Soc.* **1986**, *108*, 8299-8300.
36. Kuo, L. Y.; Kanatzidis, M. G.; Marks, T. J. *J. Am. Chem. Soc.* **1987**, *109*, 7207-7209.

37. Torres, L. M.; Marzilli, L. G. *J. Am. Chem. Soc.* **1991**, *113*, 4678-4679.
38. Bose, R. N.; Goswami, N.; Moghaddas, S. *Inorg. Chem.* **1990**, *29*, 3461-3467.
39. Bose, R. N.; Slavia, L. L.; Cameron, J. W.; Luellen, D. L.; Viola, R. E. *Inorg. Chem.* **1993**, *32*, 1795-1802.
40. Ano, S. O.; Intini, F. P.; Natile, G.; Marzilli, L. G. *J. Am. Chem. Soc.* **1998**, *120*, 12017-12022.
41. Marzilli, L. G.; Ano, S. O.; Intini, F. P.; Natile, G. *J. Am. Chem. Soc.* **1999**, *121*, 9133-9142.
42. Cramer, R. E.; Dahlstrom, P. L. *Inorg. Chem.* **1985**, *24*, 3420-3424.
43. Ano, S. O.; Intini, F. P.; Natile, G.; Marzilli, L. G. *Inorg. Chem.* **1999**, *38*, 2989-2999.
44. Marzilli, L. G.; Intini, F. P.; Kiser, D.; Wong, H. C.; Ano, S. O.; Marzilli, P. A.; Natile, G. *Inorg. Chem.* **1998**, *37*, 6898-6905.
45. Natile, G.; Marzilli, L. G. *Coord. Chem. Rev.* **2006**, *250*, 1315-1331.
46. Sullivan, S. T.; Ciccarese, A.; Fanizzi, F. P.; Marzilli, L. G. *Inorg. Chem.* **2000**, *39*, 836-842.
47. Wong, H. C.; Intini, F. P.; Natile, G.; Marzilli, L. G. *Inorg. Chem.* **1999**, *38*, 1006-1014.
48. Wong, H. C.; Shinozuka, K.; Natile, G.; Marzilli, L. G. *Inorg. Chim. Acta* **2000**, *297*, 36-46.
49. Benedetti, M.; Tamasi, G.; Cini, R.; Marzilli, L. G.; Natile, G. *Chem. Eur. J.* **2007**, *13*, 3131-3142.
50. Cramer, R. E.; Dahlstrom, P. L.; Seu, M. J. T.; Norton, T.; Kashiwagi, M. *Inorg. Chem.* **1980**, *19*, 148-154.
51. Inagaki, K.; Dijt, F. J.; Lempers, E. L. M.; Reedijk, J. *Inorg. Chem.* **1988**, *27*, 382-387.
52. Marcelis, A. T. M.; van der Veer, J. L.; Zwetsloot, J. C. M.; Reedijk, J. *Inorg. Chim. Acta* **1983**, *78*, 195-203.
53. Marzilli, L. G.; Chalilpoyil, P. *J. Am. Chem. Soc.* **1980**, *102*, 873-875.
54. Marzilli, L. G.; Chalilpoyil, P.; Chiang, C. C.; Kistenmacher, T. J. *J. Am. Chem. Soc.* **1980**, *102*, 2480-2482.
55. Saad, J. S.; Scarcia, T.; Natile, G.; Marzilli, L. G. *Inorg. Chem.* **2002**, *41*, 4923-4935.
56. Sullivan, S. T.; Ciccarese, A.; Fanizzi, F. P.; Marzilli, L. G. *Inorg. Chem.* **2001**, *40*, 455-462.

57. Wong, H. C.; Coogan, R.; Intini, F. P.; Natile, G.; Marzilli, L. G. *Inorg. Chem.* **1999**, *38*, 777-787.
58. Sigel, H.; Massoud, S. S.; Corfù, N. A. *J. Am. Chem. Soc.* **1994**, *116*, 2958-2971.
59. Song, B.; Zhao, J.; Griesser, R.; Meiser, C.; Sigel, H.; Lippert, B. *Chem. Eur. J.* **1999**, *5*, 2374-2387.
60. Williams, K. M.; Cerasino, L.; Intini, F. P.; Natile, G.; Marzilli, L. G. *Inorg. Chem.* **1998**, *37*, 5260-5268.
61. Berners-Price, S. J.; Frey, U.; Ranford, J. D.; Sadler, P. J. *J. Am. Chem. Soc.* **1993**, *115*, 8649-8659.
62. Berners-Price, S. J.; Ranford, J. D.; Sadler, P. J. *Inorg. Chem.* **1994**, *33*, 5842-5846.
63. Reily, M. D.; Marzilli, L. G. *J. Am. Chem. Soc.* **1986**, *108*, 6785-6793.
64. Song, B.; Oswald, G.; Bastian, M.; Sigel, H.; Lippert, B. *Metal-Based Drugs* **1996**, *3*, 131-141.
65. Marzilli, L. G. In *Prog. Inorg. Chem.*; Lippard, S. J., Ed.; John Wiley and Sons: New York, 1977; Vol. 23, pp 255-278.
66. Benedetti, M.; Saad, J. S.; Marzilli, L. G.; Natile, G. *Dalton Trans.* **2003**, 872-879.
67. Bhattacharyya, D.; Marzilli, P. A.; Marzilli, L. G. *Inorg. Chem.* **2005**, *44*, 7644-7651.
68. Bloemink, M. J.; Heetebrij, R. J.; Ireland, J.; Deacon, G. B.; Reedijk, J. *J. Biol. Inorg. Chem.* **1996**, *1*, 278-283.
69. Saad, J. S.; Scarcia, T.; Shinozuka, K.; Natile, G.; Marzilli, L. G. *Inorg. Chem.* **2002**, *41*, 546-557.
70. Dawson, R. M. C.; Elliott, D. C.; Elliott, W. H.; Jones, K. M. *Data for Biochemical Research*; 3rd ed.; Clarendon Press: Oxford, 1986.
71. Martin, R. B. *Acc. Chem. Res.* **1985**, *18*, 32-38.
72. Evans, D. J.; Green, M.; van Eldik, R. *Inorg. Chim. Acta* **1987**, *128*, 27-29.
73. Djuran, M. I.; Lempers, E. L. M.; Reedijk, J. *Inorg. Chem.* **1991**, *30*, 2648-2652.
74. Christoforou, A. M.; Marzilli, P. A.; Marzilli, L. G. *Inorg. Chem.* **2006**, *45*, 6771-6781.

CHAPTER 3.

REACTIONS OF *fac*-[Re(CO)₃(H₂O)₃]⁺ WITH NUCLEOSIDE DIPHOSPHATES AND THIAMINE DIPHOSPHATE IN AQUEOUS SOLUTION INVESTIGATED BY MULTINUCLEAR NMR SPECTROSCOPY*

3.1 Introduction

The participation of nucleotides in a large variety of biochemical processes, usually as metal ion complexes, has prompted a large number of investigations of metal-ion binding to nucleotides in solution.¹⁻⁴ Most of the literature is focused on nucleoside mono- and triphosphates. Because of the dynamic conformational changes characteristic of nucleotides and the lability of most biologically important metals such as Mg²⁺, nucleotide coordination propensity is often assessed by using inert metal centers, which usually afford definitive results.⁵⁻⁹ However, the binding of nucleoside diphosphates to metal centers has been the subject of very few studies, particularly with inert metal complexes.^{8,10,11}

In recent years, the importance of Pt anticancer drugs has led to many informative investigations of Pt(II) complexes of nucleoside mono- and triphosphates.¹²⁻¹⁶ However, the octahedral geometry is more relevant to natural biological processes. More recently, we and others have recognized that the octahedral *fac*-[Re(CO)₃(H₂O)₃]⁺ cation is another inert, redox-stable metal center that can be used to study metal interactions with nucleotides.¹⁷⁻¹⁹ Compared to Pt(II) compounds, the *fac*-[Re(CO)₃(H₂O)₃]⁺ cation may have a higher affinity for oxygen donors.²⁰ Previous work demonstrated that reactions of *fac*-[Re(CO)₃(H₂O)₃]⁺ and nucleoside monophosphates (NMPs) attained equilibrium, forming predominantly Re/NMP 1:1 complexes

* Reproduced with permission from American Chemical Society: Adams, K. M., Marzilli, P. A., Marzilli, L. G., "Reactions of *fac*-[Re(CO)₃(H₂O)₃]⁺ with Nucleoside Diphosphates and Thiamine Diphosphate in Aqueous Solution Investigated by Multinuclear NMR Spectroscopy," *Inorganic Chemistry*, **2007**, *46*, 9172-9181. Copyright 2007 American Chemical Society.

with Re(I) bound via N7 of the NMP; no {N7,P α } macrochelate-type complexes were identified.¹⁷ However, the second phosphate group of monoester diphosphates (MDPs) provides additional binding sites for the *fac*-[Re(CO)₃]⁺ center; thus, different products could result.



Figure 3.1. TDP (top). Base portion of 5'-UDP (middle left) and 5'-GDP (middle right) and the R group bearing the diphosphate moiety (bottom).

3.1.1 Stereochemistry and Nomenclature

The MDPs studied here (Figure 3.1) have the following characteristics: no asymmetric ribose nor Re(I)-binding base (thiamine diphosphate, TDP), an asymmetric ribose but no Re(I)-binding base (uridine 5'-diphosphate, 5'-UDP), or an asymmetric ribose and a Re(I)-binding base (guanosine 5'-diphosphate, 5'-GDP). Although there are potential metal-binding sites on all three base moieties, both N1' (thiamine, p*K*_a ~5) and N3 (uridine, p*K*_a ~10) are protonated at pH 3.6, used here; the N7 of guanine (p*K*_a < 2) is available for binding to Re(I).^{4,21} As the complexity of

the MDP increases, the number of possible adducts formed by $fac-[Re(CO)_3(H_2O)_3]^+$ increases in the order, TDP < 5'-UDP < 5'-GDP. Note: in designating the adducts, we omit the 5'- to simplify the designation, but retain the 5'- when referring to the free nucleotide.

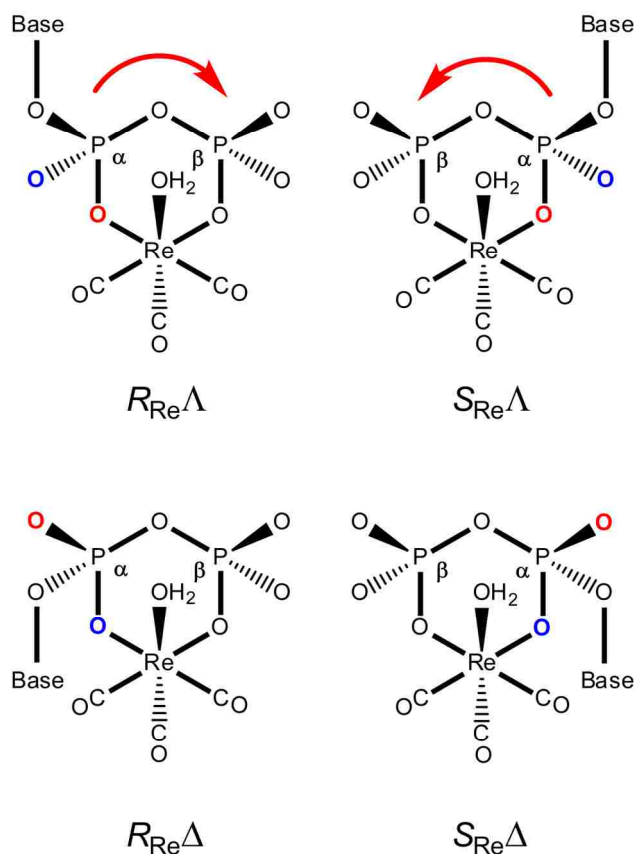


Figure 3.2. Four possible isomers of $fac-[Re(CO)_3(\{P_\alpha, P_\beta\}MDP)]^-$; $R_{Re}\Delta/S_{Re}\Delta$ and $R_{Re}\Lambda/S_{Re}\Lambda$ are mirror image pairs if the attached ester moiety has no chiral groups. Arrows indicate sense of rotation defining chirality at Re(I). The blue O and the red O are the pro- Δ and pro- Λ oxygens in the free nucleotide, respectively.

Unidentate coordination of an MDP (MDP = TDP, 5'-UDP, 5'-GDP) to $fac-[Re(CO)_3(H_2O)_3]^+$ could occur in three possible ways. Coordination via the terminal P_β group of an MDP would result in the formation of a single isomer, as the P_β group is not prochiral. Unidentate coordination of the prochiral P_α group (although unlikely) would create an

asymmetric P_α center and two isomers. The terminal oxygens of the prochiral P_α group are labeled pro- Δ and pro- Λ in Figure 3.2. Coordination via N7 of 5'-GDP would lead to a single isomer.

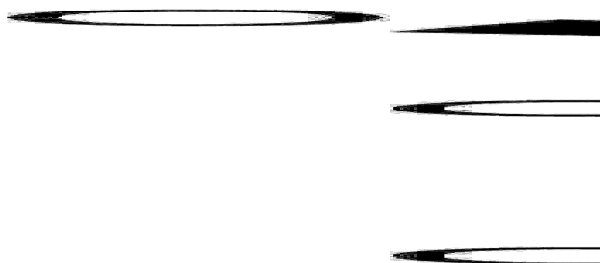


Figure 3.3. R_{Re} and S_{Re} isomers of $fac-[Re(CO)_3(H_2O)_3(\{N7,P_\beta\}GDP)]^-$. Only these two isomers are possible when P_α is not bound to $Re(I)$. The R_{Re} and S_{Re} isomers are tentatively assigned as ***M*** and ***m***, respectively.

Bidentate coordination to $fac-[Re(CO)_3(H_2O)_3]^+$ by *both* P_α and P_β of an MDP, forming $fac-[Re(CO)_3(H_2O)_3(\{P_\alpha,P_\beta\}MDP)]^-$, creates asymmetric centers at both P_α and $Re(I)$. Up to four diastereomers could exist for the MDP used here. Naming the isomers requires designation of the chirality of these asymmetric centers. First, the asymmetry at P_α depends on which oxygen (pro- Δ or pro- Λ) binds to $Re(I)$ (Figure 3.2).⁵⁻⁷ Second, designation of the asymmetry of the $Re(I)$ center is based on the direction of rotation of the MDP around a reference axis defined by a line passing through the $Re(I)$ atom perpendicular to the chelate ring (assumed to be planar as shown in Figure 3.2) and passing through the CO (away from the viewer).⁵⁻⁷ The asymmetry at $Re(I)$ is then designated as R_{Re} and S_{Re} for clockwise and counterclockwise rotation, respectively (Figure 3.2). Although we adhere to the naming protocol described here, we should note that application of the *R,S* system (according to Cahn–Ingold–Prelog priority rules) to other metal–chelate

complexes can lead to reversals of the letter designation.⁵ In *fac*-[Re(CO)₃(H₂O)({P_α,P_β}MDP)]⁻ adducts, the four possible diastereomers constitute two enantiomeric pairs (two sets of NMR signals, *R*_{Re}Δ/*S*_{Re}Λ and *R*_{Re}Λ/*S*_{Re}Δ) for TDP but four NMR-distinct isomers for 5'-UDP (*R*_{Re}Δ, *R*_{Re}Λ, *S*_{Re}Δ, *S*_{Re}Λ, Figure 3.2). Were 5'-GDP to bind in this manner, there would again be four NMR-distinct diastereomers. However, we did not detect clear evidence for such a species because 5'-GDP binds via N7 in all major species we identified; Re(I) coordination via N7 of 5'-GDP presents different possibilities for adduct formation. Bidentate coordination through N7 and P_β of 5'-GDP creates only one asymmetric center (at Re(I)). If the resulting pair of diastereomers (*R*_{Re} and *S*_{Re}) of *fac*-[Re(CO)₃(H₂O)({N7,P_β}GDP)]⁻ (Figure 3.3) is conformationally dynamic, only two sets of NMR signals are expected. Tridentate coordination of N7, P_α, and P_β of 5'-GDP, to form the *fac*-[Re(CO)₃{N7,P_α,P_β}GDP)]⁻ adduct, would result in four NMR-distinct diastereomers because this adduct contains both Re(I) and P_α asymmetric centers. The number of possible adducts and NMR-observable distinct sets of signals are summarized in Table 3.1.

Table 3.1. Possible Isomers Formed by the Reaction of *fac*-[Re(CO)₃(H₂O)₃]⁺ with MDPs

complex	diastereomers	mirror pairs	<i>possible</i> sets of signals	<i>observed</i> sets of signals
{P _α ,P _β }TDP	4	2	2	2
{P _α ,P _β }UDP	4	0	4	4
{N7,P _α ,P _β }GDP	4	0	4	^a
{N7,P _β }GDP	2	0	2	2

^aNot observed.

3.2 Experimental Section

3.2.1 Materials and Sample Preparation

Stock solutions (10 mM and 50 mM) of *fac*-[Re(CO)₃(H₂O)₃]OTf in H₂O were prepared by published procedures and maintained at pH ~1.8.²² 5'-GDP, 5'-UDP (disodium salts), TDP, sodium pyrophosphate (PP), and D₂O (99.9%) (Sigma-Aldrich) were used as received.

A typical preparation of samples for 1D NMR spectroscopy involved treatment of an appropriate amount of MDP in 0.3 mL of H₂O with 0.4 mL of an ~10 mM stock solution of *fac*-[Re(CO)₃(H₂O)₃]OTf; a small amount (0.1 mL) of D₂O was added to establish a lock signal. For 2D NMR spectroscopy, samples were prepared by removing H₂O from an aqueous 0.4 mL aliquot of a ~50 mM stock solution of *fac*-[Re(CO)₃(H₂O)₃]OTf and adding 0.4 mL of D₂O; then, the appropriate amount of MDP (in 0.4 mL D₂O) was added. The pH (uncorrected) of the samples in NMR tubes was maintained at ~3.6 by the addition of dilute HCl and NaOH (in H₂O) or DCl and NaOD (in D₂O) stock solutions, as required. The pH of each sample was adjusted before the acquisition of each NMR spectrum. Because spectra were acquired at frequent intervals relative to the ~1 day half-life of each reaction, the reactions proceeded at a pH close to 3.6. At early stages of the reactions, the pH changes were larger, and generally the pH dropped. However, our focus was on the products, not on the reaction rates of product formation.

3.2.2 NMR Spectroscopy

All NMR spectra were obtained on a Varian INOVA500 spectrometer (500.1 MHz) equipped with a variable-temperature probe that was equilibrated at 25 °C unless otherwise indicated. A 1 s presaturation pulse was used to reduce the HOD peak in 1D ¹H NMR spectra, and the residual HOD signal was used to reference the spectrum. Each FID was accumulated for

32 transients, each containing 32K data points. Before Fourier transformation, an exponential apodization window function with a 0.2 Hz line-broadening was applied. 1D proton-decoupled ^{31}P NMR spectra ($\{^1\text{H}\}\text{-}^{31}\text{P}$) were referenced to external trimethyl phosphate (TMP); each FID was accumulated for 128 transients, each containing 8K data points. Before Fourier transformation, an exponential apodization window function with a 0.5 Hz line-broadening was applied.

In general, 32 scans per block (512 blocks) were collected in $^1\text{H}\text{-}^1\text{H}$ rotating frame nuclear Overhauser effect spectroscopy (ROESY) experiments conducted by using a spectral width of ~ 6000 Hz in both dimensions and a mixing time of 500 ms at 25 °C and 32 °C. Proton-decoupled $^{31}\text{P}\text{-}^{31}\text{P}$ nuclear Overhauser effect spectroscopy (NOESY) exchange experiments were conducted by using 32 scans per block (422 blocks) and a spectral width of ~ 5000 Hz in both dimensions and a mixing time of 500 ms at 32 °C. Proton-decoupled $^{31}\text{P}\text{-}^{31}\text{P}$ correlation spectroscopy (COSY) experiments containing 32 scans per block (734 blocks) were conducted by using a spectral width of ~ 4400 Hz in both dimensions and a COSY-45 pulse sequence to aid in visualizing close coupling patterns. All NMR data were processed with VnmrJ (Varian) software.

3.2.3 Computational Methods

All models were constructed on a PC equipped with the Hyperchem 7.5²³ molecular modeling package, and all computations were performed using AMBER99 force field parameters and methods described previously.²⁴ Four models (two R_{Re} and two S_{Re} models) of *fac*- $[\text{Re}(\text{CO})_3(\text{H}_2\text{O})(\{\text{N7}, \text{P}_\beta\}\text{GDP})]^-$ were built by using information obtained through NMR studies and derived from the X-ray crystal structure of *fac*- $[\text{Re}(\text{CO})_3(\text{H}_2\text{O})(9\text{-MeG})_2]^+$.¹⁸ The Re-N7 distance in all four models was constrained to ~ 2.2 Å. The H2'-C2'-C1'-H1' angle of one R_{Re}

and one S_{Re} model was constrained to 67° (equal to a ${}^3J_{\text{H1}'\text{-H2}'}$ value of 1 Hz), and the $\text{H2}'\text{-C2}'\text{-C1}'\text{-H1}'$ angle of the other R_{Re} and S_{Re} models was constrained to 41° (equal to a ${}^3J_{\text{H1}'\text{-H2}'}$ value of 4.5 Hz). The H8 proton was oriented close in space to $\text{H2}'$ and $\text{H3}'$ in all four models, as the NOE data (see above) confirms this close proximity for all adducts formed. The models were geometrically minimized using Polak–Ribiere conjugate gradient minimization, which was terminated upon reaching an rms gradient of $0.01 \text{ kcal}/\text{\AA}\cdot\text{mol}$.

3.3 Results and Discussion

Shift changes of the ${}^1\text{H}$ and ${}^{31}\text{P}$ NMR signals of the MDP upon coordination are informative. In general, ${}^1\text{H}$ and ${}^{31}\text{P}$ NMR signals arising from atoms close to the metal binding site will shift downfield upon coordination because of an inductive effect of the metal center. Because deprotonation of $\text{fac-}[\text{Re}(\text{CO})_3(\text{H}_2\text{O})_3]^+$ begins around pH 4 and causes oligomerization, we conducted most studies at pH 3.6 as in previous work.^{17,20} In addition, $5'$ -GDP is protonated at N7 to a very limited extent at pH 3.6 (see NMR shift data in Appendix B), thereby allowing metal coordination; also, the low pH assures no significant deprotonation of N1H, thereby precluding metal binding at N1. Coordination of Re(I) at N7 of $5'$ -GMP causes a ~ 0.4 ppm downfield shift of the H8 signal and a slight upfield shift (~ 0.3 ppm) of the P_α signal, while coordination of one Re(I) metal center at N7 and another at P_α of the same $5'$ -GMP leads to a ~ 0.4 ppm downfield shift of the H8 signal but a larger ~ 4 ppm downfield shift of the P_α signal.¹⁷ At pH ~ 3.6 , the P_β group of the free MDP is protonated and the phosphate chain carries two negative charges (Figure 3.1).

Throughout this section, concentrations will be denoted as ($__ \text{ mM}$, $r = __ : __$), in which the $\text{fac-}[\text{Re}(\text{CO})_3(\text{H}_2\text{O})_3]^+$ concentration is stated and r is the ratio of the cation to added

phosphate ligand. This notation designates both the starting ligand concentration and its ratio to the starting $fac\text{-}[\text{Re}(\text{CO})_3(\text{H}_2\text{O})_3]^+$ concentration.

As a first step, we employed diprotonated pyrophosphate (PP^{2-}) to assess the effects of chelate ring formation on ^{31}P NMR shifts at pH ~ 3.6 . A single product ^{31}P NMR signal, shifted ~ 7 ppm downfield from the ^{31}P NMR signal of free PP^{2-} (Table 3.2), was observed 1 day after mixing $fac\text{-}[\text{Re}(\text{CO})_3(\text{H}_2\text{O})_3]^+$ and PP^{2-} (25 mM, $r = 1:1$ and $1:2$). At equilibrium (no changes from 3 to 6 days), $\sim 60\%$ of the PP^{2-} had reacted, indicating incomplete product formation. The appearance of one signal indicates that $fac\text{-}[\text{Re}(\text{CO})_3(\text{H}_2\text{O})(\text{PP})]^-$, in which both phosphate groups chelate Re(I), is the reaction product.

Table 3.2. ^1H and ^{31}P NMR Chemical Shifts (ppm), Coupling Constants (Hz) of TDP, 5'-UDP, PP, and Complexes Formed with $fac\text{-}[\text{Re}(\text{CO})_3(\text{H}_2\text{O})_3]^+$ ^a

complex	δ ^1H		δ ^{31}P	
PP	—	—	-13.8	
$fac\text{-}[\text{Re}(\text{CO})_3(\text{H}_2\text{O})(\text{PP})]^-$	—	—	-6.6	
	H2	H6'	$\text{P}_\alpha (J_{\alpha\beta})$	P_β
TDP	9.62	7.88	-14.7 (22.3)	-14.0
<i>M</i> pair	9.71	7.79	-9.0 (19.8)	-5.0
<i>m</i> pair	9.67	7.77	-8.4 (19.6)	-4.9
	H6	$\text{H1}' (^3J_{\text{H1}'\text{-H2}'})$	$\text{P}_\alpha (J_{\alpha\beta})$	$\text{P}_\beta (J_{\beta\alpha})$
5'-UDP	7.94 ^b	5.98 (4.5) ^c	-14.4 (20.2)	-13.8 (20.3)
<i>M</i> ₁	7.98 ^b	5.95 ^c	-9.2 (20.6)	-5.4 (20.4)
<i>m</i> ₁	7.88 ^b	5.95 ^c	-8.8 (19.8)	-5.6 (20.7)
<i>M</i> ₂	7.87 ^b	5.95 ^c	-8.5 (19.8)	-5.7 (20.2)
<i>m</i> ₂	7.86 ^b	5.95 ^c	-8.5 (19.8)	-5.5 (20.2)

^a25 mM, $r = 1:1$, pH 3.6. ^b $^3J_{\text{H5-H6}} = 8.1$ Hz. ^cH1' signals overlap with H5 signals.

3.3.1 Overview of Products Formed by *fac*-[Re(CO)₃(H₂O)₃]⁺ and MDPs

In describing the results for MDP binding to *fac*-[Re(CO)₃(H₂O)₃]⁺, we state the nature of the adducts formed before presenting all the ¹H and ³¹P NMR spectral evidence and the reasoning for adduct designations. We should note that no evidence was found for the formation of significant amounts of either unidentate adducts (bound through only one phosphate oxygen) or 1:2 adducts for any MDP, even in *r* = 1:2 reaction mixtures.

3.3.2 TDP Reaction Products

TDP formed a 1:1 adduct, *fac*-[Re(CO)₃(H₂O)({P_α,P_β}TDP)]⁻, for which four diastereomers are possible (Figure 3.2). Because these are two mirror-image pairs (*R*_{ReΔ}/*S*_{ReΛ} and *R*_{ReΛ}/*S*_{ReΔ}), only two sets of ¹H and ³¹P NMR signals for bound TDP were observed. The more intense set is labeled ***M*** for the major mirror-image pair, and the other set is labeled ***m*** for the minor mirror-image pair.

Although the 5a and 5b multiplets are for TDP protons close to the metal-binding P_α phosphate group (Figure 3.1), these multiplets have chemical shifts very close to that of residual HOD. Thus, the H2 and H6' singlets, although for protons remote from the metal-binding site, are also used to provide information about the adducts formed. Approximately 1 day after *fac*-[Re(CO)₃(H₂O)₃]⁺ and TDP (25 mM, *r* = 1:1) were mixed, the NMR spectrum showed two new H2 and two new H6' singlets, shifted slightly downfield and slightly upfield, respectively, from the corresponding H2 and H6' signals of free TDP (Table 3.2). Although partially obscured by the residual HOD peak, two sets of 5b multiplets (shifted downfield from the 5b multiplet of free TDP) were observed. At equilibrium (no changes from 3 to 6 days), the ratio of ***M*** pair/***m*** pair was 2:1 and only ~35% of the TDP had reacted, indicating incomplete product formation.

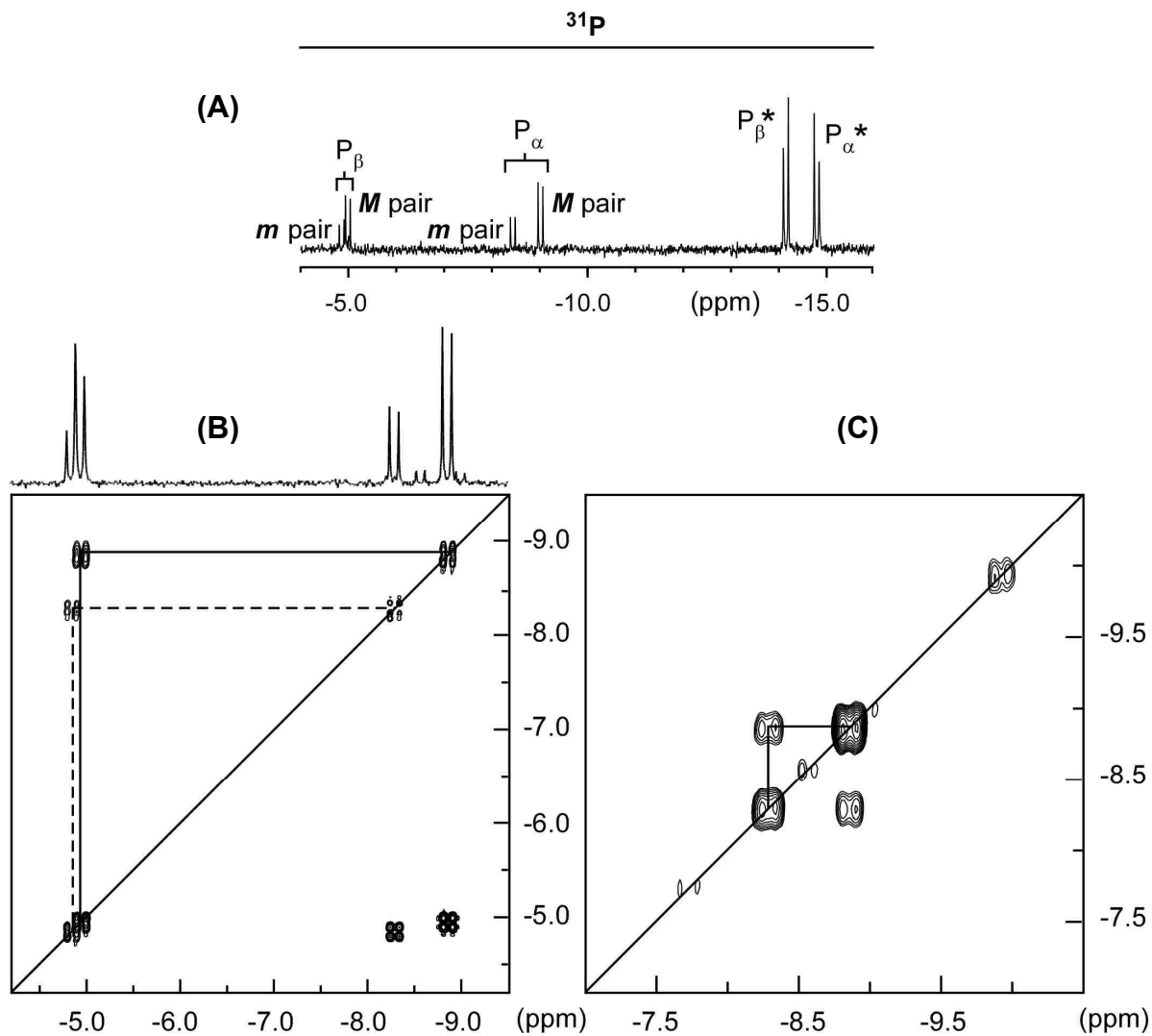


Figure 3.4. ³¹P NMR (A), ³¹P-³¹P COSY (B), and ³¹P-³¹P NOESY (C) spectra of an equilibrium mixture of *fac*-[Re(CO)₃(H₂O)₃]⁺ (25 mM, $r = 1:1$) and TDP at pH 3.6. Asterisk labels indicate peaks arising from free TDP.

The $\{^1\text{H}\}$ -³¹P NMR spectrum of the (25 mM, $r = 1:1$) reaction mixture revealed two P_α doublets at ca. -8.7 ppm and two P_β doublets at ca. -5.0 ppm, shifted ~6 and ~9 ppm downfield from the respective free TDP signals (Figure 3.4). The P_α vs P_β assignments were confirmed with a proton-coupled ³¹P NMR spectrum. A proton-decoupled ³¹P-³¹P COSY experiment (25 mM, $r = 1:1$) showed coupling between doublets at -9.0 ppm (P_α) and -5.0 ppm (P_β) for the

major pair (*M* pair), and doublets at -8.4 ppm (P_α) and -4.9 ppm (P_β) for the minor pair (*m* pair, Figure 3.4). In addition, a ^{31}P - ^{31}P NOESY spectrum showed exchange between the two P_α doublets and between the P_β doublets, indicating that interconversion of the isomers does occur, but in the slow-exchange regime of the NMR time scale (see below).

The P_β signals of *M* pair and *m* pair shifted ~ 4 ppm downfield between pH 1.5 and 3.5 during an NMR-monitored titration from pH 1.5 to 6.5, leading to a pK_a estimate of ~ 2.5 for P_β of both the *M* and *m* pairs. The low value of the estimated P_β pK_a is likely due to the presence of a proton on N1'.

3.3.3 5'-UDP Reaction Products

5'-UDP formed a 1:1 adduct, $\text{fac-}[\text{Re}(\text{CO})_3(\text{H}_2\text{O})(\{P_\alpha, P_\beta\}\text{UDP})]^-$, exhibiting ^1H and ^{31}P NMR signals of four diastereomers. (The $\text{Re}/5'\text{-UDP}$ 1:1 ratio in the adduct was confirmed in the mixed-nucleotide experiment described below.) Because the H5 and H1' signals overlap, only the H6 signals are informative. ^1H NMR spectra of $\text{fac-}[\text{Re}(\text{CO})_3(\text{H}_2\text{O})_3]^+$ treated with 5'-UDP (25 mM, $r = 1:1$) showed after ~ 1 day one large H6 doublet (*M₁*) and three smaller H6 doublets (*M₂*, *m₁*, *m₂*), shifted slightly *downfield* and slightly *upfield*, respectively, from the H6 doublet of free 5'-UDP (Figure 3.5, Table 3.2). The small size of the shifts indicates no base binding. At equilibrium (no changes from 3 to 6 days), $\sim 40\%$ of the 5'-UDP had reacted (17% large H6 and 23% other three H6's combined), indicating that 5'-UDP product formation is about as favorable as TDP product formation at $r = 1:1$. This finding is consistent with the absence of base binding for both MDPs.

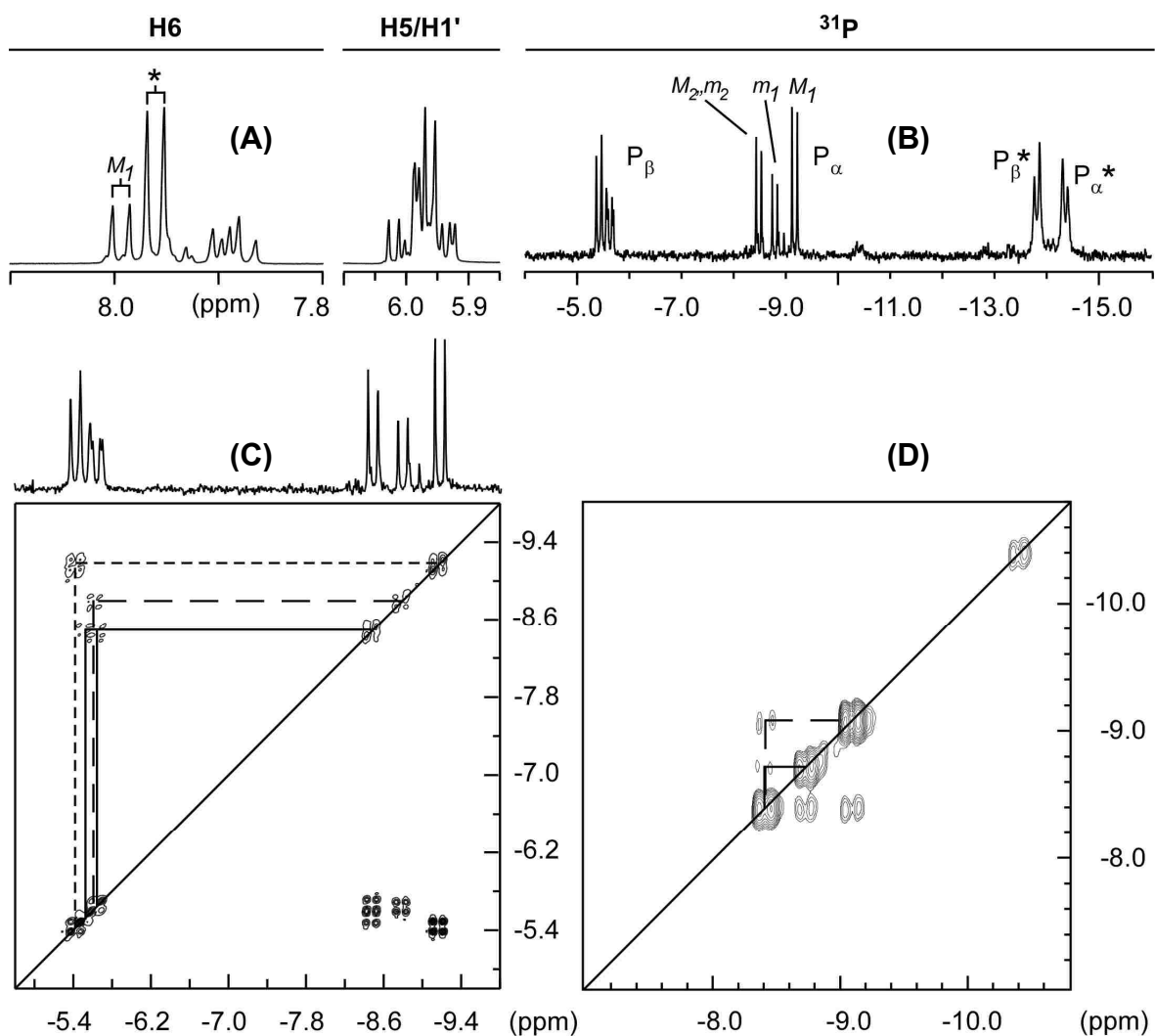


Figure 3.5. ^1H NMR (A), ^{31}P NMR (B), ^{31}P - ^{31}P COSY (C), and ^{31}P - ^{31}P NOESY (D) spectra of an equilibrium mixture of *fac*- $[\text{Re}(\text{CO})_3(\text{H}_2\text{O})_3]^+$ (25 mM, $r = 1:1$) and 5'-UDP at pH 3.6. Asterisk labels indicate peaks arising from free 5'-UDP.

The $\{^1\text{H}\}$ - ^{31}P NMR spectrum of the (25 mM, $r = 1:1$) reaction mixture revealed three well-separated P_α doublets at ca. -8.8 ppm and four overlapping P_β doublets at ca. -5.6 ppm, shifted ~ 6 and ~ 8 ppm downfield from the respective free 5'-UDP signals (Figure 3.5). The P_α doublets are assigned as follows. Most upfield, M_1 ; intermediate, m_1 ; the most downfield, both M_2 and m_2 . The P_α vs P_β assignments were confirmed with a proton-coupled ^{31}P NMR spectrum. A

proton-decoupled ^{31}P - ^{31}P COSY experiment (25 mM, $r = 1:1$) revealed the M_1/M_2 and m_1/m_2 connectivities between the P_α and P_β signals (Figure 3.5). The ^{31}P - ^{31}P NOESY spectrum showed exchange between the downfield overlapped M_2 and m_2 P_α doublet and the two M_1 and m_1 P_α doublets, but no exchange between the M_1 and m_1 P_α doublets was detected (see below).

3.3.3.1 Mixed-Nucleotide Experiment

To investigate the Re/nucleotide ratio of the products, we treated *fac*- $[\text{Re}(\text{CO})_3(\text{H}_2\text{O})_3]^+$ with a mixture of TDP and 5'-UDP (25 mM, $r = 1:0.5:0.5$ and $1:1:1$). If the adducts identified above as 1:1 adducts were in fact 1:2 adducts or 2:2 adducts, etc., new product NMR signals for mixed TDP/5'-UDP adducts would be observed. At equilibrium, no unidentified NMR signals were observed, the ratio of the four product 5'-UDP H6 signals did not change, and the total amount of reaction was comparable to that found in the (25 mM, $r = 1:1$) experiment, thus confirming that only one MDP is bound per Re(I). In addition, monitoring of a *fac*- $[\text{Re}(\text{CO})_3(\text{H}_2\text{O})_3]^+$ plus 5'-UDP (25 mM, $r = 1:1$) equilibrated reaction mixture after addition of 3 equiv of TDP confirmed that 5'-UDP dissociation was very slow ($t_{1/2} \approx 24$ h). A reviewer commented that this type of observation would support the suggested mechanism for the isomerizations described below. We postulate below that P_β does not dissociate during the isomerization process.

3.3.4 5'-GDP Reaction Products

5'-GDP formed mainly three 1:1 adducts: *fac*- $[\text{Re}(\text{CO})_3(\text{H}_2\text{O})_2(\{\text{N7}\}\text{GDP})]^-$ and two isomers of *fac*- $[\text{Re}(\text{CO})_3(\text{H}_2\text{O})(\{\text{N7},\text{P}_\beta\}\text{GDP})]^-$ (M and m). Only one set of NMR signals was observed for each species. The most informative ^1H NMR signals of 5'-GDP are H8 (on the base) and H1' (on the ribose); extensive studies with metal-G ($G =$ a guanine N9 derivative)

complexes indicate that, upon coordination of **G** via N7, the **G** H8 singlet shifts downfield.²⁵ Because of the inductive effect of the metal center, the H1' doublet shifts downfield slightly upon formation of a 1:1 adduct. An {N7,P α } macrochelate, in which the 5'-nucleotide is coordinated via both N7 and P α , has an H1' signal that appears to be a singlet.^{12,13,26} The coupling constant, $^3J_{\text{H1}'\text{-H2}'}$, is dependent upon the mole fractions of N and S sugar pucker present in dynamic equilibrium; typical free MDPs have $^3J_{\text{H1}'\text{-H2}'}$ values of ~ 6 Hz and %S $\approx 10 \times ^3J_{\text{H1}'\text{-H2}'}$ (corresponding to $\sim 60\%$ S pucker).²⁷ As the mole fraction of N sugar increases, the $^3J_{\text{H1}'\text{-H2}'}$ value decreases, approaching 0 Hz near 100% N.²⁷ However, an {N7,P α } macrochelate is rare, occurring for 5'- but not for 3'-nucleotides.^{13,28,29}

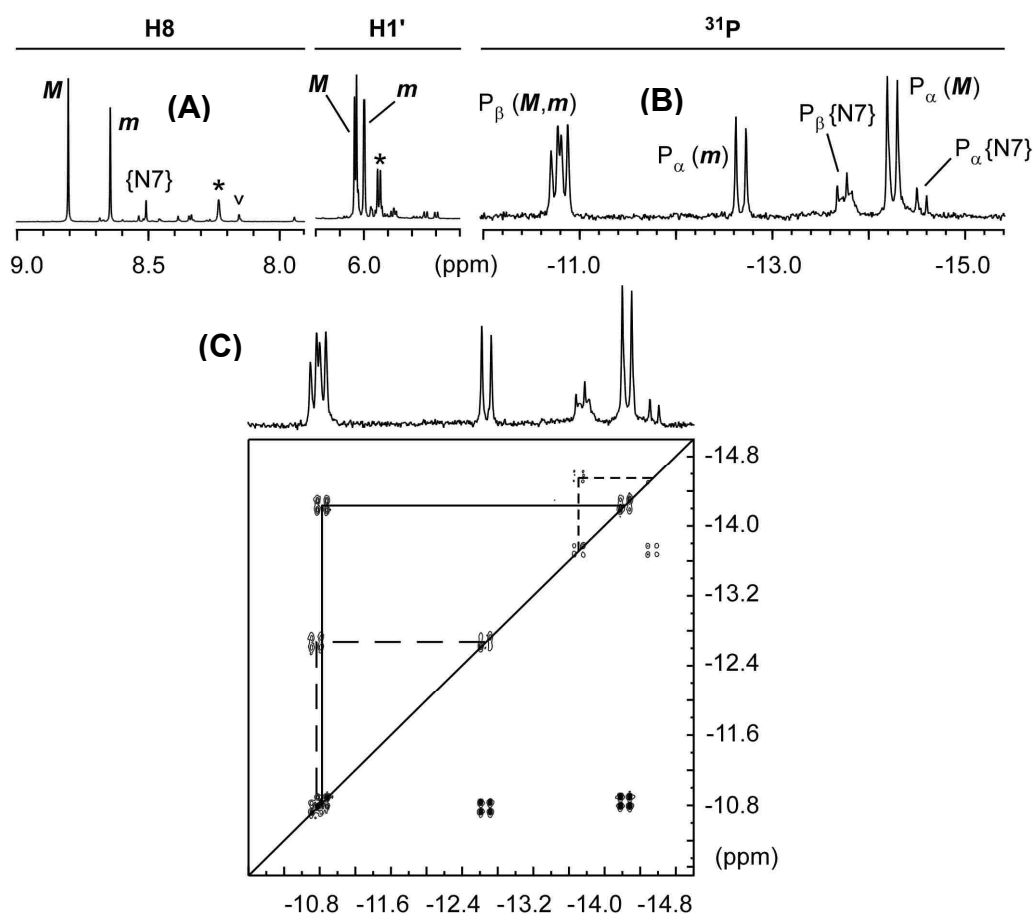


Figure 3.6. ^1H NMR (A), ^{31}P NMR (B) and ^{31}P - ^{31}P COSY (C) spectra of an equilibrium mixture of *fac*- $[\text{Re}(\text{CO})_3(\text{H}_2\text{O})_3]^+$ (25 mM, $r = 1:1$) and 5'-GDP at pH 3.6. Asterisk labels indicate peaks arising from free 5'-GDP.

Upon treatment of $fac\text{-}[\text{Re}(\text{CO})_3(\text{H}_2\text{O})_3]^+$ with 5'-GDP (25 mM, $r = 1:1$), three new H8 NMR singlets and two new H1' signals were observed immediately after mixing (Figure 3.6, Table 3.3). The two most downfield product H8 signals (8.79 and 8.67 ppm, **M** and **m**, respectively) integrate as 1:0.86, respectively, at 1 day after mixing and at equilibrium (no changes from 3 to 6 days). The smallest, least downfield product H8 singlet (8.49 ppm) decreased in intensity with time relative to the two larger H8 product signals; at equilibrium, the **M**/8.49 ppm signal ratio was 1:0.17. A number of other small H8 signals are unambiguously due to traces of free 5'-GMP present in the starting 5'-GDP, and the resulting $fac\text{-}[\text{Re}(\text{CO})_3(\text{H}_2\text{O})_2(5'\text{-GMP})]$ adduct.¹⁷ The finding that at equilibrium 83% of the 5'-GDP has reacted indicates that 5'-GDP binds more strongly than 5'-UDP or TDP.

Table 3.3. ¹H and ³¹P NMR Chemical Shifts (ppm), Coupling Constants (Hz) of 5'-GDP and Complexes Formed with $fac\text{-}[\text{Re}(\text{CO})_3(\text{H}_2\text{O})_3]^+$ ^a

complex	δ ¹ H		δ ³¹ P	
	H8	H1' (³ J _{H1'-H2'})	P _α (J _{αβ})	P _β
5'-GDP	8.21	5.92 (6.0)	-14.6 (21.5)	-13.8
$fac\text{-}[\text{Re}(\text{CO})_3(\text{H}_2\text{O})_2(\{\text{N7}\}\text{GDP})]^-$	8.49	6.03 ^b	-14.6 (19.7)	-13.7
M	8.79	6.03 (4.5)	-14.3 (21.5)	-10.8
m	8.67	6.00 (1.0)	-12.7 (21.5)	-10.8

^a25 mM, $r = 1:1$, pH 3.6. ^bAssigned by a ¹H-¹H ROESY experiment.

All free 5'-GDP was consumed in an experiment with an excess of Re(I) (25 mM, $r = 1:0.5$). Five hours after mixing, we observed at least three new H8 signals, shifted ca. 0.4 ppm downfield from the H8 signal of free 5'-GDP, in addition to the H8 signals of **M**, **m**, and $fac\text{-}[\text{Re}(\text{CO})_3(\text{H}_2\text{O})_2(\{\text{N7}\}\text{GDP})]^-$. **M**, **m**, and $fac\text{-}[\text{Re}(\text{CO})_3(\text{H}_2\text{O})_2(\{\text{N7}\}\text{GDP})]^-$ accounted for 78% of the reacted 5'-GDP, while the three new H8 signals accounted for 22% of the reacted 5'-GDP. At $r = 1:0.5$, the **m** H8 signal appears to be larger than the **M** H8 signal, but this result is likely due to overlap of the **m** H8 signal with another new H8 signal. The $\{^1\text{H}\}\text{-}^{31}\text{P}$ NMR spectrum

showed three new P_{α} doublets between -7.5 and -8.5 ppm; these shifts are within ~ 0.5 ppm of the P_{α} doublets of the TDP and $5'$ -UDP adducts (ca. -8.5 ppm for both). Likewise, the shifts of the two sets of two new P_{β} doublets at ca. -4 and -4.5 ppm are within ~ 1 ppm of those for the P_{β} doublets of the TDP and $5'$ -UDP adducts (-5 and -5.5 ppm, respectively). Thus, these results indicate that the new products all have N7, P_{α} , and P_{β} of $5'$ -GDP bound to Re(I). An increase in the amount of these new products upon addition of an excess of fac - $[\text{Re}(\text{CO})_3(\text{H}_2\text{O})_3]^+$ indicates that more than one Re(I) is bound per $5'$ -GDP. Therefore, the new products are undoubtedly dinuclear species with N7 bound to one Re(I) moiety and P_{α} and P_{β} chelating a second Re(I) moiety.

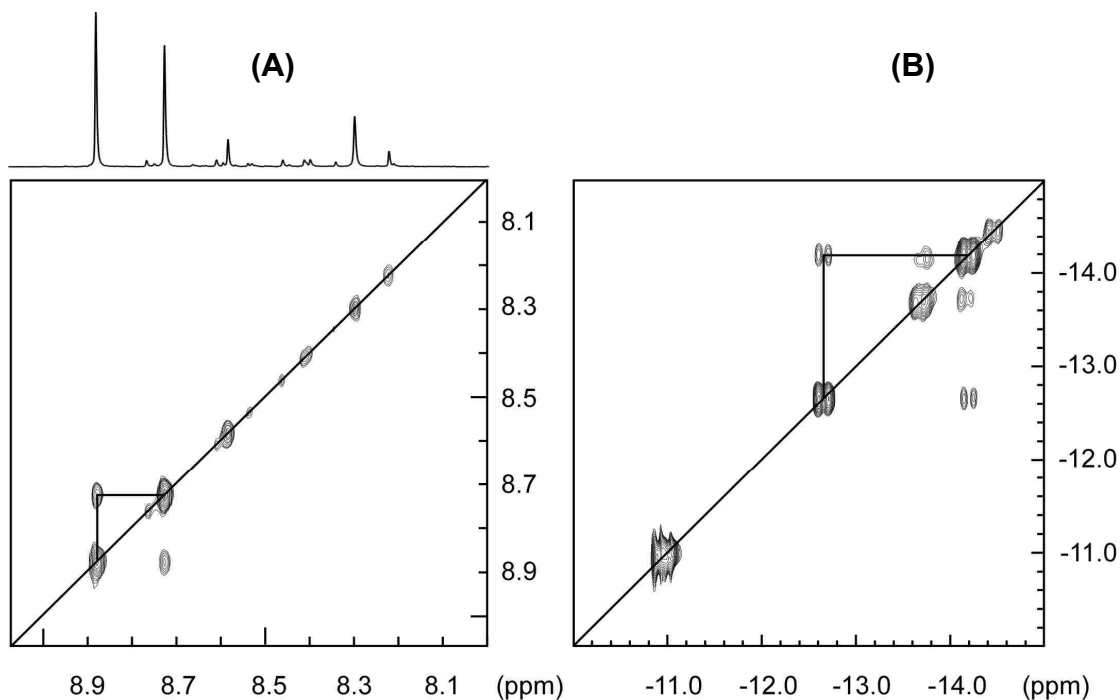


Figure 3.7. ^1H - ^1H ROESY (A) and ^{31}P - ^{31}P NOESY (B) spectra of an equilibrium mixture of fac - $[\text{Re}(\text{CO})_3(\text{H}_2\text{O})_3]^+$ (25 mM, $r = 1:1$) and $5'$ -GDP at pH 3.6.

3.3.5 Further Considerations

Our evidence demonstrates that all three products of the $r = 1:1$ reaction are N7-bound 1:1 adducts, $fac-[Re(CO)_3(H_2O)_x(GDP)]^-$ ($x = 1$ or 2). There are four types of evidence for N7 binding: First, the downfield shift changes of the H8 singlets (~ 0.5 ppm) and the H1' NMR signals (~ 0.1 ppm) of these products relative to free 5'-GDP are consistent with N7-bound adducts (Table 3.2).¹⁷ Second, the three H8 singlets were insensitive to changing the pH from 3.6 to 1.5 (Appendix B).¹⁷ Third, $^3J_{H1'-H2'}$ decreased from ~ 5.6 Hz (free 5'-GDP) to ~ 4.5 Hz and ~ 1 Hz, a feature consistent with metal coordination at N7 (Table 3.2).¹⁷ Furthermore, $^3J_{H1'-H2'} \approx 1$ Hz is indicative of an N7-coordinated, macrochelate-type structure having a highly N-puckered ribose.²⁷ Fourth, titration of a solution of Mn^{2+} ion (1 mM) into an equilibrated solution of $fac-[Re(CO)_3(H_2O)_3]^+$ and 5'-GDP (5 mM, $r = 1:1$) confirmed that N7 was bound to Re(I) in all three products, as none of the three H8 NMR signals of bound 5'-GDP broadened significantly at 5 μM Mn^{2+} ion, a concentration at which the H8 signal of free 5'-GDP became broadened to the point of disappearance (Appendix B). Two types of evidence demonstrate that all products have one Re(I) per 5'-GDP: First, all three H8 signals have different integrals (Appendix B). Two of the three H8 signals would integrate equally if they were due to a bis adduct, in which both nucleotides are coordinated to the same Re(I) center.¹⁷ Second, addition of a second equivalent of 5'-GDP to a previously equilibrated sample (25 mM, $r = 1:1$) such that $r = 1:2$ resulted in 57% of the 5'-GDP remaining unbound. Taken together, the above findings leave no doubt that all three products contain one N7-bound 5'-GDP.

The ribose 1H NMR signals of the $fac-[Re(CO)_3(H_2O)(\{N7,P_\beta\}GDP)]^-$ isomers were assigned by using $^1H-^1H$ COSY and $^1H-^{13}C$ HMQC experiments (Table 3.4). The H1' signals at 6.03 and 6.00 ppm belong to ***M*** and ***m***, respectively. $^3J_{H1'-H2'}$ values of ~ 4.5 (***M***) and ~ 1 (***m***) Hz

correspond to ~55% and ~90% N pucker, respectively. Most notably, the H2' NMR signal of *m* is shifted *upfield* (~0.3 ppm) relative to the H2' NMR signals of *M* or *fac*-[Re(CO)₃(H₂O)₂({N7}GDP)]⁻. Previous studies have shown that the H2' NMR signal of *cis*-[Pt(NH₂CH₃)₂({N7,P_α}5'-IMP)] is shifted significantly *downfield* (0.4 ppm) relative to the H2' NMR signals of *cis*-[Pt(NH₂CH₃)₂({N7}5'-IMP)] or free 5'-IMP; in this adduct, the sugar is N, the base is anti and the anisotropic downfield shift of H2' is likely due to the placement of H2' in the plane of the pyrimidine ring near N3.^{12,13} Conversely, an *upfield* shift of H2' (0.08 ppm) is seen for N, high anti *cis*-[Pt(ND₂CH₃)₂({N7,P_γ}5'-ITP)]; the upfield shift of H2' is likely caused by anisotropy.^{12,13} Therefore, these results indicate that in *m*, the sugar is N, the base is high anti, and the H2' proton is *not* located near N3 of the base pyrimidine ring.

Table 3.4. Ribose ¹H NMR Chemical Shifts (ppm) of 5'-GDP and Complexes Formed with *fac*-[Re(CO)₃(H₂O)₃]⁺ ^a

complex	δ ¹ H			
	H2'	H3'	H4'	H5'/H5''
5'-GDP	4.70	4.54	4.30	4.18/4.18
<i>fac</i> -[Re(CO) ₃ (H ₂ O) ₂ ({N7}GDP)] ⁻	4.63	4.53	4.36	^b
<i>M</i>	4.59	4.48	4.34	4.35/4.15
<i>m</i>	4.35	4.43	4.29	4.19/4.13

^a25 mM, *r* = 1:1, pH 3.6. ^bNot observed.

The syn or anti conformation of bound 5'-GDP in the products was evaluated by using the intensities of the H8–H1' and H8–H2' NOE cross-peaks in a ¹H–¹H ROESY experiment (25 mM, *r* = 1:1). Weak H8–H1' and strong H8–H2' NOE cross-peaks indicate an anti conformation of 5'-GDP, while the reverse is found for 5'-GDP with a syn conformation. The H8–H1' NOE cross-peaks of *M*, *m*, and *fac*-[Re(CO)₃(H₂O)₂({N7}GDP)]⁻ were weak compared to the H8–H2' NOE cross-peaks, indicating that the nucleotides in all adducts are in the anti conformation. Also

apparent in the ROESY spectrum were *M*–*m* H8–H8 EXSY cross-peaks (Figure 3.7), consistent with the ³¹P EXSY data, indicating *M*-to-*m* interchange.

3.3.5.1 pH Study of *fac*-[Re(CO)₃(H₂O)(N7,P_β)GDP][−] Isomers

In an effort to identify differences between the two *fac*-[Re(CO)₃(H₂O)(N7,P_β)GDP][−] isomers, we carried out an NMR-monitored titration from pH ~1.5 to 6.5 in 1 unit steps. The H8 NMR signals of the two *fac*-[Re(CO)₃(H₂O)(N7,P_β)GDP][−] isomers shifted downfield ~0.2 ppm between pH 3.5 and 5.5; this small downfield shift is most likely a result of deprotonation of the P_β group (Appendix B). In addition, the H8 signal of *fac*-[Re(CO)₃(H₂O)₂(N7)GDP][−] disappeared around pH 4.5, indicating that this species is not stable at higher pH, converting to the macrochelate isomers. Previous work has shown that 1:1 complexes containing 5'-GMP bound to Re(I) via N7 only are unstable above pH 4.¹⁷ The P_α signals of *M* and *m* are affected similarly by P_β deprotonation, shifting downfield slightly (~0.6 ppm). The P_β signals of *M* and *m* shifted downfield ~5 ppm between pH 3.5 and 5.5, indicating that the pK_a of this group has been lowered by ~2 pH units compared to free 5'-GDP (pK_a ~6.5, Appendix B). The similar behavior of the ³¹P NMR signals over the pH range studied provides additional evidence that *M* and *m* have closely related structures, as expected if they differ mainly in the chirality at the Re(I) metal center (*R*_{Re} and *S*_{Re}, see above).

3.3.5.2 Mn²⁺ Relaxation NMR Titrations of *fac*-[Re(CO)₃(H₂O)(N7,P_β)GDP][−] Isomers

To investigate the possible differences between the two *fac*-[Re(CO)₃(H₂O)(N7,P_β)GDP][−] isomers, Mn²⁺ ion was used to assess the environment surrounding the H8 proton of each isomer. For example, the H8 NMR signal will broaden upon

addition of Mn^{2+} ion if uncoordinated phosphate groups reside near the H8 proton. The magnitude of this line-broadening is slight compared to that observed when N7 is not bound to Re(I), allowing the two phenomena to be distinguished (see above). At increasing concentrations of Mn^{2+} ion, the line width of the H8 NMR signals increased more for *m* than for *M*, while the *fac*- $[\text{Re}(\text{CO})_3(\text{H}_2\text{O})_2(\{\text{N7}\}\text{GDP})]^-$ H8 NMR signal line width remained small in comparison (Appendix B). This result suggests that the H8 protons of *M* and *m* are, respectively, farther from and closer to uncoordinated phosphate groups. The distance from H8 to the uncoordinated phosphate group is long for *fac*- $[\text{Re}(\text{CO})_3(\text{H}_2\text{O})_2(\{\text{N7}\}\text{GDP})]^-$, as this signal did not broaden greatly even at high concentrations of Mn^{2+} ion (70 μM).

Because the Mn^{2+} ion titration indicated that phosphate groups are closer to H8 in *m* than in *M* (see above), we used HyperChem²³ to construct molecular models, allowing us to estimate the distance from H8 to each phosphate oxygen (Table 3.5). The results obtained are compared to computational results reported for *cis*- $[\text{Pt}(\text{NH}_3)_2(\text{nucleoside triphosphate})]$ macrochelate complexes (Table 3.5).^{12,13} On the basis of the pseudorotation phase angle (P, calculated from the endocyclic sugar torsion angles⁴) and the N-glycosidic bond torsion angle (χ , defined by O4'-C1'-N7-C4 values⁴), the 5'-GDP moieties in all four models have N sugars with a high anti orientation (P = 325–330° and χ = -59° to -67°). We should note that these values are comparable to the P and χ values reported for models of *cis*- $[\text{Pt}(\text{NH}_3)_2(\{\text{N7}, \text{P}_\beta\}5'\text{-GTP})]$ (Table 3.5). The H8-P_β distances (Table 3.6) are shorter for the two *S*_{Re} models of *fac*- $[\text{Re}(\text{CO})_3(\text{H}_2\text{O})_2(\{\text{N7}, \text{P}_\beta\}\text{GDP})]^-$ (4.88 Å) than for the two *R*_{Re} models (5.72 Å). The average H8-P_α distance was ~5.30 Å for all models (Table 3.6). Thus, we suggest that *m* is the *S*_{Re} isomer.

Table 3.5. Characteristics of Selected Pt(II) and Re(I) Nucleotide Complexes

complex	P (°)	χ (°)	N/S	syn/anti
<i>cis</i> -[Pt(NH ₃) ₂ ({N7,P _{γ} }5'-GTP)] ^a	346	-26.5	N	syn
<i>cis</i> -[Pt(NH ₃) ₂ ({N7,P _{β} }5'-GTP)] ^a	332	-60.1	N	borderline syn/high anti
<i>cis</i> -[Pt(NH ₃) ₂ ({N7,P _{α} }5'-GTP)] ^a	327	-81.5	N	high anti
<i>fac</i> -[Re(CO) ₃ (H ₂ O)({N7,P _{β} }GDP)] ⁻				
$S_{\text{Re}} \text{}^3J_{\text{H1}'\text{-H2}'} = 1.0 \text{ Hz}^b$	326	-67.8	N	high anti
$S_{\text{Re}} \text{}^3J_{\text{H1}'\text{-H2}'} = 4.5 \text{ Hz}^b$	325	-66.1	N	high anti
<i>fac</i> -[Re(CO) ₃ (H ₂ O)({N7,P _{β} }GDP)] ⁻				
$R_{\text{Re}} \text{}^3J_{\text{H1}'\text{-H2}'} = 1.0 \text{ Hz}^b$	330	-58.9	N	borderline syn/high anti
$R_{\text{Re}} \text{}^3J_{\text{H1}'\text{-H2}'} = 4.5 \text{ Hz}^b$	330	-59.1	N	borderline syn/high anti

^aData from ref 12. ^bCalculated from lowest-energy models built and minimized in HyperChem.²³

Table 3.6. Distances (Å) between H8 Proton and Phosphate Oxygens of *fac*-[Re(CO)₃(H₂O)({N7,P _{β} }GDP)]⁻ Macrochelate Models

complex	P _{α(O/pro-Δ)}	P _{α(O/pro-Λ)}	P _{α(avg)} ^a	P _{β(O)}	P _{β(O)}	P _{β(avg)} ^a
S_{Re}						
$\text{}^3J_{\text{H1}'\text{-H2}'} = 1.0 \text{ Hz}$	5.11	5.40	{5.26}	4.49	5.23	{4.86}
$\text{}^3J_{\text{H1}'\text{-H2}'} = 4.5 \text{ Hz}$	5.18	5.45	5.32	4.54	5.27	{4.91}
R_{Re}						
$\text{}^3J_{\text{H1}'\text{-H2}'} = 1.0 \text{ Hz}$	5.72	4.85	{5.28}	6.16	5.25	5.71
$\text{}^3J_{\text{H1}'\text{-H2}'} = 4.5 \text{ Hz}$	5.78	4.85	5.31	6.19	5.28	5.73

^a{Values} represent shortest average distances.

3.3.6 Rate Constants of Interchange for TDP, 5'-UDP, and 5'-GDP Products

The rate constants of H₂O exchange for *fac*-[Re(CO)₃(H₂O)₃]⁺ ($\sim 5.5 \times 10^{-3} \text{ s}^{-1}$) and *fac*-[Re(CO)₃(H₂O)₂(OH)] ($\sim 27 \text{ s}^{-1}$) indicate a large range of exchange rates dependent on the coordinated ligand; thus, we assessed the rate constants of interchange between isomers of *fac*-[Re(CO)₃(H₂O)({P _{α} ,P _{β} }TDP)]⁻, *fac*-[Re(CO)₃(H₂O)({P _{α} ,P _{β} }UDP)]⁻, and *fac*-[Re(CO)₃(H₂O)({N7,P _{β} }GDP)]⁻ adducts at 32 °C.³⁰ The rate constants of interchange were

estimated from ^1H - ^1H ROESY and ^{31}P - ^{31}P NOESY experiments at 500 ms mixing time (t_m) (Table 3.7). The rate constant (k) can be calculated by using the ratio of the relative intensities (peak amplitude, as measured by integration) of the diagonal peaks (I_{AA} and I_{BB}) and the EXSY cross-peaks (I_{AB} and I_{BA}) and the following equation:³¹

$$k = \frac{1}{t_m} \ln \frac{R+1}{R-1}, \text{ where } R = \frac{(I_{AA} + I_{BB})}{(I_{AB} + I_{BA})}$$

Using ^{31}P - ^{31}P NOESY data for the *fac*-[Re(CO)₃(H₂O)($\{P_\alpha, P_\beta\}$ TDP)]⁻ and *fac*-[Re(CO)₃(H₂O)($\{P_\alpha, P_\beta\}$ UDP)]⁻ isomers, we calculated an average k value of $\sim 0.8 \text{ s}^{-1}$ (Table 3.7). The four isomers of *fac*-[Re(CO)₃(H₂O)($\{P_\alpha, P_\beta\}$ MDP)]⁻ (Figure 3.2) can isomerize in four different ways. If either P_α or P_β interchanges coordination positions with H₂O (and the phosphate oxygen bound to Re(I) does not change), the Re(I) chirality (R_{Re} or S_{Re}) changes to S_{Re} or R_{Re} , respectively. If the change is between O(pro- Δ) and O(pro- Λ) of P_α (Figure 3.2), with no change in coordination position, then the P_α chirality changes. If both types of interchange occur, for example, via an intermediate in which both O(pro- Δ) and O(pro- Λ) of P_α are bound to Re(I), then both the Re(I) and P_α chiralities change (Figure 3.8).

Table 3.7. Rate Constants of Interchange Obtained from ^1H - ^1H ROESY and ^{31}P - ^{31}P NOESY Experiments ^a

complex	R	k (s ⁻¹)
TDP (M pair – m pair) - P_α	3.80	1.08
UDP (M_1 – M_2) - P_α	6.37	0.63
UDP (m_1 – m_2) - P_α	7.36	0.55
GDP (M – m) - P_α	9.51	0.42
GDP (M – m) - H8	6.38	0.63

^a25 mM, $r = 1:1$, pH 3.6, 32 °C.

The EXSY cross-peak observed between the P_α doublets of the two mirror pairs of fac - $[\text{Re}(\text{CO})_3(\text{H}_2\text{O})(\{P_\alpha, P_\beta\}\text{TDP})]^-$ indicates that interchange involves a chirality change only at one chiral center, either Re(I) or P_α . Thus, simultaneous changes of both the Re(I) and the P_α chiralities, leading to a synergistic interchange of members of the different mirror pairs, are ruled out.

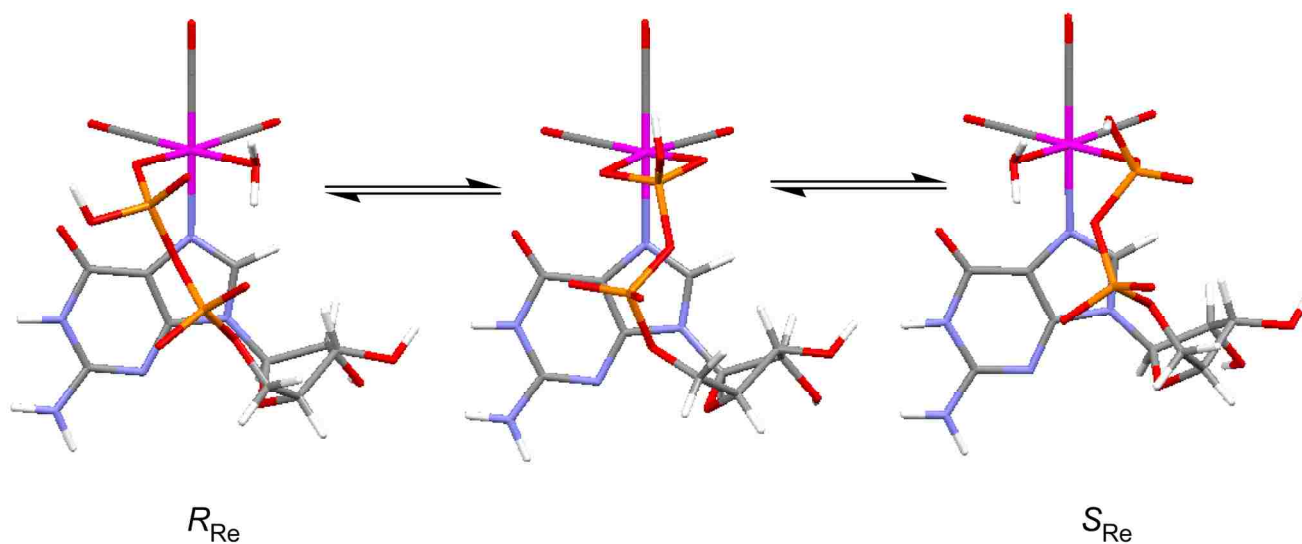


Figure 3.8. Possible mode of conversion between the R_{Re} and S_{Re} isomers of fac - $[\text{Re}(\text{CO})_3(\text{H}_2\text{O})\{\text{N7}, P_\beta\}\text{GDP}]^-$.

For fac - $[\text{Re}(\text{CO})_3(\text{H}_2\text{O})(\{P_\alpha, P_\beta\}\text{UDP})]^-$, EXSY peaks connect each of the two upfield P_α doublets with the downfield P_α doublet, but no EXSY peak between the two upfield P_α doublets was detected. Rate constants of interchange calculated from the EXSY peaks for fac - $[\text{Re}(\text{CO})_3(\text{H}_2\text{O})(\{P_\alpha, P_\beta\}\text{UDP})]^-$ ($\sim 0.6 \text{ s}^{-1}$) are similar to that found ($\sim 1 \text{ s}^{-1}$) for fac - $[\text{Re}(\text{CO})_3(\text{H}_2\text{O})(\{P_\alpha, P_\beta\}\text{TDP})]^-$ isomers (Table 3.7). These results indicate that interchange among the isomers of fac - $[\text{Re}(\text{CO})_3(\text{H}_2\text{O})(\{P_\alpha, P_\beta\}\text{UDP})]^-$ is undoubtedly due to a chirality

change at only one chiral center, either Re(I) or P_α, as was found for *fac*-[Re(CO)₃(H₂O)({P_α,P_β}TDP)]⁻.

Using ³¹P-³¹P and ¹H-¹H NOESY data for *fac*-[Re(CO)₃(H₂O)({N7,P_β}GDP)]⁻ (Table 3.7), we calculated an average *k* of ~0.5 s⁻¹ for interchange between the isomers. When P_α is *not* bound to Re(I), as in *fac*-[Re(CO)₃(H₂O)({N7,P_β}GDP)]⁻, there can be only one mechanism for interchange (Figure 3.3). Interchange of P_β and H₂O coordination positions (via an intermediate in which two oxygens of P_β are bound to Re(I)) leads to a chirality change only at Re(I) (Figure 3.8).

Because the rate constant for interchange between the *R*_{Re} and *S*_{Re} isomers of *fac*-[Re(CO)₃(H₂O)({N7,P_β}GDP)]⁻ is similar to the rate constants for interchange for both *fac*-[Re(CO)₃(H₂O)({P_α,P_β}TDP)]⁻ and *fac*-[Re(CO)₃(H₂O)({P_α,P_β}UDP)]⁻ isomers, the chirality change at Re(I) for *fac*-[Re(CO)₃(H₂O)({P_α,P_β}TDP)]⁻ and *fac*-[Re(CO)₃(H₂O)({P_α,P_β}UDP)]⁻ isomers most likely occurs by P_β interchanging coordination positions with H₂O, and *not* by interchange between O(pro-Δ) and O(pro-Λ) of P_α or by P_α interchanging coordination positions with H₂O. As mentioned above, this suggested mechanism is supported by the very slow dissociation of 5'-UDP from *fac*-[Re(CO)₃(H₂O)({P_α,P_β}UDP)]⁻ adducts, an indication that P_β remains bound to Re(I) during isomerization.

3.4 Conclusions

The nucleotide adducts described in this study and possessing the *fac*-[Re(CO)₃]⁺ moiety are sufficiently inert to allow the various products to be distinguished by NMR spectroscopy, but the adducts are reactive enough for equilibrium amounts to be assessed. In comparison to studies with other inert metal centers,^{7,11} the ³¹P NMR signals found here are notably sharp, allowing the

coupling to be observed. This relatively rare combination of properties allows us to conclude that there is little stereochemical preference for a given diastereomer over other possible diastereomers. Thus, when metal nucleotide complexes act as cofactors with enzymes as part of their natural biochemical function,^{6,32-36} the preferred (active) stereochemistry of the metal nucleotide complex is very likely imparted by the enzyme rather than by any intrinsic stereochemical preference dictated by the configuration and geometric parameters of the nucleotide itself. The metals that function in biological roles are generally hard metals such as Mg^{2+} , which have little affinity for the endocyclic nitrogens of nucleotides.³ Our study suggests that transition metal ions may not have been selected for this role because the affinity of the metal for nitrogen leads to nucleobase binding. The resulting complexes have less metal-to-phosphate interaction compared to other metal–phosphate complexes,³⁷⁻³⁹ and thus, the phosphate hydrolysis needed for the biological activity⁵ is less favored.

Few other metal centers are likely to possess the useful combination of properties that the *fac*- $[Re(CO)_3]^+$ center provides. In addition, unlike some metal centers (e.g., Pt(II) adducts derived from Pt(II) anticancer drugs³⁷) the rate of metal-promoted phosphate hydrolysis is very slow, thus avoiding complications in spectral analysis caused by formation of adducts of both the hydrolyzed nucleotide and inorganic phosphate.

3.5 References

1. Lippard, S. J.; Berg, J. M. *Principles of Bioinorganic Chemistry*; University Science Books: Mill Valley, CA, 1994.
2. Martin, R. B.; Mariam, Y. H. *Met. Ions Biol. Syst.* **1979**, *8*, 57-124.
3. Marzilli, L. G. In *Progress in Inorganic Chemistry*; Lippard, S. J., Ed.; John Wiley and Sons: New York, 1977; Vol. 23, pp 255-278.
4. Saenger, W. *Principles of Nucleic Acid Structure*; 1st ed.; Springer-Verlag: New York, 1984.

5. Cleland, W. W. *Methods Enzymol.* **1982**, *87*, 159-179.
6. Cornelius, R. D.; Cleland, W. W. *Biochemistry* **1978**, *17*, 3279-3286.
7. Cornelius, R. D.; Hart, P. A.; Cleland, W. W. *Inorg. Chem.* **1977**, *16*, 2799-2805.
8. Dunaway-Mariano, D.; Cleland, W. W. *Biochemistry* **1980**, *19*, 1496-1505.
9. Lu, Z.; Shorter, A. L.; Lin, I.; Dunaway-Mariano, D. *Inorg. Chem.* **1988**, *27*, 4135-4139.
10. Sajadi, S. A. A.; Song, B.; Gregán, F.; Sigel, H. *Inorg. Chem.* **1999**, *38*, 439-448.
11. Bose, R. N.; Slavin, L. L.; Cameron, J. W.; Luellen, D. L.; Viola, R. E. *Inorg. Chem.* **1993**, *32*, 1795-1802.
12. Reily, M. D.; Hambley, T. W.; Marzilli, L. G. *J. Am. Chem. Soc.* **1988**, *110*, 2999-3007.
13. Reily, M. D.; Marzilli, L. G. *J. Am. Chem. Soc.* **1986**, *108*, 8299-8300.
14. Wong, H. C.; Shinozuka, K.; Natile, G.; Marzilli, L. G. *Inorg. Chim. Acta* **2000**, *297*, 36-46.
15. Benedetti, M.; Tamasi, G.; Cini, R.; Marzilli, L. G.; Natile, G. *Chem. Eur. J.* **2007**, *13*, 3131-3142.
16. Natile, G.; Marzilli, L. G. *Coord. Chem. Rev.* **2006**, *250*, 1315-1331.
17. Adams, K. M.; Marzilli, L. G. *Inorg. Chem.* **2007**, *46*, 4926-4936.
18. Zobi, F.; Blacque, O.; Schmalke, H. W.; Spingler, B.; Alberto, R. *Inorg. Chem.* **2004**, *43*, 2087-2096.
19. Zobi, F.; Spingler, B.; Fox, T.; Alberto, R. *Inorg. Chem.* **2003**, *42*, 2818-2820.
20. Egli, A.; Hegetschweiler, K.; Alberto, R.; Abram, U.; Schibli, R.; Hedinger, R.; Gramlich, V.; Kissner, R.; Schubiger, P. A. *Organometallics* **1997**, *16*, 1833-1840.
21. Malandrinos, G.; Louloudi, M.; Koukkou, A. J.; Sovago, I.; Drainas, C.; Hadjiliadis, N. *J. Biol. Inorg. Chem.* **2000**, *5*, 218-226.
22. He, H.; Lipowska, M.; Xu, X.; Taylor, A. T.; Carlone, M.; Marzilli, L. G. *Inorg. Chem.* **2005**, *44*, 5437-5446.
23. HyperChem, Version 7.5; Hypercube, Inc.: Gainesville, FL.
24. He, H.; Lipowska, M.; Christoforou, A. M.; Marzilli, L. G.; Taylor, A. T. *Nucl. Med. Biol.* **2007**, *34*, 709-716.

25. Ano, S. O.; Kuklenyik, Z.; Marzilli, L. G. In *Cisplatin: Chemistry and Biochemistry of a Leading Anticancer Drug*; Lippert, B., Ed.; Wiley-VCH: Weinheim, 1999, pp 247-291.
26. Girault, J.-P.; Chottard, G.; Lallemand, J.-Y.; Chottard, J.-C. *Biochemistry* **1982**, *21*, 1352-1356.
27. Altona, C.; Sundaralingam, M. *J. Am. Chem. Soc.* **1973**, *95*, 2333-2344.
28. Kuo, L. Y.; Kanatzidis, M. G.; Marks, T. J. *J. Am. Chem. Soc.* **1987**, *109*, 7207-7209.
29. Torres, L. M.; Marzilli, L. G. *J. Am. Chem. Soc.* **1991**, *113*, 4678-4679.
30. Salignac, B.; Grundler, P. V.; Cayemittes, S.; Frey, U.; Scopelliti, R.; Merbach, A. E.; Hedinger, R.; Hegetschweiler, K.; Alberto, R.; Prinz, U.; Raabe, G.; Kölle, U.; Hall, S. *Inorg. Chem.* **2003**, *42*, 3516-3526.
31. Perrin, C. L.; Dwyer, T. J. *Chem. Rev.* **1990**, *90*, 935-967.
32. Cleland, W. W.; Mildvan, A. S. In *Advances in Inorganic Biochemistry*; Eichhorn, G. L., Marzilli, L. G., Eds.; Elsevier / North-Holland: New York, 1979; Vol. 1, pp 163-191.
33. Dunaway-Mariano, D.; Cleland, W. W. *Biochemistry* **1980**, *19*, 1506-1515.
34. Lu, Z.; Shorter, A. L.; Dunaway-Mariano, D. *Biochemistry* **1993**, *32*, 2378-2385.
35. Bakhtina, M.; Lee, S.; Wang, Y.; Dunlap, C.; Lamarche, B.; Tsai, M.-D. *Biochemistry* **2005**, *44*, 5177-5187.
36. Yang, L.; Arora, K.; Beard, W. A.; Wilson, S. H.; Schlick, T. *J. Am. Chem. Soc.* **2004**, *126*, 8441-8453.
37. Bose, R. N.; Cornelius, R. D.; Viola, R. E. *Inorg. Chem.* **1984**, *23*, 1181-1182.
38. Haromy, T. P.; Gilletti, P. F.; Cornelius, R. D.; Sundaralingam, M. *J. Am. Chem. Soc.* **1984**, *106*, 2812-2818.
39. Haromy, T. P.; Knight, W. B.; Dunaway-Mariano, D.; Sundaralingam, M. *Biochemistry* **1982**, *21*, 6950-6956.

CHAPTER 4.

fac-[Re(CO)₃(H₂O)₃]⁺ NUCLEOSIDE TRIPHOSPHATE ADDUCTS INVESTIGATED IN AQUEOUS SOLUTION BY MULTINUCLEAR NMR SPECTROSCOPY

4.1 Introduction

Nucleoside triphosphates (NTPs) such as adenosine 5'-triphosphate (5'-ATP) and guanosine 5'-triphosphate (5'-GTP) play a vital role in numerous biochemical reactions.¹ Virtually all biological reactions involving NTPs require divalent metal cations, most commonly Mg²⁺ or Zn²⁺.² NTPs contain a variety of potential metal-binding sites, including the base, ribose and phosphate moieties.^{3,4} Because of this complexity, and because of the lability of key metal ions (such as Mg²⁺), understanding the solution structure of metal–NTP complexes has captured the interest of investigators for nearly fifty years.³⁻¹⁶ This lability also impedes crystallization and makes it risky to use solid-state structural information for interpreting [Mg(ATP)] solution behavior. The simultaneous interaction of a metal with both purine N7 and the phosphate moiety (of the same NTP), giving rise to a macrochelate, has been the subject of considerable study.^{3,4,13} Such macrochelates can be inner- or outer-sphere with respect to metal coordination at N7.^{4,13} Both types of macrochelates possess direct bonds to a P_β and a P_γ phosphate group oxygen; however, inner-sphere macrochelates are proposed to have a direct metal–N7 bond (and a metal-bound H₂O molecule intervening between metal and the P_α phosphate group). Outer-sphere macrochelates have a direct bond to a P_α phosphate group oxygen (with an intervening H₂O molecule between the metal and N7).¹³

Substitution-inert [Co(III)(NTP)] and [Rh(III)(NTP)] complexes have been used as models for labile metal–NTP complexes.^{5,10,17} In NMR spectroscopic studies of Co(III) and

Rh(III) complexes of 5'-ATP, the 5'-ATP is bound as a tridentate $\{P_\alpha, P_\beta, P_\gamma\}$ chelate, with the formation of multiple isomers that can be separated chromatographically.^{5,10,17} Despite this, no evidence has been found for the formation of inner- or outer-sphere macrochelates in either system, thus precluding any potential studies providing insight into macrochelate structure. In addition, the isomers of these relatively inert Co(III) and Rh(III) adducts may not be at equilibrium, and the distribution of products may be influenced by kinetic pathways. On the other hand, NTP complexes of labile metals such as Mg(II), while at equilibrium, show NMR spectra containing only time-averaged signals that are difficult to interpret.^{5,18}

We are particularly interested in the use of the substitution-inert, redox-stable *fac*- $[\text{Re}(\text{I})(\text{CO})_3]^+$ metal core for assessing nucleoside and nucleotide binding.^{19,20} Adducts containing this core typically exhibit favorable characteristics. Previous studies (performed at pH 3.6, to avoid deprotonation and oligomerization of the *fac*- $[\text{Re}(\text{CO})_3]^+$ core²¹) have shown that reactions of *fac*- $[\text{Re}(\text{CO})_3(\text{H}_2\text{O})_3]^+$ and nucleoside mono- and diphosphates attain equilibrium at a convenient rate, and the products formed undergo exchange slowly on the NMR time scale.^{19,20} In addition, the products formed are dependent upon the properties of the nucleotide.^{19,20} When mixed with guanosine 5'-monophosphate (5'-GMP) or guanosine 5'-diphosphate (5'-GDP), *fac*- $[\text{Re}(\text{CO})_3(\text{H}_2\text{O})_3]^+$ forms a 1:1 monodentate $\{\text{N7}\}$ complex and a 1:1 bidentate $\{\text{N7}, P_\beta\}$ macrochelate, respectively; we found no evidence of a bidentate $\{\text{N7}, P_\alpha\}$ macrochelate.^{19,20} These results indicate that a simultaneous interaction of *fac*- $[\text{Re}(\text{CO})_3]^+$ with N7 and P_α (of the same nucleotide) is not favorable. However, the reaction of uridine 5'-diphosphate (5'-UDP) with *fac*- $[\text{Re}(\text{CO})_3(\text{H}_2\text{O})_3]^+$ resulted in a bidentate $\{P_\alpha, P_\beta\}$ chelate, indicating that P_α coordination is favored when a simultaneous base interaction is absent.²⁰ In this work, we exploit the favorable properties of the *fac*- $[\text{Re}(\text{I})(\text{CO})_3]^+$ core for studying the interaction of *fac*- $[\text{Re}(\text{CO})_3(\text{H}_2\text{O})_3]^+$

with NTPs in aqueous solution at pH 3.6, with the objective of shedding light on [Mg(ATP)] solution behavior.

4.2 Experimental Section

4.2.1 Materials and Sample Preparation

Stock solutions (10 mM and 50 mM) of *fac*-[Re(CO)₃(H₂O)₃]OTf in water were prepared by published procedures and maintained at pH ~ 1.8.²² 5'-UTP, 5'-ATP, 5'-GTP (disodium salts), sodium tripolyphosphate, and D₂O (99.9%) (Sigma-Aldrich) were used as received.

A typical preparation of samples for 1D NMR spectroscopy involved treatment of an appropriate amount of NTP in 0.3 mL of H₂O with 0.4 mL of an ~10 mM stock solution of *fac*-[Re(CO)₃(H₂O)₃]OTf; a small amount (0.1 mL) of D₂O was added to establish a lock signal. Samples for 2D NMR spectroscopy were prepared by removing H₂O from an aqueous 0.4 mL aliquot of an ~50 mM stock solution of *fac*-[Re(CO)₃(H₂O)₃]OTf and adding 0.4 mL D₂O; the appropriate amount of NTP (in 0.4 mL D₂O) was then added. The pH (uncorrected) of the samples in NMR tubes was maintained at ~3.6 by the addition of dilute HCl and NaOH (in H₂O) or DCl and NaOD (in D₂O) stock solutions, as required. The sample pH was adjusted to ~3.6 immediately after mixing, and before the acquisition of each NMR spectrum.

4.2.2 NMR Spectroscopy

All NMR spectra were obtained on a Varian INOVA500 spectrometer (500.1 MHz) equipped with a variable temperature probe that was equilibrated at 25 °C unless otherwise indicated. A 1 s presaturation pulse was used to reduce the HOD peak in 1D ¹H NMR spectra, and the residual HOD signal was used to reference the spectrum. Each FID was accumulated for 32 transients, each containing 32K data points. Before Fourier transformation, an exponential

apodization window function with a 0.2 Hz line broadening was applied. 1D proton-decoupled ^{31}P NMR spectra ($\{^1\text{H}\}-^{31}\text{P}$) were referenced to external trimethyl phosphate (TMP); each FID was accumulated for 128 transients, each containing 8K data points. Before Fourier transformation, an exponential apodization window function with a 0.5 Hz line broadening was applied.

In general, $^{31}\text{P}-^{31}\text{P}$ nuclear Overhauser effect spectroscopy (NOESY) experiments were conducted by using 32 scans per block (512 blocks), a spectral width of $\sim 10\text{K}$ Hz in both dimensions, and a mixing time of 500 ms at $25\text{ }^\circ\text{C}$. $^{31}\text{P}-^{31}\text{P}$ correlation spectroscopy (COSY) experiments containing 32 scans per block (734 blocks) were conducted by using a spectral width of ~ 4400 Hz in both dimensions and a COSY-45 pulse sequence to aid in visualizing close coupling patterns. All NMR data were processed with VnmrJ (Varian) software.

4.2.3 Computational Methods

All models were constructed by using methods described previously²⁰ on a PC equipped with the Hyperchem 7.5²³ molecular modeling package, and all computations were performed using AMBER99 force field parameters and literature methods.²⁴ The Re-N7 and Re-phosphate oxygen distances in all four models were constrained to $\sim 2.2\text{ \AA}$. Each model was geometrically minimized by using Polak-Ribiere conjugate gradient minimization and terminated upon reaching an rms gradient of $0.01\text{ kcal/\AA}\cdot\text{mol}$.

4.3 Results and Discussion

4.3.1 General Considerations, Including Nomenclature

Although the base moieties of uridine 5'-triphosphate (5'-UTP), 5'-ATP, and 5'-GTP possess potential metal-binding sites, N3 (5'-UTP, $pK_a \sim 9.6$) and N1 (5'-ATP, $pK_a \sim 4$; 5'-GTP,

$pK_a \sim 9.6$) are protonated at pH 3.6, while the N7 atoms of 5'-GTP ($pK_a \sim 2.9$) and 5'-ATP ($pK_a \sim 2.7$)²⁵ are available for binding to Re(I) (Figure 4.1).²⁶ Each NTP also possesses an asymmetric ribose moiety with potential metal-binding sites; however, Re(I) binding to these sites is unlikely under the conditions used here.⁴

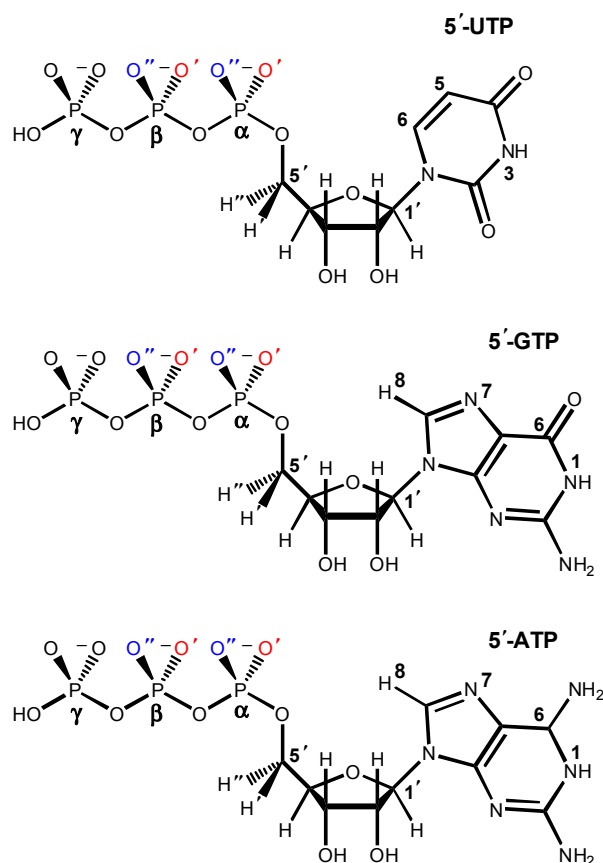


Figure 4.1. 5'-UTP (top), 5'-GTP (middle), and 5'-ATP (bottom). At pH ~ 3.6 , the P_γ group of the free NTP is protonated and the phosphate chain carries three negative charges. See text for protocol used to designate phosphate oxygen atoms.

Unidentate coordination of an NTP to $fac\text{-}[\text{Re}(\text{CO})_3(\text{H}_2\text{O})_3]^+$ can occur in four possible ways. Coordination via the terminal P_γ group of an NTP would result in the formation of a single isomer. Unidentate coordination of the prochiral P_α or P_β groups (although unlikely) would create an asymmetric P_α or P_β center and two isomers. Coordination via N7 of 5'-GTP would lead to a single isomer.

For the purposes of the following discussion, the terminal phosphate oxygen atoms of P_α and P_β are labeled O' and O'' by utilizing the $H5'$ and $H5''$ hydrogens. The O' and O'' are then labeled by aligning the $O-P-O$ and $H-C5'-H$ groupings, leading to the designations in Figure 4.1.

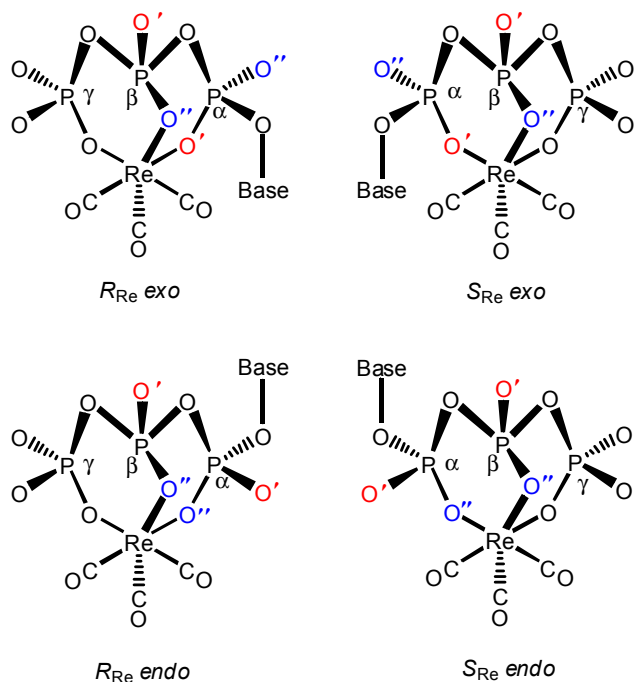


Figure 4.2. The four possible isomers of $fac-[Re(CO)_3(\{P_\alpha, P_\beta, P_\gamma\}NTP)]^{2-}$. The asymmetry of the $Re(I)$ center (R_{Re} or S_{Re}) is based on the direction of rotation of the NTP around a reference axis defined by a line passing through the $Re(I)$ atom perpendicular to the $P_\alpha-Re(I)-P_\gamma$ chelate ring (assumed to be planar as shown above) and passing through the CO (away from the viewer). *Endo* and *exo* isomers result from $P_\alpha O''$ and $P_\alpha O'$ coordination to $Re(I)$, respectively.

Bidentate coordination of an NTP through the P_α and P_β phosphate groups creates asymmetric centers at $Re(I)$, P_α and P_β . Because either O' and O'' of both P_α and P_β can coordinate, eight $\{P_\alpha, P_\beta\}$ isomers are possible. Bidentate coordination through the P_β and P_γ phosphate groups creates asymmetric centers at $Re(I)$ and P_β , leading to four possible $\{P_\beta, P_\gamma\}$ isomers. (Bidentate $\{P_\alpha, P_\gamma\}$ coordination is unlikely.) Bidentate $\{N7, P_\alpha\}$ coordination of 5'-GTP or 5'-ATP is likely to be unfavorable for $Re(I)$, as this sterically strained coordination mode has not been observed for reactions of $fac-[Re(CO)_3(H_2O)_3]^+$ with 5'-GMP and 5'-GDP.^{19,20} In contrast, bidentate $\{N7, P_\beta\}$ or $\{N7, P_\gamma\}$ coordination (resulting in four and two possible isomers,

respectively) is sterically feasible. However, products exhibiting this type of {N7,P} chelation are unlikely to build up to a detectable level because the adjacent P_γ or P_β group is brought in close proximity to a coordination position bearing an aqua ligand, and the {N7, P_β , P_γ } tridentate adduct (see below) is favored.

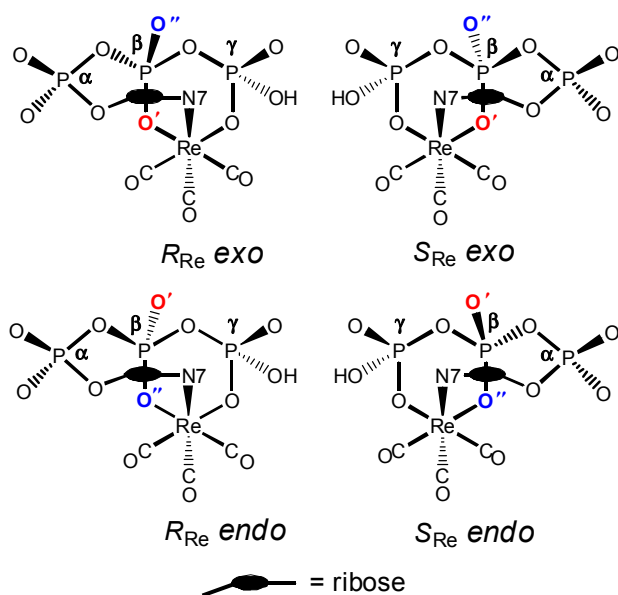


Figure 4.3. The four possible isomers of $fac\text{-}[\text{Re}(\text{CO})_3(\{\text{N}7,\text{P}_\beta,\text{P}_\gamma\}\text{NTP})]^{2-}$. The asymmetry of the Re(I) center (R_{Re} or S_{Re}) is based on the direction of rotation of the NTP around a reference axis defined by a line passing through the Re(I) atom perpendicular to the $\text{P}_\beta\text{-Re(I)-P}_\gamma$ chelate ring (assumed to be planar as shown above) and passing through the CO (away from the viewer). *Endo* and *exo* isomers result from $\text{P}_\beta\text{O}''$ and $\text{P}_\beta\text{O}'$ coordination to Re(I), respectively.

Tridentate coordination of an NTP via the P_α , P_β and P_γ phosphate groups results in asymmetric centers at Re(I), P_α and P_β . For a facial arrangement of a triphosphate moiety, either $\text{P}_\alpha\text{O}'$ or $\text{P}_\alpha\text{O}''$ can coordinate, resulting in *endo* and *exo* diastereomers. Furthermore, the triphosphate chain can “wrap” around the octahedral face of the $fac\text{-}[\text{Re}(\text{CO})_3]^+$ moiety in either a right-handed or left-handed fashion, resulting in R_{Re} and S_{Re} diastereomers, respectively. (Previously established nomenclature designates the R_{Re} and S_{Re} diastereomers as Δ and Λ , respectively.^{5,7,8}) However, binding of only $\text{P}_\beta\text{O}''$ is possible (coordination through $\text{P}_\beta\text{O}'$ gives a

meridional arrangement); thus, the $P_{\beta}O''$ coordination mode is fixed. Thus, for a given NTP, up to four diastereomers could exist, designated as $R_{Re} \textit{exo}$, $R_{Re} \textit{endo}$, $S_{Re} \textit{exo}$, and $S_{Re} \textit{endo}$ (Figure 4.2).

Table 4.1. Possible Isomers Formed by the Reaction of $fac\text{-}[\text{Re}(\text{CO})_3(\text{H}_2\text{O})_3]^+$ with NTPs

	N = U, A	N = G
<i>monodentate</i>		
$\text{Re}\{\text{N7}\}\text{NTP}$	^a	1
$\text{Re}\{\text{P}_{\alpha}^*\}\text{NTP}$	2^b	2^b
$\text{Re}\{\text{P}_{\beta}^*\}\text{NTP}$	2^b	2^b
$\text{Re}\{\text{P}_{\gamma}\}\text{NTP}$	1	1
<i>bidentate</i>		
$\text{Re}^*\{\text{P}_{\alpha}^*, \text{P}_{\beta}^*\}\text{NTP}$	8	8
$\text{Re}^*\{\text{P}_{\alpha}^*, \text{P}_{\gamma}\}\text{NTP}$	4^c	4^c
$\text{Re}^*\{\text{P}_{\beta}^*, \text{P}_{\gamma}\}\text{NTP}$	4	4
$\text{Re}^*\{\text{N7}, \text{P}_{\alpha}^*\}\text{NTP}$	^a	4^c
$\text{Re}^*\{\text{N7}, \text{P}_{\beta}^*\}\text{NTP}$	^a	4
$\text{Re}^*\{\text{N7}, \text{P}_{\gamma}\}\text{NTP}$	^a	2
<i>tridentate</i>		
$\text{Re}^*\{\text{N7}, \text{P}_{\alpha}^*, \text{P}_{\beta}^*\}\text{NTP}$	^a	8^c
$\text{Re}^*\{\text{N7}, \text{P}_{\beta}^*, \text{P}_{\gamma}\}\text{NTP}$	^a	4
$\text{Re}^*\{\text{N7}, \text{P}_{\alpha}^*, \text{P}_{\gamma}\}\text{NTP}$	^a	4^d
$\text{Re}^*\{\text{P}_{\alpha}^*, \text{P}_{\beta}, \text{P}_{\gamma}\}\text{NTP}$	4	4

*chiral center. ^anot applicable. ^bunlikely that only P_{α} or P_{β} is bound. ^cunlikely that both N7 and P_{α} are bound. ^dunlikely that P_{α} and P_{γ} are bound, and P_{β} remains unbound.

Consequently, four NMR-distinct isomers are possible for $fac\text{-}[\text{Re}(\text{CO})_3(\{\text{P}_{\alpha}, \text{P}_{\beta}, \text{P}_{\gamma}\}\text{UTP})]^{2-}$ and $fac\text{-}[\text{Re}(\text{CO})_3(\{\text{P}_{\alpha}, \text{P}_{\beta}, \text{P}_{\gamma}\}\text{ATP})]^{-}$. (Note: In formulae for the

nucleotide complexes, the 5'- is omitted to save space.) Were 5'-GTP to bind in this manner, there would again be four NMR-distinct diastereomers. However, we did not detect clear evidence for such a species because 5'-GTP binds via N7 in all major species we identified; N7 coordination is also found for the major 5'-ATP adduct. Re(I) coordination via N7 of 5'-GTP (or 5'-ATP) presents different possibilities for adduct formation. Neither {N7,P_α,P_β} nor {N7,P_α,P_γ} tridentate coordination is likely because the N7–Re–P_α chelate ring is sterically strained.^{19,20} {N7,P_β,P_γ} tridentate coordination of 5'-GTP (or 5'-ATP) creates asymmetric centers at Re(I) and P_β; thus, four NMR-distinct isomers are possible for *fac*-[Re(CO)₃({N7,P_β,P_γ}GTP)]²⁻ and *fac*-[Re(CO)₃({N7,P_β,P_γ}ATP)]⁻ (*R*_{Re} *endo*, *R*_{Re} *exo*, *S*_{Re} *endo*, *S*_{Re} *exo*; Figure 4.3). The number of isomers likely to be formed upon the reaction of the NTPs studied here with *fac*-[Re(CO)₃(H₂O)₃]⁺ are summarized in Table 4.1.

Table 4.2. ¹H and ³¹P NMR Chemical Shifts (ppm), Coupling Constants (Hz) of H₂PPP³⁻, 5'-UTP, and Complexes Formed with *fac*-[Re(CO)₃(H₂O)₃]⁺ ^a

complex	δ ¹ H		δ ³¹ P		
		P _{α/α'} (<i>J</i> _{α/α'β})	P _β	P _γ (<i>J</i> _{βγ})	configuration
H ₂ PPP ³⁻	^b	-13.4 (18.7)	-25.6		
<i>fac</i> -[Re(CO) ₃ (H ₂ PPP)] ²⁻	^b	-7.0 (18.5)	-16.8		
	H6 ^c	P _α (<i>J</i> _{αβ})	P _β	P _γ (<i>J</i> _{βγ})	configuration
5'-UTP ^d	7.93(5)	-14.5 (19.7)	-26.2	-13.9 (19.4)	^b
1-U	7.85(6)	-10.6 (20.1)	-17.0 ^e	-5.8 (20.1)	<i>S</i> _{Re} <i>exo</i>
2-U	7.86(0)	-10.4 (20.1)	-17.0 ^e	-5.7 (19.9)	<i>R</i> _{Re} <i>exo</i>
3-U	7.89(1)	-9.5 (17.9)	-17.0 ^e	-6.4 (19.6)	<i>R</i> _{Re} <i>endo</i>
4-U	7.94(2)	-9.2 (17.2)	-17.0 ^e	-6.6 (19.6)	<i>S</i> _{Re} <i>endo</i>

^a[Re] = 25 mM, pH 3.6. ^bNot applicable. ^cThird decimal place is given to distinguish adducts; ³*J*_{H5-H6} = 8.1 Hz for all species observed. ^dH6 signals could not be correlated to ³¹P signals. ^eAll P_β signals are overlapped.

Table 4.3. ^{31}P NMR Chemical Shift Data (ppm) of Selected Reference Co(III) and Rh(III) Complexes Compared to Similar Re(I) Complexes

complex	pH	$\delta^{31}\text{P}$			ref
		P_α	P_β	P_γ	
free $\text{H}_2\text{PPP}^{3-}$	3	-13.7	-26.2	<i>d</i>	<i>b</i>
$[\text{Rh}(\text{H}_2\text{O})_3(\text{PPP})]^{a,e}$	3	2.8	-9.0	<i>d</i>	18
coordination chemical shift (ccs)		16.5	17.2		
free ATP^{2-}	2.5	-14.4	-26.1	-13.9	<i>b</i>
$[\text{Rh}(\text{H}_2\text{O})_3(\{\text{P}_\alpha, \text{P}_\beta, \text{P}_\gamma\}\text{ATP})]^{a,e}$	2.5	-2.5	-10.5	4.3	11
ccs		11.9	15.6	18.2	
free $\text{H}_2\text{PPP}^{3-}$	3.6	-13.4	-25.6	<i>d</i>	<i>b</i>
<i>fac</i> - $[\text{Re}(\text{CO})_3(\text{H}_2\text{PPP})]^{2-}$	3.6	-7.0	-16.8	<i>d</i>	<i>b</i>
ccs		6.4	8.8		
free UTP^{3-}	3.6	-14.5	-26.2	-13.9	<i>b</i>
<i>fac</i> - $[\text{Re}(\text{CO})_3(\{\text{P}_\alpha, \text{P}_\beta, \text{P}_\gamma\}\text{UTP})]^{2-}$	3.6	-9.9	-17.0	-6.1	<i>b</i>
ccs		4.6	9.2	7.8	
free GTP^{3-}	3.6	-14.4	-26.1	-13.9	<i>b</i>
<i>fac</i> - $[\text{Re}(\text{CO})_3(\{\text{N7}, \text{P}_\beta, \text{P}_\gamma\}\text{GTP})]^{2-}$	3.6	-14.2	-21.2	-7.7	<i>b</i>
ccs		0.2	4.9	6.2	
free ATP^{2-}	3.6	-14.4	-26.1	-13.8	<i>b</i>
<i>fac</i> - $[\text{Re}(\text{CO})_3(\text{H}_2\text{O})(\{\text{P}_\beta, \text{P}_\gamma\}\text{ATP})]^-$	3.6	-14.1	-20.8	-7.9	<i>b</i>
ccs		0.3	5.2	5.9	
<i>fac</i> - $[\text{Re}(\text{CO})_3(\{\text{P}_\alpha, \text{P}_\beta, \text{P}_\gamma\}\text{ATP})]^-$	3.6	-10.0	-16.9	-6.3	<i>b</i>
ccs		4.4	9.1	7.5	
free $\text{ATP}^{3-a,c}$	4.8	-14.5	-26.0	-14.5	17
$[\text{MgATP}]^{a,c,e}$	4.8	-14.3	-23.9	-12.2	17
ccs		0.2	2.1	2.3	
free ATP^{3-}	5.8	-14.4	-25.9	-13.2	<i>b</i>
$[\text{Co}(\text{NH}_3)_3(\{\text{P}_\alpha, \text{P}_\beta, \text{P}_\gamma\}\text{ATP})]^{a,e}$	5.8	-4.2	-11.2	1.5	15
ccs		10.2	14.7	14.7	

^a ^{31}P NMR chemical shifts converted to TMP reference by subtracting 3.54 ppm from the ^{31}P chemical shift measured relative to 85% H_3PO_4 . ^bThis work. ^cEstimated from graphical representation. ^dNot applicable. ^eOverall charge on complex is taken from the corresponding literature reference.

Previous work with 5'-GDP and 5'-GMP has shown that upon Re(I) coordination via N7 of the nucleotide, both the H8 and H1' signals of the nucleotide shift downfield, $^3J_{H1'-H2'}$ decreases in magnitude, and no significant shift change occurs for the P_α and P_β signals.^{19,20} Coordination of one Re(I) metal center at N7 and another Re(I) chelating P_α and P_β of the same 5'-GDP leads to a ~0.4 ppm downfield shift of the H8 signal but larger (~6 and ~10 ppm) downfield shifts for the P_α and P_β signals, respectively.²⁰ Re(I) coordination via only the phosphate moiety of 5'-UDP resulted in negligible shift changes for the NMR signals of uracil; however, a slight decrease in the magnitude of $^3J_{H1'-H2'}$ was noted, indicating a decrease in the percent S character (% S) in the dynamic equilibrium between N and S puckers of the ribose.^{19,20}

As a first step in understanding the effects of coordination on ^{31}P NMR shifts, we studied the reaction of *fac*-[Re(CO)₃(H₂O)₃]⁺ with diprotonated tripolyphosphate (H₂PPP³⁻)²⁷ at pH 3.6. A ^{31}P NMR spectrum recorded one day after mixing *fac*-[Re(CO)₃(H₂O)₃]⁺ and H₂PPP³⁻ (25 mM, *r* = 1:1 and 1:2) contained a P_β triplet, shifted ~9 ppm downfield from the P_β signal of free H₂PPP³⁻, and a $P_\alpha/P_{\alpha'}$ doublet, shifted ~7 ppm downfield from the $P_\alpha/P_{\alpha'}$ doublet of free H₂PPP³⁻ (Table 4.2). The $P_\alpha/P_{\alpha'}$ and P_β signals of the product integrate as 2:1, demonstrating that both terminal phosphate groups are bound to Re(I). At equilibrium (no changes from 3 to 6 days), ~85% of the H₂PPP³⁻ had reacted and there was only one set of product signals. These results indicate that *fac*-[Re(CO)₃(H₂PPP)]²⁻, in which all three phosphate groups chelate Re(I), is the favorable reaction product.

Of particular note, the ~7 ppm downfield shift change for the $P_\alpha/P_{\alpha'}$ doublet of *fac*-[Re(CO)₃(H₂PPP)]²⁻ is similar to the downfield shift change (~7 ppm) observed for the ^{31}P NMR signal of the coordinated phosphate groups of *fac*-[Re(CO)₃(H₂O)(H₂PP)]⁻ at pH 3.6 (H₂PP²⁻ = diprotonated pyrophosphate).²⁰ In general, the coordination shift changes observed here for the

$P_{\alpha/\alpha'}$ and P_{β} signals of $fac-[Re(CO)_3(H_2PPP)]^{2-}$ (and for the coordinated phosphate groups of 5'-UTP, 5'-ATP, and 5'-GTP, see below) are smaller than those observed for the related tridentate chelate adduct, $[Rh(H_2O)_3(H_2PPP)]$ (Table 4.3).¹⁷ This result is attributable to the lower oxidation state (and lower electrophilicity) of Re(I) compared to Rh(III).

4.3.2 Overview of Products Formed by $fac-[Re(CO)_3(H_2O)_3]^+$ and NTPs

Throughout this work, concentrations will be denoted as ($__ \text{ mM}, r = __:__$), in which the $fac-[Re(CO)_3(H_2O)_3]^+$ concentration is stated and r is the ratio of the cation to added phosphate ligand. This notation designates both the starting ligand concentration and its ratio to the starting $fac-[Re(CO)_3(H_2O)_3]^+$ concentration.

In the following discussion, we first identify the adducts formed as a result of NTP binding to $fac-[Re(CO)_3(H_2O)_3]^+$; we then present the ^1H and ^{31}P NMR spectral evidence and the reasoning for such adduct designations. We did not detect any evidence suggesting formation of a significant amount of either uni- or bidentate adducts (bound through only one or two phosphate oxygens, respectively), or 1:2 adducts (even in $r = 1:2$ reaction mixtures) for 5'-UTP, 5'-GTP, or 5'-ATP.

4.3.3 5'-UTP Reaction Products

5'-UTP formed a tridentate 1:1 adduct, $fac-[Re(CO)_3(\{P_{\alpha}, P_{\beta}, P_{\gamma}\}UTP)]^{2-}$, exhibiting ^1H and ^{31}P NMR signals for four diastereomers. ^1H NMR spectra of $fac-[Re(CO)_3(H_2O)_3]^+$ treated with 5'-UTP (25 mM, $r = 1:1$) showed after ~ 1 day four product H6 doublets; one H6 doublet was shifted slightly *downfield* and three H6 doublets were shifted slightly *upfield*, respectively, from the H6 doublet of free 5'-UTP (Table 4.2 and Figure 4.4). The small size of the shifts indicates no base binding. Signal overlap prevented analysis of the H5 and H1' signals. At

equilibrium (no changes from 3 to 6 days), ~70% of the 5'-UTP had reacted, indicating that formation of $fac\text{-}[\text{Re}(\text{CO})_3(\{\text{P}_\alpha, \text{P}_\beta, \text{P}_\gamma\}\text{UTP})]^{2-}$ is slightly less favorable than $fac\text{-}[\text{Re}(\text{CO})_3(\text{PPP})]^{2-}$ formation at $r = 1:1$.

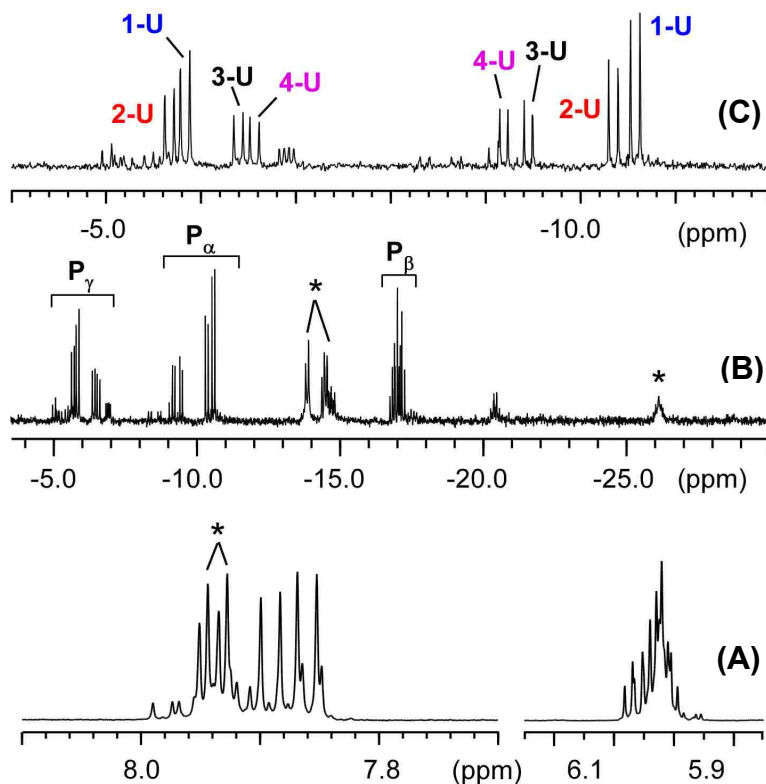


Figure 4.4. ^1H NMR (A), ^{31}P NMR (B) and expanded region of ^{31}P NMR (C) spectra of an equilibrium mixture of $fac\text{-}[\text{Re}(\text{CO})_3(\text{H}_2\text{O})_3]^+$ (25 mM, $r = 1:1$) and 5'-UTP at pH 3.6. Asterisk labels indicate peaks arising from free 5'-UTP.

The $\{^1\text{H}\}\text{-}^{31}\text{P}$ NMR spectrum of the (25 mM, $r = 1:1$) reaction mixture (Figure 4.4) contained two sets of two P_α doublets between -9.0 and -11.0 ppm, overlapping P_β doublets at -17.0 ppm, and two sets of two P_γ doublets between -5.0 and -7.0 ppm, shifted ~ 4.5 , ~ 9 and ~ 8 ppm downfield from the respective free 5'-UTP signals (Table 4.2). The P_α vs P_γ assignments were confirmed by a proton-coupled ^{31}P NMR experiment. The P_α doublets are labeled as follows from most upfield to most downfield: **1-U**, **2-U**, **3-U**, and **4-U** (Figure 4.4). This

numbering coincidentally reflects the relative abundance of the isomers, **1-U** being the most abundant. On chelate ring formation, the ${}^3J_{\alpha\beta}$ coupling constants for **3-U** and **4-U** decreased to ~ 17.6 Hz from 19.7 Hz (free 5'-UTP), whereas the ${}^3J_{\alpha\beta}$ values for **1-U** and **2-U** increased to 20.1 Hz; the ${}^3J_{\beta\gamma}$ coupling constants for all four isomers were relatively unaffected by chelate formation (Table 4.2). The P_α - P_β and P_β - P_γ connectivities in a proton-decoupled ${}^{31}\text{P}$ - ${}^{31}\text{P}$ COSY experiment (25 mM, $r = 1:1$) allowed the P_γ doublets to be assigned from most upfield to most downfield as follows: **4-U**, **3-U**, **1-U**, and **2-U** (Figure 4.4, Figure 4.5 and Appendix C).

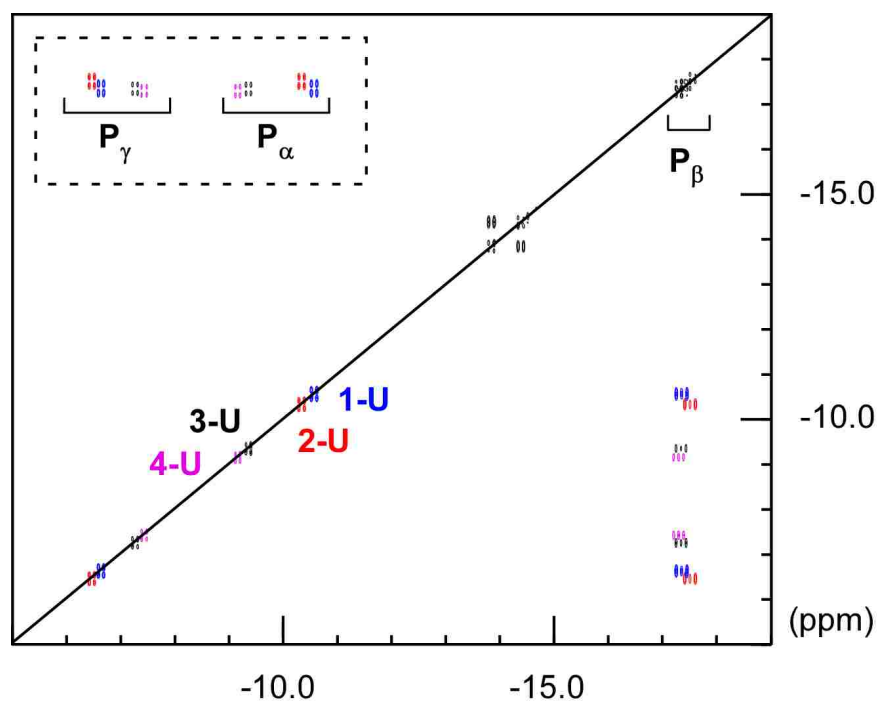


Figure 4.5. ${}^{31}\text{P}$ - ${}^{31}\text{P}$ COSY spectrum of an equilibrium mixture of *fac*- $[\text{Re}(\text{CO})_3(\text{H}_2\text{O})_3]^+$ (25 mM, $r = 1:1$) and 5'-UTP at pH 3.6. Expansion of cross-peaks encircled by dotted line appears in Appendix C.

No NMR studies of similar 5'-UTP complexes of octahedral metals were found in the literature. However, $[\text{Rh}(\text{H}_2\text{O})_3(\{P_\alpha, P_\beta, P_\gamma\}\text{ATP})]^{10}$ and $[\text{Co}(\text{NH}_3)_3(\{P_\alpha, P_\beta, P_\gamma\}\text{ATP})]^{15}$ (at pH 2.5 and 5.8, respectively) have been studied by ${}^{31}\text{P}$ NMR spectroscopy (Table 4.3). Downfield coordination shifts (~ 10 ppm) for P_α , P_β , and P_γ of 5'-ATP indicate that all three phosphate

groups are coordinated in both $[\text{Rh}(\text{H}_2\text{O})_3(\{\text{P}_\alpha, \text{P}_\beta, \text{P}_\gamma\}\text{ATP})]$ and $[\text{Co}(\text{NH}_3)_3(\{\text{P}_\alpha, \text{P}_\beta, \text{P}_\gamma\}\text{ATP})]$; the appearance of four sets of NMR signals for each complex indicates the presence of four $\{\text{P}_\alpha, \text{P}_\beta, \text{P}_\gamma\}$ tridentate diastereomers (Δ *endo*, Λ *endo*, Δ *exo*, and Λ *exo*, see above).^{8,10,15}

Diastereomers of $[\text{Rh}(\text{H}_2\text{O})_3(\{\text{P}_\alpha, \text{P}_\beta, \text{P}_\gamma\}\text{ATP})]$ and $[\text{Co}(\text{NH}_3)_3(\{\text{P}_\alpha, \text{P}_\beta, \text{P}_\gamma\}\text{ATP})]$ give characteristic patterns of ^{31}P NMR signals. For example, the P_α signals of *endo* isomers are more downfield than those of *exo* isomers for both $[\text{Rh}(\text{H}_2\text{O})_3(\{\text{P}_\alpha, \text{P}_\beta, \text{P}_\gamma\}\text{ATP})]$ and $[\text{Co}(\text{NH}_3)_3(\{\text{P}_\alpha, \text{P}_\beta, \text{P}_\gamma\}\text{ATP})]$.^{10,15} For $[\text{Co}(\text{NH}_3)_3(\{\text{P}_\alpha, \text{P}_\beta, \text{P}_\gamma\}\text{ATP})]$, P_α signals of the Λ isomers appear downfield from those of the Δ isomers for both the *exo* and *endo* configurations.¹⁵ For $[\text{Rh}(\text{H}_2\text{O})_3(\{\text{P}_\alpha, \text{P}_\beta, \text{P}_\gamma\}\text{ATP})]$, the P_α signal of the Λ *endo* isomer appears downfield from that of the Δ *endo* isomer.¹⁰ (The P_α signals of the two *exo* isomers have nearly identical chemical shifts; the downfield and upfield *exo* P_α signal are assigned as Δ and Λ by using circular dichroism spectroscopy.¹⁰) Also, Speckhard et al. noted that the $^3J_{\alpha\beta}$ coupling constants of the *exo* isomers are several Hz larger than those for the *endo* isomers; the $^3J_{\alpha\beta}$ coupling constants are larger than the $^3J_{\beta\gamma}$ coupling constants for all isomers.¹⁵ Thus, using these patterns, we tentatively assign the P_α NMR signals of *fac*- $[\text{Re}(\text{CO})_3(\{\text{P}_\alpha, \text{P}_\beta, \text{P}_\gamma\}\text{UTP})]^{2-}$ as follows: **1-U** and **2-U** belong to the R_{Re} and S_{Re} *exo* isomers, respectively; and **3-U** and **4-U** belong to the R_{Re} and S_{Re} *endo* isomers, respectively (Figure 4.6).

For $[\text{Co}(\text{NH}_3)_3(\{\text{P}_\alpha, \text{P}_\beta, \text{P}_\gamma\}\text{ATP})]$, the P_β signals of the *exo* isomers are upfield from those of the *endo* isomers.¹⁵ However, the P_β NMR signals of *fac*- $[\text{Re}(\text{CO})_3(\{\text{P}_\alpha, \text{P}_\beta, \text{P}_\gamma\}\text{UTP})]^{2-}$ overlap, thus precluding assignment of signals to individual isomers. In contrast to the behavior observed for the P_α signals of both $[\text{Rh}(\text{H}_2\text{O})_3(\{\text{P}_\alpha, \text{P}_\beta, \text{P}_\gamma\}\text{ATP})]$ and $[\text{Co}(\text{NH}_3)_3(\{\text{P}_\alpha, \text{P}_\beta, \text{P}_\gamma\}\text{ATP})]$, the P_γ signals of the *endo* isomers are *upfield* from those of the *exo*

4.3.4 5'-GTP Reaction Products

When treated with $fac\text{-}[\text{Re}(\text{CO})_3(\text{H}_2\text{O})_3]^+$, 5'-GTP formed primarily a tridentate 1:1 adduct, $fac\text{-}[\text{Re}(\text{CO})_3(\{\text{N}_7, \text{P}_\beta, \text{P}_\gamma\}\text{GTP})]^{2-}$. Immediately after mixing, an NMR spectrum of $fac\text{-}[\text{Re}(\text{CO})_3(\text{H}_2\text{O})_3]^+$ mixed with 5'-GTP (25 mM, $r = 1:1$) showed two new H8 singlets (partially overlapped at ~ 8.43 ppm and shifted ~ 0.2 ppm downfield from the H8 singlet of free 5'-GTP, Table 4.4) and two new H1' doublets (6.00 and 6.06 ppm) (Figure 4.7). At equilibrium, $>90\%$ of the 5'-GTP has reacted, indicating that 5'-GTP binds more strongly than 5'-UTP or $\text{H}_2\text{PPP}^{3-}$ at pH 3.6. A number of other small H8 signals are unambiguously assigned to traces of free and coordinated 5'-GMP and 5'-GDP arising from impurities in the starting 5'-GTP.^{19,20}

The $\{^1\text{H}\}\text{-}^{31}\text{P}$ NMR spectrum of the (25 mM, $r = 1:1$) reaction mixture supports the ^1H NMR data indicating the presence of mainly two products. An apparent triplet at -21.0 ppm (**1-G**) and a doublet of doublets near -21.4 ppm (**2-G**) are without question P_β signals (Figure 4.7). From broadening seen in a proton-coupled ^{31}P NMR spectrum, the doublets at -14.3 (**1-G**) and at -14.0 (**2-G**) ppm are P_α signals. Thus, the doublets at -7.9 (**1-G**) and at -7.5 (**2-G**) ppm are P_γ signals. The product P_α , P_β and P_γ signals are shifted ~ 0.2 , ~ 5 , and ~ 6 ppm downfield from the respective free 5'-GTP signals (Table 4.4). These results demonstrate that N_7 , P_β and P_γ are, and P_α is not, directly coordinated to $\text{Re}(\text{I})$ in both **1-G** and **2-G**. Because the overlapped H8 singlets of **1-G** and **2-G** precluded integration, the approximate product distribution (60% **1-G** / 40% **2-G**) was obtained by integrating the P_β NMR signals. T_1 values for the P_β signals of **1-G** and **2-G** were similar (~ 1 s); nevertheless, a relaxation delay of $5 \times T_1$ was used between pulses to minimize any error introduced by incomplete ^{31}P relaxation. The product distribution observed initially was the same as that found at equilibrium (no changes from 3 to 6 days). Thus, product formation is not influenced noticeably by kinetic control. A proton-decoupled $^{31}\text{P}\text{-}^{31}\text{P}$ COSY

experiment (25 mM, $r = 1:1$) allowed identification of ^{31}P nuclei within the same spin system (Figure 4.7). A ^{31}P - ^{31}P NOESY spectrum contained no EXSY peaks, indicating that **1-G** and **2-G** do not interconvert even in the slow exchange regime of the NMR time scale.

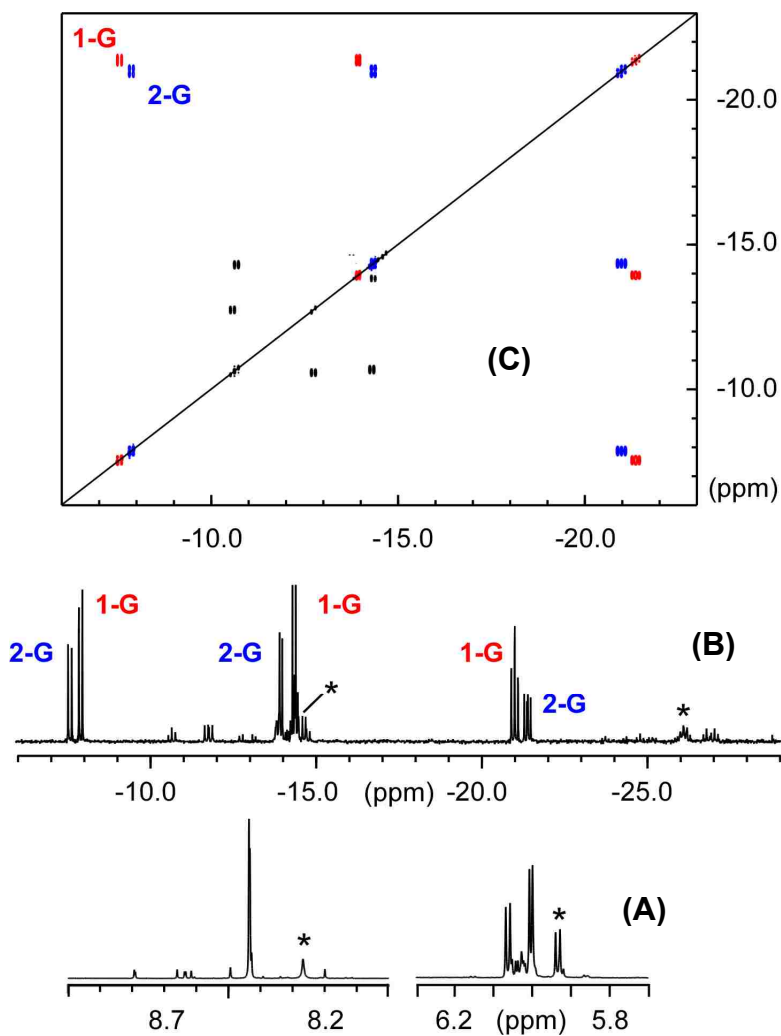


Figure 4.7. ^1H NMR (A), ^{31}P NMR (B) and ^{31}P - ^{31}P COSY (C) spectra of an equilibrium mixture of *fac*- $[\text{Re}(\text{CO})_3(\text{H}_2\text{O})_3]^+$ (25 mM, $r = 1:1$) and $5'$ -GTP at pH 3.6. Asterisk labels indicate peaks arising from free $5'$ -GTP.

Several types of evidence demonstrate that both **1-G** and **2-G** are N7 bound, 1:1 *fac*- $[\text{Re}(\text{CO})_3(\text{GTP})]^{2-}$ adducts. First, the downfield shift changes of the H8 singlets (~ 0.2 ppm) and the H1' NMR signals (~ 0.1 ppm) of these products relative to free $5'$ -GTP are consistent with

N7-bound adducts (Table 4.4).¹⁹ Second, both H8 singlets were insensitive to a decrease in pH from 3.6 to 1, indicating that Re(I) coordination blocks N7 protonation.¹⁹ Third, $^3J_{\text{H1}'\text{-H2}'}$ decreased from ~5.7 Hz (free 5'-GTP) to ~5.5 Hz and ~4.0 Hz, a feature consistent with metal coordination at N7 (Table 4.4).¹⁹ Fourth, titration of a 1 mM solution of Cu^{2+} ion into a previously equilibrated solution containing **1-G** and **2-G** did not result in broadening of the H8 signals of the products at 15 μM Cu^{2+} ion, a concentration at which the H8 signal of free 5'-GTP is broadened to the point of disappearance; thus N7 is bound to Re(I) in both **1-G** and **2-G**.

Table 4.4. ^1H and ^{31}P NMR Chemical Shifts (ppm), Coupling Constants (Hz) of 5'-GTP and Complexes Formed with $\text{fac-}[\text{Re}(\text{CO})_3(\text{H}_2\text{O})_3]^+$ ^a

complex	δ ^1H			δ ^{31}P	
	H8	H1' ($J_{\text{H1}'\text{-H2}'}$)	P_α ($J_{\alpha\beta}$)	P_β	P_γ
5'-GTP	8.26	5.93 (5.7)	-14.4 (19.7)	-26.1	-13.9
1-G	8.43(2)	6.00 (4.0)	-14.3 (20.0)	-21.0	-7.9
2-G	8.43(0)	6.06 (5.5)	-14.0 (16.7)	-21.3, -21.4	-7.5

^a[Re] = 25 mM, pH 3.6. ^b $^3J_{\text{H1}'\text{-H2}'}$ (free 5'-GTP) = ~6 Hz and ~60% S pucker (estimated by % S $\approx 10 \times ^3J_{\text{H1}'\text{-H2}'}$).⁴²

Two types of evidence demonstrate that both **1-G** and **2-G** have one Re(I) per 5'-GTP. First, a 1:2 adduct would have two H8 signals and the two H8 signals would integrate equally.¹⁹ The observed signals do not have the same intensity. Second, addition of a second equivalent of 5'-GTP to a previously equilibrated sample (25 mM, $r = 1:1$) such that $r = 1:2$ resulted in ~50% of the 5'-GTP remaining unbound. (The amount of the GDP adduct decreased.) Taken together, the above findings leave no doubt that the two H8 signals are from two 1:1 adducts and that both contain one N7-bound 5'-GTP. This result also rules out the very remote possibility that the NMR data reflect a mixture of 1:1 and 1:2 adducts with overlapping H8 signals.

4.3.5 Effect of Re(I) Binding on P_γ pK_a of the fac -[Re(CO)₃({N7,P_β,P_γ}GTP)]²⁻ and fac -[Re(CO)₃({P_α,P_β,P_γ}UTP)]²⁻ Adducts

The effect of pH changes on the chemical shifts of fac -[Re(CO)₃({N7,P_β,P_γ}GTP)]²⁻ and fac -[Re(CO)₃({P_α,P_β,P_γ}UTP)]²⁻ were assessed by monitoring the NMR spectrum as the pH was raised from ~1 to ~7 in steps of 1 pH unit (Appendix C). No significant shift changes were observed for the H8 and P_α signals of fac -[Re(CO)₃({N7,P_β,P_γ}GTP)]²⁻ over the pH range studied. However, the P_β and P_γ signals of fac -[Re(CO)₃({N7,P_β,P_γ}GTP)]²⁻ shifted ~1.5 and ~3.5 ppm downfield, respectively, between pH 3 and 5 (Appendix C). This suggests a P_γ pK_a decrease to ~4.5 for fac -[Re(CO)₃({N7,P_β,P_γ}GTP)]²⁻ compared to the P_γ pK_a of free 5'-GTP (pK_a ~6.5, Appendix C), which is undoubtedly due to direct Re(I)–phosphate binding.

No significant shift changes were observed for the H6 or P_α signals of fac -[Re(CO)₃({P_α,P_β,P_γ}UTP)]²⁻ over the pH range in experiments performed as described above for 5'-GTP. The P_β and P_γ signals of fac -[Re(CO)₃({P_α,P_β,P_γ}UTP)]²⁻ were more affected, shifting ~1.5 and ~3.5 ppm downfield, respectively, between pH 1.4 and 4.3 (Appendix C). These data suggest a P_γ pK_a of ~4, a decrease compared to that of free 5'-UTP (pK_a ~7, Appendix C). These results are consistent with previous findings that metal coordination to the triphosphate chain lowers the P_γ pK_a by ~2-4 units vs the P_γ pK_a value for free NTP.^{10,11,26,28}

4.3.6 Nature of the GTP Products

The similar dependence of the ¹H and ³¹P NMR signals of **1-G** and **2-G** on pH provides evidence for a close structural relationship between the **1-G** and **2-G** products. However, as discussed above, four diastereomers (R_{Re} *endo*, R_{Re} *exo*, S_{Re} *endo* and S_{Re} *exo*) (and four sets of NMR signals) are possible for fac -[Re(CO)₃({N7,P_β,P_γ}GTP)]²⁻. However, only two sets of

NMR signals are observed, and the lack of exchange between the NMR signals of **1-G** and **2-G** (see above) suggests that the products have the same chirality about the Re(I) metal center. We have previously established that the R_{Re} and S_{Re} diastereomers of $fac\text{-}[\text{Re}(\text{CO})_3(\text{H}_2\text{O})(\{\text{N}7, \text{P}_\beta\}\text{GDP})]^-$ interchange in the slow exchange regime of the NMR time scale, giving rise to EXSY cross-peaks.²⁰

Lower energy diastereomers were identified by using HyperChem²³ to construct models of the four conceivable diastereomers of $fac\text{-}[\text{Re}(\text{CO})_3(\{\text{N}7, \text{P}_\beta, \text{P}_\gamma\}\text{GTP})]^{2-}$; the results of the modeling are shown in Figure 4.8 and **Table 4.5**. We found that the two S_{Re} diastereomers of $fac\text{-}[\text{Re}(\text{CO})_3(\{\text{N}7, \text{P}_\beta, \text{P}_\gamma\}\text{GTP})]^{2-}$ are 10-20 kcal/mol lower in energy than the two R_{Re} diastereomers, and the S_{Re} *endo* and S_{Re} *exo* diastereomers differ in energy by ~ 1.5 kcal/mol. These results indicate that the two sets of NMR signals observed for $fac\text{-}[\text{Re}(\text{CO})_3(\{\text{N}7, \text{P}_\beta, \text{P}_\gamma\}\text{GTP})]^{2-}$ can be attributed to the S_{Re} *endo* and S_{Re} *exo* diastereomers; it is unlikely that the R_{Re} diastereomers are formed.

The 5'-GTP moieties in the S_{Re} *endo* and S_{Re} *exo* models of $fac\text{-}[\text{Re}(\text{CO})_3(\{\text{N}7, \text{P}_\beta, \text{P}_\gamma\}\text{GTP})]^{2-}$ have N sugars with N-glycosidic bond torsion angles (given by χ , O4'-C1'-N9-C4) in the anti ($\chi = -91.9^\circ$, $\chi_{\text{range}} = 180^\circ \pm 90^\circ$) and high anti ($\chi = -81.5^\circ$, $\chi_{\text{range}} = -60^\circ$ to -90°) ranges, respectively.²⁷ The conformation of the sugar-phosphate linkage is determined by the torsion angle γ (O5'-C5'-C4'-C3'); γ values of 43° and 41° for the S_{Re} *endo* and S_{Re} *exo* models of $fac\text{-}[\text{Re}(\text{CO})_3(\{\text{N}7, \text{P}_\beta, \text{P}_\gamma\}\text{GTP})]^{2-}$, respectively, indicate that the preferred conformation of the sugar-phosphate linkage is *gauche*, *gauche* (*gg*, $\gamma_{\text{range}} = 30^\circ$ to 90°).²⁷ Past modeling studies have shown that the S_{Re} diastereomer of $fac\text{-}[\text{Re}(\text{CO})_3(\text{H}_2\text{O})(\{\text{N}7, \text{P}_\beta\}\text{GDP})]^-$ has an N sugar with a high anti conformation around the glycosidic bond ($\chi = -67.4^\circ$), and the preferred conformation of the sugar-phosphate linkage is *gg* ($\gamma = 51.0^\circ$).²⁰

Table 4.5. Characteristics of *fac*- $[\text{Re}(\text{CO})_3(\{\text{N}7, \text{P}_\beta, \text{P}_\gamma\} \text{GTP})]^{2-}$ Model Complexes ^a

	χ (deg)	γ (deg)
S_{Re}		
<i>endo</i>	-91.9 (anti)	43.0 (<i>gg</i>)
<i>exo</i>	-81.5 (high anti)	45.0 (<i>gg</i>)

^aAngles χ and γ are defined by torsion angles O4'-C1'-N9-C4 and O5'-C5'-C4'-C3', respectively.²⁷

The results presented above for the S_{Re} diastereomers of both *fac*- $[\text{Re}(\text{CO})_3(\text{H}_2\text{O})(\{\text{N}7, \text{P}_\beta\} \text{GDP})]^-$ and *fac*- $[\text{Re}(\text{CO})_3(\{\text{N}7, \text{P}_\beta, \text{P}_\gamma\} \text{GTP})]^{2-}$ are in good agreement with results found for other metal-nucleotide macrochelate complexes.²⁹ NMR spectroscopic studies (of *cis*- $[\text{Pt}(\text{ND}_2\text{CH}_3)_2(\{\text{N}7, \text{P}_\gamma\} \text{ITP})]^{12}$), molecular mechanics studies (of *cis*- $[\text{Pt}(\text{NH}_3)_2(\{\text{N}7, \text{P}_\gamma\} \text{GTP})]^{12}$ and *cis*- $[\text{Pt}(\text{NH}_3)_2(\{\text{N}7, \text{P}_\alpha\} \text{GMP})]^{12}$) and X-ray structural studies (of the cyclic trimer $[(\eta^6\text{-}p\text{-MeC}_6\text{H}_4\text{Pr}^i)\text{Ru}(\{\text{N}7\} \text{AMP})]_3$)³⁰ have demonstrated a nearly exclusive preference for N sugars with an anti (or high anti) conformation around the glycosidic bond and a *gg* conformation of the sugar-phosphate linkage.

During this study, we noted that the ~0.2 ppm downfield shift of the H8 signals of *fac*- $[\text{Re}(\text{CO})_3(\{\text{N}7, \text{P}_\beta, \text{P}_\gamma\} \text{GTP})]^{2-}$ upon Re(I) coordination (free 5'-GTP, 8.26 ppm; **1-G** and **2-G**, 8.43 ppm) is considerably smaller than the ~0.5 ppm downfield shift of the H8 signals of *fac*- $[\text{Re}(\text{CO})_3(\text{H}_2\text{O})(\{\text{N}7, \text{P}_\beta\} \text{GDP})]^-$ (free 5'-GDP, 8.21 ppm; products, ~8.74 ppm).²⁰ Distance measurements taken from *fac*- $[\text{Re}(\text{CO})_3(\{\text{N}7, \text{P}_\beta, \text{P}_\gamma\} \text{GTP})]^{2-}$ and *fac*- $[\text{Re}(\text{CO})_3(\text{H}_2\text{O})(\{\text{N}7, \text{P}_\beta\} \text{GDP})]^-$ model complexes show that the H8 proton is ~1 Å closer to the phosphate backbone in the S_{Re} *endo* and S_{Re} *exo* diastereomers of *fac*-

$[\text{Re}(\text{CO})_3(\{\text{N7},\text{P}_\beta,\text{P}_\gamma\}\text{GTP})]^{2-}$ (average H8-O5' distances = 2.5 Å), compared to the S_{Re} diastereomer of $\text{fac}-[\text{Re}(\text{CO})_3(\text{H}_2\text{O})(\{\text{N7},\text{P}_\beta\}\text{GDP})]^-$ (H8-O5' distance = 3.2 Å). This proximity may result in a larger shielding effect near the H8 proton of $\text{fac}-[\text{Re}(\text{CO})_3(\{\text{N7},\text{P}_\beta,\text{P}_\gamma\}\text{GTP})]^{2-}$ compared to $\text{fac}-[\text{Re}(\text{CO})_3(\text{H}_2\text{O})(\{\text{N7},\text{P}_\beta\}\text{GDP})]^-$, resulting in a larger downfield shift of the H8 proton of the latter upon Re(I) coordination.

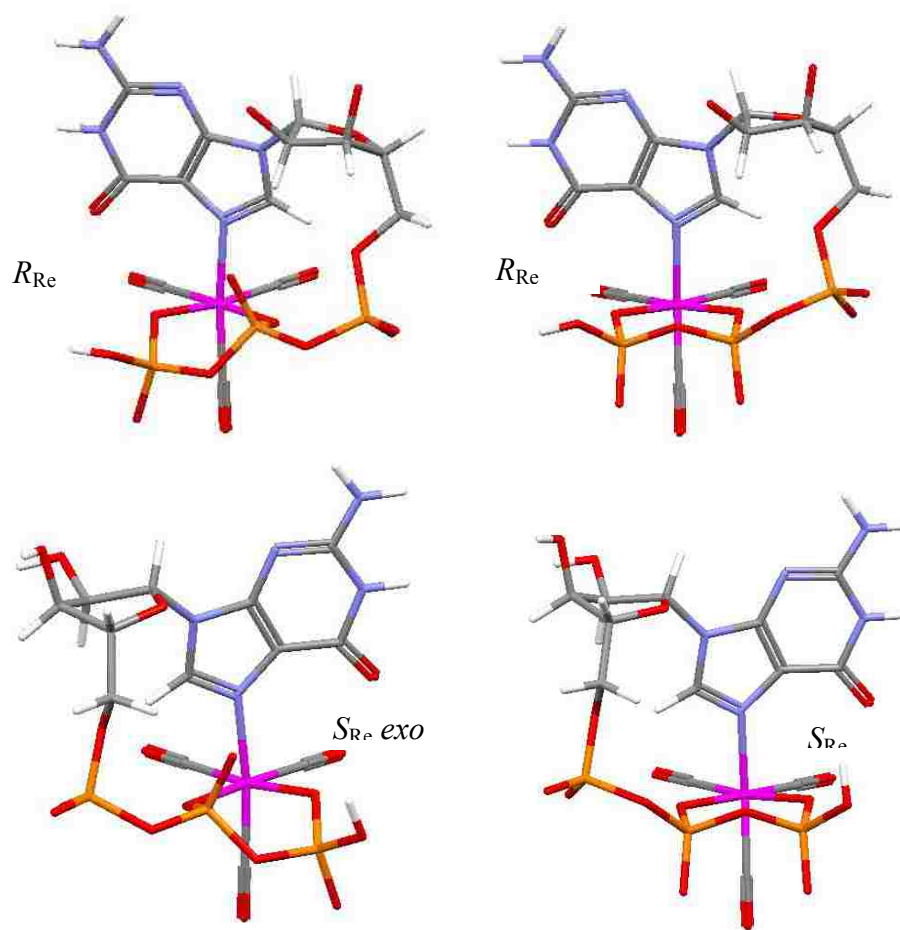


Figure 4.8. Models of four possible diastereomers of $\text{fac}-[\text{Re}(\text{CO})_3(\{\text{N7},\text{P}_\beta,\text{P}_\gamma\}\text{GTP})]^{2-}$.

4.3.7 5'-ATP Reaction Products

When treated with $\text{fac}-[\text{Re}(\text{CO})_3(\text{H}_2\text{O})_3]^+$, 5'-ATP formed primarily a macrochelate 1:1 adduct, $\text{fac}-[\text{Re}(\text{CO})_3(\{\text{N7},\text{P}_\beta,\text{P}_\gamma\}\text{ATP})]^-$; the tridentate 1:1 phosphato chelate $\text{fac}-$

$[\text{Re}(\text{CO})_3(\{\text{P}_\alpha, \text{P}_\beta, \text{P}_\gamma\}\text{ATP})]^-$ was also formed as a minor product. One hour after mixing *fac*- $[\text{Re}(\text{CO})_3(\text{H}_2\text{O})_3]^+$ with 5'-ATP (25 mM, $r = 1:1$), five new H8 ^1H NMR singlets were present. Two H8 signals of nearly equal intensity at 8.84 and 8.86 ppm are approximately three times more intense than an apparent H8 triplet centered at 8.64 ppm (it is likely that the apparent H8 triplet is the result of four overlapping H6 signals); these products are thus designated as the major (**1-A**) and minor (**2-A**) products, respectively (Table 4.6). The shift changes upon coordination of the H8 signals of **1-A** and **2-A** are ~ 0.15 ppm *downfield*, and ~ 0.1 ppm *upfield*, respectively. Two new H2 signals (at 8.45 and 8.48 ppm) and two new H1' signals (at 6.31 and 6.37 ppm) were observed; these signals can be assigned to **1-A**. The H2 and H1' signals of **1-A** are only slightly shifted compared to the same signals of free 5'-ATP (Table 4.6). The H2 and H1' signals of **2-A** are small and are obscured by the respective signals of the free nucleotide. At equilibrium, **1-A** and **2-A** account for 60% and 20% of the total 5'-ATP, respectively; $\sim 20\%$ of the added 5'-ATP remains unreacted. Under pH 3.6 conditions, 5'-ATP binding is more favorable than 5'-UTP or $\text{H}_2\text{PPP}^{3-}$ binding, but slightly less favorable than 5'-GTP binding.

Table 4.6. ^1H and ^{31}P NMR Chemical Shifts (ppm), Coupling Constants (Hz) of 5'-ATP and Complexes Formed with *fac*- $[\text{Re}(\text{CO})_3(\text{H}_2\text{O})_3]^+$ ^a

complex	$\delta \text{ } ^1\text{H}$			$\delta \text{ } ^{31}\text{P}$		
	H8	H2	H1' ($J_{\text{H1}'\text{-H2}'}$)	P_α ($J_{\alpha\beta}$)	P_β	P_γ
5'-ATP	8.71	8.48	6.25 (5.2)	-14.4 (18.6)	-25.9	13.8
	8.84	8.45	6.31 (3.1)			-7.7
1-A	8.86	8.48	6.36 (3.6)	-14.1 ^b	-20.8	-8.0
		^c	^c	-9.0 (17.3), -9.2 (18.0)		-5.9
2-A	8.64			-10.2 (18.1), -10.4 (20.0)	-16.9	-6.5

^a[Re] = 25 mM, pH 3.6. ^bCoupling not observed due to signal overlap. ^cSignals obscured by signals of free 5'-ATP.

The $\{^1\text{H}\}-^{31}\text{P}$ NMR spectrum of the (25 mM, $r = 1:1$) reaction mixture supports the ^1H NMR data indicating the presence of two products (Table 4.6). Two multiplets, due to their presence in the most upfield region of the ^{31}P NMR spectrum, are without question P_β signals. A large P_β multiplet (-20.8 ppm) and a small P_β multiplet (-16.9 ppm) can be assigned to **1-A** and **2-A**, respectively. Broadening observed in a proton-coupled ^{31}P NMR spectrum confirmed that two large doublets near -14.1 ppm and four smaller doublets near -10.0 ppm are P_α signals. Thus, two large doublets at -8.0 ppm and two smaller (apparent) triplets (it is likely that the two triplets result from overlapping of four doublets) near -6.0 ppm are P_γ signals. The P_α - P_β and P_β - P_γ connectivities observed in a proton-decoupled ^{31}P - ^{31}P COSY experiment (25 mM, $r = 1:1$) allowed identification of ^{31}P nuclei within the same spin system. Thus, the P_β multiplet at -20.8 ppm, two P_α doublets at -14.1 ppm and two P_γ doublets at -8.0 ppm can be assigned to **1-A**; and the P_β multiplet at -16.9 ppm, four P_α doublets at -10.0 ppm and two P_γ (apparent) triplets at -6.0 ppm can be assigned to **2-A**. Compared to the respective free 5'-ATP signals, the P_α , P_β and P_γ signals are shifted downfield by ~ 0.3 , ~ 5 , and ~ 6 ppm for **1-A**, and ~ 4.5 , ~ 9 , and ~ 7.5 ppm for **2-A** (Table 4.6). These results demonstrate that P_β and P_γ are directly coordinated to Re(I) in both **1-A** and **2-A**; however, P_α is directly coordinated to Re(I) only in **2-A**. The downfield shift upon Re(I) coordination for the two H8 signals of **1-A** indicates that Re(I) is bound via N7 of the adenine base; the slight *upfield* shift upon Re(I) coordination for the H8 signals of **2-A** indicates that Re(I) is likely not bound via N7 of the adenine base. Thus, we can conclude that **1-A** is *fac*- $[\text{Re}(\text{CO})_3(\{\text{N7}, \text{P}_\beta, \text{P}_\gamma\} \text{ATP})]^-$, and **2-A** is *fac*- $[\text{Re}(\text{CO})_3(\{\text{P}_\alpha, \text{P}_\beta, \text{P}_\gamma\} \text{ATP})]^-$.

Raising the pH of a sample containing 60% **1-A**, 20% **2-A**, and 20% free 5'-ATP from ~ 3.6 to ~ 7 resulted in significant sharpening of the ^{31}P NMR signals of **1-A** and **2-A**. At pH ~ 7 , the sample contained 75% **1-A**, 19% **2-A**, and 6% free 5'-ATP. Thus, as the pH of the sample is

increased, unbound 5'-ATP reacts with *fac*-[Re(CO)₃(H₂O)₃]⁺ to form more of the tridentate macrochelate **1-A**. The amount of **2-A** in the sample decreased slightly from 20% to 19% on raising the pH from ~3.6 to ~7; this result indicates that formation of **2-A** is not pH-dependent. No change in the chemical shift of the P_α signals of **1-A** and **2-A** was observed on raising the pH to ~7. However, the P_β signals shift ~1 and ~0.5 ppm for **1-A** and **2-A**, respectively; and the P_γ signals shift ~1.5 and ~1.2 ppm for **1-A** and **2-A**, respectively.

4.3.8 Considerations Regarding the Solution Structure of [Mg(ATP)]

The [Mg(ATP)] complex is the natural substrate for a variety of enzymatic processes. Thus, determining the coordination mode of the nucleotide in [Mg(ATP)] has been the focus of a large number of investigations. The results of these experiments have been analyzed to suggest that Mg²⁺ binds 5'-ATP only via P_β and P_γ oxygen atoms,¹⁸ while results from other experiments have been interpreted to suggest that Mg²⁺ binds 5'-ATP via P_α, P_β, and P_γ oxygen atoms.³¹ Early ³¹P NMR spectroscopic studies performed by Cohn et al. showed that the addition of Mg²⁺ caused the P_α, P_β, and P_γ ³¹P NMR signals of 5'-ATP to shift ~0.2, 2.1 and 2.3 ppm downfield (Table 4.3), leading these researchers to suggest that the [Mg(ATP)] complex exists predominantly as a bidentate {P_β,P_γ} phosphato chelate in solution.¹⁸ Later, broadening observed in ¹⁷O NMR spectroscopic studies was interpreted as an indication that P_α was also involved in chelation of Mg²⁺, leading to a tridentate {P_α,P_β,P_γ} phosphato chelate.³¹ In addition, molecular dynamics studies of the conformational equilibria of [Mg(ATP)] in aqueous solution have suggested that [Mg(ATP)] is equally likely to exist as either the {P_α,P_β,P_γ} or the {P_β,P_γ} phosphato chelate.³² Originally proposed by Szent-Györgyi in 1956¹⁶, Martin and Mariam⁴ also suggested that [Mg(ATP)] exists as a {N7,P_β,P_γ} macrochelate, in which Mg²⁺ has an inner-

sphere interaction with N7, P_β, and P_γ. However, space-filling models, generated by Sigel et al., have indicated that a simultaneous inner-sphere interaction of both N7 and P_α is possible without “much” strain.^{33,34} Despite this, Sigel and coworkers have recently interpreted stability constant data as indicating no direct Mg²⁺ to adenine base interaction.²

Several researchers have suggested that the use of Rh(III) and Co(III) complexes of 5'-ATP as models for [Mg(ATP)]. ³¹P NMR spectroscopic studies of [Rh(H₂O)₃({P_α,P_β,P_γ}ATP)] and [Co(NH₃)₃({P_α,P_β,P_γ}ATP)] have shown that the P_α, P_β, and P_γ signals shifted between 10 and 18 ppm *downfield* from the same ³¹P NMR signals of 5'-ATP upon metal coordination (Table 4.3).^{8,10,15} These results demonstrate that P_α, P_β, and P_γ are directly bound to the Rh(III) (or Co(III)) metal center in both [Rh(H₂O)₃({P_α,P_β,P_γ}ATP)] and [Co(NH₃)₃({P_α,P_β,P_γ}ATP)]. Also, the *magnitude* of the downfield shift upon coordination is significantly larger in [Rh(H₂O)₃({P_α,P_β,P_γ}ATP)] and [Co(NH₃)₃({P_α,P_β,P_γ}ATP)], compared to [Mg(ATP)], indicating that Rh(III) and Co(III) have a much greater deshielding effect than Mg(II). These results demonstrate that Rh(III) and Co(III) complexes of 5'-ATP are not accurate models for the [Mg(ATP)] complex.

The results presented here suggest that the *fac*-[Re(CO)₃]⁺ core could be used as a more accurate model for the biologically relevant [Mg(ATP)] complex. The *fac*-[Re(CO)₃]⁺ core is both octahedral and exchange-inert, and is not prone to oligomer formation.

4.4 Conclusions

The nucleoside triphosphate adducts described here contain the kinetically inert, octahedral *fac*-[Re(CO)₃]⁺ core. When *fac*-[Re(CO)₃(H₂O)₃]⁺ is allowed to react with NTPs, an equilibrium distribution of product diastereomers is established, and sharp ³¹P NMR signals

arising from each diastereomer can be distinguished. Thus, we can conclude that when all three phosphate groups are coordinated to Re(I), as in *fac*-[Re(CO)₃({P_α,P_β,P_γ}UTP)]²⁻, there is a significant stereochemical preference for diastereomers with the base moiety directed away from the coordinated phosphate chain (*exo*) compared to those diastereomers with the base directed toward the phosphate chain (*endo*). We found no evidence indicating a preference for one Re(I) chirality over the other for {P_α,P_β,P_γ} chelate complexes. Thus, these results provide additional support for our suggestion that when metal nucleotide complexes act as enzyme cofactors,^{6,7,35-38} the preferred stereochemistry of the active, enzyme-bound metal-nucleotide complex is likely to be controlled by the enzyme and not by the stereochemical preference of the nucleotide adduct.²⁰

Metals ions in biological roles, such as Mg²⁺, are generally hard metals that have little affinity for the endocyclic nitrogens of nucleotides.³ Placement of the *fac*-[Re(CO)₃]⁺ cation in Pearson's hard-soft acids and bases³⁹ scheme, using a modification by Martin,⁴⁰ indicates that Re(I) is a "borderline" metal center.⁴¹ Such a classification is somewhat unexpected for a monovalent third-row transition metal, as these metals are typically quite soft. However, a significant amount of electron density is displaced onto the three π-backbonding CO ligands, effectively increasing the hardness of Re(I). The "borderline" hardness of Re(I) most likely increases the affinity of the metal center for the phosphate oxygen atoms of a nucleotide, but does not preclude an interaction between Re(I) and N7 of the base moiety.

Only one clear example of an NTP macrochelate having a direct metal–N7 bond has been reported; [Ru(η⁶-C₆H₆)]²⁺ forms a tridentate {N7,P_β,P_γ} macrochelate when allowed to react with 5'-ATP.³⁰ However, this system is not suitable as a general model for macrochelates containing an octahedral metal center, because [Ru(η⁶-C₆H₆)]²⁺ readily forms oligomers in aqueous solution, and the ³¹P NMR signals of the resulting [(Ru(η⁶-C₆H₆)({N7,P_β,P_γ}ATP)]⁻

complex are not well defined.³⁰ We have demonstrated that the *fac*-[Re(CO)₃]⁺ core could be used as a general model for further investigations into the structure of macrochelates, as *fac*-[Re(CO)₃({N₇,P_β,P_γ}GTP)]²⁻ and *fac*-[Re(CO)₃({N₇,P_β,P_γ}ATP)]⁻ are both stable and easily accessible via the reaction of *fac*-[Re(CO)₃(H₂O)₃]⁺ with 5'-GTP or 5'-ATP.

4.5 References

1. Lippard, S. J.; Berg, J. M. *Principles of Bioinorganic Chemistry*; University Science Books: Mill Valley, CA, 1994.
2. Sigel, H.; Griesser, R. *Chem. Soc. Rev.* **2005**, *34*, 875-900.
3. Marzilli, L. G. In *Prog. Inorg. Chem.*; Lippard, S. J., Ed.; John Wiley and Sons: New York, 1977; Vol. 23, pp 255-278.
4. Martin, R. B.; Mariam, Y. H. *Met. Ions Biol. Syst.* **1979**, *8*, 57-124.
5. Cleland, W. W. *Methods Enzymol.* **1982**, *87*, 159-179.
6. Cleland, W. W.; Mildvan, A. S. In *Advances in Inorganic Biochemistry*; Eichhorn, G. L., Marzilli, L. G., Eds.; Elsevier / North-Holland: New York, 1979; Vol. 1, pp 163-191.
7. Cornelius, R. D.; Cleland, W. W. *Biochemistry* **1978**, *17*, 3279-3286.
8. Cornelius, R. D.; Hart, P. A.; Cleland, W. W. *Inorg. Chem.* **1977**, *16*, 2799-2805.
9. Korn, S.; Sheldrick, W. S. *Inorg. Chim. Acta* **1997**, *254*, 85-91.
10. Lu, Z.; Shorter, A. L.; Lin, I.; Dunaway-Mariano, D. *Inorg. Chem.* **1988**, *27*, 4135-4139.
11. Pecoraro, V. L.; Hermes, J. D.; Cleland, W. W. *Biochemistry* **1984**, *23*, 5262-5271.
12. Reily, M. D.; Hambley, T. W.; Marzilli, L. G. *J. Am. Chem. Soc.* **1988**, *110*, 2999-3007.
13. Sigel, H. *Eur. J. Biochem.* **1987**, *165*, 65-72.
14. Sigel, H. *Pure Appl. Chem.* **2004**, *76*, 375-388.
15. Speckhard, D. C.; Pecoraro, V. L.; Knight, W. B.; Cleland, W. W. *J. Am. Chem. Soc.* **1986**, *108*, 4167-4171.

16. Szent-Györgyi, A. In *Enzymes, Units of Biological Structure and Function*; Gaebler, O. H., Ed.; Academic Press: New York, 1956, pp 393-397.
17. Lin, I.; Knight, W. B.; Ting, S.-J.; Dunaway-Mariano, D. *Inorg. Chem.* **1984**, *23*, 988-991.
18. Cohn, M.; Hughes Jr., T. R. *J. Biol. Chem.* **1962**, *237*, 176-181.
19. Adams, K. M.; Marzilli, L. G. *Inorg. Chem.* **2007**, *46*, 4926-4936.
20. Adams, K. M.; Marzilli, P. A.; Marzilli, L. G. *Inorg. Chem.* **2007**, *46*, 9172-9181.
21. Egli, A.; Hegetschweiler, K.; Alberto, R.; Abram, U.; Schibli, R.; Hedinger, R.; Gramlich, V.; Kissner, R.; Schubiger, P. A. *Organometallics* **1997**, *16*, 1833-1840.
22. He, H.; Lipowska, M.; Xu, X.; Taylor, A. T.; Carlone, M.; Marzilli, L. G. *Inorg. Chem.* **2005**, *44*, 5437-5446.
23. HyperChem Version 7.5, Hypercube, Inc., Gainesville, FL.
24. He, H.; Lipowska, M.; Christoforou, A. M.; Marzilli, L. G.; Taylor, A. T. *Nucl. Med. Biol.* **2007**, *34*, 709-716.
25. Sigel, H., details to be published; personal communication, Nov. 2007.
26. Sigel, H.; Bianchi, E. M.; Corfù, N. A.; Kinjo, Y.; Tribolet, R.; Martin, R. B. *J. Chem. Soc., Perkin Trans. 2* **2001**, 507-511.
27. Saenger, W. *Principles of Nucleic Acid Structure*; 1st ed.; Springer-Verlag: New York, 1984.
28. Tribolet, R.; Malini-Balakrishnan, R.; Sigel, H. *J. Chem. Soc., Dalton Trans.* **1985**, 2291-2303.
29. Aoki, K. *Met. Ions Biol. Syst.* **1996**, *32*, 91-134.
30. Korn, S.; Sheldrick, W. S. *J. Chem. Soc., Dalton Trans.* **1997**, *12*, 2191-2199.
31. Huang, S. L.; Tsai, M.-D. *Biochemistry* **1982**, *21*, 951-959.
32. Liao, J.-C.; Sun, S.; Chandler, D.; Oster, G. *Eur. Biophys. J.* **2004**, *33*, 29-37.
33. Sigel, H.; Scheller, K. H. *Eur. J. Biochem.* **1984**, *138*, 291-299.
34. Sigel, H.; Tribolet, R.; Malini-Balakrishnan, R.; Martin, R. B. *Inorg. Chem.* **1987**, *26*, 2149-2157.

35. Dunaway-Mariano, D.; Cleland, W. W. *Biochemistry* **1980**, *19*, 1506-1515.
36. Lu, Z.; Shorter, A. L.; Dunaway-Mariano, D. *Biochemistry* **1993**, *32*, 2378-2385.
37. Bakhtina, M.; Lee, S.; Wang, Y.; Dunlap, C.; Lamarche, B.; Tsai, M.-D. *Biochemistry* **2005**, *44*, 5177-5187.
38. Yang, L.; Arora, K.; Beard, W. A.; Wilson, S. H.; Schlick, T. *J. Am. Chem. Soc.* **2004**, *126*, 8441-8453.
39. Pearson, R. G. *Chemical Hardness: Applications from Molecules to Solids*; Wiley-VCH Verlag GmbH: Weinheim, Germany, 1997.
40. Martin, R. B. *Inorg. Chim. Acta* **2002**, *339*, 27-33.
41. Salignac, B.; Grundler, P. V.; Cayemittes, S.; Frey, U.; Scopelliti, R.; Merbach, A. E.; Hedinger, R.; Hegetschweiler, K.; Alberto, R.; Prinz, U.; Raabe, G.; Kölle, U.; Hall, S. *Inorg. Chem.* **2003**, *42*, 3516-3526.
42. Altona, C.; Sundaralingam, M. *J. Am. Chem. Soc.* **1973**, *95*, 2333-2344.

CHAPTER 5.

PROGRESS TOWARDS X-RAY CRYSTALLOGRAPHIC CHARACTERIZATION OF COMPLEXES CONTAINING 5-6 BICYCLIC BIOLIGANDS BOUND TO THE *fac*-[Re(CO)₃]⁺ CORE

5.1 Introduction

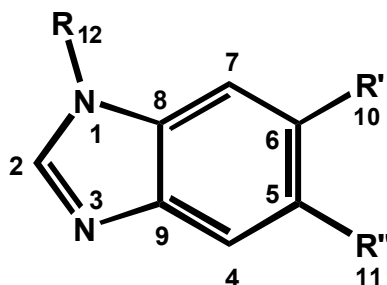
In recent years, the great success of the antineoplastic agent cisplatin has fueled the search for other metal-based cytotoxic agents having high levels of efficacy with fewer toxic effects. Although much of the focus has been directed towards complexes based on the square-planar, inert, and redox-stable Pt(II) metal center, octahedral metal centers are more likely to form kinetically inert, redox-stable complexes. Several octahedral metal complexes have shown modest anticancer properties; some of the most promising complexes contain Ru(II) and dinuclear Rh(II)/Rh(II) metal centers.¹⁻⁹

Complexes containing the *fac*-[Re(CO)₃]⁺ core have also displayed modest cytotoxic activity against a number of murine and human leukemia and lymphoma tumor cell lines.¹⁰ However, the mechanism of action of octahedral metal-containing complexes is generally not well understood. A broader understanding of the behavior of *fac*-[Re(CO)₃]⁺ complexes in biological systems, and that displayed by other octahedral metal-based complexes, can be gained by exploring interactions of the *fac*-[Re(CO)₃]⁺ core with nucleotides and other bioligands in both the solid and solution states.¹¹⁻¹⁷

Recently, the first *cis*-bis(**G**) (**G** = guanine base derivative) complexes containing the *fac*-[Re(CO)₃]⁺ core, *fac*-[Re(CO)₃(MeG)₂(H₂O)]ClO₄, were characterized by X-ray crystallography (MeG = 9-methylguanine, 7-methylguanine).^{16,17} X-ray structural evidence confirmed that the *fac*-[Re(CO)₃]⁺ moiety can bind two guanine bases in a *cis* fashion, and the two bases can assume either a head-to-head (HH) or a head-to-tail (HT) orientation around the Re(I) metal

center.^{16,17} Although some researchers have noted¹⁸ that the purine O6 can become sterically demanding in octahedral complexes, the ~ 2.2 Å Re–N7 bond (~ 0.2 Å longer a Pt–N7 bond) lessens the steric effect imposed by the purine O6. In conclusion, these studies found that rotation about the Re–N7 bond is unrestricted by steric hindrance imposed by O6 of the coordinated guanines, and that neither steric hindrance nor intramolecular H-bonding were factors deciding the preferred conformation of the product *cis*-bis(MeG) complexes.¹⁷

Chart 5.1. Structure of Bzm Ligands with Numbering of Relevant Atoms



Bzm	$R = R' = R'' = -H$
MeBzm	$R = -CH_3, R' = R'' = -H$
Me₂Bzm	$R = -H, R' = R'' = -CH_3$
Me₃Bzm	$R = R' = R'' = -CH_3$

Planar aromatic N-donor ligands (L) containing a five-membered imidazole ring, such as purine bases and benzimidazoles, constitute an important class of bioligands. Benzimidazole (Bzm), the simplest of these ligands, possesses no exocyclic groups, while the more complex purine base analog 1,5,6-trimethylbenzimidazole (Me₃Bzm) is non-*C*₂-symmetric (i.e. lopsided, Chart 5.1). Previous studies of octahedral Ru(II) *cis*-bis(Me₃Bzm) complexes have shown that the orientation of the Me₃Bzm ligands is dependent upon both steric and electronic factors.^{19,20} The N₂CH proton (H2) of the imidazole ring is somewhat acidic and bears a partial positive charge, and the amount of the positive charge on H2 increases upon imidazole ring binding to metal centers.^{19,20} The positively charged H2 can be electrostatically attracted to nearby

negatively charged ligands (such as halides), thus exerting electrostatic control over the observed conformation of the product complex.²⁰ In order to gain greater understanding of the steric and electronic forces controlling the orientation of N-donor ligands in *cis*-bis(L) complexes containing the *fac*-[Re(CO)₃]⁺ core, we have synthesized and crystallized a series of *fac*-[Re(CO)₃(L)₂Br] and *fac*-[Re(CO)₃(L)₂(O-donor)]⁺ complexes, where L = Bzm, 1-methylbenzimidazole (MeBzm), 5,6-dimethylbenzimidazole (Me₂Bzm), and Me₃Bzm; and O-donor = H₂O or OTf. Specifically, the compounds reported here include: *fac*-[(Bzm)₂Re(CO)₃Br] (**5.1**), *fac*-[(MeBzm)₂Re(CO)₃Br] (**5.2**), *fac*-[(Me₂Bzm)₂Re(CO)₃Br] (**5.3**), *fac*-[(Me₃Bzm)₂Re(CO)₃Br] (**5.4**), *fac*-[(Bzm)₂Re(CO)₃(H₂O)]OTf (**5.5**), *fac*-[(MeBzm)₂Re(CO)₃(H₂O)]OTf (**5.6**), *fac*-[(Me₂Bzm)₂Re(CO)₃(H₂O)]OTf (**5.7**), and *fac*-[(Me₃Bzm)₂Re(CO)₃(H₂O)]OTf (**5.8**). The crystal structures of **5.1-5.3**, **5.6** and **5.7** have been determined, as has that of *fac*-[(Me₂Bzm)₂Re(CO)₃(OTf)] (**5.7a**).

5.2 Experimental Section

5.2.1 Starting Materials

[Re(CO)₅Br]²¹, [Re(CO)₅OTf]²² (OTf = trifluoromethanesulfonate), and Me₃Bzm²³ were prepared as described in the literature. Bzm, MeBzm, and Me₂Bzm and all solvents were obtained from Sigma-Aldrich and were used as received.

5.2.2 Synthetic Procedures

***fac*-[Re(CO)₃(L)₂(H₂O)]OTf and *fac*-[Re(CO)₃(L)₂Br]. Method A.** A benzene solution (20 mL) containing either [Re(CO)₅Br] or [Re(CO)₅OTf] (0.137 mmol) was treated with L (0.274 mmol), and the reaction mixture was heated at reflux for ~4 h. After allowing the reaction mixture to cool to room temperature, the volume of the solvent was reduced to ~1 ml under a

stream of N₂. The resulting white powdery solids were precipitated with hexanes, filtered, washed with hexanes, and dried in vacuo. Use of this method resulted in high yields of powdered *fac*-[Re(CO)₃(L)₂(H₂O)]OTf and *fac*-[Re(CO)₃(L)₂Br] complexes that required no further purification.

***fac*-[(Bzm)₂Re(CO)₃Br] (5.1).** Method A gave a white precipitate: yield, 33 mg (41%). X-ray quality crystals were obtained by recrystallization from benzene/hexanes. ¹H NMR (ppm) in CDCl₃: 9.93 (s, 2H, N1H), 8.28 (s, 2H, B2H), 7.54 (d, 2H, B4H), 7.40 (d, 2H, B7H), 7.20 (m, 4H, B5H/B6H).

***fac*-[(MeBzm)₂Re(CO)₃Br] (5.2).** Method A gave a white precipitate: yield, 63 mg (75%). X-ray quality crystals were obtained by recrystallization from benzene/hexanes. ¹H NMR (ppm) in CDCl₃: 8.44 (s, 2H, B2H), 7.63 (d, 2H, B4H), 7.41 (d, 2H, B7H), 7.30 (m, 4H, B5H/B6H), 3.78 (s, 6H, B12H₃).

***fac*-[(Me₂Bzm)₂Re(CO)₃Br] (5.3).** Method A gave a white precipitate: yield, 37 mg (43%). X-ray quality crystals were obtained by recrystallization from benzene/hexanes. ¹H NMR (ppm) in CDCl₃: 9.69 (s, 2H, N1H), 8.04 (s, 2H, B2H), 7.22 (s, 2H, B4H), 7.10 (s, 2H, B7H), 2.25 (s, 6H, B10H₃), 2.17 (s, 6H, B11H₃).

***fac*-[(Me₃Bzm)₂Re(CO)₃Br] (5.4).** Method A gave a white precipitate: yield, 75 mg (81%). ¹H NMR (ppm) in CDCl₃: 8.29 (s, 2H, B2H), 7.35 (s, 2H, B4H), 7.14 (s, 2H, B7H), 3.71 (s, 6H, B12H₃), 2.37 (s, 6H, B10H₃), 2.24 (s, 6H, B11H₃).

***fac*-[(Bzm)₂Re(CO)₃(H₂O)]OTf (5.5).** Method A gave a white precipitate: yield, 49 mg (54%).

***fac*-[(MeBzm)₂Re(CO)₃(H₂O)]OTf (5.6).** Method A gave a white precipitate: yield, 41 mg (42%). X-ray quality crystals were obtained by recrystallization from benzene/hexanes. ¹H

NMR (ppm) in CDCl₃: 8.10 (s, 2H, B2H), 7.63 (d, 2H, B4H), 7.41 (d, 2H, B7H), 7.30 (m, 4H, B5H/B6H), 3.83 (s, 6H, B12H₃).

***fac*-[(Me₂Bzm)₂Re(CO)₃(H₂O)]OTf (5.7).** Method A gave a white precipitate; yield, 83 mg (85%). Colorless, block-shaped, X-ray quality crystals of [(Me₂Bzm)₂Re(CO)₃(H₂O)]OTf (**7**) were collected directly from the reaction solution, after allowing the open vessel to stand overnight at room temperature. The reaction vessel was then sealed and allowed to stand overnight once more. Colorless plate-like crystals, identified as [(Me₂Bzm)₂Re(CO)₃OTf] (**5.7a**) by X-ray crystallography, were deposited after ~24 h.

***fac*-[(Me₃Bzm)₂Re(CO)₃(H₂O)]OTf (5.8).** Method A gave a white precipitate; yield, 91 mg (93%).

5.2.3 NMR Spectroscopy

All NMR spectra were obtained on either a Bruker DPX400 spectrometer (400.1 MHz) or a Varian INOVA500 spectrometer (500.1 MHz); both were equipped with a variable temperature probe that was equilibrated at 25 °C unless otherwise indicated. 1D ¹H NMR spectra were referenced to the residual HOD peak, and presaturation was used to reduce the residual HOD peak. Each FID was accumulated for 64 transients, each containing 16K data points. Before Fourier transformation, an exponential apodization window function with a 0.2 Hz line broadening was applied. All NMR data were processed with either XWINNMR (Bruker) or VnmrJ (Varian) software.

5.2.4 X-Ray Crystallographic Data Collection and Structure Determination

Single crystals were mounted in a cooled N₂ gas stream at 90 K (or 297 K for complex **5.2**) on a Nonius Kappa CCD diffractometer (equipped with an Oxford Cryostream cooler) with

graphite-monochromated Mo-K α ($\lambda = 0.71073 \text{ \AA}$) radiation. Data reduction included absorption corrections by the multi-scan method, using HKL DENZO and SCALEPACK.²⁴ All X-ray structures were solved by direct methods and refined by full-matrix least-square on F^2 using the SIR97²⁵ and SHELXL97²⁶ crystallographic software packages. All non-hydrogen atoms were refined anisotropically. Hydrogen atoms were visible in difference maps, but were placed in idealized locations. All non-hydrogen atoms were refined anisotropically.

5.3 Results and Discussion

5.3.1 X-ray Characterization

All complexes have a slightly distorted octahedral structure with three CO ligands occupying one face. Two of the three other coordination sites are occupied by an imidazole nitrogen of **L**, while the third site is occupied by either a bromide ligand (as in **5.1**, **5.2** and **5.3**) or an oxygen atom (of H₂O, as in **5.6** and **5.7**; or of OTf, as in **5.7a**) (Figure 5.1). Crystallographic data and structure refinement parameters for complexes **5.1-5.3**, **5.6-5.7**, and **5.7a** are listed in Table 5.1. Selected bond lengths and angles are given in Table 5.2.

In all complexes, the Re–N and Re–O bond lengths ($\sim 2.2 \text{ \AA}$) and the N–Re–N bond angles ($\sim 85^\circ$) are comparable to values for other complexes containing similar N-donor ligands.^{16,17,27} The near bisection of the CO–Re–CO angle by the plane of the benzimidazole ligands is another universal feature of the crystal structures studied here. This feature is commonly observed in other *cis*-bis(**G**) and *cis*-bis(**L**) complexes of octahedral metals such as Re(I) and Ru(II).^{16,17,19,20} However, it is quite interesting to note that, for all complexes except for **5.3**, the benzimidazole ligands are in the HH orientation (with the H2's on the same side of the N–Re–N coordination plane). A unique example, complex **5.3** crystallizes with an HH (**5.3a**)

and an HT (**5.3b**, Figure 5.2) conformer in the unit cell. A more detailed analysis of the solid state conformation of complexes **5.1-5.3**, **5.6**, **5.7** and **5.7a** appears below in Section 5.2.1.3.

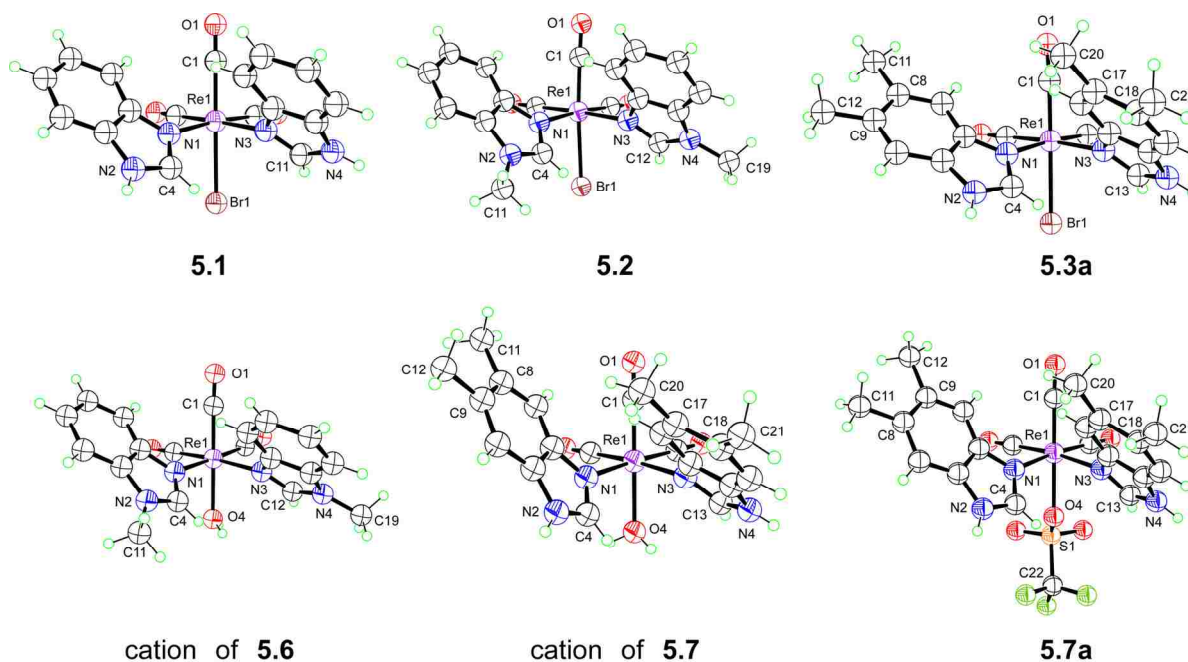


Figure 5.1. Perspective drawings of $[(\text{Bzm})_2\text{Re}(\text{CO})_3\text{Br}]$ (**5.1**), $[(\text{MeBzm})_2\text{Re}(\text{CO})_3\text{Br}]$ (**5.2**), $[(\text{Me}_2\text{Bzm})_2\text{Re}(\text{CO})_3\text{Br}]$ (HH, **5.3a**), $[(\text{MeBzm})_2\text{Re}(\text{CO})_3(\text{H}_2\text{O})]\text{OTf}$ (**5.6**), $[(\text{Me}_2\text{Bzm})_2\text{Re}(\text{CO})_3(\text{H}_2\text{O})]\text{OTf}$ (**5.7**) and $[(\text{Me}_2\text{Bzm})_2\text{Re}(\text{CO})_3\text{OTf}]$ (**5.7a**). Counter ions have been omitted for clarity. Thermal ellipsoids are drawn with 50% probability.

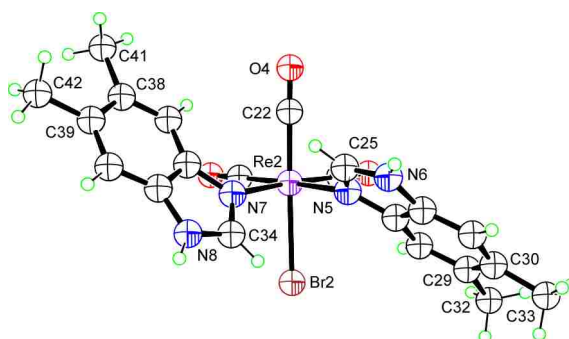


Figure 5.2. Perspective drawing of $[(\text{Me}_2\text{Bzm})_2\text{Re}(\text{CO})_3\text{Br}]$ (HT, **5.3b**). Thermal ellipsoids are drawn with 50% probability.

Table 5.1. Crystal Data and Structure Refinement for [(Bzm)₂Re(CO)₃Br] (**5.1**), [(MeBzm)₂Re(CO)₃Br] (**5.2**), [(Me₂Bzm)₂Re(CO)₃Br] (**5.3**), [(MeBzm)₂Re(CO)₃(H₂O)]OTf (**5.6**), [(Me₂Bzm)₂Re(CO)₃(H₂O)]OTf (**5.7**), and [(Me₂Bzm)₂Re(CO)₃(OTf)] (**5.7a**)

<i>Crystal data</i>	5.1	5.2	5.3	5.6	5.7	5.7a
Chemical formula	C ₁₇ H ₁₂ BrN ₄ O ₃ Re·2.5(C ₆ H ₆)	C ₁₉ H ₁₆ BrN ₄ O ₃ Re·1.5(C ₆ H ₆)	C ₂₁ H ₂₀ BrN ₄ O ₃ Re·C ₆ H ₆	C ₁₉ H ₁₈ N ₄ O ₄ Re·CF ₃ O ₃ S·C ₆ H ₆	C ₂₁ H ₂₂ N ₄ O ₄ Re·CF ₃ O ₃ S·0.5(C ₆ H ₆)·H ₂ O	C ₂₂ H ₂₀ F ₃ N ₄ O ₆ ReS·C ₆ H ₆
<i>M_r</i>	781.69	731.63	720.63	779.75	787.77	789.79
Cell setting, space group	Triclinic, <i>P</i> -1	Monoclinic, <i>C</i> 2/ <i>c</i>	Monoclinic, <i>P</i> 2 ₁ / <i>n</i>	Triclinic, <i>P</i> -1	Monoclinic, <i>C</i> 2/ <i>c</i>	Monoclinic, <i>P</i> 2 ₁ / <i>n</i>
Temperature (K)	90	297	90	90	90 (2)	90
<i>a</i> , <i>b</i> , <i>c</i> (Å)	10.9826 (14), 11.6453 (15), 12.1719 (16)	32.2569 (14), 9.3265 (2), 22.9218 (10)	13.2275 (10), 13.4881 (10), 30.793 (3)	11.1993 (16), 12.200 (2), 12.696 (2)	25.414 (2), 17.994 (2), 15.5564 (15)	11.4329 (15), 23.594 (3), 11.4625 (10)
β (°)	97.756 (6), 99.657 (7), 100.375 (6)	126.1351 (11)	95.183 (4)	69.105 (7), 64.011 (8), 87.796 (9)	123.510 (5)	91.015 (7)
<i>V</i> (Å ³)	1487.5 (3)	5569.3 (4)	5471.4 (8)	1442.3 (4)	5931.5 (10)	3091.5 (6)
<i>Z</i>	2	8	8	2	8	4
<i>D_x</i> (Mg m ⁻³)	1.745	1.745	1.750	1.795	1.764	1.697
Radiation type	Mo <i>K</i> α	Mo <i>K</i> α	Mo <i>K</i> α	Mo <i>K</i> α	Mo <i>K</i> α	Mo <i>K</i> α
μ (mm ⁻¹)	5.47	5.83	5.94	4.36	4.24	4.06
Crystal form, colour	Parallelepiped, colorless	Needle, colorless	Lath, colorless	Lath, colorless	Fragment, colorless	Plate, colorless
Crystal size (mm)	0.25 × 0.20 × 0.10	0.25 × 0.05 × 0.04	0.20 × 0.12 × 0.03	0.20 × 0.12 × 0.03	0.12 × 0.10 × 0.07	0.18 × 0.10 × 0.03
<i>Data collection</i>						
Diffractometer	Nonius KappaCCD (with Oxford Cryostream)	Nonius KappaCCD	Nonius KappaCCD (with Oxford Cryostream)	Nonius KappaCCD (with Oxford Cryostream)	Nonius KappaCCD (with Oxford Cryostream)	Nonius KappaCCD (with Oxford Cryostream)
Data collection method	ω scans with κ offsets	ω scans with κ offsets	ω scans with κ offsets	ω scans with κ offsets	ω scans with κ offsets	ω scans with κ offsets
Absorption correction	Multi-scan (based on symmetry-related measurements)	Multi-scan (based on symmetry-related measurements)	Multi-scan (based on symmetry-related measurements)	Multi-scan (based on symmetry-related measurements)	Multi-scan (based on symmetry-related measurements)	Multi-scan (based on symmetry-related measurements)

(Table 5.1 continued)

T_{\min}	0.342	0.323	0.383	0.476	0.630	0.528
T_{\max}	0.611	0.800	0.842	0.880	0.756	0.888
No. of measured, independent and observed reflections	45519, 13429, 11734	32826, 8538, 5013	67503, 19619, 12814	34655, 7555, 6783	48785, 9210, 7536	48513, 7439, 5090
Criterion for observed reflections	$I > 2\sigma(I)$	$I > 2\sigma(I)$	$I > 2\sigma(I)$	$I > 2\sigma(I)$	$I > 2\sigma(I)$	$I > 2\sigma(I)$
R_{int}	0.033	0.047	0.055	0.023	0.026	0.047
$\theta_{\max} (\infty)$	35.7	30.8	32.6	30.0	30.8	29.2
<i>Refinement</i>						
Refinement on	F^2	F^2	F^2	F^2	F^2	F^2
$R[F^2 > 2\sigma(F^2)]$, $wR(F^2)$, S	0.033, 0.077, 1.04	0.046, 0.064, 1.00	0.042, 0.086, 0.95	0.028, 0.062, 1.04	0.033, 0.077, 1.03	0.040, 0.069, 1.01
No. of reflections	13429 reflections	8538 reflections	19619 reflections	7555 reflections	9210 reflections	7439 reflections
No. of parameters	371	337	657	382	396	393
H-atom treatment	Constrained to parent site	Constrained to parent site	Constrained to parent site	Constrained to parent site	Mixture of independent and constrained refinement	Constrained to parent site
Weighting scheme	Calculated $w = 1/[\sigma^2(F_o^2) + (0.0362P)^2 + 1.2027P]$ where $P = (F_o^2 + 2F_c^2)/3$	Calculated $w = 1/[\sigma^2(F_o^2) + (0.0032P)^2 + 12.1288P]$ where $P = (F_o^2 + 2F_c^2)/3$	Calculated $w = 1/[\sigma^2(F_o^2) + (0.0336P)^2]$ where $P = (F_o^2 + 2F_c^2)/3$	Calculated $w = 1/[\sigma^2(F_o^2) + (0.0263P)^2 + 2.6506P]$ where $P = (F_o^2 + 2F_c^2)/3$	Calculated $w = 1/[\sigma^2(F_o^2) + (0.0337P)^2 + 24.730P]$ where $P = (F_o^2 + 2F_c^2)/3$	Calculated $w = 1/[\sigma^2(F_o^2) + (0.0271P)^2]$ where $P = (F_o^2 + 2F_c^2)/3$
$(\Delta/\sigma)_{\max}$	0.002	0.003	0.003	0.001	0.005	0.001
$\Delta\rho_{\max}, \Delta\rho_{\min} (e \approx^{-3})$	2.21, -3.15	0.84, -0.91	2.63, -3.79	2.69, -1.47	2.73, -1.21	1.27, -1.91
Extinction method	SHELXL			SHELXL	SHELXL	SHELXL
Extinction coefficient	0.0012 (2)			0.00070 (19)	0.00021 (2)	0.00058 (8)

5.3.1.1 Crystal Packing

As shown in Table 5.2, the average distance between Re(I) centers in adjacent complexes ranges from 6.60 Å (complex **5.3**) to 9.27 Å (complex **5.2**), with an average Re–Re separation of

8.39 Å. The shorter than average distance between Re(I) centers observed for complex **5.3** is likely because the solid state structure is highly stabilized by both π -stacking interactions and H-bonding (see next section). In **5.3**, one Me₂Bzm ligand in an HT complex is π -stacked nearly parallel to a Me₂Bzm ligand in an HH complex. The stacked benzimidazoles are slightly tilted relative to one another, as the C2 atoms are separated by 3.4 Å, but the C6 and C5 atoms are separated by 3.8 Å and 3.9 Å, respectively.

Table 5.2. Selected Bond Distances (Å) and Angles (°) for [(Bzm)₂Re(CO)₃Br] (**5.1**), [(MeBzm)₂Re(CO)₃Br] (**5.2**), [(Me₂Bzm)₂Re(CO)₃Br] (HH, **5.3a**; HT, **5.3b**), [(MeBzm)₂Re(CO)₃(H₂O)]OTf (**5.6**), [(Me₂Bzm)₂Re(CO)₃(H₂O)]OTf (**5.7**) and [(Me₂Bzm)₂Re(CO)₃OTf] (**5.7a**)

	5.1	5.2	5.3a	5.3b	5.6	5.7	5.7a
bond distances							
Re–N1	2.194 (2)	2.190 (3)	2.185 (3)	2.192 (3)	2.171 (3)	2.178 (3)	2.174 (3)
Re–N3	2.196 (2)	2.202 (3)	2.196 (3)	2.192 (3)	2.182 (2)	2.183 (3)	2.182 (3)
Re–Br	2.6511 (4)	2.6442 (5)	2.6583 (4)	2.6724 (4)	2.185 (2) ^a	2.205 (2) ^a	2.211 (3) ^a
Re–Re ^b	7.86	9.27	6.60		8.96	8.89	8.73
bond angles							
N1–Re–N3	84.41 (7)	85.37 (12)	84.99 (12)	84.53 (11)	86.07 (9)	84.09 (10)	83.34 (12)

^a Re–O4 distance. ^b average distance between Re(I) metal centers.

Despite having a less than average separation between Re(I) centers (7.86 Å), no evidence for π -stacking interactions between benzimidazole ligands was found in the solid state structure of complex **5.1**. Conversely, the solid state structure of **5.2** is stabilized only by antiparallel π -stacking between the benzimidazole ligands of two adjacent HH molecules, with a mean separation of 3.59 Å, leading to a longer than average distance between Re(I) centers. These results indicate that the distance between Re(I) centers is shorter in complexes having both types of interactions, while the presence of only H-bonding interactions or only π -stacking results in a greater distance between Re(I) centers. In contrast to complexes containing Br, no

evidence for π -stacking interactions was found for complexes **5.6**, **5.7** and **5.7a** (in which the sixth coordination position is occupied by an oxygen atom of H₂O, in **5.6** and **5.7**; and of OTf in **5.7a**).

5.3.1.2 Hydrogen Bonding

A complete table of hydrogen bonding interactions appears in Table 5.3. As mentioned above, the solid state structure of complex **5.3** is highly stabilized by H-bonds; both N1H's of a HT molecule are H-bonded to the Br ligand of an adjacent HH molecule (average N to Br distance = 3.34 Å); likewise, both N1H's of an HH molecule are H-bonded to the Br ligand of an adjacent HT molecule (average N to Br distance = 3.36 Å). Complex **5.1** is stabilized only by intermolecular H-bonds between the N1H's of the Bzm ligands and the Br ligands of adjacent molecules (average N to Br distance = 3.51 Å). Conversely, complex **5.2** (the remaining Br-containing complex) is the only complex studied here lacking H-bonding interactions. The lack of H-bonds leads to a longer than average separation between Re(I) centers (9.27 Å) in **5.2**.

The three OTf-containing solid state structures (complexes **5.6**, **5.7** and **5.7a**) possess a number of H-bonds, leading to slightly longer than average distances between Re(I) centers. Complex **5.6** is stabilized by two H-bonds between the H₂O ligand and adjacent counter ion OTf oxygen atoms (average O to O distance = 2.68 Å). In complex **5.7**, the N1H of each coordinated Me₂Bzm has an H-bond to a counter ion OTf oxygen atom (average N to O distance = 2.96 Å). In addition, the coordinated H₂O ligand in **5.7** is stabilized by one H-bond to a solvent H₂O oxygen (O to O distance = 2.90 Å) and one H-bond to a counter ion OTf oxygen (O to O distance = 2.73 Å). In complex **5.7a**, intermolecular H-bonding is observed between the coordinated OTf oxygen atoms and the N1H of adjacent molecules in the unit cell (average N to O distance = 2.89 Å).

Table 5.3. Hydrogen bond geometry

D–H···A ^a	D–H (Å)	H···A (Å)	D···A (Å)	D–H···A (°)
5.1				
N2–H2N···Br1(a)	0.88	2.85	3.503(2)	132.0
N4–H4N···Br1(b)	0.88	2.98	3.518(2)	121.0
5.3				
N2–H2N···Br2(c)	0.88	2.58	3.404 (3)	156.2
N4–H4N···Br2(d)	0.88	2.57	3.307 (3)	141.4
N6–H6N···Br1(e)	0.88	2.59	3.356 (3)	145.5
N8–H8N···Br1(f)	0.88	2.53	3.328 (4)	151.8
5.6				
O4–H1W···O5(g)	0.82	1.84	2.656 (3)	173
O4–H2W···O7	0.82	1.89	2.709 (3)	173
5.7				
O4–H4A···O5	0.84	1.89	2.730 (4)	176.6
O4–H4B···O9(h)	0.84	2.07	2.900 (4)	167.7
N2–H2N···O6(h)	0.84 (4)	2.46 (4)	3.033 (4)	127 (3)
N4–H4N···O5(i)	0.80 (4)	2.09 (4)	2.888 (4)	172 (4)
5.7a				
N2–H2N···O5(j)	0.88	2.04	2.881 (4)	159.1
N4–H4N···O6(k)	0.88	2.06	2.898 (4)	158.8

^aSymmetry codes: (a) 2-x, 1-y, 1-z; (b) 1-x, 1-y, 1-z; (c) 1/2-x, 1/2+y, 3/2-z; (d) x, 1+y, z; (e) x, y-1, z; (f) 3/2-x, y-1/2, 3/2-z; (g) -x+1, -y+1, -z; (h) 1-x, 1-y, 1-z; (i) x, 1-y, z-1/2; (j) x-1/2, 3/2-y, 1/2+z; (k) x-1/2, 3/2-y, z-1/2.

5.3.1.3 Base Orientation

For an octahedral complex with three facial CO ligands, each *cis*-coordinated **L** can have two possible orientations, “up” or “down” (Figure 5.3). (“Up” and “down” refer to the direction H2 is pointing, towards the axial CO in the former case and towards X in the latter.) Thus, there are a total of four possible isomers for a *cis*-bis(**L**) complex containing the *fac*-[Re(CO)₃]⁺ core. Because the H2 atom experiences a different chemical environment in the “up” and “down” positions, the HH_u and HH_d conformers are distinguishable both by X-ray crystallography and

NMR spectroscopy. However, for complexes containing two identical nonchiral L's (such as those studied here), the Δ HT and Λ HT conformers are distinguishable only by X-ray crystallography, as both conformers would give identical NMR spectra.

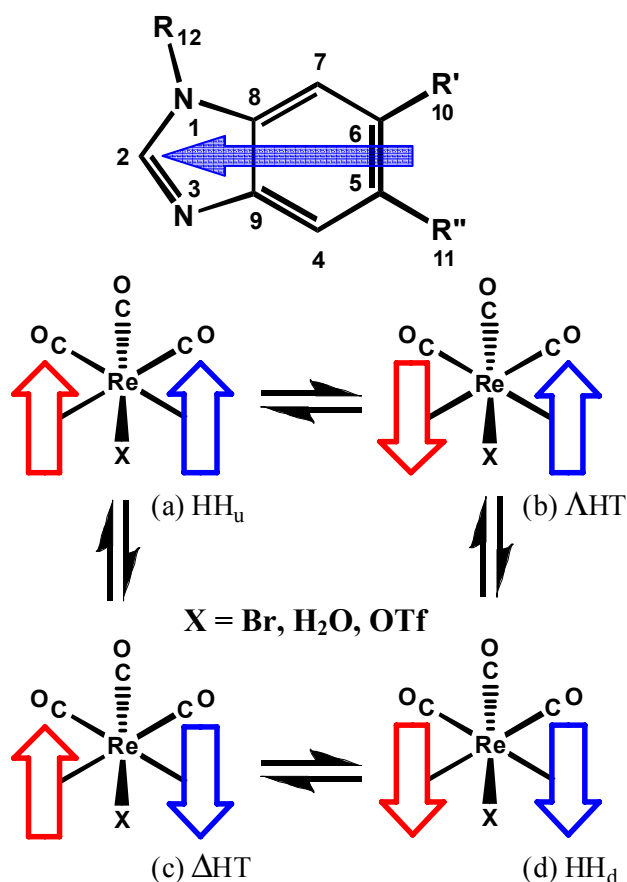


Figure 5.3. The arrow and its head represent the 6-membered ring and B2H, respectively. The red and blue arrows represent ligands **B** and **B'**; these designations are used in the text to refer to coordination positions occupied by benzimidazole ligands.

In the solid state structure of the HT conformer of fac -[Re(CO)₃(9-MeG)₂(H₂O)]⁺ (9-MeG = 9-methylguanine), the H2 of base **B** points down towards the axial H₂O ligand, while the H2 of base **B'** points up, towards the axial CO ligand (the Λ HT orientation, Figure 5.3). In this ligand arrangement, two stabilizing intra- and intermolecular H-bonds are formed; the

As noted previously, the ligands are in the HH orientation for all complexes reported here (with the exception of complex **5.3**, see above). Furthermore, the H2 atoms of both coordinated ligands are directed downwards, toward the axial X (for X = Br or O), indicating that all HH complexes show exclusively the HH_d conformation (Figure 5.3). In the only HT complex found here (in the same unit cell as the HH_d conformer of complex **5.3**), the H2 of Me₂Bzm in position **B** is directed downwards, while the H2 of ligand **B'** is directed upwards; this pattern describes the Λ HT conformation (Figure 5.3).

coordinated H₂O ligand has an *intramolecular* H-bond to the O6 atom of the ligand in the **B'** position and an *intermolecular* H-bond to an O6 atom in an adjacent complex.¹⁷ In addition, the positively charged H2 of the **B** ligand is electrostatically attracted to the negatively charged oxygen atom of the axial H₂O ligand ($H \cdots O = 2.57 \text{ \AA}$). In both solid state and solution studies of *cis*-bis(Me₃Bzm) complexes of Ru(II), the electrostatic interaction between the negatively charged axial ligand and the positively charged H2 proton on the imidazole ring was found to be the most important factor determining the specific orientation of *one* Me₃Bzm ligand,^{19,20,28,29} thus, the exclusive formation of the HH_d conformation for complexes **5.1**, **5.2**, **5.3a**, **5.6**, **5.7**, **5.7a** in the solid state corroborates this previous finding. However, it seems that with the lack of any exocyclic H-bonding groups (e.g., O6 for purine bases) on the ligands used here, the electrostatic interaction between the H2 protons of *both* benzimidazole ligands and the negatively charged X ligand controls the specific orientation (namely, HH_d) of the product complexes in the solid state.

5.3.1.4 Dihedral Angles

Several useful parameters have been developed to compare the structural features of square-planar metal-purine complexes; these same parameters can also be used to describe and compare octahedral metal-purine complexes of other 5-6 bicyclic ligands (e.g., benzimidazoles).^{17,28,30} The **B/B'** dihedral angle is measured at the intersection of the planes passing through the *cis*-coordinated ligands. The **B/CP** and **B'/CP** angles are measured at the intersection of the plane passing through the **B** and **B'** ligands, respectively, and the plane defined by Re, the two N's of the coordinated ligands, and the two C's *trans* to the coordinated N's (CP = coordination plane).

As shown in Table 5.4, the **B/B'** dihedral angle for the complexes described herein ranges from 50° to 71°, with an average **B/B'** angle of 61°. This average **B/B'** angle is comparable to that reported for *fac*-[Re(CO)₃(9-MeG)₂(H₂O)]ClO₄ and *fac*-[Re(CO)₃(9-MeG)₂(H₂O)]Br.¹⁷ The **B/CP** angles observed in the benzimidazole complexes do not vary significantly, however, it is notable that complex **5.3** possesses both the smallest (**5.3a**) and the largest (**5.3b**) **B/CP** angles (40° and 52°, respectively). The **B'/CP** angles are slightly more diverse, ranging from 42° (**5.3b**) to 56° (**5.7**).

Table 5.4. Relevant Conformational Parameters for [(Bzm)₂Re(CO)₃Br] (**5.1**), [(MeBzm)₂Re(CO)₃Br] (**5.2**), [(Me₂Bzm)₂Re(CO)₃Br] (HH, **5.3a**; HT, **5.3b**), [(MeBzm)₂Re(CO)₃(H₂O)]OTf (**5.6**), [(Me₂Bzm)₂Re(CO)₃(H₂O)]OTf (**5.7**) and [(Me₂Bzm)₂Re(CO)₃OTf] (**5.7a**)

	dihedral angles (°)			bite angle (°)	conformation	close contacts (Å)	
	B/B'	B/CP	B'/CP	NB-Re-NB'		X-BH2	X-B'H2
5.1	67	49	47	84.41 (7)	HH _d	2.91	3.09
5.2	71	50	47	85.37 (12)	HH _d	2.96	2.97
5.3a	59	40	45	84.99(12)	HH _d	3.02	3.18
5.3b	61	52	42	84.53 (11)	ΔHT	2.92	4.85
5.6	56	44	46	86.07 (9)	HH _d	2.87	2.98
5.7	50	46	56	84.09 (10)	HH _d	2.63	2.91
5.7a	64	51	51	83.34 (12)	HH _d	2.53	2.76
5.A^a	66	48	50	83.06(17)	ΔHT	2.57	4.43
5.B^b	57	51	46	81.9(4)	HH _u	4.50	4.50

^a**5.A** = *fac*-[Re(CO)₃(9-MeG)₂(H₂O)]ClO₄¹⁷; ^b**5.B** = *fac*-[Re(9-MeG)₂(H₂O)(CO)₃]Br¹⁷.

Previous studies of the effects of intra- and interligand interactions on the solid state molecular conformation of *cis*-[(en)(1,3,9-TMX)₂Pt]²⁺ cations (1,3,9-TMX = 1,3,9-trimethylhypoxanthine) found that intermolecular H-bonding favors a small **B/CP** angle, while interligand steric factors favor a larger **B/CP** angle.³⁰ Indeed, this trend is apparent in this work,

as the smallest **B**/CP and **B'**/CP angles belong to complex **5.3**, a structure that is highly stabilized by both π -stacking and interligand H-bonds (see above). It has been suggested that π -stacking interactions result in large **B**/CP angles;¹⁷ however, we do not find this to be the case for Re(I) complexes containing benzimidazole ligands. For example, complex **5.2** is stabilized only by antiparallel π -stacking interactions between the MeBzm ligands of two adjacent HH molecules; the **B**/CP and **B'**/CP angles for **5.2** are nearly identical to those of complex **5.1**, in which no π -stacking interactions are present (Table 5.4).

5.4 Conclusions

The results presented here demonstrate clearly that benzimidazole and similar methyl-substituted ligands can have either a HH or an HT conformation within an octahedral complex containing the *fac*-[Re(CO)₃]⁺ core. However, the HH conformation appears to be preferred in the solid state, with the positively charged H2 of each ligand electrostatically attracted to the negatively charged axial X (for X = Br or O) ligand; thus, the HH complexes show exclusively the HH_d conformation. The solid state HH_d conformation of *cis*-bis(L) complexes of Re(I) is stabilized by either π -stacking interactions or H-bonding, or a combination of both factors. It is generally accepted that the **G** bases in the cytotoxic intrastrand Pt-DNA cross-link have the HH orientation; thus, any potential metal drugs should show accessibility to an HH conformation. These results offer hope that novel drugs based on the *fac*-[Re(CO)₃]⁺ core can be developed, having fewer toxic side effects in conjunction with increased cytotoxic activity.

5.5 References

1. Alessio, E.; Mestroni, G.; Bergamo, A.; Sava, G. *Curr. Top. Med. Chem.* **2004**, *4*, 1525-1535.
2. Chifotides, H. T.; Dunbar, K. R. *Acc. Chem. Res.* **2005**, *38*, 146-156.

3. Chifotides, H. T.; Koshlap, K. M.; Pérez, L. M.; Dunbar, K. R. *J. Am. Chem. Soc.* **2003**, *125*, 10714-10724.
4. Frausin, F.; Scarcia, V.; Cocchietto, M.; Furlani, A.; Serli, B.; Alessio, E.; Sava, G. *J. Pharmacol. Exp. Ther.* **2005**, *313*, 227-233.
5. Galanski, M.; Arion, V. B.; Jakupec, M. A.; Keppler, B. *Curr. Pharm. Des.* **2003**, *9*, 2078-2089.
6. Guichard, S. M.; Else, R.; Reid, E.; Zeitlin, B.; Aird, R.; Muir, M.; Dodds, M.; Fiebig, H.; Sadler, P. J.; Jodrell, D. I. *Biochem. Pharmacol.* **2006**, *71*, 408-415.
7. Hayward, R. L.; Schornagel, Q. C.; Tente, R.; Macpherson, J. S.; Aird, R. E.; Guichard, S.; Habtemariam, A.; Sadler, P.; Jodrell, D. I. *Cancer Chemother. Pharmacol.* **2005**, *55*, 577-583.
8. Velders, A. H.; Bergamo, A.; Alessio, E.; Zangrando, E.; Haasnoot, J. G.; Casarsa, C.; Cocchietto, M.; Zorzet, S.; Sava, G. *J. Med. Chem.* **2004**, *47*, 1110-1121.
9. Yan, Y. K.; Melchart, M.; Habtemariam, A.; Sadler, P. J. *Chem. Commun.* **2005**, 4764-4776.
10. Yan, Y.-K.; Cho, S. E.; Shaffer, K. A.; Rowell, J. E.; Barnes, B. J.; Hall, I. H. *Pharmazie* **2000**, *55*, 307-313.
11. Adams, K. M.; Marzilli, L. G. *Inorg. Chem.* **2007**, *46*, 4926-4936.
12. Adams, K. M.; Marzilli, P. A.; Marzilli, L. G. *Inorg. Chem.* **2007**, *46*, 9172-9181.
13. Alberto, R.; Schibli, R.; Waibel, R.; Abram, U.; Schubiger, P. A. *Coord. Chem. Rev.* **1999**, *190-192*, 901-919.
14. He, H.; Lipowska, M.; Xu, X.; Taylor, A. T.; Carlone, M.; Marzilli, L. G. *Inorg. Chem.* **2005**, *44*, 5437-5446.
15. Lipowska, M.; Cini, R.; Tamasi, G.; Xu, X.; Taylor, A. T.; Marzilli, L. G. *Inorg. Chem.* **2004**, *43*, 7774-7783.
16. Zobi, F.; Spingler, B.; Fox, T.; Alberto, R. *Inorg. Chem.* **2003**, *42*, 2818-2820.
17. Zobi, F.; Blacque, O.; Schmalte, H. W.; Spingler, B.; Alberto, R. *Inorg. Chem.* **2004**, *43*, 2087-2096.
18. Vliet, P. M. v.; Haasnoot, J. G.; Reedijk, J. *Inorg. Chem.* **1994**, *33*, 1934-1939.
19. Alessio, E.; Calligaris, M.; Iwamoto, M.; Marzilli, L. G. *Inorg. Chem.* **1996**, *35*, 2538-2545.

20. Alessio, E.; Iengo, E.; Zangrando, E.; Geremia, S.; Marzilli, P. A.; Calligaris, M. *Eur. J. Inorg. Chem.* **2000**, 2207-2219.
21. Schmidt, S. P.; Trogler, W. C.; Basolo, F. *Inorg. Synth.* **1990**, 28, 160-165.
22. Schmidt, S. P.; Nitschke, J.; Trogler, W. C. *Inorg. Synth.* **1989**, 26, 113-117.
23. Simonov, A. M.; Pozharskii, A. E.; Marianovskii, V. M. *Indian J. Chem.* **1967**, 5, 81-82.
24. Otwinowski, Z.; Minor, W. *Methods Enzymol.* **1997**, 276, 307-326.
25. Altomare, A.; Burla, M. C.; Camalli, M.; Cascarano, G. L.; Giacovazzo, C.; Guagliardi, A.; Moliterni, A. G. G.; Polidori, G.; Spagna, R. *J. Appl. Crystallogr.* **1999**, 32, 115-119.
26. Sheldrick, G. M. *SHELXL-97, A Program for the Solution of Crystal Structures from X-ray Data*; **1997**, University of Göttingen: Göttingen, Germany.
27. Oriskovich, T. A.; White, P. S.; Thorp, H. H. *Inorg. Chem.* **1995**, 34, 1629-1631.
28. Marzilli, L. G.; Iwamoto, M.; Alessio, E.; Hansen, L.; Calligaris, M. *J. Am. Chem. Soc.* **1994**, 116, 815-816.
29. Marzilli, L. G.; Marzilli, P. A.; Alessio, E. *Pure Appl. Chem.* **1998**, 70, 961-968.
30. Orbell, J. D.; Wilkowski, K.; Castro, B. d.; Marzilli, L. G.; Kistenmacher, T. J. *Inorg. Chem.* **1982**, 21, 813-821.

CHAPTER 6.

PROGRESS TOWARDS SYNTHESIS, CHARACTERIZATION AND X-RAY CRYSTALLOGRAPHIC STUDIES OF *fac*-[Re(CO)₃]⁺ COMPLEXES CONTAINING N,N'-BIDENTATE AROMATIC N-DONOR LIGANDS

6.1 Introduction

The success of cisplatin (*cis*-[Pt(NH₃)₂Cl₂]) as an antineoplastic agent has fueled the search for other highly efficacious metal-based cytotoxic agents with fewer toxic side effects. Complexes based on the square-planar, inert Pt(II) metal center have historically been the primary focus of the search for new drugs. However, we and others have recognized that complexes containing octahedral metal centers are more likely to form kinetically inert, redox-stable complexes. Several complexes containing Re(I), Ru(II), and dinuclear Rh(II)/Rh(II) metal centers have displayed modest cytotoxic activity.¹⁻¹⁰ Despite this, the mechanism of action of octahedral metal-based complexes has not been extensively studied and thus is generally not well understood.

Recent studies performed in our laboratory have focused on the structural aspects of square-planar Pt(II) complexes containing *N,N'*-bidentate aromatic N-donor ligands (N–N) such as 2,2'-bipyridine (and derivatives thereof).¹¹⁻¹³ In an effort to learn more about the solid-state structure of octahedral complexes containing *N,N'*-bidentate aromatic N-donor ligands, we undertook the synthesis of a series of Re(I) complexes having the general formula *fac*-[(N–N)Re(CO)₃X], where N–N = 4,4'-dimethyl-2,2'-bipyridine (4,4'-Me₂bpy), 5,5'-dimethyl-2,2'-bipyridine (5,5'-Me₂bpy), 6,6'-dimethyl-2,2'-bipyridine (6,6'-Me₂bpy), and 2,2'-bipyridine (bpy) (Figure 6.1); and X = Br, H₂O, and OTf. In this chapter, the synthesis and NMR characterization of several *fac*-[(N–N)Re(CO)₃X] complexes is reported, along with X-ray crystallographic structure determinations for *fac*-[(5,5'-Me₂bpy)Re(CO)₃Br] (**6.1**), *fac*-[(6,6'-Me₂bpy)Re(CO)₃Br]

(6.2), *fac*-[(2,9-Me₂phen)Re(CO)₃Br] (6.5). Also reported are X-ray crystallographic structure determinations for *fac*-[(4,4'-Me₂bpy)Re(CO)₃(H₂O)]OTf (6.6), *fac*-[(5,5'-Me₂bpy)Re(CO)₃(H₂O)]OTf (6.7), and *fac*-[(6,6'-Me₂bpy)Re(CO)₃(H₂O)]OTf (6.8). In addition, a unique case is presented in which the triflate anion is coordinated to the Re(I) metal center, and the resulting *fac*-[(6,6'-Me₂bpy)Re(CO)₃(OTf)] complex crystallizes in two different crystal morphologies (6.9a and 6.9b). Finally, deviations from planarity of the N–N ligand in the abovementioned complexes are presented and then compared to the calculated deviations from planarity of published Pt complexes containing N–N ligands.

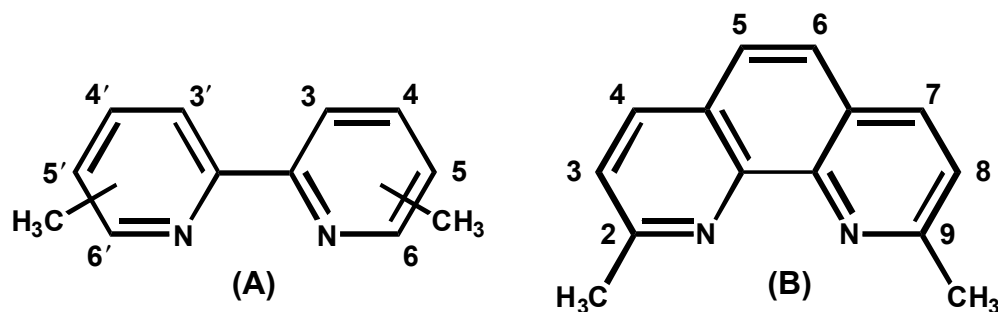


Figure 6.1. Graphical representation and atom numbering schemes for coordinated (A) dimethyl-2,2'-bipyridine derivatives, and (B) 2,9-dimethyl-1,10-phenanthroline (2,9-Me₂phen).

6.2 Experimental Section

6.2.1 Starting Materials

2,2'-Bipyridine (bpy), 4,4'-dimethyl-2,2'-bipyridine (4,4'-Me₂bpy), 5,5'-dimethyl-2,2'-bipyridine (5,5'-Me₂bpy), 6,6'-dimethyl-2,2'-bipyridine (6,6'-Me₂bpy), and 2,9-dimethyl-1,10-phenanthroline (2,9-Me₂phen) were used as received (Aldrich). [Re(CO)₅Br]¹⁴ and [Re(CO)₅OTf]¹⁵ were prepared as described in the literature. Other reagents were of analytical grade from commercial sources and were used without further purification.

6.2.2 Synthetic Procedures

***fac*-[(bpy)Re(CO)₃Br] Complexes. Method A.** A methanol solution (10 mL) containing [Re(CO)₅Br] (0.10 g, 0.05 M) and the desired N–N ligand (0.05 M) was heated at reflux for 4 hrs. After reducing the volume of the solvent by evaporation, the resulting yellow crystalline solid was precipitated with water, washed successively with methanol and diethyl ether, and dried in vacuo. Use of this method resulted in high yields, and no further purification of the product complex was required. X-ray quality crystals of **6.1** and **6.2** were obtained by mixing equimolar quantities (0.1 M) of the N–N ligand and [Re(CO)₅Br] in 1 mL methanol in an NMR tube, and allowing the capped tube to stand undisturbed for ~2 weeks. All other complexes were recrystallized from a mixture of acetone/diethyl ether.

Bromo(5,5'-dimethyl-2,2'-bipyridyl)tricarbonylrhenium(I) (**[(5,5'-Me₂bpy)Re(CO)₃Br]**, **6.1**). Method A gave a yellow powdery precipitate: yield, 90 mg (68%). Recrystallization afforded yellow block-shaped crystals. C₁₅H₁₂BrN₂O₃Re: ¹H NMR (CDCl₃, ppm): 8.87 (s, H6/6'), 8.02 (d, H3/3'), 7.82 (d, H4/4'), 2.51 (s, 5/5'-CH₃).

Bromo(6,6'-dimethyl-2,2'-bipyridyl)tricarbonylrhenium(I) (**[(6,6'-Me₂bpy)Re(CO)₃Br]**, **6.2**). Method A gave a yellow powder: yield, 70 mg (53%). Recrystallization afforded yellow prisms. C₁₅H₁₂BrN₂O₃Re: ¹H NMR (CDCl₃, ppm): 8.00 (d, H3/3'), 7.88 (t, H4/4'), 7.46 (d, H5/5'), 3.14 (s, 6/6'-CH₃).

Bromo(4,4'-dimethyl-2,2'-bipyridyl)tricarbonylrhenium(I) (**[(4,4'-Me₂bpy)Re(CO)₃Br]**, **6.3**). Method A gave a yellow powder: yield, 100 mg (76%). ¹H NMR (CDCl₃, ppm): 8.89 (d, H6/6'), 8.00 (s, H3/3'), 7.33 (d, H5/5'), 2.58 (s, 4/4'-CH₃).

Bromo(2,2'-bipyridyl)tricarbonylrhenium(I) (**[(bpy)Re(CO)₃Br]**, **6.4**). Method A gave a yellow powder: yield, 90 mg (72%). ¹H NMR (CDCl₃, ppm): 9.10 (d, H6/6'), 8.21 (d, H3/3'), 8.07 (m, H4/4'), 7.55 (m, H5/5').

Bromo(2,9-dimethyl-1,10-phenanthroline)tricarbonylrhenium(I) (**[(2,9-Me₂phen)Re(CO)₃Br]**, **6.5**). Method A gave a yellow powder. Recrystallization afforded X-ray quality, thin yellow needles.

fac-[(bpy)Re(CO)₃(H₂O)]OTf Complexes. Method B. A methanol solution (10 ml) of [Re(CO)₅OTf] (0.24 g, 0.1 M) and the desired N–N ligand (0.09 g, 0.1 M) was heated at reflux overnight. After cooling, the yellow solid was precipitated with diethyl ether, collected via gravity filtration, washed with diethyl ether and dried in vacuo. The resultant complexes (in powder form) required no further purification. X-ray quality crystals were obtained by recrystallization from a mixture of acetone/diethyl ether and allowing the open vessel to stand for ~1 week.

Aquo(4,4'-dimethyl-2,2'-bipyridyl)tricarbonylrhenium(I) triflate (**[(4,4'-Me₂bpy)Re(CO)₃(H₂O)]OTf**, **6.6**). Method B gave a yellow-orange powdery precipitate: yield, 130 mg (41%). Recrystallization afforded X-ray quality, thin yellow lath-shaped crystals. C₁₆H₁₄F₃N₂O₇SRe: ¹H NMR (CD₃OD, ppm): 8.95 (d, H6/6'), 8.56 (s, H3/3'), 7.64 (d, H5/5'), 2.64 (s, 4/4'–CH₃).

Aquo(5,5'-dimethyl-2,2'-bipyridyl)tricarbonylrhenium(I) triflate (**[(5,5'-Me₂bpy)Re(CO)₃(H₂O)]OTf**, **6.7**). Method B gave a light yellow powdery precipitate: yield, 170 mg (54%). Recrystallization afforded X-ray quality, thin yellow lath-shaped crystals. C₁₆H₁₄F₃N₂O₇SRe: ¹H NMR (CD₃OD, ppm): 8.95 (s, H6/6'), 8.50 (d, H3/3'), 8.19 (d, H4/4'), 2.56 (s, 5/5'–CH₃).

Aquo(6,6'-dimethyl-2,2'-bipyridyl)tricarbonylrhenium(I) triflate (**[(6,6'-Me₂bpy)Re(CO)₃(H₂O)]OTf**, **6.8**) and **triflate(6,6'-dimethyl-2,2'-bipyridyl)tricarbonylrhenium(I)** (**[(6,6'-Me₂bpy)Re(CO)₃(OTf)]**, **6.9**) Method B gave a yellow crystalline precipitate of **6.8**: yield, 220 mg (70%). Recrystallization afforded X-ray quality, thin yellow lath-shaped crystals. C₁₆H₁₄F₃N₂O₇SRe: ¹H NMR (CD₃OD, ppm): 8.46 (d, H3/3'), 8.18 (t, H4/4'), 7.76 (d, H5/5'), 3.12 (s, 6/6'-CH₃). A further recrystallization of **6.8** from a mixture of acetone/diethyl ether kept isolated from the environment yielded **[(6,6'-Me₂bpy)Re(CO)₃(OTf)]** (**6.9**). X-ray quality crystals having two different morphologies were isolated from the mother liquor. Complexes **6.9a** and **6.9b** are characterized by yellow lath-shaped crystals and by yellow block-shaped crystals, respectively.

6.2.3 NMR Spectroscopy

All NMR spectra were obtained on a Varian INOVA500 spectrometer (500.1 MHz) equipped with a variable temperature probe that was equilibrated at 25 °C unless otherwise indicated. 1D ¹H NMR spectra were referenced to the residual HOD peak, and presaturation was used to reduce the residual HOD peak. Each FID was accumulated for 64 transients, each containing 16K data points. Before Fourier transformation, an exponential apodization window function with a 0.2 Hz line broadening was applied. All NMR data were processed with VnmrJ (Varian) software.

6.2.4 X-Ray Crystallographic Data Collection and Structure Determination

Single crystals were mounted in a cooled N₂ gas stream at 110 K on a Nonius Kappa CCD diffractometer (equipped with an Oxford Cryostream cooler) with graphite-monochromated Mo-K α ($\lambda = 0.71073$ Å) radiation. Data reduction included absorption

corrections by the multi-scan method, using HKL DENZO and SCALEPACK.¹⁶ All X-ray structures were solved by direct methods and refined by full-matrix least-square on F^2 using the SIR97¹⁷ and SHELXL97¹⁸ crystallographic software packages. All non-hydrogen atoms were refined anisotropically. Hydrogen atoms were visible in difference maps, but were placed in idealized locations. All non-hydrogen atoms were refined anisotropically.

6.3 Results and Discussion

6.3.1 X-Ray Characterization

In general, the complexes discussed here have a distorted octahedral geometry, with three CO ligands occupying one face of the molecule in each complex. Two of the three other coordination sites are occupied by the nitrogen atoms of a chelating N–N ligand, resulting in the formation of a five-membered ring. The sixth coordination site is occupied by either a bromide ligand (as in **6.1**, **6.2** and **6.5**), or an oxygen atom (of H₂O, as in **6.6**, **6.7** and **6.8**, Figure 6.2; or of OTf, as in **6.9a** and **6.9b**, Figure 6.3). Crystallographic data and structure refinement parameters are listed in Table 6.1 for complexes **6.1**, **6.2**, and **6.5-6.8**; and selected bond lengths and angles are given in Table 6.2. A unique example, complex **6.9** crystallizes with the OTf counter ion coordinated to the Re(I) metal center, giving rise to two different crystal morphologies. The –CF₃ moiety of the OTf counter ion is directed towards a pyridyl ring of 6,6'-Me₂bpy in **6.9a** ([[(6,6'-Me₂bpy)Re(CO)₃(OTf_{up})]]), and away from the pyridine rings of 6,6'-Me₂bpy in **6.9b** ([[(6,6'-Me₂bpy)Re(CO)₃(OTf_{down})]]), Figure 6.3). Crystallographic data and structure refinement parameters are listed in Table 6.3 for complexes **6.9a** and **6.9b**; selected bond lengths and angles are given in Table 6.4.

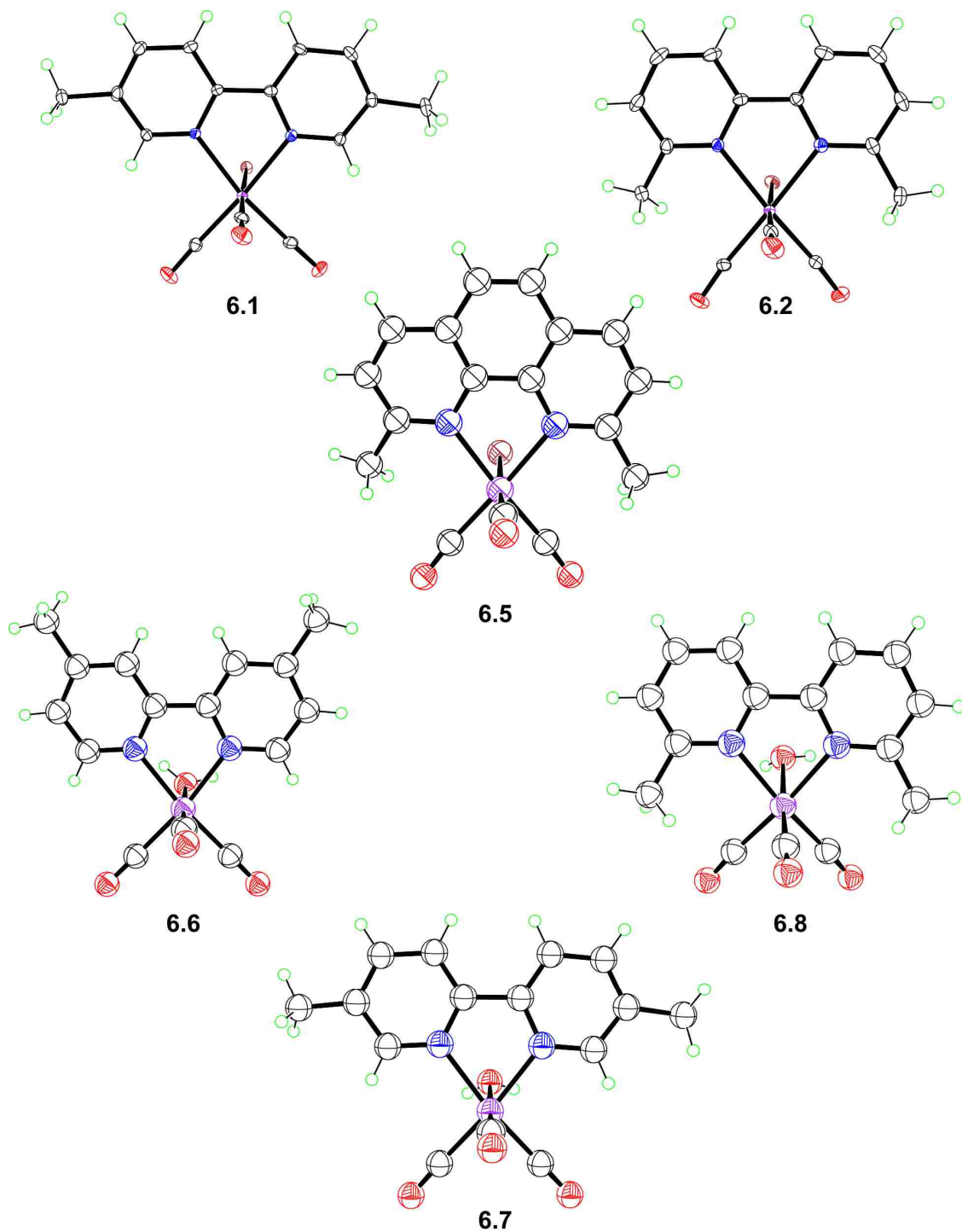


Figure 6.2. Perspective drawings of [(5,5'-Me₂bpy)Re(CO)₃Br] (**6.1**), [(6,6'-Me₂bpy)Re(CO)₃Br] (**6.2**), [(2,9-Me₂phen)Re(CO)₃Br] (**6.5**), [(4,4'-Me₂bpy)Re(CO)₃(H₂O)]OTf (**6.6**), [(5,5'-Me₂bpy)Re(CO)₃(H₂O)]OTf (**6.7**), and [(6,6'-Me₂bpy)Re(CO)₃(H₂O)]OTf (**6.8**). Counter ions have been omitted for clarity. Thermal ellipsoids are drawn with 50% probability.

Table 6.1. Crystal Data and Experimental Details for [(5,5'-Me₂bpy)Re(CO)₃Br] (**6.1**), [(6,6'-Me₂bpy)Re(CO)₃Br] (**6.2**), [(2,9-Me₂phen)Re(CO)₃Br] (**6.5**), [(4,4'-Me₂bpy)Re(CO)₃(H₂O)]OTf (**6.6**), [(5,5'-Me₂bpy)Re(CO)₃(H₂O)]OTf (**6.7**), and [(6,6'-Me₂bpy)Re(CO)₃(H₂O)]OTf (**6.8**)

complex	6.1	6.2	6.5	6.6	6.7	6.8
<i>Crystal data</i>						
Chemical formula	C ₁₅ H ₁₂ BrN ₂ O ₃ Re	C ₁₅ H ₁₂ BrN ₂ O ₃ Re	C ₁₇ H ₁₂ BrN ₂ O ₃ Re	C ₁₅ H ₁₄ N ₂ O ₄ Re ¹⁺ .CF ₃ O ₃ S ¹⁻	C ₁₅ H ₁₄ N ₂ O ₄ Re ¹⁺ .CF ₃ O ₃ S ¹⁻	C ₁₅ H ₁₄ N ₂ O ₄ Re ¹⁺ .CF ₃ O ₃ S ¹⁻
<i>M_r</i>	534.38	534.38	558.40	621.55	621.55	621.55
Cell setting	Monoclinic	Monoclinic	Monoclinic	Monoclinic	Monoclinic	Monoclinic
Space group	<i>P</i> 2 ₁ / <i>c</i>	<i>P</i> 2 ₁ / <i>c</i>	<i>P</i> 2 ₁ / <i>c</i>	<i>P</i> 2 ₁ / <i>n</i>	<i>P</i> 2 ₁ / <i>n</i>	<i>P</i> 2 ₁ / <i>n</i>
Temperature (K)	110	110	90	90	90	110
<i>a</i> , <i>b</i> , <i>c</i> (Å)	14.755 (3), 11.4799 (15), 9.3441 (10)	7.7268 (10), 20.891 (3), 9.8144 (12)	7.8414 (10), 21.825 (3), 9.5633 (12)	10.8811 (15), 9.8466 (14), 19.125 (2)	11.197 (2), 10.4487 (12), 16.846 (3)	12.998 (2), 8.0981 (10), 19.344 (3)
α , β , γ (°)	90, 105.609 (8), 90	90, 106.440 (7), 90	90, 104.012 (7), 90	95.249 (6)	91.883 (6)	100.102 (5)
<i>V</i> (Å ³)	1524.4 (4)	1519.5 (4)	1588.0 (4)	2040.5 (5)	1969.8 (5)	2004.6 (5)
<i>Z</i>	4	4	4	4	4	4
<i>D_x</i> (Mg m ⁻³)	2.328	2.336	2.336	2.023	2.096	2.060
Radiation type	Mo <i>K</i> α	Mo <i>K</i> α	Mo <i>K</i> α	Mo <i>K</i> α	Mo <i>K</i> α	Mo <i>K</i> α
μ (mm ⁻¹)	10.61	10.64	10.19	6.13	6.35	6.24
Crystal form, colour	Parallelepiped, yellow	Prism, yellow	Needle, yellow	Fragment, yellow	Lath, yellow	Fragment, yellow
Crystal size (mm)	0.22 × 0.10 × 0.10	0.22 × 0.13 × 0.07	0.22 × 0.08 × 0.03	0.20 × 0.10 × 0.07	0.20 × 0.05 × 0.02	0.17 × 0.12 × 0.10
<i>Data collection</i>						
Diffractometer	KappaCCD (with Oxford Cryostream)	KappaCCD (with Oxford Cryostream)	Nonius KappaCCD (with Oxford Cryostream)	Nonius KappaCCD (with Oxford Cryostream)	Nonius KappaCCD (with Oxford Cryostream)	KappaCCD (with Oxford Cryostream)
Data collection method	ω scans with κ offsets	ω scans with κ offsets	ω scans with κ offsets			
Absorption correction	Multi-scan (based on symmetry-related measurements)	Multi-scan (based on symmetry-related measurements)	Multi-scan (based on symmetry-related measurements)			

(Table 6.1 continued)

T_{\min}	0.169	0.203	0.213	0.374	0.363	0.417
T_{\max}	0.346	0.523	0.750	0.674	0.884	0.574
No. of measured, independent and observed reflections	34647, 5487	6965, 23986, 5312	6256, 28246, 3907	4932, 28845, 7555	9230, 24469, 5250	6058, 32486, 6085, 5313
Criterion for observed reflections	$I > 2\sigma(I)$					
R_{int}	0.038	0.030	0.035	0.029	0.023	0.023
$\theta_{\max} (\infty)$	35.7	34.2	30.8	35.6	30.8	30.5
<i>Refinement</i>						
Refinement on	F^2	F^2	F^2	F^2	F^2	F^2
$R[F^2 > 2\sigma(F^2)]$, $wR(F^2)$, S	0.032, 1.03	0.067, 1.03	0.029, 1.03	0.067, 1.04	0.037, 1.04	0.091, 1.04
No. of reflections	6965 reflections	6256 reflections	4932 reflections	9230 reflections	6058 reflections	6085 reflections
No. of parameters	202	202	221	274	274	280
H-atom treatment	Constrained to parent site	Mixture of independent and constrained refinement				
Weighting scheme	Calculated $w = 1/[\sigma^2(F_o^2) + (0.0291P)^2]$ where $P = (F_o^2 + 2F_c^2)/3$	Calculated $w = 1/[\sigma^2(F_o^2) + (0.0256P)^2]$ where $P = (F_o^2 + 2F_c^2)/3$	Calculated $w = 1/[\sigma^2(F_o^2) + (0.0471P)^2]$ where $P = (F_o^2 + 2F_c^2)/3$	Calculated $w = 1/[\sigma^2(F_o^2) + (0.0346P)^2]$ where $P = (F_o^2 + 2F_c^2)/3$	Calculated $w = 1/[\sigma^2(F_o^2) + (0.0243P)^2]$ where $P = (F_o^2 + 2F_c^2)/3$	Calculated $w = 1/[\sigma^2(F_o^2) + (0.0025P)^2]$ where $P = (F_o^2 + 2F_c^2)/3$
$(\Delta/\sigma)_{\max}$	0.002	0.001	0.002	0.003	0.002	0.003
$\Delta\rho_{\max}$, $\Delta\rho_{\min}$ ($\text{e} \text{ \AA}^{-3}$)	1.89, -1.99	2.22, -1.77	2.31, -2.85	1.84, -1.91	1.96, -2.14	0.66, -1.01
Extinction method	SHELXL	SHELXL		SHELXL	SHELXL	SHELXL
Extinction coefficient	0.00137 (10)	0.00137 (12)		0.00086 (12)	0.00107 (10)	0.00072 (6)

Table 6.2. Selected Bond Distances (Å) and Angles (°) for [(5,5'-Me₂bpy)Re(CO)₃Br] (**6.1**), [(6,6'-Me₂bpy)Re(CO)₃Br] (**6.2**), [(2,9-Me₂phen)Re(CO)₃Br] (**6.5**), [(4,4'-Me₂bpy)Re(CO)₃(H₂O)]OTf (**6.6**), [(5,5'-Me₂bpy)Re(CO)₃(H₂O)]OTf (**6.7**), and [(6,6'-Me₂bpy)Re(CO)₃(H₂O)]OTf (**6.8**)

	6.1	6.2	6.5	6.6	6.7	6.8
bond distances						
Re–N1	2.187 (2)	2.218 (3)	2.212 (4)	2.178 (2)	2.170 (3)	2.1968 (19)
Re–N2	2.178 (3)	2.224 (3)	2.227 (4)	2.172 (2)	2.163 (3)	2.1948 (18)
Re–Br	2.6352 (5)	2.6271 (4)	2.6104 (6)	2.1916 (17) ^a	2.199 (3) ^a	2.1852 (16) ^a
Re–Re ^b	6.29	6.46	6.28	6.28	7.64	7.74
bond angles						
N1–Re–N2	75.14 (9)	75.59 (10)	75.84 (15)	75.11 (8)	75.15 (11)	76.08 (7)

^aRe–O4 distance. ^baverage distance between Re(I) metal centers.

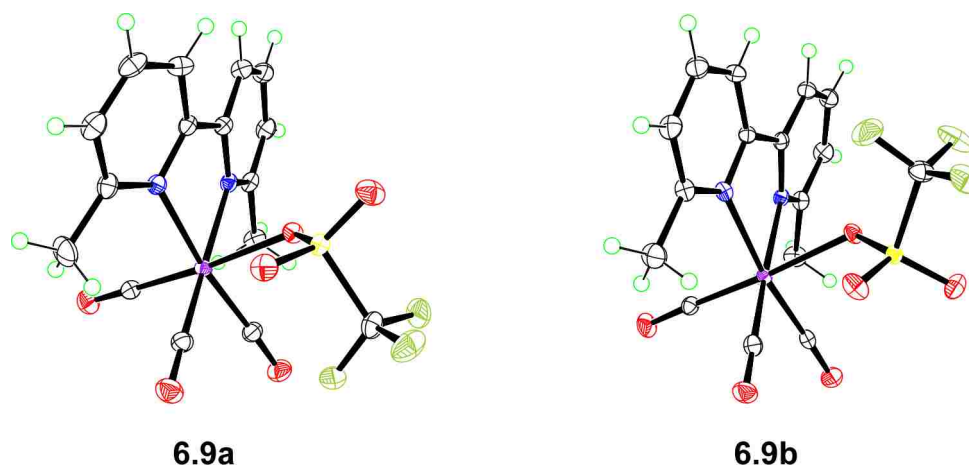


Figure 6.3. Perspective drawings of [(6,6'-Me₂bpy)Re(CO)₃(OTf)] (**6.9a** and **6.9b**). Thermal ellipsoids are drawn with 50% probability.

In all complexes, the Re–N and Re–O bond lengths (~2.2 Å) are comparable to values for other complexes containing similar N-donor ligands.¹⁹ The N–Re–N bond angles are considerably smaller than 90° (~75°); this result is a consequence of the small bite angle between pyridyl rings of the bipyridine ligand.

Table 6.3. Crystal Data and Experimental Details for [(6,6'-Me₂bpy)Re(CO)₃(OTf)] (**6.9a** and **6.9b**)

complex	6.9a	6.9b
<i>Crystal data</i>		
Chemical formula	C ₁₆ H ₁₂ F ₃ N ₂ O ₆ ReS	C ₁₆ H ₁₂ F ₃ N ₂ O ₆ ReS
M_r	603.54	603.54
Cell setting	Monoclinic	Monoclinic
Space group	$P2_1/n$	$P2_1/c$
Temperature (K)	110	110
a, b, c (Å)	8.3897 (10), 14.738 (2), 15.026 (2)	13.551 (3), 10.168 (3), 13.543 (3)
α, β, γ (°)	91.166 (7)	96.109 (13)
V (Å ³)	1857.5 (4)	1855.4 (8)
Z	4	4
D_x (Mg m ⁻³)	2.158	2.161
Radiation type	Mo $K\alpha$	Mo $K\alpha$
μ (mm ⁻¹)	6.72	6.73
Crystal form, colour	Lath fragment, yellow	Parallelepiped, yellow
Crystal size (mm)	0.33 \diamond 0.22 \diamond 0.10	0.27 \diamond 0.25 \diamond 0.20
<i>Data collection</i>		
Diffractometer	KappaCCD (with Oxford Cryostream)	KappaCCD (with Oxford Cryostream)
Data collection method	ω scans with κ offsets	ω scans with κ offsets
Absorption correction	Multi-scan (based on symmetry-related measurements)	Multi-scan (based on symmetry-related measurements)
T_{\min}	0.215	0.264
T_{\max}	0.553	0.346
No. of measured, independent and observed reflections	35351, 7366, 5618	20370, 5492, 4630
Criterion for observed reflections	$I > 2\sigma(I)$	$I > 2\sigma(I)$
R_{int}	0.023	0.033

(Table 6.2 continued)

$\theta_{\max} (\infty)$	33.7	30.5
<i>Refinement</i>		
Refinement on	F^2	F^2
$R[F^2 > 2\sigma(F^2)],$ $wR(F^2), S$	0.033, 0.093, 1.04	0.025, 0.059, 1.03
No. of reflections	7366 reflections	5492 reflections
No. of parameters	265	265
H-atom treatment	Constrained to parent site	Constrained to parent site
Weighting scheme	Calculated $w = 1/[\sigma^2(F_o^2) + (0.0504P)^2 + 2.5873P]$ where $P = (F_o^2 + 2F_c^2)/3$	Calculated $w = 1/[\sigma^2(F_o^2) + (0.020P)^2 + 1.2029P]$ where $P = (F_o^2 + 2F_c^2)/3$
$(\Delta/\sigma)_{\max}$	0.001	0.001
$\Delta\rho_{\max}, \Delta\rho_{\min}$ (e \AA^{-3})	2.40, -3.67	1.23, -1.19
Extinction method	SHELXL	SHELXL
Extinction coefficient	0.0028 (2)	0.00085 (11)

6.3.2 Distortion of Re(I) Complexes Containing Bipyridine Ligands

The two pyridyl rings of an uncoordinated bipyridine ligand are *anti* to one another; thus, an uncoordinated bipyridine ligand is essentially planar because any steric repulsion between H3 and H3' (see Figure 6.1 for atom numbering scheme) is minimized. However, upon bidentate coordination to a metal center (**M**), the two pyridyl rings become *syn* and H3–H3' repulsive forces can cause significant distortions from planarity in complexes with **M**–N distances of ~2.0 to 2.2 \AA .²⁰ Distortions from planarity can occur both in and out of the plane of the coordinated bipyridine ligand. In-plane distortion is described in terms of in-plane bending (θ_p) (Figure 6.4).²¹ Out-of-plane distortions can be described in terms of bowing (θ_b) and twisting (θ_t) and to a lesser extent in terms of an S-shaped distortion (d_s) (Figure 6.4).²¹

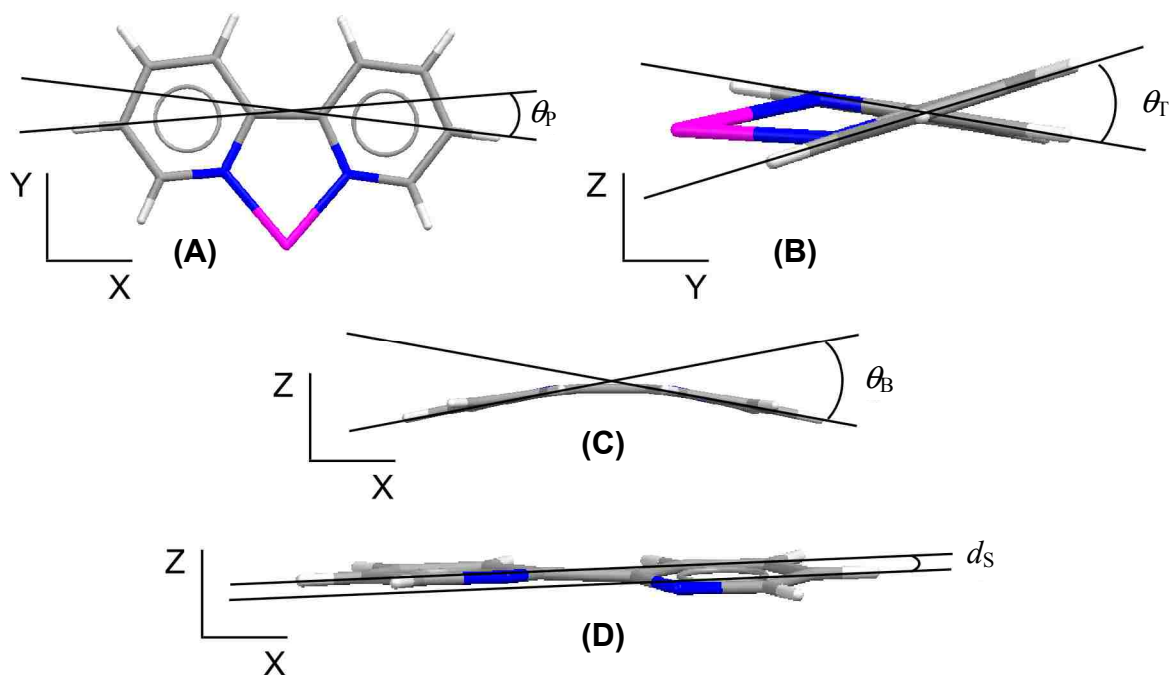


Figure 6.4. Distortions in N–N ligands as defined by Hazell: **(A)** in-plane bending (θ_p , in deg); **(B)** twisting (θ_T , in deg); **(C)** bowing (θ_B , in deg); **(D)** S-shaped distortion (d_s , in Å). θ_T , θ_B and θ_p are the angles between the best straight lines ($ax + c = z$) through each pyridyl ring of the bipyridine ligand in the XY, YZ, and XZ projections, respectively.

Table 6.4. Selected Bond Distances (Å) and Angles (°) for $[(6,6'\text{-Me}_2\text{bpy})\text{Re}(\text{CO})_3(\text{OTf})]$ (**6.9a** and **6.9b**)

	6.9a	6.9b
	bond distances	
Re–N1	2.196 (2)	2.194 (3)
Re–N2	2.205 (3)	2.192 (3)
Re–O	2.201 (2)	2.203 (2)
Re–Re ^b		
	bond angles	
N1–Re–N2	75.64 (9)	75.09 (10)

^aaverage distance between Re(I) metal centers.

In a recent comprehensive study, Hazell compared 551 metal complexes containing bpy or substituted bpy ligands from the Cambridge Structural Database²² and calculated θ_T , θ_B , d_S , and θ_P for each metal complex.²¹ The values of θ_T and θ_B ranged from 0.0° to 26.1° and from 0.0° to 19.8°, respectively. The least significant parameter, d_S , ranged from 0.0 to 0.127 Å, with nearly 90% of the values being less than 0.053 Å. The θ_P angles ranged from +2.9 Å to +12.5 Å, with a mean value of +7.8 Å (positive sign indicates that distortion is directed toward the metal).

Table 6.5. Ligand Deformation in Octahedral Re(I) and Square-Planar Pt(II)/Pd(II) Complexes

complex	Twist angle (θ_T)	Bow angle (θ_B)	S-shaped distortion (d_S)	In-plane distortion (θ_P)	M–N distance (Å)	Dihedral angle (θ_{di})	Ref
[(5,5'-Me ₂ bpy)Re(CO) ₃ Br] (6.1)	2.3	2.0	0.011	+6.5	2.187 (2) 2.178 (3) 2.218 (3)	3.1	^b
[(6,6'-Me ₂ bpy)Re(CO) ₃ Br] (6.2)	9.0	0.8	0.065	+2.8	2.224 (3) 2.211	9.1	^b
[(2,9-Me ₂ phen)Re(CO) ₃ Br] (6.5)	–	–	–	–	2.227	–	^b
[(4,4'-Me ₂ bpy)Re(CO) ₃ (H ₂ O)]OTf (6.6)	2.9	2.1	0.012	+5.9	2.178 (2) 2.172 (2)	3.6	^b
[(5,5'-Me ₂ bpy)Re(CO) ₃ (H ₂ O)]OTf (6.7)	0.9	0.1	0.007	+7.7	2.170 (3) 2.163 (3)	0.9	^b
[(6,6'-Me ₂ bpy)Re(CO) ₃ (H ₂ O)]OTf (6.8)	15.2	9.4	0.060	+3.6	2.196 (8) 2.194 (8)	18.1	^b
[(6,6'-Me ₂ bpy)Re(CO) ₃ (OTf _{up})] (6.9a)	6.6	10.1	0.076	+4.3	2.196 (2) 2.205 (3)	12.1	^b
[(6,6'-Me ₂ bpy)Re(CO) ₃ (OTf _{down})] (6.9b)	10.3	18.0	0.032	+5.2	2.194 (3) 2.192 (3)	21.0	^b
[(bpy)Re(CO) ₃ (H ₂ O)]OTf	2.2	0.1	0.034	+7.1	2.161 2.165 2.023 (3)	2.3	19
[(4,4'-Me ₂ bpy)PtCl ₂]	2.4	0.1	0.02	+5.9	2.027 (3)	2.8 (6)	13
[(5,5'-Me ₂ bpy)PtCl ₂]	5.5	0.0	0.075	+8.9	2.017 (3) 2.028 (2)	5.56 (6)	13
[(6,6'-Me ₂ bpy)PtCl ₂]	6.1	19.2	0.000	+10.9	2.030 (2)	20.18 (14)	13
[(bpy)PtCl ₂]	0.0	0.0	0.000	+8.8	2.009 (6)	0.0	23
[(bpy)PdCl ₂]	2.3	1.9	0.009	+8.9	2.03 (1)	3.0	24

^a θ_T , θ_B , d_S , θ_P , and θ_{di} values were calculated by using a FORTRAN program provided by Dr. Alan Hazell. θ_{di} angles for complexes reported in this work were checked using Mercury; in all cases, the two θ_{di} values were comparable within 0.1 Å. ^bThis work.

6.3.2.1 Out-of-Plane Distortions

In general, the Re(I) complexes in Table 6.5 have θ_T angles ranging from 0.9° to 15.2°, and an average θ_T angle of 6.7°. While these values are within the range reported by Hazell²¹, the average θ_T angle is somewhat larger than the θ_T angle of 2.2° for the reference compound, [(bpy)Re(CO)₃(H₂O)]OTf (Table 6.5).¹⁹ Complexes containing bpy, 4,4'-Me₂bpy or 5,5'-Me₂bpy ligands have smaller θ_T angles than complexes having 6,6'-Me₂bpy ligands; in fact, the magnitude of θ_T is greatly increased for these latter complexes (Table 6.5). This result can be attributed to steric repulsion between the 6,6' methyl groups and the cis CO ligands (Figure 5.2). Of the complexes containing 6,6'-Me₂bpy ligands, [(6,6'-Me₂bpy)Re(CO)₃(OTf_{up})] has the smallest θ_T angle (6.6°). In contrast, [(6,6'-Me₂bpy)Re(CO)₃(OTf_{down})] has a θ_T angle of 10.3°. The smaller θ_T angle for [(6,6'-Me₂bpy)Re(CO)₃(OTf_{up})] indicates that the interaction between the -CF₃ moiety with the 6,6'-Me₂bpy ligand results in less twisting about the central C-C bond of the 6,6'-Me₂bpy ligand.

A comparison of θ_T angles for square-planar Pt(II)/Pd(II) vs octahedral Re(I) complexes reveals that the magnitude of θ_T depends primarily upon the nature of the bipyridine ligand; the coordination geometry of **M** plays a minor role in determining the magnitude of θ_T . Inspection of Table 6.5 shows that the θ_T angles are nearly equal for Pt(II) and Re(I) complexes of 4,4'-Me₂bpy. However, the Re(I) complexes of 5,5'-Me₂bpy and 6,6'-Me₂bpy have smaller and larger θ_T angles, respectively, when compared to Pt(II) complexes of the same ligands.

The Re(I) complexes studied here have θ_B angles ranging from 0.1° to 18.0° (Table 6.5). The average θ_B angle is 6.1°, indicating that these complexes are significantly more bowed than complexes containing unsubstituted bpy ligands ($\theta_B = 0.1^\circ$ for [(bpy)Re(CO)₃(H₂O)]OTf, Table

6.5). These values for θ_B are within the range reported by Hazell; however, the θ_B angle calculated for [(6,6'-Me₂bpy)Re(CO)₃(OTf_{down})] (18.0°) is near the upper limit of 19.8°.²¹ As was discussed above for twist distortions, complexes containing bpy, 4,4'-Me₂bpy or 5,5'-Me₂bpy ligands have smaller θ_B values than complexes having 6,6'-Me₂bpy ligands. However, [(6,6'-Me₂bpy)Re(CO)₃Br] is one exception, with a θ_B value of 0.8° (Table 6.5). The two highest θ_B values belong to [(6,6'-Me₂bpy)Re(CO)₃(OTf_{up})] (10.1°) and [(6,6'-Me₂bpy)Re(CO)₃(OTf_{down})] (18.0°). This result indicates that the presence of OTf in the coordination sphere of Re(I) causes substantial bowing of the bpy ligand. The smaller θ_B value for [(6,6'-Me₂bpy)Re(CO)₃(OTf_{up})] indicates that an interaction between the -CF₃ moiety and 6,6'-Me₂bpy results in less bowing of the 6,6'-Me₂bpy ligand, as compared to [(6,6'-Me₂bpy)Re(CO)₃(OTf_{down})].

An overall comparison of θ_B angles for square-planar Pt(II)/Pd(II) vs octahedral Re(I) complexes reveals greater θ_B angles for the latter (Table 6.5); indicating that the coordination geometry of **M** has a more significant effect on θ_B as compared to θ_T . However, [(6,6'-Me₂bpy)PtCl₂] has the largest θ_B angle (19.2°) in Table 6.5. This result is most likely due to significant steric repulsion between the 6,6' methyl groups and the chloride ligands of [(6,6'-Me₂bpy)PtCl₂].¹³ It is likely that longer Re-N bonds alleviate some of the steric strain upon forming Re(I) complexes of 6,6'-Me₂bpy.

The d_S values range from 0.007 Å to 0.076 Å (for [(5,5'-Me₂bpy)Re(CO)₃(H₂O)]OTf and [(6,6'-Me₂bpy)Re(CO)₃(OTf_{up})], respectively; Table 6.5). Thus, the Re(I) complexes discussed herein do not have a significant amount of S-shaped deformity. The d_S values for square-planar Pt(II) and Pd(II) complexes are equally negligible (Table 6.5), a result indicating that the magnitude of d_S is not significantly dependent upon the coordination geometry of **M**, or upon the **M**-N bond length.

Distortion of coordinated bipyridine ligands can also be described in terms of the dihedral angle between the best planes through each of the two pyridyl rings, θ_{di} .¹³ The magnitude of θ_{di} is influenced by both θ_{T} and θ_{B} ; thus, θ_{di} is a descriptor of the overall distortion of the coordinated bipyridine ligand. The θ_{di} angles range from 0.9° to 21.0° for Re(I) complexes, and from 0.0° to 20.18° for Pt(II)/Pd(II) complexes (Table 6.5). The largest θ_{di} angles are for complexes containing 6,6'-Me₂bpy ligands (θ_{di} for Re(I) and Pt(II)/Pd(II) complexes are nearly equal), indicating that the magnitude of θ_{di} is mostly independent of the **M** coordination geometry and the **M**-N bond length.

6.3.2.2 In-plane Bending Distortions

The Re(I) complexes reported here have θ_{p} angles ranging from +2.8° to +7.7° (Table 6.5). The average θ_{p} angle is +5.1°, indicating that Re(I) complexes with substituted bpy ligands have less in-plane distortion than those complexes containing unsubstituted bpy ligands (θ_{p} = +7.1° for [(bpy)Re(CO)₃(H₂O)]OTf, Table 6.5). Generally, Re(I) complexes containing 4,4'-Me₂bpy or 5,5'-Me₂bpy ligands have larger θ_{p} angles than those with 6,6'-Me₂bpy ligands. It is likely that the interaction of the 6,6' methyl groups with the cis CO ligands in an octahedral coordination environment prevents significant in-plane bending in complexes containing 6,6'-Me₂bpy.

A comparison of the magnitude of θ_{p} and the **M**-N bond length in Table 6.5 shows that, as observed by Hazell²¹, the magnitude of θ_{p} decreases with increasing **M**-N bond length. This effect is illustrated by comparing data for the Re(I) and Pt(II)/Pd(II) complexes in Table 6.5. The average θ_{p} angle is +8.7° for the Pt(II)/Pd(II) complexes (average **M**-N bond length of 2.05 Å),

compared to an average θ_p angle of $+5.1^\circ$ for the Re(I) complexes (average **M**-N bond length of 2.19 Å).

6.4 Conclusions

The Re(I) complexes described here have longer than average **M**-N distances of ~ 2.2 Å; thus, these complexes cannot be considered as general models for pseudo-octahedral metal complexes of bipyridine and other similar ligands. However, comparison of the data collected here with literature data for square-planar Pt(II) and Pd(II) complexes allows for some conclusions to be made about the effect of **M**-N bond length and coordination geometry on intramolecular interactions that can result in the distortion of bipyridine-type ligands.

Although five different parameters (θ_T , θ_B , d_S , θ_p , θ_{di}) have been introduced to describe distortions of bipyridine-type ligands coordinated to metal centers, distortions in both octahedral and square-planar complexes can be described primarily in terms of θ_T and θ_B . The similar magnitudes of θ_T and θ_B calculated for Re(I) and Pt(II)/Pd(II) complexes indicates that interligand interactions between the 6,6' substituents and the *cis*-coordinated ligands play a significant role in determining θ_T and θ_B , while **M** coordination geometry and length of the **M**-N bond appear to have only a minor effect on θ_T and θ_B . These results offer hope that novel drugs based on the *fac*-[Re(CO)₃]⁺ core can be developed with similar levels of antineoplastic activity, but lower toxicity, than cisplatin.

6.5 References

1. Alessio, E.; Mestroni, G.; Bergamo, A.; Sava, G. *Curr. Top. Med. Chem.* **2004**, *4*, 1525-1535.
2. Chifotides, H. T.; Dunbar, K. R. *Acc. Chem. Res.* **2005**, *38*, 146-156.
3. Chifotides, H. T.; Koshlap, K. M.; Pérez, L. M.; Dunbar, K. R. *J. Am. Chem. Soc.* **2003**, *125*, 10714-10724.

4. Frausin, F.; Scarcia, V.; Cocchietto, M.; Furlani, A.; Serli, B.; Alessio, E.; Sava, G. *J. Pharmacol. Exp. Ther.* **2005**, *313*, 227-233.
5. Galanski, M.; Arion, V. B.; Jakupec, M. A.; Keppler, B. *Curr. Pharm. Des.* **2003**, *9*, 2078-2089.
6. Guichard, S. M.; Else, R.; Reid, E.; Zeitlin, B.; Aird, R.; Muir, M.; Dodds, M.; Fiebig, H.; Sadler, P. J.; Jodrell, D. I. *Biochem. Pharmacol.* **2006**, *71*, 408-415.
7. Hayward, R. L.; Schornagel, Q. C.; Tente, R.; Macpherson, J. S.; Aird, R. E.; Guichard, S.; Habtemariam, A.; Sadler, P.; Jodrell, D. I. *Cancer Chemother. Pharmacol.* **2005**, *55*, 577-583.
8. Velders, A. H.; Bergamo, A.; Alessio, E.; Zangrando, E.; Haasnoot, J. G.; Casarsa, C.; Cocchietto, M.; Zorzet, S.; Sava, G. *J. Med. Chem.* **2004**, *47*, 1110-1121.
9. Yan, Y.-K.; Cho, S. E.; Shaffer, K. A.; Rowell, J. E.; Barnes, B. J.; Hall, I. H. *Pharmazie* **2000**, *55*, 307-313.
10. Yan, Y. K.; Melchart, M.; Habtemariam, A.; Sadler, P. J. *Chem. Commun.* **2005**, 4764-4776.
11. Bhattacharyya, D.; Marzilli, P. A.; Marzilli, L. G. *Inorg. Chem.* **2005**, *44*, 7644-7651.
12. Maheshwari, V.; Bhattacharyya, D.; Fronczek, F. R.; Marzilli, P. A.; Marzilli, L. G. *Inorg. Chem.* **2006**, *45*, 7182-7190.
13. Maheshwari, V.; Carlone, M.; Fronczek, F. R.; Marzilli, L. G. *Acta Crystallogr., Sect. B: Struct. Sci.* **2007**, *B63*, 603-611.
14. Schmidt, S. P.; Trogler, W. C.; Basolo, F. *Inorg. Synth.* **1990**, *28*, 160-165.
15. Schmidt, S. P.; Nitschke, J.; Trogler, W. C. *Inorg. Synth.* **1989**, *26*, 113-117.
16. Otwinowski, Z.; Minor, W. *Methods Enzymol.* **1997**, *276*, 307-326.
17. Altomare, A.; Burla, M. C.; Camalli, M.; Cascarano, G. L.; Giacovazzo, C.; Guagliardi, A.; Moliterni, A. G. G.; Polidori, G.; Spagna, R. *J. Appl. Crystallogr.* **1999**, *32*, 115-119.
18. Sheldrick, G. M. *SHELXL-97, A Program for the Solution of Crystal Structures from X-ray Data*; **1997**, University of Göttingen: Göttingen, Germany.
19. Salignac, B.; Grundler, P. V.; Cayemittes, S.; Frey, U.; Scopelliti, R.; Merbach, A. E.; Hedinger, R.; Hegetschweiler, K.; Alberto, R.; Prinz, U.; Raabe, G.; Kölle, U.; Hall, S. *Inorg. Chem.* **2003**, *42*, 3516-3526.
20. Hazell, A.; Simensen, O.; Wernberg, O. *Acta Crystallogr., Sect. C: Cryst. Struct. Commun.* **1986**, *C42*, 1707-1711.

21. Hazell, A. *Polyhedron* **2004**, 23, 2081-2083.
22. Allen, F. H. *Acta Crystallogr., Sect. B: Struct. Sci.* **2002**, B58, 380-388.
23. Connick, W. B.; Henling, L. M.; Marsh, R. E.; Gray, H. B. *Inorg. Chem.* **1996**, 35, 6261-6265.
24. Canty, A. J.; Skelton, B. W.; Traill, P. R.; White, A. H. *Aust. J. Chem.* **1992**, 45, 417-422.

CHAPTER 7.

CONCLUSION

In general, this work represents a significant contribution to the current body of knowledge surrounding the coordination chemistry of the biologically relevant $fac-[Re(CO)_3]^+$ core. The $fac-[Re(CO)_3]^+$ core has potential chemotherapeutic applications; and complexes containing unstable rhenium isotopes have additional applications, such as radiolabeling, radiodiagnostics and radiotherapy.

We found that, unlike cisplatin, equilibrium is achieved in reaction mixtures containing $fac-[Re(CO)_3(H_2O)_3]^+$ and nucleotides, thus allowing measurement of the relative stability of the adducts formed under both kinetic and thermodynamic conditions. In addition, the adducts formed are dependent upon the nature of the base moiety and the number of phosphate groups. Notably, $fac-[Re(CO)_3(H_2O)_3]^+$ was found to have a *higher* affinity for oxygen donors, but a *much lower* affinity for sulfur donors than cisplatin. This result offers hope that chemotherapeutic agents based on the $fac-[Re(CO)_3]^+$ core could be developed with higher efficacy, and lower toxicity, than cisplatin, as the latter side effect has been linked to platination of sulfur-containing proteins and peptides.

Studying the adducts formed in the reaction between the $fac-[Re(CO)_3]^+$ core and N-donor ligands such as benzimidazoles and bipyridines revealed that the $fac-[Re(CO)_3]^+$ core prefers to bind to two N-donor ligands in a *cis* fashion, in a manner reminiscent of cisplatin binding to two adjacent guanine bases. In addition, two coordinated benzimidazole ligands preferentially adopt a head-to-head orientation (as opposed to a head-to-tail arrangement); access to the HH orientation has been suggested to be responsible for the cytotoxic activity observed for cisplatin.

APPENDIX A

SUPPORTING INFORMATION FOR CHAPTER 2

A.1 Sugar Pucker of Nucleotides Coordinated to *fac*-[Re(CO)₃(H₂O)₃]⁺

Clearly resolved H1' signals allowed measurement of ³J_{H1'-H2'} coupling constants, which are useful for assessing the degree of S or N sugar pucker. Literature values for ³J_{H1'-H2'} of a typical NMP range from 6.2 to 6.9 Hz at pH ~7;² we found ³J_{H1'-H2'} = ~6.0 Hz at pH 3.6. The ³J_{H1'-H2'} coupling constant decreased by ~2.3 Hz upon coordination of one 5'-GMP (3.7 Hz) or one 3'-GMP (3.6 Hz) to *fac*-[Re(CO)₃(H₂O)₃]⁺ (Table 2.1). Similar results were found for the coordination of one 5'-IMP (3.0 Hz) or one 3'-IMP (3.5 Hz) to *fac*-[Re(CO)₃(H₂O)₃]⁺. The decrease in ³J_{H1'-H2'} upon adduct formation indicate that coordination causes an increase in the population of nucleotides possessing an N pucker.^{2,3}

In general, the ³J_{H1'-H2'} coupling constants for each of the coordinated nucleotides in the 1:2 adducts are approximately the same as the ³J_{H1'-H2'} coupling constants for the nucleotides in the 1:1 adducts. However, the observation of different ³J_{H1'-H2'} values (5.1 Hz and 3.9 Hz, Table 2.1) for each of the two 5'-GMP's of *fac*-[Re(CO)₃(H₂O)(5'-GMP)₂]⁻ indicates that the ribose ring of one coordinated 5'-GMP has more N character than the ribose ring of the other coordinated 5'-GMP.

A.2 Exclusion of the Presence of 2:2 Cyclic Dimer

Two different experiments were used to exclude the possibility that a 2:2 cyclic dimeric adduct is formed in the reaction between *fac*-[Re(CO)₃(H₂O)₃]⁺ and 5'-GMP. First, we utilized an increased concentration of both Re and 5'-GMP (*r* = 1:1, [Re] = 100 mM). The spectra from this experiment, in contrast to spectra when *r* = 4:1, have no signals previously ascribed to the

dinuclear adduct, $fac-[Re_2(CO)_6(H_2O)_4(5'-GMP)]^+$. The relative intensity of these dinuclear signals would have increased if they were due to a 2:2 cyclic dimeric adduct.

We also used a mixture of 5'- and 3'-GMP, which helps to assess the presence of a cyclic 2:2 dimeric adduct (Figure 2.3) because of the formation of isomers. If two GMP's are coordinated to two $fac-[Re(CO)_3(H_2O)]^+$ moieties in a cyclic 2:2 dimeric adduct, three different adducts with a Re/GMP ratio of 2:2 are possible for a mixture of 5'-GMP and 3'-GMP. In addition to the 1:2 adducts of 5'-GMP and 3'-GMP found above, a new Re/5'-GMP/3'-GMP cyclic 2:2 dimeric adduct can form, resulting in two new H8 singlets.

The H8 signal previously attributed to a dinuclear species (but which could be due to the formation of a cyclic 2:2 dimeric adduct) is largest when there is a large excess of Re over GMP; therefore, the formation reaction was carried out by mixing $fac-[Re(CO)_3(H_2O)_3]^+$ (100 mM) with 12.5 mM 5'-GMP and 12.5 mM 3'-GMP, for a total Re/GMP ratio of 4:1. No new 1H or ^{31}P NMR signals were observed, indicating that no new mixed-nucleotide cyclic 2:2 dimeric adduct was formed. Because the different positions of the 3'-phosphate and the 5'-phosphate groups could possibly prevent formation of the mixed cyclic dimeric adduct (because of different distances spanning the Re atoms), we examined a similar reaction but with a mixture of 5'-GMP and 5'-IMP. Again, no new 1H or ^{31}P NMR signals were observed. These results confirm that no cyclic 2:2 dimeric adducts are formed in the reaction of $fac-[Re(CO)_3(H_2O)_3]^+$ with 5'- or 3'-nucleotides.

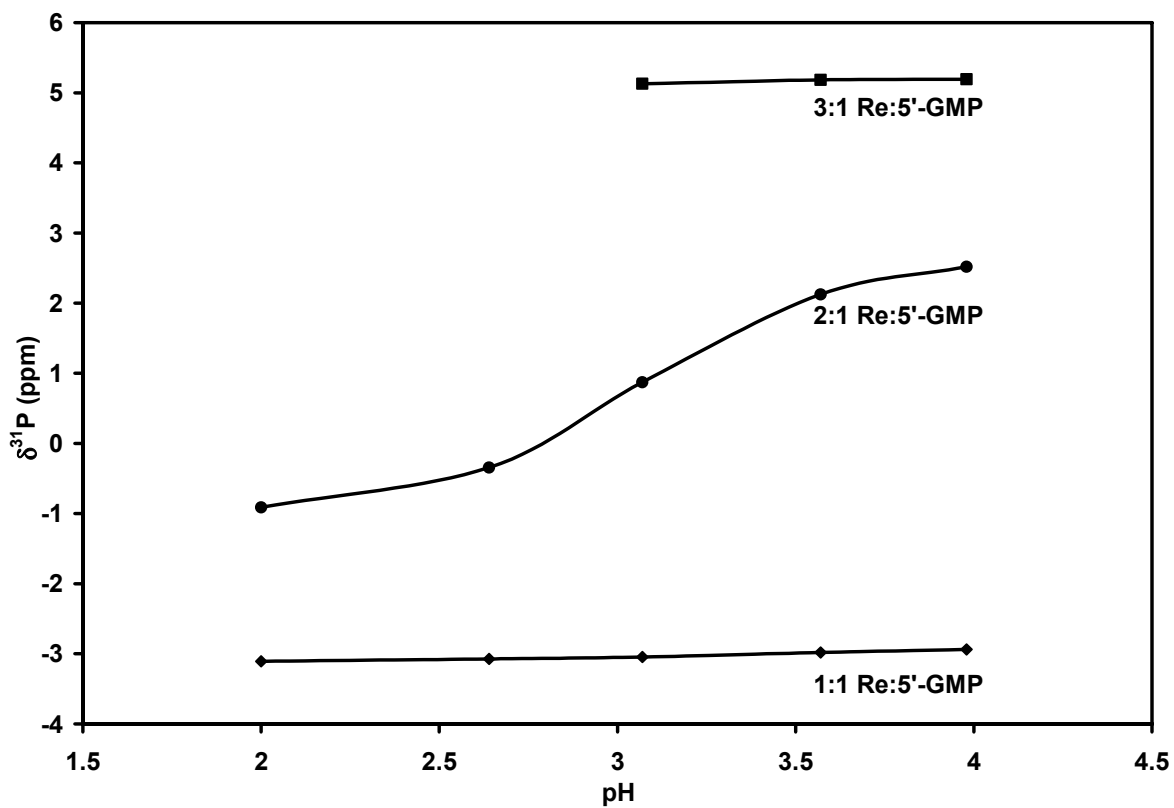


Figure A.1. Chemical shift vs. pH for the P_{α} signals of *fac*-[Re(CO)₃(H₂O)₂(5'-GMP)], *fac*-[Re₂(CO)₆(H₂O)₄(5'-GMP)] and *fac*-[Re₃(CO)₉(H₂O)₆(5'-GMP)]⁺. The P_{α} signals of the 1:2 Re:GMP adduct do not shift over the pH range studied and therefore the curve(s) are not shown because these signals flank the P_{α} signal of the 1:1 Re:5'-GMP adduct.

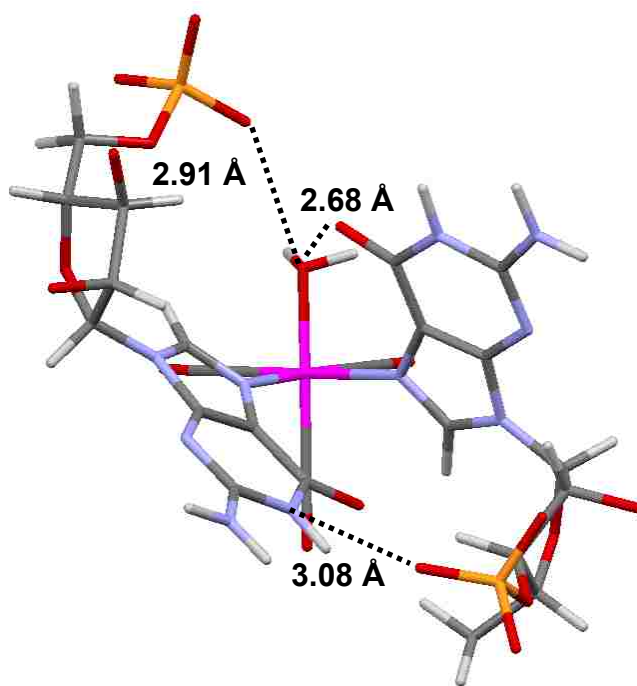


Figure A.2. Idealized model (constructed using HyperChem¹) of proposed favored *fac*-[Re(CO)₃(H₂O)(5'-GMP)(3'-GMP)]⁺ adduct, showing the possibility for an Δ HT conformer with three H-bonding contacts. N7–Re bond lengths and N7–Re–N7 bond angle are fixed using values found in the crystal structure of *fac*-[Re(CO)₃(H₂O)(9-MeG)₂]⁻ (9-MeG = 9-methylguanine).⁴

A.3 References

1. HyperChem(TM) Version 7.5, Hypercube, Inc., 1115 NW 4th Street, Gainesville, Florida 32601, USA.
2. Davies, D. B.; Danyluk, S. S. *Biochemistry* **1974**, *13*, 4417-4434.
3. Okamoto, K.; Benham, V.; Viet, M. T. P.; Polissiou, M.; Gauthier, J.-Y.; Hanessian, S.; Theophanides, T. *Inorg. Chim. Acta* **1986**, *123*, L3-L5.
4. Zobi, F.; Blacque, O.; Schmalte, H. W.; Spingler, B.; Alberto, R. *Inorg. Chem.* **2004**, *43*, 2087-2096.

APPENDIX B

SUPPORTING INFORMATION FOR CHAPTER 3

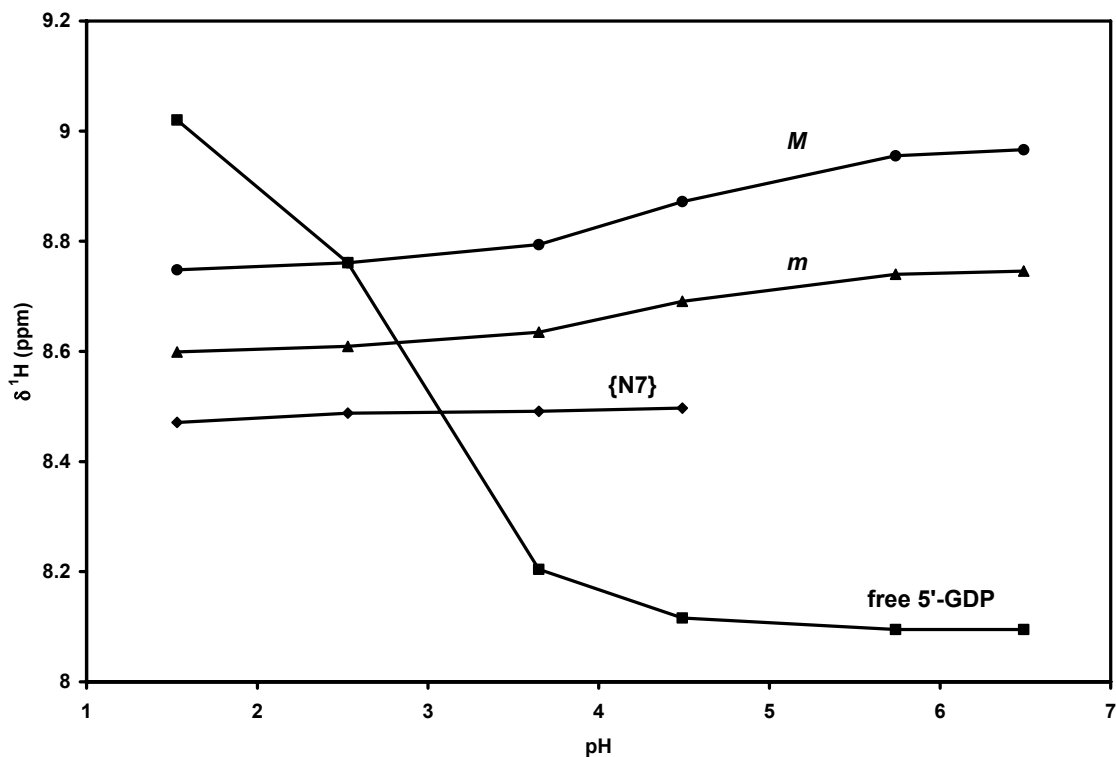


Figure B.1. Chemical shift vs pH for the H8 NMR signals of *M*, *m*, *fac*-[Re(CO)₃(H₂O)₂({N7}GDP)]⁻ and free 5'-GDP²⁻. Because *fac*-[Re(CO)₃(H₂O)₂({N7}GDP)]⁻ is unstable above pH ~4, no data could be obtained above this pH. Charges indicated in the captions of Figures B.1-B.4 are those for each species at pH 3.6.

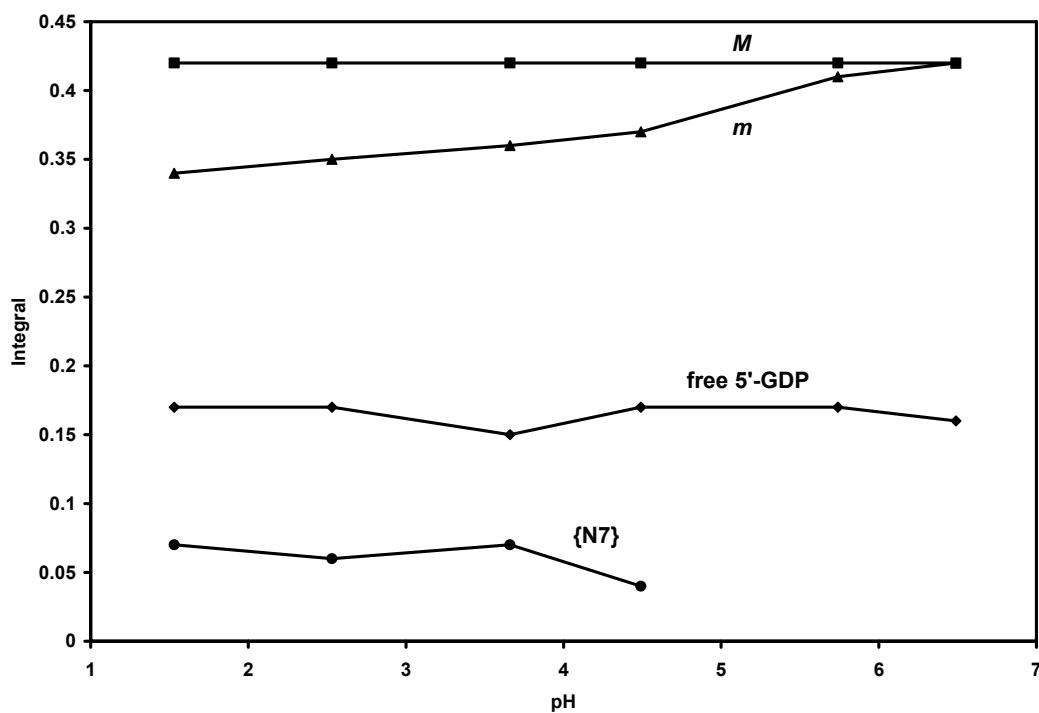


Figure B.2. Area under peak (integral) vs pH for the H8 NMR signals of *M*, *m*, *fac*-[Re(CO)₃(H₂O)₂({N7}GDP)]⁻ and free 5'-GDP²⁻.

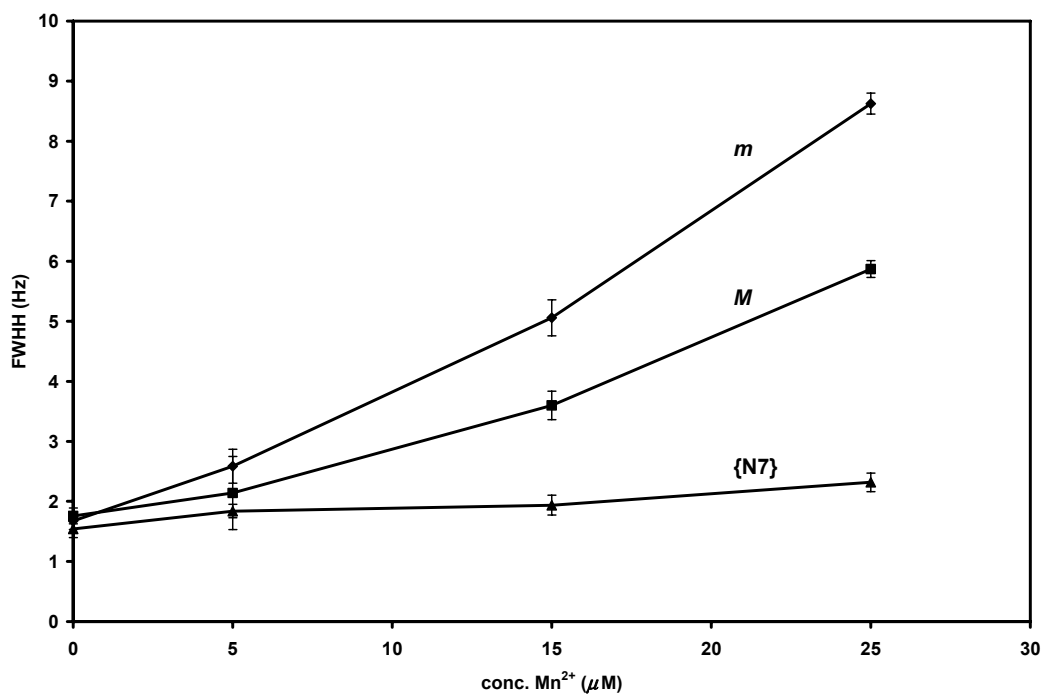


Figure B.3. Linewidth at full width half height (fwhh, in Hz) vs concentration of Mn²⁺ (in μM) for the H8 NMR signals of *M*, *m* and *fac*-[Re(CO)₃(H₂O)₂({N7}GDP)]⁻.

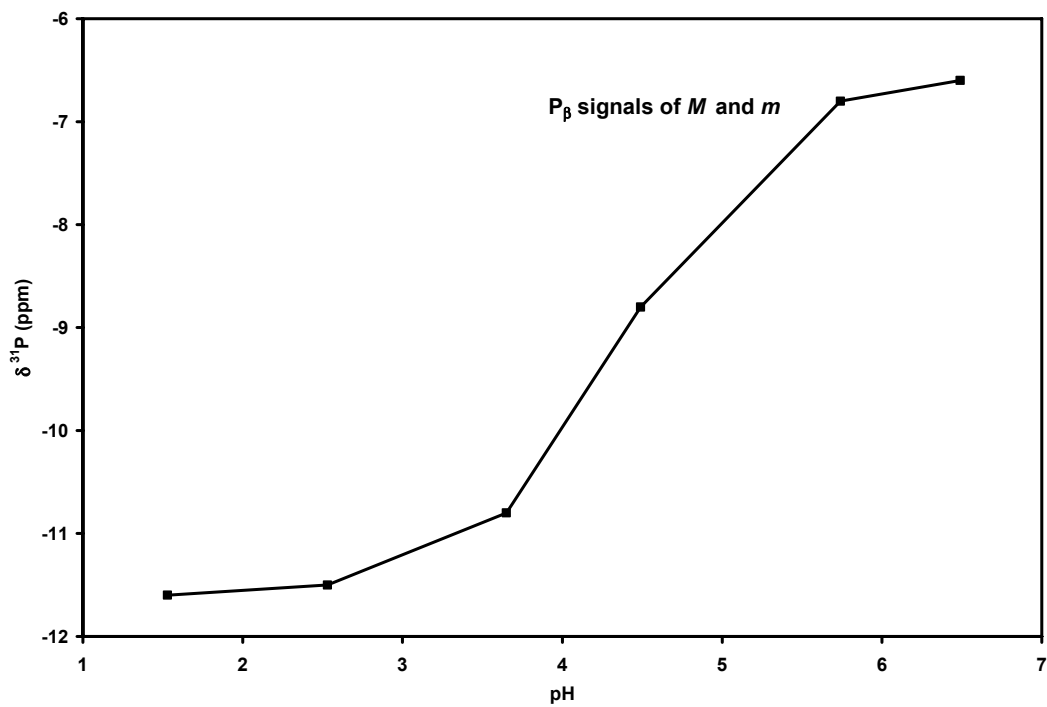


Figure B.4. Chemical shift vs pH for the P_β NMR signals of *M*, *m* and *fac*-[Re(CO)₃(H₂O)({N7,P_β}GDP)]⁻. Note the change in pK_a of the terminal P_β group, from ~6.5 for free 5'-GDP²⁻ to ~4.5 for *M* and *m*.

APPENDIX C

SUPPORTING INFORMATION FOR CHAPTER 4

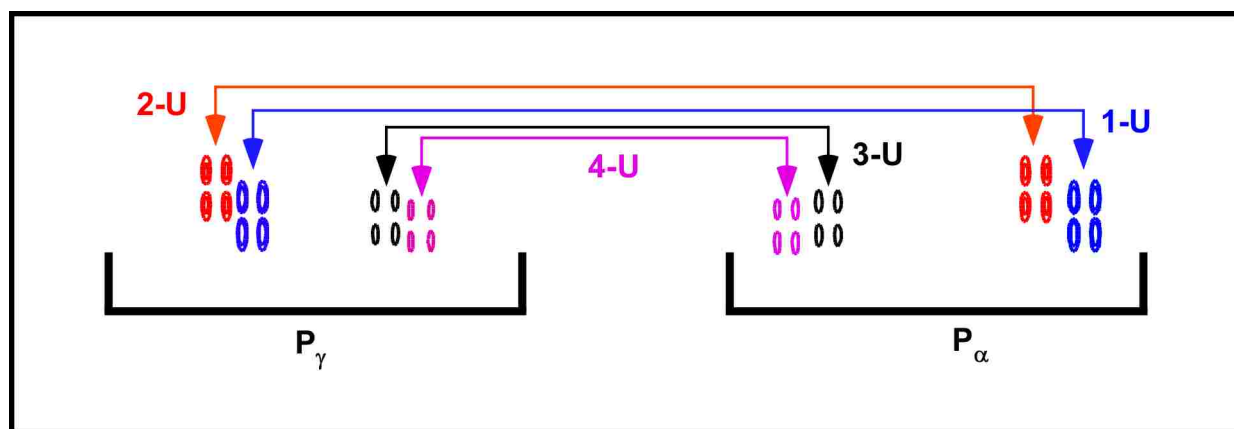


Figure C.1. Expansion of the P_α - P_β and P_β - P_γ cross-peak region in the ^{31}P - ^{31}P COSY spectrum of an equilibrium mixture of *fac*- $[\text{Re}(\text{CO})_3(\text{H}_2\text{O})_3]^+$ (25 mM, $r = 1:1$) and 5'-UTP at pH 3.6 (Figure 5, main text). P_α and P_γ cross-peaks with identical P_β chemical shifts arise from the same diastereomer (1-U, 2-U, 3-U and 4-U).

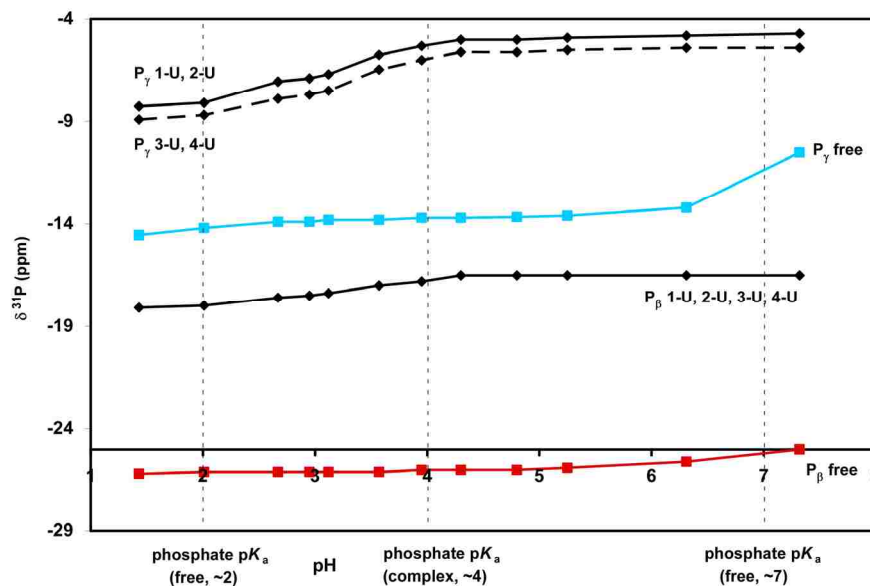


Figure C.2. Chemical shift vs pH for the P_{α} , P_{β} and P_{γ} NMR signals of 1-U, 2-U, 3-U, and 4-U. Note the decrease in the P_{γ} pK_a , from ~ 7 in free 5'-UTP to ~ 4 for the products. Literature values for phosphate pK_a 's of free 5'-UTP from ref 25.

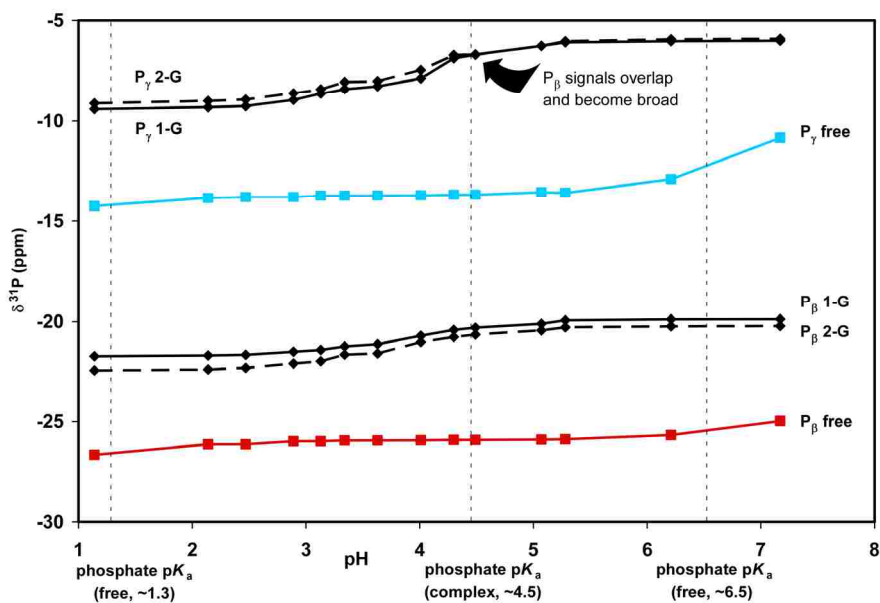


Figure C.3. Chemical shift vs pH for the P_{α} , P_{β} and P_{γ} NMR signals of 1-G and 2-G. The P_{γ} pK_a has decreased from ~ 7 in free 5'-GTP to ~ 4.5 for 1-G and 2-G. Literature values for phosphate pK_a 's of free 5'-GTP from ref 25.

APPENDIX D

REGARDING THE SYNTHESIS, PURIFICATION, AND CHARACTERIZATION OF THIAMINE TRIPHOSPHATE

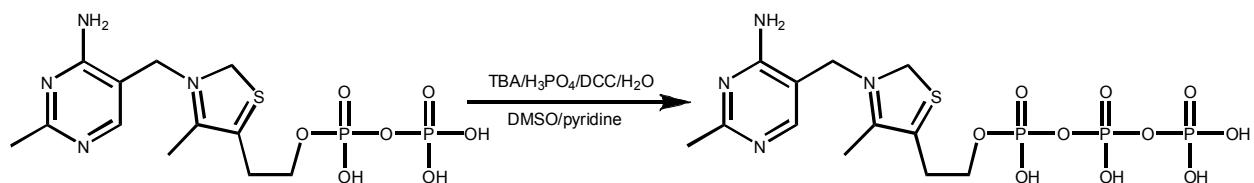


Figure D.1. Synthesis of thiamine triphosphate from thiamine diphosphate and H₃PO₄.

D.1 Synthesis, Purification and Characterization of Thiamine Triphosphate

Methods of phosphorylation often require strictly anhydrous conditions.¹ These methods are typically not successful if attempted outside of a glovebox or without the use of a Schlenk line. Thus, we were quite intrigued to find a piece of literature claiming the successful phosphorylation of nucleoside monophosphates and thiamine diphosphate (to form nucleoside triphosphates and thiamine triphosphate, respectively) in reaction mixtures containing *added* water.² As a result, we set out to reproduce the literature claim.

Thiamine triphosphate was prepared from thiamine diphosphate (TDP) as follows (Figure D.1).² First, TDP (0.5 g) was added to a round-bottom flask containing 1.05 mL tributylamine ($\geq 98.5\%$), 82.5 μL 85% H₃PO₄ (99.999%, 85 wt % solution in H₂O), and 0.75 mL H₂O (HPLC grade). The flask was then strongly agitated until all solid TDP went into solution. With stirring, 200 mL DMSO (anhydrous, $\geq 99.9\%$) and 178 mL pyridine (anhydrous, $\geq 99.9\%$) were added to the round-bottom flask. In a separate beaker, 1,3-dicyclohexyl carbodiimide (DCC, 18 g) was dissolved in 7 mL pyridine and subsequently added to the round-bottom flask containing TDP. The clear reaction mixture was stirred overnight at room temperature, over which time the color

of the solution changed from colorless to orange. A large excess of diethyl ether was added to precipitate out the reaction product as a gelatinous, extremely hygroscopic orange solid.

After filtration and collection of the orange solid, the filter paper was washed thoroughly with H₂O (HPLC grade, 10 mL) and the orange, aqueous solution was poured into a separation funnel. The orange aqueous solution was then extracted with (4) 100 mL aliquots of CHCl₃ (to remove residual DMSO and pyridine). The volume of the resulting aqueous solution was then reduced to ~2 mL using rotary evaporation and applied to the top of a 2.5 cm×5 cm Dowex 50W×8 (200-400 mesh) column (previously prepared in a 60 mL disposable syringe). The column was then eluted with H₂O (HPLC grade, pH 4, adjusted with HCl), and 10 mL aliquots were collected. NMR spectroscopic analysis showed that the first fraction contained predominantly H₃PO₄, and fractions 2-4 contained mainly DMSO. Fractions 5-8 contained *pure* thiamine triphosphate, free of contamination by pyridine, DMSO, and H₃PO₄. Fractions 5-8 were then pooled and the volume of the solution was reduced to ~1 mL using rotary evaporation. After addition of ~4 mL of absolute ethanol, the flask is covered and placed in a freezer (–20 °C) overnight. The mixture is then filtered, and the product thiamine triphosphate is retained on the filter paper as a white powder (yield: 125 mg, 25%; ³¹P NMR (ppm): –14.8 (d, P_α, ³J_{αβ} = 19.8 Hz), –26.7 (P_β, t), –14.2 (d, P_γ, ³J_{βγ} = 18.5 Hz)).

While phosphorylation was effected using the literature procedure, we were able to increase the overall yield and purity of the product thiamine triphosphate by (1) using *ultrapure*, *high-quality* reagents; (2) extracting the crude reaction mixture with a large volume of CHCl₃ to remove residual DMSO and pyridine from the product; and (3) using a cation-exchange column to further reduce the amount of contaminating pyridine, DMSO and unreacted H₃PO₄ remaining in the final product.

D.2 References

1. Burgess, K.; Cook, D. *Chem. Rev.* **2000**, *100*, 2047-2059.
2. Bettendorff, L.; Nghiêm, H.-O.; Wins, P.; Lakaye, B. *Anal. Biochem.* **2003**, *322*, 190-197.

VITA

Kristie Marie Adams was born on Wednesday, December 13th, 1978, to Elaine S. and Mark R. Adams in Indianapolis, Indiana. Kristie completed grades K-2 in Indianapolis, grades 3-6 in Casper, Wyoming, and grades 7-12 in Billings, Montana. After one year of concurrent enrollment at Montana State University–Billings, Kristie graduated from high school in May, 1997. With one year of college already completed, she continued to pursue a Bachelor of Science degree in business administration. Kristie was soon encouraged to pursue a Bachelor of Science degree in chemistry by Dr. William G. Wickun. After moving to Denver, Colorado, in 1999, Kristie resumed her studies at the University of Colorado–Denver, where she completed an undergraduate research program under the direction of Dr. Xiaotai Wang. In 2001, Kristie moved to her “final” alma mater, Louisiana State University and Agricultural and Mechanical College, graduating with Honors and a Bachelor of Science degree in chemistry in May, 2002. Kristie then accepted a Board of Regents Fellowship to pursue a Doctor of Philosophy in chemistry at Louisiana State University. Kristie joined the bioinorganic chemistry research laboratory of Dr. Luigi G. Marzilli in January, 2003.

While at LSU, Kristie attended several national scientific meetings. She attended the 232nd ACS National Meeting in September 2006, where she participated in two poster sessions. Kristie also attended the 62nd ACS Southwest Regional Meeting in October 2006, where she presented a poster. She is a member of the American Chemical Society (ACS) and the American Association for the Advancement of Science (AAAS). Kristie also served as the LSU Chemistry Graduate Student Council President and performed chemistry experiments for children in grades K-12 as a part of the ChemDemo outreach program. Kristie has received several awards and honors while at LSU, including a Proctor & Gamble Research Fellowship (2007), the Troy H.

Middleton Scholarship (2006), the ACS Division of Inorganic Chemistry Graduate Travel Award (2006), the Charles E. Coates Travel Award (2006) and the ACS Women Chemists Committee Travel Award (2006). Notably, Kristie was one of 250 outstanding senior graduate students nationwide chosen to attend the 2nd National Graduate Student Research Festival at the National Institutes of Health in Bethesda, Maryland, in October, 2007.

Kristie will receive her Doctor of Philosophy degree in chemistry on December 21, 2007, during the Fall Commencement ceremony. After recovering for an indeterminate period of time, Kristie plans to begin a postdoctoral appointment, and start repaying her student loans.